

*Ion-exchange studies of yttrium doped
zirconium phosphates for use in the remediation
of nuclear waste*

by

Gurpreet Singh Suri

A thesis submitted in partial fulfilment for the requirements for the degree of
Doctor of Philosophy (PhD) at the University of Central Lancashire

January 2016

The School of Forensic & Investigative Sciences

University of Central Lancashire

Preston, UK.

STUDENT DECLARATION FORM

Concurrent registration for two or more academic awards

Either *I declare that while registered as a candidate for the research degree, I have not been a registered candidate or enrolled student for another award of the University or other academic or professional institution

or *I declare that while registered for the research degree, I was with the University's specific permission, a *registered candidate/*enrolled student for the following award:

Material submitted for another award

Either *I declare that no material contained in the thesis has been used in any other submission for an academic award and is solely my own work

or *I declare that the following material contained in the thesis formed part of a submission for the award of

(state award and awarding body and list the material below):

* *delete as appropriate*

Collaboration

Where a candidate's research programme is part of a collaborative project, the thesis must indicate in addition clearly the candidate's individual contribution and the extent of the collaboration. Please state below:

Signature of Candidate _____

Type of Award _____

School _____

ABSTRACT

There has been considerable amount of interest in the ion-exchange properties of layered zirconium phosphates. This interest has been renewed due to potential applications in the remediation of nuclear waste. They are believed to be preferred to the conventional ion-exchange materials due to their increased stability under acid conditions. The ability of the material to withstand low pH is crucial as the legacy waste pools have very low pH. It has been well documented that substituting metals with different radii into material's framework can alter the ion-exchange properties of the material due to differences in the crystal structure and the interactions between the framework and the non-framework ions. Perhaps one of the best known examples is the microporous titanium silicate sitinakite, which when 25% of the titanium is substituted for niobium the resulting material has increased ion-exchange selectivity for caesium.

The work presented here focuses on the synthesis and characterisation of a series of α -zirconium phosphate materials doped with trivalent cations (Y, Fe, Ce) of which the results indicate that complete solid solutions were not formed for iron-zirconium phosphate and cerium-zirconium phosphate, whereas solubility limits exist for yttrium-zirconium phosphate. The new yttrium-zirconium phosphates obtained were characterised by analytical techniques such as XRD, XRF, SEM/EDAX, MAS-NMR and FT-IR. The structural refinement of these materials was carried out and a study of the doping effect was also done to conclude that yttrium substitution into the zirconium phosphate framework did not follow Vegard's law. Finally, ion exchanges of the inactive ions of Cs, Sr and Co commonly found in nuclear waste was carried out using single ion exchange and competitive exchange experiments with Na, Mg and Ca as interfering ions. The results indicate that the yttrium doped zirconium phosphates showed higher efficiency for exchanging strontium and cobalt compared to α -zirconium phosphate. Although, structural solution of these exchanged phases was not carried out, a number of characterisation methods were used to understand the degree of exchange and order of affinity to determine their use as potential nuclear waste stores.

Acknowledgement

It is with great respect and honour that I would like to thank my Director of Studies, Dr. Jennifer. E. Readman for providing me an opportunity to explore the vast field of inorganic chemistry and contribute to the valuable research ongoing in her group. Dr. Jennifer has been a great mentor and guide both in and out of the laboratory and I will lifelong cherish every piece of advice and knowledge that I have received from her. Special thanks go to my second supervisors, Prof. Gary Bond and Prof. Richard McCabe for providing constant support and guidance whenever needed and adding enormously to my learning experience here at UCLan.

I would like to specifically acknowledge Prof. Abraham Clearfield who had provided his pioneer knowledge and expertise through emails and was very kind to communicate with me without prior introduction. I see the legendary Clearfield as my path finder for all his service and contributions in the field of zirconium phosphates since decades. Special mentioning goes to Prof. Jai Paul Singh for being my Research Degree Tutor and acting as a guardian here at UCLan and providing all the professional and emotional support needed at times. Secondly, I would like to mention a special thank you to the lab technicians: James Charles Donnelly (Jim), Patric Daniel Cookson (Pat) and Dr. Runjie Mao for their constant guidance while operating analytical machines.

Finally, but nonetheless, I would like to thank my lovely parents, my elder brother and my grandparents for their strong prayers and love towards me which always make me feel blessed. I would also like to extend my token of regards and humbleness to the members of Sikh Temple (Guru Nanak Gurudwara Singh Sabha, Bow Lane, Preston) for the blissful communions and family-like support throughout my stay here. It would not be possible to maintain spiritual sanctity and high morality without the presence of blessed aura and wisdom around myself, as I have received from the Preston community members.

Above all, I would like to thank the divine being (Akaal Purakh) – who is always there for everyone without discrimination, the true being, the only doer, fearless, loving, formless, immortal, enlightener and achieved by salvation (Mool Mantar translation).

List of Abbreviations

α -ZrP	Alpha Zirconium Phosphate
Y-ZrP	Yttrium-Zirconium Phosphate
Fe-ZrP	Iron-Zirconium Phosphate
Ce- ZrP	Cerium-Zirconium Phosphate
NMR	Nuclear Magnetic Resonance
XRD	Powder X-Ray Diffraction
XRF	X-Ray Fluorescence spectroscopy
SEM	Scanning Electron Microscopy
EDX	Energy Dispersive X-ray spectroscopy
BET	Brunauer, Emmett and Teller
GSAS	General Structural Analysis System
FT-IR	Fourier Transform Infrared Spectroscopy

Table of Contents

Chapter 1: INTRODUCTION

1.1.	Research background – ‘An insight’	1
1.2.	Ion-exchangers	4
1.3.	Layered transition metal (IV) phosphates.....	5
1.4.	Alpha-zirconium phosphate – ‘The template’	6
1.5.	Structure of α -ZrP.....	15
1.6.	Ion-exchange chemistry of α -zirconium phosphate	18
1.7.	Layered mixed metal phosphates.....	25
1.8.	Aims of the study	29
1.9.	References	31

CHAPTER 2: EXPERIMENTAL METHODOLOGY

2.1	Introduction.....	37
2.2	Synthesis procedure	37
2.2.1	Synthesis of α -zirconium phosphate.....	38
2.2.2	Synthesis of yttrium-zirconium phosphate.....	39
2.3	Acid stability test.....	40
2.4	Ion-exchange	41
2.5	Characterisation techniques	42
2.5.1	X-ray Diffraction (XRD).....	42
2.5.2	X-ray florescence (XRF) spectroscopy	49
2.5.3	Scanning electron microscopy (SEM).....	50
2.5.4	Physical-adsorption study using BET.....	52
2.5.5	Fourier transform infrared spectroscopy (FT-IR)	54
2.5.6	Solid state nuclear magnetic resonance (MAS-NMR).....	55
2.5.7	Inductively coupled plasma mass spectrometry (ICP-MS).....	57
2.5.8	Particle size measurement.....	58
2.6	Rietveld refinement	59
2.7	References	63

CHAPTER 3: RESULTS AND DISCUSSIONS FOR SYNTHESIS AND CHARACTERISATION OF MIXED METAL PHOSHPHATES

3.1	Synthesised alpha zirconium phosphate	65
3.1.1	X-ray diffraction (XRD) analysis.....	65

3.1.2	X-ray fluorescence (XRF) analysis.....	69
3.1.3	Scanning electron microscopy (SEM) analysis	71
3.1.4	Mastersizer analysis.....	72
3.1.5	FT-IR analysis.....	74
3.1.6	Nuclear magnetic resonance (NMR) analysis	75
3.1.7	Rietveld Refinement	79
3.2	Synthesis of yttrium-zirconium phosphate (Y-ZrP)	85
3.2.1	X-ray diffraction of Y-ZrP samples.....	86
3.2.2	X-ray fluorescence (XRF)	90
3.2.3	Scanning electron microscopy (SEM) analysis	92
3.2.4	Mastersizer analysis.....	94
3.2.5	BET surface area analysis	96
3.2.6	FT-IR of synthesised Y-ZrP.....	97
3.2.7	Solid State ³¹ P MAS-NMR of Y-ZrP samples.....	99
3.2.8	Rietveld Refinement of Y-ZrP.....	102
3.2.9	Acid Stability test	114
3.3	Mixed phase Y-ZrP products.....	115
3.3.1	X-ray diffraction (XRD) analysis.....	116
3.3.2	X-ray fluorescence analysis.....	117
3.3.3	SEM analysis of the mixed phase products.....	118
3.4	Other attempted mixed metal phosphates	121
3.4.1	XRD analysis of Ce-ZrP and Fe-ZrP	122
3.4.2	XRF analysis of the mixed phase products.....	124
3.5	References	126

CHAPTER 4: SINGLE ION EXCHANGE STUDIES

4.1.	Introduction.....	129
4.2.	Strontium ion exchanges of Y-ZrP samples.....	129
4.2.1	XRD analysis of strontium exchanged products.....	130
4.2.2	pH analysis of strontium exchanged solutions	134
4.2.3	XRF analysis of strontium exchanged products	135
4.2.4	FT-IR analysis of strontium exchanged products	137
4.2.5	ICP-MS of the strontium exchanged products.....	142
4.3.	Caesium ion exchange.....	145
4.3.1	XRD analysis of caesium exchanged products	145

4.3.2	pH analysis of caesium exchanged products	150
4.3.3	XRF analysis of caesium exchanged products.....	151
4.3.4	FT-IR analysis of caesium exchanged products.....	152
4.3.5	ICP-MS analysis of caesium exchanged products	157
4.4.	Cobalt ion exchange	160
4.4.1	XRD analysis of the cobalt exchanged products	160
4.4.2	XRF analysis of cobalt exchanged products	163
4.4.3	pH analysis of the cobalt exchanged products	165
4.4.4	FT-IR analysis of the cobalt exchanged products.....	166
4.4.5	ICP-MS analysis of the cobalt exchanged products	169
4.5.	Summary of single ion-exchange results.....	171
4.6.	References	173

CHAPTER 5: COMPETITIVE ION EXCHANGE

5.1.	Introduction.....	174
5.2.	Strontium – caesium exchange.....	174
5.2.1	XRD analysis of strontium-caesium exchange	174
5.2.2	XRF analysis of strontium-caesium exchange	176
5.2.3	pH analysis of strontium-caesium exchange	178
5.2.4	ICP-MS analysis of strontium-caesium exchange	179
5.3.	Caesium-Cobalt exchange.....	181
5.3.1	XRD analysis of the caesium-cobalt exchange	181
5.3.2	XRF analysis of caesium-cobalt exchange.....	183
5.3.3	pH analysis of caesium-cobalt exchange	184
5.3.4	ICP-MS of caesium-cobalt exchange	186
5.4.	Strontium - cobalt exchange	189
5.4.1	XRD analysis of strontium-cobalt exchange.....	189
5.4.2	XRF analysis of strontium-cobalt exchange	190
5.4.3	pH analysis of strontium-cobalt exchange.....	192
5.4.4	ICP-MS analysis of strontium-cobalt exchange.....	193
5.5.	Strontium-caesium- cobalt exchange.....	195
5.5.1	XRD analysis of strontium-caesium-cobalt exchange	195
5.5.2	XRF analysis of strontium-caesium-cobalt exchange.....	196
5.5.3	pH analysis of strontium-caesium-cobalt exchange	197
5.5.4	ICP-MS analysis of strontium-caesium-cobalt exchange	199

5.6.	Competitive exchange with calcium	202
5.6.1	XRD analysis of competitive exchange with calcium	202
5.6.2	XRF analysis of competitive exchange with calcium.....	207
5.6.3	pH analysis of competitive exchange with calcium	209
5.6.4	ICP-MS analysis for competitive exchange with calcium.....	211
5.7.	Competitive exchange with magnesium	217
5.7.1	XRD analysis of competitive exchange with magnesium.....	218
5.7.2	EDX/SEM results for competitive exchange with magnesium.....	221
5.7.3	pH analysis of competitive exchange with magnesium.....	223
5.7.4	ICP-MS analysis of the competitive exchange with magnesium	225
5.8.	Competitive exchange with sodium	230
5.8.1	XRD analysis of competitive exchange with sodium.....	230
5.8.2	EDX/SEM analysis of the competitive exchange with sodium.....	235
5.8.3	pH analysis of competitive exchange with sodium.....	236
5.8.4	ICP-MS analysis of competitive exchange with sodium.....	238
5.9.	Unit cell refinement of the ion-exchanged samples	244
5.10.	Summary of the results	246
5.11.	References	249

CHAPTER 6: CONCLUSION AND FUTURE WORK

6.1.	Mixed Metal Phosphates.....	250
6.2.	Ion Exchange Studies.....	252
6.3.	Summary of the work reported in this thesis.....	253
6.4.	Future Work.....	254
6.5.	References	256

APPENDICES

Appendix 1	258
Appendix 2	266
Appendix 3	269
Appendix 4	281
Appendix 5	286
Appendix 6	299

CHAPTER 1: INTRODUCTION

1.1. Research background – ‘An insight’

The quest for harnessing nuclear power began with scientific developments that were taking place across the world in the fields of chemistry and physics. The discovery of Uranium in 1789 by a German Chemist named Martin Klaproth and subsequent studies on its physical and chemical properties by many researchers helped in understanding the nature of radiations that were emitted from it, thus enabling Marie and Pierre Curie to coin the term as ‘radioactivity’ in 1896. However, it was not until 1939, when Otto Frisch and Lise Meitner while working under Niels Bohr, quantified the nuclear energy and provided an experimental figure for the estimated nuclear power that could be harnessed proportional to the mass of the radioactive material. Still, the use of nuclear energy at large scale was brought to light during World War II with the United States carrying out a highly confidential Manhattan Project during which the atomic bombs were produced to aid the U.S and create dominance over other countries. This not only led to the most well-known and ill reputed nuclear attacks on Japan’s Hiroshima and Nagasaki in the years 1944-1945 but also gave way to higher research and expansibility of nuclear power in the world.

Shortly after the nuclear weapons were created during the WWII, small nuclear reactors were designed to produce the world’s first nuclear electricity in the U.S at Shippingport, Pennsylvania (1957-1982), Dresden (1960-1978) and also in United Kingdom at Calder Hall – 1 (1956-2003).^[1] This was followed by other countries such as Canada, Russia, Germany, India, etc that soon realised the potential of nuclear power. But due to the large scale disasters that occurred at the nuclear power plant sites all over the world such as Three Mile Island in 1979, Chernobyl in 1986 and the most recent Fukushima Daiichi nuclear disaster on March 11th 2011, the nuclear industry is facing strict regulations and monitoring.

Currently, more than 30 countries are producing electricity generated by nuclear plants but due to the rising concerns over the legacy nuclear wastes and past nuclear disasters that have occurred, many countries have cancelled or restrained their future projects on nuclear power. Germany and Italy had already announced to

shut down all the nuclear power plants and withdraw completely from nuclear energy production by 2022, and Switzerland plans to do the same by 2034. ^[2] But on the other hand, United Kingdom and China have plans to expand their nuclear power generation in the coming years and many new plants are being planned. The increase in production of nuclear energy also leads to increased nuclear waste generation and therefore poses greater challenges to deal with it. This renews the interest in the technology and measures to encounter the radioactive waste which is generated in tonnes across the globe and it is disposed off into the environment causing a risk of pollution. ^[1, 2] One of the most efficient ways of treating the radioactive waste is to use ion exchangers that remove the radionuclides such as strontium, caesium and cobalt from the waste solutions.

The nuclear effluents from the nuclear power plants across the world typically generate large quantities of radioactive waste that is known as 'spent fuel'. The typical spent fuel from a nuclear reactor consists of elements such as uranium, plutonium, neptunium, americium and curium. These are in turn split into radioactive ⁹⁰Sr and ¹³⁷Cs along with the production of corrosion products such as ⁶⁰Co. These radionuclides are then discharged into the environment in the form of nuclear wastes which is categorised as low-level, medium-level or high level wastes. ^[2, 3] The low-level wastes are generally produced by industries and laboratories in the form of tools, rags, gloves, etc that accounts to short-lived radioactivity. The medium level waste mostly consists of contaminated materials and parts from nuclear reactors, chemical sludges and decommissioned weapons, etc that accounts to about 4% of the total radioactivity in the environment. Finally, the high-level waste consists of mostly fission products and spent fuel concentrated with uranium and plutonium isotopes which accounts to about 95% of the total radioactivity.

These effluents are then discharged or are leaked through primary pipelines into the spent fuel pond water storage and floor drain water systems. This spent fuel is highly radioactive and also contains large quantities of unused uranium and plutonium which is often re-used by many nuclear plants in countries like UK, Russia and Japan. ^[3] This is achieved by dissolving the spent fuel in acidic solutions such as nitric acid, producing a solution which contains cations such as ⁹⁰Sr, ¹³⁷Cs and ²⁴¹Am along with that of anionic nuclides such as ⁹⁹Tc and ¹⁰⁶Ru. The solution is

concentrated and stored in stainless steel tanks or can be immobilised in concrete and cements. Finally the waste is stored in underground repository sites located away from the human habitat. ^[4]

Another well-established process of immobilising the radioactive waste is vitrification. This uses borosilicate glass as a host material to make a vitreous product by incorporating the waste acidic salts into a suitable cast form. ^[5, 6] Although these processes are well known and desirable in the early stages, but in a longer run they prove to be expensive and complex. It is argued that employment of highly selective process to remove the radionuclides from the liquid nuclear wastes would prove more beneficial. This will not only reduce the volume of the nuclear waste which needs to be handled and disposed but will also significantly reduce the amount of radioactive waste dumped into the environment. The process of exchanging the radionuclides from the nuclear waste solution will generate only medium or low level residual waste which can be easily solidified using simpler and inexpensive processes and will pose lower risk to the environment. However, one of the main disadvantages of underground disposal of immobilised nuclear waste is the leaching of the radionuclides into the underground water table.

The half-lives of the most common radionuclides are shown in the Table 1.1 below ^[7], highlighting the problem of leaching of nucleotides back into the environment.

Table 1.1 Half-Lives of the most common radionuclides

Radionuclide	Half-life (years)
^{238}U	4.5 billion
^{235}U	700 million
^{239}Pu	24,000
^{60}Co	5.27
^{90}Sr	28.5
^{137}Cs	30.2

More recently, nuclear weapons make use of caesium, cobalt and strontium, as seen in the two caesium containing undetonated bombs found in Chechnya in mid and late 1990's. These radionuclides would contaminate the land and other water supplies after detonation. [8] Therefore it is important to tackle the spread of these radionuclides by efficiently removing it from the environment by employing highly selective materials such as the ion-exchangers.

1.2. Ion-exchangers

Various different types of ion-exchangers have been used for the remediation of nuclear waste over the last few decades. Both organic and inorganic exchangers and composites are used for this purpose. Although the selection of a type of ion-exchanger strongly depends on the targeted chemical composition of the waste solution but it has been found that organic resins are not thermally stable at high temperatures and are not stable towards ionising radiation. [9-11] In contrast, the inorganic ion-exchangers have higher thermal and radiation stability. Cost analysis of both types of ion-exchangers shows inorganic ion-exchangers can save up to 5 to 10% of the cost of treating nuclear waste as compared to organic resins. [9]

Zeolites have been one of the most widely used inorganic ion-exchangers for remediation of nuclear waste due to their high selectivity towards radionuclides and high ion-exchange capacity. [10] Zeolites are crystalline hydrated alumina-silicates which are made up of $[\text{SiO}_4]^{-4}$ and $[\text{AlO}_4]^{-5}$ tetrahedra connected vertex sharing by oxygen atoms to form 3D structures with cavities and tunnels of varying sizes to trap ions of interest. [11] The cationic exchange is facilitated by isomorphous substitution of the Si^{4+} ions of the tetrahedral with Al^{3+} ions that results in a net negative charge in the framework which is balanced by the cations that can be exchanged within the cavities. The Si/Al ratio can be varied to tailor for the specific cavity size and ion-sieving effect for cations of interest. For example, the zeolite A has a pore size of 4 Å in the sodium form which is reduced to 3 Å on exchange of Na^+ ions with K^+ ions and to 5 Å on exchange of 2 Na^+ ions with a Ca^{2+} ion. [10, 11]

One of the disadvantages of using zeolites for the remediation of nuclear waste is the extremely acidic pH environment found in the legacy waste pools. Under the acidic conditions the aluminium and silicon units break apart, making the zeolites

unstable. For example, it has been well documented that separating chromium (Cr^{3+}) ions from that of iron (Fe^{3+}) and aluminium ions (Al^{3+}) in streams of tanning bath effluent is problematic. This led to the discovery of acid stable inorganic ion-exchangers which are also efficient in hot organic solutions to selectively remove cations, called metal (IV) phosphates such as zirconium phosphate and titanium phosphate in the early and mid 1900's.^[12] But many of the early materials produced were amorphous and with varying degrees of composition. As a result the ion-exchange mechanism was not fully understood and the knowledge on the physical and chemical properties was limited. It was not until 1964 when Clearfield and Stynes synthesised the first crystalline zirconium phosphate phase that it was possible to determine the structure and understand the ion-exchange mechanism.^[13] Various other types of inorganic ion-exchangers have been developed over the years including silico-titanates (CST) and hexacyanoferrate compounds, of which crystalline silico-titanate (CST) and layered sodium titanate ($\text{Na}_4\text{Ti}_9\text{O}_{20}\cdot n\text{H}_2\text{O}$) are one of the most efficient inorganic exchangers for the removal of radioactive caesium and strontium respectively from broad pH ranges of high nuclear salt waste solutions.^[14]

1.3. Layered transition metal (IV) phosphates

The insoluble acid salts of the tetravalent metal have been used as efficient ion-exchangers for many decades for various applications but recently the interest in them is renewed due to their higher resistance to radiation and extreme temperatures. They are present in various degrees of crystallinity based on the preparation techniques and stoichiometry of the chemical reagents used, starting from amorphous gels to single crystals^[13, 14] and the crystalline forms of the metal (IV) phosphates are found to be more stable than the amorphous gels.^[15]

The most well studied metal (IV) phosphates includes titanium phosphates, tin phosphates, germanium phosphates and zirconium phosphates as mentioned before. Titanium phosphates are isomorphic to zirconium phosphates and can be produced in both crystalline and amorphous forms starting with precipitation of TiCl_4 solutions in phosphoric acid^[16-18]. The alpha and gamma phases of TiP can be produced using similar methodology as of α -ZrP and γ -ZrP but they tend to have

narrower passages which restricts the cations with larger radii as seen in the case of K^+ ion exchanges done on α -ZrP and α -TiP, the former being a good ion-exchanger of K^+ compared to the latter ^[19].

Tin phosphate, on the other hand is a well-established ion-exchanger used for decades for both water purification and nuclear waste remediation ^[20]. α -SnP was first synthesised by Merz *et al.* ^[21] in 1959 and showed similar ion-exchange properties compared to α -ZrP even though it was a gelatinous sample. Later Rietveld analysis ^[22] showed that α -SnP is isomorphous to α -ZrP and α -TiP, but it was also shown by Costantino *et.al* that tin phosphates can be hydrolysed in alkaline and even neutral pH environments by most of the alkali metal cations, as opposed to α -ZrP ^[23].

One of the chemically least stable phosphates of the metal (IV) phosphates is known as α -GeP. ^[24] Most of the attempts to synthesise α -GeP resulted in poorly crystalline and often impure products which were easily hydrolysed. The structural studies report the unit cell to be monoclinic ^[25] but due to the instability of the structure, number of studies done using this ion-exchanger is far lesser compared to other related materials.

1.4. Alpha-zirconium phosphate – ‘The template’

Most of the recent studies on the ion-exchangers are utilising the α -ZrP as a ‘template’ to synthesise a variety of novel ion-exchangers (both organic and inorganic). The detailed framework studies which are done on α -ZrP over the years prove its higher ion-exchange selectivity and capacity to remove most of the cations across the periodic table at varying pH solutions. As previously mentioned, the preparation of α -ZrP was reported first by Clearfield and Stynes in 1964 ^[13] and later by Alberti and Torracca. ^[26] The investigation of mixed compounds of this and other types is also of interest because of the potential for fine tuning of the ion-exchange selectivity through chemical control. As the properties of materials are directly linked to their structure, slightly changing the structure of a material can significantly change or enhance its properties.

Clearfield *et al.* [27] reported that slight variation in acidity of the phosphoric acid used in the synthesis changes the crystallinity of the product. Also, there were other similar layered materials such as the largely hydrated γ -ZrP (gamma form) and the anhydrous β -ZrP (beta form). Hodson and Whittaker [28] reported how materials with the same chemical formula, but synthesised using different synthesis routes had differing surface areas which affected their success as catalysts. Trobajo *et al.* [29] showed that crystalline α -ZrP can be obtained directly by co-precipitation of a zirconium source and an excess of phosphoric acid without the need of a subsequent step and that the washing up of precipitate causes hydrolysis which is the cause for the formation of amorphous product. However, the fresh unwashed precipitate was thermally unstable and showed the presence of mixture of α -ZrP and H_3PO_4 which affects the surface area and ion exchange properties of the α -ZrP.

Andersen *et al.* [30] showed that amorphous zirconium phosphate products can be crystallised by using hydrothermal methods. This hydrothermal pressure vessel can then be placed in a hot oven at desired temperature between 0 to 200°C. As the temperature increases in the vessel, an elevated pressure develops inside, corresponding to the liquid-vapour pressure relationship of the solvent (for example at 180°C, water and steam co-exist at about 10 bars pressure). Hydrothermal methods normally provide higher working temperatures and a uniform heating mechanism due to the product being under pressure.

Recently, Yuan *et al.* [31] has provided evidence for fast synthesis of ordered mesoporous materials using a microwave which resulted in uniform particle size. However, there has been little work reported on microwave synthesis of layered α -ZrP, although there has been work published on mesoporous zirconium phosphate synthesis recently by Panda *et al.* [32] however, the product obtained was amorphous.

Different phases of the crystalline phosphates are also known and synthesised over the last few decades and are briefly summarised below along with their interlayer spacing in angstroms shown in Table 1.2.

Table 1.2 Different crystalline phases of zirconium phosphate ^[34]

Phase	Chemical Formula	Interlayer Spacing (Å)
α-ZrP	Zr(HPO ₄) ₂ ·H ₂ O	7.56
β-ZrP	Zr(HPO ₄) ₂	9.4
γ-ZrP	Zr(HPO ₄) ₂ ·2H ₂ O	12.2
δ-ZrP	Zr(HPO ₄) ₂ · ¹ / ₂ H ₂ O	7.13
ε-ZrP	Zr(HPO ₄) ₂	5.59
ζ-ZrP	Zr(HPO ₄) ₂	7.41
η-ZrP	Zr(HPO ₄) ₂	7.37
θ-ZrP	Zr(HPO ₄) ₂ ·8H ₂ O	10.4
τ-ZrP	Zr(HPO ₄) ₂ ·2H ₂ O	12.25

Gamma-zirconium phosphate (γ-ZrP) was first synthesized by Clearfield *et al.* ^[35] in 1968 alongside beta-zirconium phosphate (β-ZrP). The samples were prepared by refluxing ZrOCl₂ solution with that of P₂O₅ for approximately 25 hours. The product obtained was washed with HCl acid, phosphoric acid and finally with a small amount of de-ionized water. It was then either air dried which led to the formation of the γ-ZrP or dried in a vacuum desiccators over anhydrous calcium phosphate to produce β-ZrP. Subsequent work by other groups showed that γ-ZrP can be produced by different synthetic routes, for example, Alberti *et al.* ^[36] prepared crystalline sample of γ-ZrP by first forming the mono-ammonium form directly followed by ion-exchange, whereas, Poojary *et al.* ^[37] prepared a highly crystalline sample of γ-ZrP by hydrothermal methods.

Determination of the structure of γ-ZrP proved quite difficult due to the difficulty of achieving a satisfactory crystalline sample. One of the very first crystallographic models of γ-ZrP was reported in 1979 by Yamanaka and Tanaka ^[79] showing that γ-ZrP structure is monoclinic with unit cell parameters $a = 5.376 \text{ \AA}$, $b = 6.636 \text{ \AA}$, $c =$

24.56 Å and $\beta = 93.94^\circ$. It was later found that the phosphate groups were mistakenly assigned as the monohydrogen groups. Clayden *et al.* [80] in 1987 performed a study on γ -ZrP using solid state NMR and showed that in contrast to the α -ZrP which shows a single resonance at -18.7 ppm, two different ^{31}P resonances were observed for γ -ZrP at -9.4 ppm and -27.4 ppm respectively. This provided evidence that two different phosphate environments were present in γ -ZrP which were due to the presence of two distinct phosphate groups, with H_2PO_4^- groups giving a peak at -9.4 ppm and PO_4^{3-} groups at -27.4 ppm.

The crystal structure of γ -ZrP was finally resolved by Alberti *et al.*, [36] when a crystalline sample of γ -ZrP was indexed. The crystalline γ -ZrP was produced by slow decomposition reaction for the fluoro complexes followed by ion-exchange mechanisms. It was found that γ -ZrP crystals were monoclinic with lattice parameters: $a = 5.386(3)$ Å, $b = 6.636(1)$ Å, $c = 12.403(4)$ Å and $\beta = 98.70(3)^\circ$ and later, Poojary *et al.* [81] provided the structure of the monoammonium exchanged form of γ -ZrP where it was found that $\text{Zr}(\text{PO}_4)(\text{NH}_4\text{HPO}_4)$ also crystallised in monoclinic crystal system with a space group of $\text{P}2_1/m$ and the lattice parameters were found to be: $a = 5.3284(4)$ Å, $b = 6.6217(2)$ Å, $c = 11.326(1)$ Å and $\beta = 96.63(1)^\circ$.

Finally, Poojary *et al.* [37] determined the exact structure of γ -Zr $(\text{PO}_4)(\text{H}_2\text{PO}_4)\cdot 2\text{H}_2\text{O}$ using hydrothermal methods. It was found that one of the phosphate groups along with the metal atoms were nearly located in a plane with an octahedral coordination, where the metal atoms were bonded to four of the oxygen atoms of the phosphate group along with two of the oxygen atoms from the dihydrogenphosphate group. Protons bind to the other two oxygen atoms of the dihydrogenphosphate group forming hydroxyl groups which project out into the interlayer spaces. Water molecules are then bonded with these hydroxyl groups using hydrogen bonds to form pockets which accommodate the water molecules forming a zigzag chain along the perpendicular axis. Another study was carried out by Rajeh and Szirtes [121] in the same year confirming that structure of γ -ZrP crystal was monoclinic with about similar lattice parameters. By using IR spectrophotometry they confirmed the presence of two different phosphate groups (H_2PO_4^- and PO_4^{3-}) in equal ratio with two moles of water between the layers.

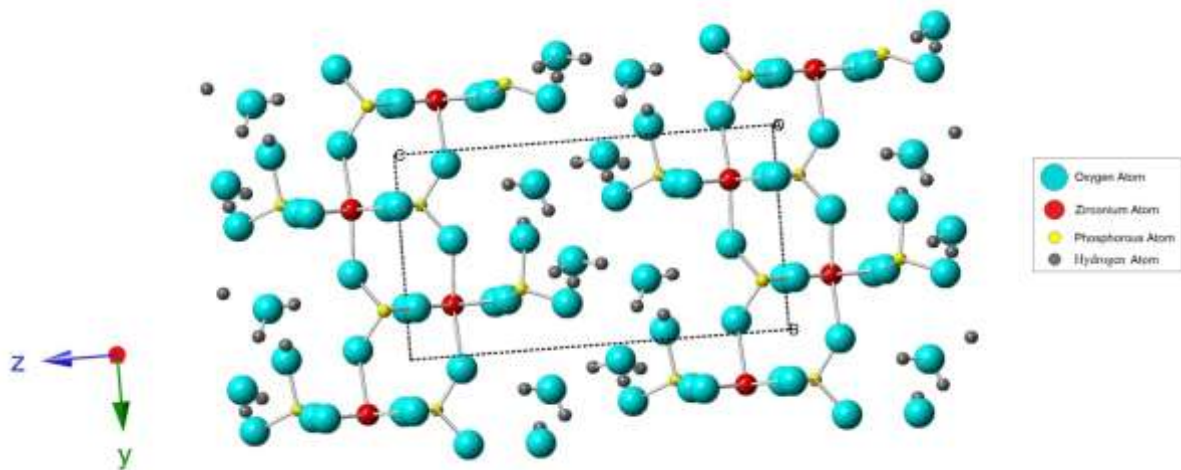


Figure 1.1 Structural representation of γ -ZrP as reported by Poojary and Shpeiz ^[37]

Gamma-zirconium phosphate (γ -ZrP) has varied intercalation chemistry however, because of strong hydrogen bonds between the zirconium phosphate layers, the rate of intercalation is usually very slow. The use of γ -ZrP for ion-exchange has not been extensively studied, as discussed before. However, it is believed that due to the rigid framework as a result of strong hydrogen bonds, γ -ZrP would be a more stable cationic exchanger over a wide range of temperature. One of the first reported cases of the ion exchange was reported by Clearfield and Garces ^[82] in which the alkali metal ions were exchanged into γ -ZrP in the presence of excess water content (2 moles per mole of exchanger) in its framework which aids accommodation of various ions without changing the interlayer spacing. The initial selectivity of γ -ZrP for alkali metal ions were in the order of $K^+ > Rb^+ > Cs^+ > Na^+ > Li^+$ which was later changed to $K^+ > Rb^+ > Na^+ > Cs^+ > Li^+$ over the increase in contact time. It was observed that the x-ray diffraction pattern changed in cases of Li^+ exchange up to 25% leading to two phases which consisted of a partially exchanged phase and a pure γ -ZrP phase. Similar lattice changes were observed for potassium, rubidium and caesium where a single phase was observed up to 50% exchange but led to a decrease in interlayer spacing. ^[82]

It was observed that potassium and rubidium were irreversibly exchanged whereas lithium and sodium could easily be back exchanged out of γ -ZrP. Another study carried out by Clearfield and Kalnins ^[83] observed that first row transition metal

acetates led to an increased uptake from solution for γ -ZrP with little change in the interlayer spacing. The order of selectivity was similar to that of α -ZrP: $\text{Cu}^{2+} > \text{Zn}^{2+} > \text{Mn}^{2+} > \text{Ni}^{2+} \approx \text{Co}^{2+}$. Finally Nilchi *et al.* [84] carried out an ion exchange study on γ -ZrP and concluded that the strontium exchanged capacity of γ -ZrP exceeded beyond the total theoretical capacity, which was explained by the fact that the hydrolysis of the exchanger took place above 80% Sr^{2+} exchange and strontium phosphate precipitation occurred.

Beta zirconium phosphate (β -ZrP) has a similar structure to that of α -ZrP but the layers in β -ZrP are arranged differently relative to each other. The layers are not staggered and lie directly over one another, producing larger cavities and providing different ion-exchange behaviour. [85] β -ZrP has similar behaviour to clay like substance when it comes in contact with water molecules. It rapidly absorbs 2 moles of water and causes a subsequent increase of the interlayer spacing transforming to a gamma phase. Likewise, when α -ZrP loses a mole of water upon heating at 100°C , it has the composition of β -ZrP but usually there is no change in the x-ray diffraction pattern or structure and as a result the material behaves in a similar fashion to α -ZrP. Overall the main distinction between β -ZrP and other phases of ZrP is that β -ZrP can act as a drying agent and shows unique catalytic and ion-exchange properties but it is not easily synthesised at low temperatures. Andersen and Norby [86] provided a complete study on the phase transition of zirconium phosphate at different temperatures and by indexing powder patterns found, the lattice parameters of β -ZrP were shown to be: $a = 8.3127(5) \text{ \AA}$, $b = 6.6389(4) \text{ \AA}$, $c = 5.3407(3) \text{ \AA}$.

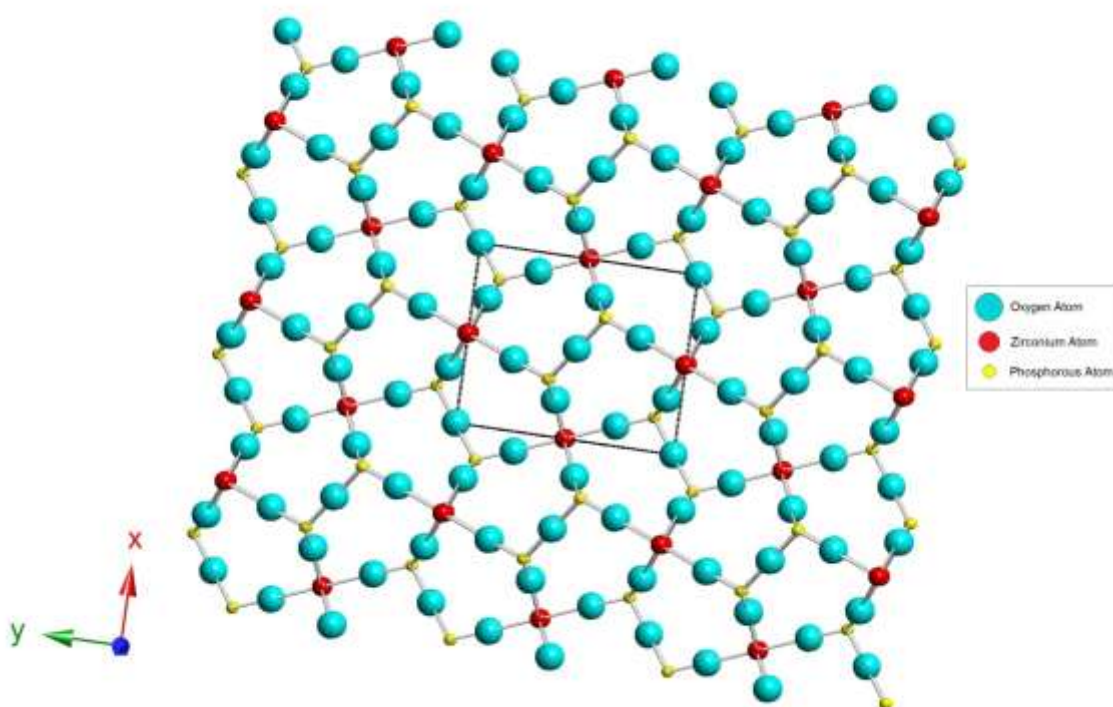


Figure 1.2 Structural representation of β -ZrP reported by Andersen and Norby ^[86]

Anderson *et al.* ^[30] prepared the 3D τ -ZrP by using hydrothermal synthesis but its synthesis is quite difficult since it forms under similar conditions as compared to that of zirconium pyrophosphate. This phase was formed by using amorphous ZrP and mixing it with phosphoric acid to form a gel which was then heated in a Teflon lined autoclave to 190°C for 4-6 days after which it was cooled and separated followed by washing with distilled water. The products were then analysed using XRD which exhibited similar patterns as reported by Clearfield *et al.* ^[34] and Segawa *et al.* ^[87] for the unknown phases which they obtained. The indexed patterns showed a tetragonal unit cell with a space group of $I4_1cd$. The unit cell parameters were found to be $a = 11.259(1) \text{ \AA}$ and $c = 10.764(1) \text{ \AA}$. Little work has been carried out on this phase of ZrP with respect to ion-exchange or catalytic applications since its synthesis is quite complex and the product obtained is quite unstable.

The structure of τ -ZrP consists of ZrO_6 octahedra which are linked to each other via HPO_4 tetrahedra that give rise to a 3-dimensional network with 4-ring channels that

are extending along c-axis. The hydroxyl groups point in to these channels and leads to the formation of a hydrogen bonded spiral along the 4_1 axis. One hydrogen bond is accepted and donated by each hydrogen phosphate and the lengths of these hydrogen bonds are longer at 2.2 Å as compared to α -ZrP (1.85 Å). This shows that τ -ZrP has a more rigid structure compared to the layered α -ZrP, which leads to highly constrained hydrogen bonds that affect the overall stability of the structure.

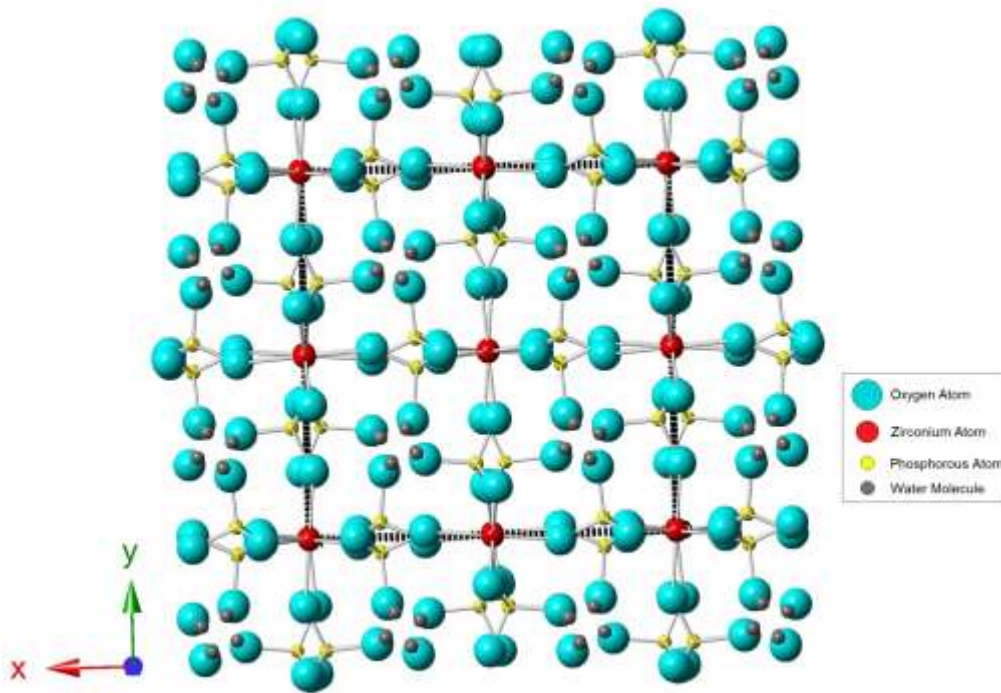


Figure 1.3 Structural representation of τ -ZrP as reported by Andersen and Norby [30]

Another intermediate phase of ZrP which was studied by Andersen and Norby [86] in 2000 was designated as ρ -ZrP (rho-zirconium phosphate). The structure of ρ -ZrP was found to consist of a 3-dimensional orthorhombic structure in which the ZrO_6 octahedra are connected via the vertices with HPO_4 tetrahedra. The ZrO_6 octahedra were observed to be almost regular ordered with bond lengths of 2.056(7) Å and 2.084(4) Å, whereas the HPO_4 tetrahedra are distorted. An in-depth structural study led to an orthorhombic structure with a space group of $Pn\bar{m}$ and unit cell parameters of $a = 8.1856(7)$ Å, $b = 7.6984(7)$ Å and $c = 5.4019(4)$ Å being

proposed. The structure closely resembled to that of τ -ZrP where the orthorhombic a and b axis of ρ -ZrP were equivalent to the half diagonal of the tetragonal unit cell of τ -ZrP except for the fact that the c -axis of ρ -ZrP was halved.

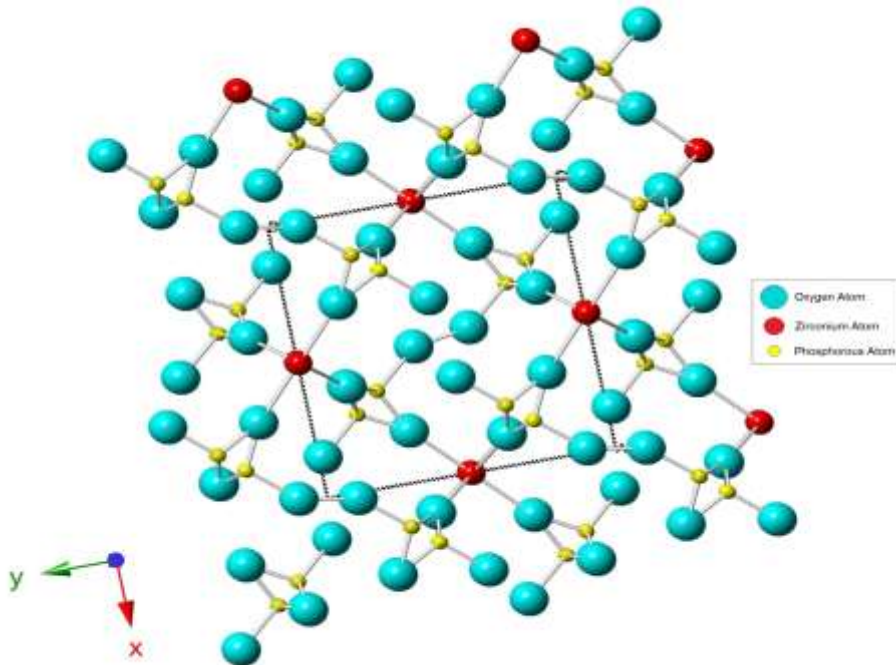


Figure 1.4 Structural representation of ρ -ZrP as reported by Andersen and Norby ^[86]

In 1973, Clearfield *et al.* ^[34] reported the synthesis of several other ZrP phases. All the reported phases were produced from the crystalline α -ZrP by various treatments as described below:

θ -ZrP with the formula $Zr(HPO_4) \cdot 8H_2O$ is an octahydrate which was produced when the half sodium exchanged form of α -ZrP was treated with 0.1M HCl solution. The resulting mixture was then stored in a desiccator at 10°C. The removal of sodium ions led to a highly hydrated form of α -ZrP, which upon standing in air converts back to α -ZrP.

Clearfield *et al.* ^[34] synthesised τ -ZrP using α -ZrP and mixing with 0.1M NaCl and NaOH which was shaken for several hours. After filtration and washing with distilled water, the product was dried at 100°C. This was then heated to 900°C to form the anhydrous phase after which the sodium ions were removed by washing with 1M

HCl. The new τ -ZrP phase was formed which did not revert back to the α -ZrP phase upon cooling and washing.

κ -ZrP synthesis was achieved by dissolving α -ZrP in concentrated hydrofluoric acid using platinum crucible for gentle heating. A small amount of SiO_2 was added once the α -ZrP was completely dissolved and then again it was heated to evaporate the acid forming a thick paste. Boric acid solution was added to this paste and the resulting solid was filtered and dried at 150°C . A new X-ray diffraction pattern which was observed, did not match to those of the materials previously reported.

The phases of δ -ZrP and ϵ -ZrP were synthesised by refluxing α -ZrP in a concentrated phosphoric acid solution (15.7M). These phases were found to be poor ion-exchangers and little work has been carried out to determine their structure or other physical and chemical properties.

ζ -ZrP and η -ZrP were formed by dehydration of α -ZrP. It was found that ζ -ZrP is stable as rehydration to α -ZrP is not achieved. Prolonged heating to high temperatures induces a phase change to η -ZrP. It was also suggested that ζ -ZrP has interlayer spaces similar to those found in α -ZrP.

1.5. Structure of α -ZrP

The family of zirconium phosphate materials have layered structures in most of the phases. The most widely characterised zirconium phosphate phase is α -ZrP in which the zirconium atoms lie in a pseudo hexagonal arrangement in plane. The phosphate groups are situated alternatively above and below the Zr atom plane forming a bridge between the zirconium octahedral such that three of the oxygen atoms from each phosphate group is octahedrally coordinated by three of the zirconium atoms. The fourth oxygen atom of the phosphate group has an exchangeable proton which gives rise to the ion exchange properties of this material. These layers are stacked with an interlayer distance of 7.6 \AA and held together by van der Waals forces alone.

The single crystal x-ray diffraction studies confirmed the initial results of Clearfield and Smith.^[38] It was reported that α -ZrP synthesized had a crystallised monoclinic system with $P2_1/c$ space group and have the lattice parameters as shown in the

Table 1.3 below. This table also shows the confirmatory results produced over the years by Albertsson *et al.* [39] and Troup & Clearfield [40] until the most recent Rietveld refinement done by Burnell and Readman. [41]

Table 1.3 Reported lattice parameters for α -ZrP

Formula	Space Group	a (Å)	b (Å)	c (Å)	β (°)	Ref.
α -Zr(HPO ₄) ₂ .H ₂ O	P2 ₁ /c	9.076(3)	5.298(6)	16.22(2)	111.15(1)	38
α -Zr(HPO ₄) ₂ .H ₂ O (Neutron refinement)	P2 ₁ /c	9.061(1)	5.2873(7)	16.248(1)	111.41(1)	39
α -Zr(HPO ₄) ₂ .H ₂ O	P2 ₁ /n	9.060(2)	5.297(1)	15.414(3)	101.71(2)	40
α -Zr(HPO ₄) ₂ .H ₂ O	P2 ₁ /c	9.063(4)	5.2906(1)	16.246(1)	111.40(2)	41

(Note - The values in bracket show the precision in the last digit and is regarded as the estimated standard deviation or error)

The interlayer spacing of 7.56Å or 7.6Å can increase as the water content increases or with the presence of counter ions. Normally, the Zr-O bond distance is approximately 2.064(5) Å with a O-Zr-O bond angle of approximately 90°. Troup and Clearfield [40] concluded that the fourth oxygen on the phosphate group carrying the negative charge is bonded to a H⁺ ion forming a P-OH group. These groups are hydrogen bonded to the water molecules sitting between the layers. Also, layers pack with P-OH above and below the zirconium atoms, forming water filled hexagonal shaped zeolitic type cavities. These cavities are interconnected by openings of maximum size 2.64Å which restricts the counter ions with a larger diameter from diffusing in unless sufficient energy is supplied to spread the layers. This could be done by adjusting the pH or using higher temperatures. [38]

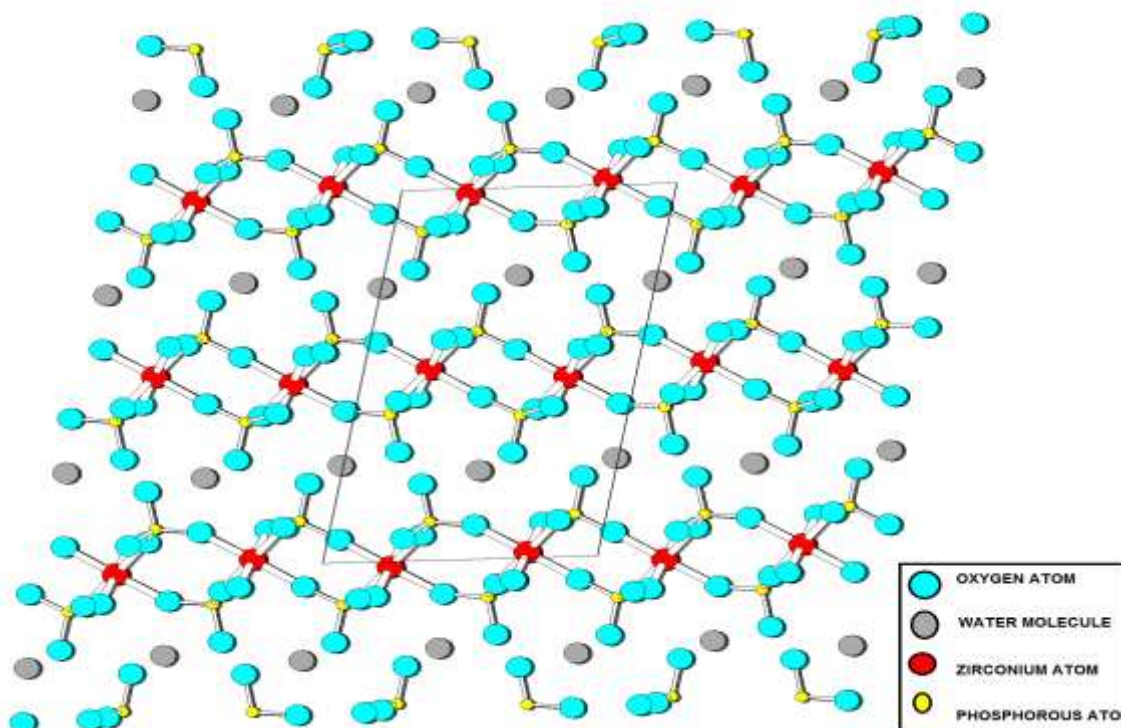


Figure 1.5 Structural representation of α -ZrP as reported by Clearfield & Troup ^[40]

The debate of how layers were bound together was again brought to light in 1972 by Leigh and Dyer ^[42]. They believed that the lattice had a net negative charge which was compensated by half of the available hydrogen ions. The other halves were involved in interlayer hydrogen bonding. Leigh and Dyer also pointed out some similarities between α -ZrP and clay materials. They both consist of layers, both showed interlayer expansion upon ion-exchange and both have large unit cell parameters in the direction perpendicular to the lattice layer.

In 1977, Troup and Clearfield ^[40] published a single crystal x-ray diffraction study of α -ZrP using high quality crystals obtained using hydrofluoric and boric acid. The Zr was found to be octahedrally coordinated with an average Zr-O bond distance of 2.064 Å. The O-Zr-O bond angles were 90°, indicating regular coordination about Zr. The oxygen groups not bound to Zr (i.e. P-OH) led to significantly longer P-O bonds. This study also aimed to clarify the hydrogen bonding scheme. A water molecule sits in the centre of each cavity with two hydrogen bonds from P-OH donor groups. These two groups are in the same layer and form short hydrogen bonds with the water molecule acting as a hydrogen bond donor again to the same layer. They

claimed that no hydrogen bonds were formed between the layers. The entrance to the cavity was recalculated to be 2.61 Å instead of 2.64 Å. They also claimed that the model proposed by Dyer and Leigh *et al.* [42] was incorrect and there would be a large negative charge residing on the layers.

Albertsson *et al.* [39] used neutron powder diffraction of α -ZrP to clear the misconception of hydrogen bonding between the layers of α -ZrP and suggested that van der Waals forces hold the layers together, which change to ionic when the hydrogen ions are replaced by other cations due to the fixed negative charges on adjacent layers; as hydrogen is no longer present to neutralise the charge.

The structure of hemi-hydrate α -ZrP ($\text{Zr}(\text{HPO}_4)_2 \cdot 0.5\text{H}_2\text{O}$) was studied by Alberti *et al.* [43] They determined the structure to be monoclinic with a $C2/c$ space group with lattice parameters: $a = 9.1478(5)$ Å, $b = 5.3242(3)$ Å, $c = 15.288(1)$ Å, $\beta = 103.848(6)^\circ$. Alberti *et al.* also found that at 70°C a phase transition occurred resulting in trigonal symmetry. This is accompanied by a reduction in the interlayer spacing to 7.30Å; however no further loss of water occurs. Unlike the monohydrate structure in which only intra-layer hydrogen bonds exist, interlayer hydrogen bonds were found in the hemi-hydrate structure and it is believed that these are responsible for some of the differences between the two materials.

1.6. Ion-exchange chemistry of α -zirconium phosphate

One of the very first investigations into ion-exchange applications of layered metal phosphates was focussed on determining the number of replaceable hydrogen ions in α -ZrP by Clearfield and Stynes. [13] By carrying out NaCl and NaOH titrations with crystalline α -ZrP they concluded that two hydrogen ions per formula unit could be replaced of α -ZrP. On the other hand, the amorphous gels of ZrP gave an unstable end point which disappeared after 1-2 hours of standing which was believed to be due to hydrolysis of the phosphate groups. X-ray diffraction patterns were obtained at different stages of the exchange and it was shown that as Na^+ ions were exchanged into zirconium phosphate, the peak at 7.46Å split into two peaks with d-spacings of 7.24Å and 7.56Å. With increasing Na^+ exchange, the peaks shifted to lower angles and finally merged into a single peak at 10Å. It was concluded that ion exchange in α -ZrP occurs in two stages; first the cations initially replace the

hydrogen from the P-OH groups which are bonded to water molecules by hydrogen bonds. Then these protons form H_3O^+ ions, letting the cations to occupy the space it formally occupied. The second stage occurs when all the water molecules have moved out and it is believed that it causes the breaking up of hydrogen bonds between layers, hence the layers move apart and cations become incorporated between them.

Over the years, many researchers have studied the ion-exchange properties and capabilities of α -ZrP for various purposes. The presence of ionisable groups of HPO_4 provides sites for ion-exchange since the matrix of α -ZrP is inert, rigid and stable at $\text{pH} \leq 7$ and the ion-exchange behaviour can be easily studied by using titration experiments where the protons are replaced by the ions of interest. A series of lanthanides and actinides were exchanged recently to observe the versatility of α -ZrP as an ion exchange material such as thorium, plutonium, protactinium, uranium and neptunium [72-74].

Torracca *et al.* [45] showed the exchange of mercury ions (Hg^{2+}) from HgCl_2 between the layers of α -Na-ZrP ($\text{NaZrH}(\text{PO}_4)_2 \cdot 5\text{H}_2\text{O}$). It was concluded that Hg^{2+} replaces both the Na^+ and H^+ in the exchanger and the uptake is pH dependent (pH range of 3.5 to 4.5) with the maximum Hg^{2+} uptake at pH 4.5. Reverse exchange of Hg^{2+} is also possible using NaCl where the Na^+ ions are replaced by Hg^{2+} complexing with chloride ions. Temperature was found to play a significant role in exchange of Hg^{2+} since the rate of uptake into α -Na-ZrP was slow due to strong complexation with the chloride ions. Overall the kinetics of the Na^+/H^+ exchange curves displayed a hysteresis highlighting the difference in the reverse and forward reactions along with the presence of 3 plateau regions in pH ranges of $\text{pH} < 7$, $\text{pH} = 7$ to 9 and $\text{pH} > 9$ due to the weaker activity of the HPO_4 groups.^[122] The counter ions also affected the rate of the ion-exchange and it was found that the rate of uptake increased in the following order: $\text{I}^- < \text{Br}^- < \text{Cl}^- < \text{ClO}_4^- < \text{NO}_3^- < \text{SO}_4^-$.

Clearfield and Djuric [45] also performed exchanges of Cu^{2+} and Ca^{2+} with crystalline α -ZrP and concluded that the cations can be exchanged between the layers of α -ZrP without using increased temperature provided sufficient time and low pH conditions were used. The exchanged cations are tightly bound and are difficult to

reverse exchange unless sufficient energies in the form of severe acid conditions are used.

Clearfield and Cheng ^[46] also succeeded to fully exchange Ag^+ into crystalline α -ZrP and showed that silver ions have a higher affinity towards α -ZrP compared to any of the alkali metal ions. This is believed to be due to the high positive entropy of the reaction as Ag^+ brings in 2 moles of water lesser into the lattice than Na^+ or other alkali atoms.

Dyer *et al.* ^[47] showed that amorphous α -ZrP could take up caesium and strontium from polluted water. The process was found to be temperature independent but the uptake can be altered by the presence of smaller radii alkali atoms such as potassium and calcium which have a greater affinity towards α -ZrP but this problem can be overcome by using mixed metal products of α -ZrP such as Na-ZrP.

Recently, work has been done to remove radioactive wastes from the nuclear spent fuel and fission products. Zhuravlev *et al.* ^[48] used the H^+ form and K^+ forms of ZrP and TiP modified with Al^{3+} and Fe^{3+} between the layers to absorb uranium (IV) from uranyl acetate and concluded that even though potassium form of the ZrP and TiP absorbs about 85% of uranium in first 15 minutes as compared to 50% by hydrogen form of ZrP and TiP, it is the latter which is an efficient ion-exchanger of uranium and absorbs almost completely all the uranium present. These ion exchangers are shown to work efficiently in acidic environment with pH of 5 and below. When the pH was increased to 5.5 and above, the ion exchange capacities of these exchangers dropped.

Pan *et al.* ^[49] showed the uptake of heavy metal ions such as lead, cadmium and zinc into amorphous α -ZrP. It was concluded from the sorption kinetics that the uptake was very quick followed by a gradual sorption approaching to equilibrium within 1 hour. The uptake was pH dependent and reduced gradually as the pH decreases which is consistent with the Le Chatelier principle. The Pb^{2+} was favoured over Zn^{2+} to Cd^{2+} than to Ca^{2+} . Also complete regeneration of the heavy metal exchanged α -ZrP was possible using exchange with dilute HCl acid. Nakayama *et al.* ^[50] also immobilised strontium in crystalline α -ZrP lattice and studied the effects of temperature on ion-exchange capacities. It was found that strontium

immobilised material did not form at temperatures below 400°C, which in turn affected the leaching resistance of the sample.

An overview of the various ion-exchanges done using the α -ZrP as present in literatures is summarised in the table 1.4 below:

Table 1.4 Summary of ion exchange studies using α -ZrP

Type of ZrP matrices	Ions successfully exchanged	Study focussed on	Ref
α -ZrP embedded in wool	Lithium, Sodium, Potassium and Caesium.	Behaviour of α -ZrP towards different ions	90
α -ZrP	Gold, Copper and Silver	Separating impurities in valuable metals	91
α -ZrP crystalline	Strontium and Barium	Behaviour of α -ZrP	92
α -ZrP crystalline	Strontium, Magnesium, Calcium and Barium	Hydroxide uptake of metals	93
α -ZrP	Sodium, Magnesium and Caesium	Behaviour of α -ZrP	94
α -ZrP crystalline	Caesium and Rubidium	Behaviour of α -ZrP	95
α -ZrP crystalline	Manganese, Cobalt, Nickel, Copper and Zinc	Behaviour of α -ZrP	96
α -ZrP gel	Copper, Iron (II), Iron (III) and Aluminium	Separating impurities for extraction of pure metals	97
α -ZrP crystalline	Rubidium, Sodium, Silver and Lithium	Selectivity of α -ZrP	98
α -ZrP	Ammonium	Behaviour of α -ZrP	99

α -ZrP	Magnesium, Cobalt, Nickel, Copper and Zinc	Behaviour of α -ZrP	73
α -ZrP crystalline	Chromium, Lanthanum and Thallium	Behaviour of α -ZrP	74
α -ZrP crystalline	Ammonia and Ammonium	Behaviour of α -ZrP	100
α -ZrP crystalline	Magnesium, Cobalt, Nickel and Zinc	Mechanism of α -ZrP	101
α -ZrP	Alkaline metals	Acetate uptake of metals	102
α -ZrP	Uranyl	Behaviour of α -ZrP	103
α -ZrP amorphous	Alkali metals	Thermodynamics	104
α -ZrP crystalline	Alkali metals	Thermodynamics	105
α -ZrP gel	Strontium and Yttrium	Behaviour of α -ZrP	106
α -ZrP	Silver and Copper	Molten salts of metals	107

Intercalation is another way of exchanging ions of interest by binding them to a host template using ionic, hydrophobic and other types of interactions within the matrix. This occurs when the binding free energy of the ions is more than the interlayer energy of interaction of the ions with the matrix therefore the interlayer spacing of the host molecules needs to be increased or the temperature of the reaction needs to be increased to force the ions in between the layers. This property of α -ZrP has been studied over the years and used for various applications. The use of short chain surfactant molecules is one of the common techniques to exchange ions of interests by tuning the interlayer spacing so that the surfactant molecules can be easily exchanged by the ions of interest which have a high affinity. This technique normally makes use of amines (RNH_2) of various chain lengths and was demonstrated recently by Sun *et al* ^[51] by demonstrating the intercalation of

monoamine into the α -ZrP lattice and studying the effect of heating time on intercalation. It was found that intercalation reached a maximum when longer heating times were used.

In another study it was seen by using thermal analysis that the intercalation of amines in α -ZrP leads to three different phase transitions which indicate dehydration, deamination and dehydroxylation steps where the temperature for dehydroxylation and dehydration depends on the capacity of the amine intercalated [75].

Considerable work has been carried out on the intercalation of neutral molecules between the layers of α -ZrP such as alcohols and glycols. It was observed from the x-ray diffraction patterns that the glycols form a single layer, whereas the alcohols formed a bilayer within the interlayer spacing. Ethanol, on the other hand, was studied using vibrational spectroscopy and molecular simulations showed that the α -ZrP and ethanol structure was preserved indicating that the α -ZrP layers are rigid and the binding between alcohols and host matrix is weak which leads to the easy exchange of polar organic molecules such as urea, acetonitrile and dimethylformamide for alcohols [76, 77].

Some recent studies showed the use of microwave radiation for the intercalation reaction of alkanediols and alkanols into the α -ZrP layers. The extent of intercalation is dependent on the number of the hydroxyl groups present in the alkanediols and alkanols. The heating by microwave causes a change in the torsion angle of O – C₁ – C₂ – C₃ bond from a straight chain 180° to 136° and shows that a positive ions is not necessary for the intercalation and hydrogen bonding or other type of interactions such as ion-dipole can aid in intercalation as well [78]. One recent study so far by Naik *et al* [33] showed the use of microwave for the synthesis of crystalline α -Na-ZrP and immobilising caesium, strontium and tellurium between the layers of NZP at high temperatures. The fission products doped NZP materials were analysed for the possibility of leaching with deionised water and 80% brine solution as a leachant. The results showed that even after 28 days, the concentration of the fission products into the leachant was only 10% and hence it was concluded that with 90% immobilising ability, α -Na-ZrP is a potential candidate for remediation of nuclear waste.

An overview of the various molecules intercalated into the α -ZrP matrices as present in literatures is summarised in the table 1.5 below:

Table 1.5 A summary of molecules intercalated in different α -ZrP matrices

Type of ZrP matrix	Molecules Intercalated	Study focussed on	Ref
α -ZrP microcrystal	Methylene Blue	Behaviour of α -ZrP	108
α -ZrP crystalline	<i>n</i> -butylamine and Pyridine	Behaviour of α -ZrP	109
α -ZrP	Glycols and Alkanols	Behaviour of α -ZrP	76
α -ZrP	L-lysine and L-Histidine	Behaviour of α -ZrP	110
α -ZrP	L-alanine and L-asparagine	Behaviour of α -ZrP	111
α -ZrP	Monoalkylamines	Behaviour of α -ZrP	112
α -ZrP	<i>n</i> -alkylamines	Behaviour of α -ZrP	113
α -ZrP	Imidazole, Histamine, Benzimidazole and Histidine	Formation of organic molecules	114
α -ZrP	Diamines	Behaviour of α -ZrP	115
α -ZrP	2,9-dimethyl-1,10-phenanthroline, 1,10-phenanthroline	Behaviour of α -ZrP	116
α -ZrP	Palladium(II) and 2,2'-bipyridyl	Behaviour of α -ZrP	117
α -ZrP	<i>n</i> -alkylamine	Thermal decomposition	75
α -ZrP	Isoquinolinium, <i>n</i> -alkylquinolinium and acridinium	Fluorescence of molecules	118
α -ZrP	Ethanol	Characterisation	119
α -ZrP	<i>N,N'</i> -bis(3-aminopropyl)-1,3-propandiamine	Conformational change of molecule	120

1.7. Layered mixed metal phosphates

Over the last few decades, many mixed metal phosphates have been synthesised for their use in various applications such as ion-exchange and catalysis. Mixed metal phosphates consisting of a tetravalent metal cation and two or more anions have been widely studied with numerous compounds synthesised, whereas the layered mixed metal compounds having two or more cations and one anion are very rare. Of the Mixed metal phosphates consisting of zirconium and phosphate groups reported, zirconium-titanium phosphate (ZTP) has been the most widely studied.

Zirconium-titanium phosphate (ZTP) can be synthesised as both amorphous^[54-57] and crystalline^[58-61] forms. One of the early reported mixed metal phosphates containing both zirconium and titanium metal ions was reported by Clearfield and Frianeza.^[62] It was synthesised by precipitating zirconium and titanium metal solutions in phosphoric acid and then refluxing the amorphous gel in concentrated phosphoric acid. The results showed a single phase when 20% or less of either zirconium or titanium was replaced in the structure, but any higher percentage of metal substitution (such as 33%) resulted in a two phase product. Another successful ZTP synthesis was reported in 1979 by Tomita *et al.*^[52] where they synthesised a single phase zirconium-titanium phosphate (ZTP) by mixing varying compositions of the chloride solutions of the individual metal salts and precipitating it in 2M phosphoric acid at 60-70°C and refluxing the obtained amorphous salt in concentrated phosphoric acid for 48-200 hours. The synthesised material was then used for sodium ion-exchange reactions and it was found that ZTP was more efficient ion-exchanger than α -TiP due to higher resistance to hydrolysis.

The ion-exchange behaviour towards alkali ions^[53] was then studied and it was seen that ZTP was an efficient ion-exchanger of alkali ions and the selectivity of these ions were in the following order: $\text{Na}^+ > \text{K}^+ > \text{Li}^+$, but as the load of the ion-exchanger is increased above 4.5 meq/g Li^+ ions were favoured above all and the K^+ ions uptake were nearly zero. In another study^[54], it was shown that amorphous ZTP had a higher ion-exchange capacity (3.36 meq/g) compared to its single metal salts such as α -TiP (3.09 meq/g) and α -ZrP (2.77 meq/g). As reported by Yazawa *et.al.*^[61] this higher ion-exchange capacity is credited to the less ordered structure of

ZTP as opposed to the regular lattice of the single metal salts. This is caused by the substitution of the metal ions with those of differing ionic radii ($Zr^{4+} = 0.79 \text{ \AA}$ and $Ti^{4+} = 0.68 \text{ \AA}$). This causes the P-O bonds on the phosphate group to deform and leads to an expansion of the layer, resulting in the exchangeable hydrogen ion to be more easily exchanged with the cations from the solution.

Later during early 1990's, Farfan-Torres *et al.* ^[18] reported the synthesis of ZTP by employing a sol-gel route using zirconium and titanium isopropoxide precursors and was followed by hydrolysis with phosphoric acid to form an amorphous product which was later crystallised by refluxing in concentrated phosphoric acid. The results showed that α -ZrP had a solubility limit of 3:1 whereas α -TiP had a solubility of 2:1 for the end members of the ZTP series. Following this, Thakkar and Chudasama ^[60] synthesised ZTP by an alternative sol-gel method and experimentally calculated the composition of the synthesised product to be $Zr_{0.51}Ti_{0.49}(H_2PO_4) \cdot 0.5H_2O$, but it was unclear if a single phase product had been formed.

Recently, Hodson and Whittaker ^[28] reported the preparation of mixed metal phosphates using two synthesis routes. The materials showed enhanced catalytic activity for cyclohexanol dehydration. Several samples of zirconium-titanium phosphate, zirconium-yttrium phosphate and zirconium-niobium phosphates were prepared with varying compositions by co-precipitation method using a mixture of the metal chloride salts and refluxing a 1:1 mixture of their individual phosphates in phosphoric acid followed by neutralisation. Also a triple-metal phosphate (Y-Zr-Nb) was produced by a reflux method. It was concluded from the results that the prepared materials were mostly crystalline via both routes but had different physical and chemical properties. The materials had an increased surface area and different x-ray diffraction patterns compared to α -ZrP or α -TiP. Also it was not understood if the mixed-metal phosphates were prepared by substitution within the layers or by interaction between different metal layers or if the fragments of individual layered metal phosphates were bonded together.

One of the most recent preparations of ZTP carried out by Hassan *et al.* ^[63] used 4M HCl solution along with 12% H_3PO_4 to precipitate out ZTP from the mixed metal solutions of zirconyl chloride and titanium tetrachloride in 4M HCl. This produced an

amorphous product but its application in synthesis of ammonium ion potentiometric sensor was explored and was shown to be very efficient. In 2011, Khan *et al.* [64] synthesised polyaniline exchanged ZTP by using a sol-gel method and the product obtained was semi-crystalline. It was later used for an ion-exchange study of toxic metals and was shown to exhibit enhanced ion-exchange capacity (4.52 meq/g) as compared to pure ZTP (3.36 meq/g). In 2014, Shakshooki *et al.* [65] prepared α -ZTP for synthesis of ZTP - cerium phosphate composite fibrous membranes by refluxing the amorphous parent members of the phosphates (zirconium phosphate and titanium phosphate) in a 10M phosphoric acid solution for 100 hours. The product obtained was shown to be crystalline and single phase with the composition of $Zr_{0.8}Ti_{0.2}(HPO_4)_2 \cdot H_2O$.

Apart from ZTP, many other layered mixed metal phosphate ion-exchangers have been synthesised over the last few decades such as germanium-titanium phosphates, germanium-zirconium phosphates, mixed titanium-tin phosphates, zirconium-tin phosphates, cerium-zirconium phosphate, iron-zirconium phosphate, zinc-cobalt phosphate, lead-manganese phosphate, silver-nickel phosphate, silver-cobalt phosphate and many other dense forms of the mixed metal phosphates have also been prepared. Since most of these phosphates are not fully characterised due to the limited study and absence of a single crystalline phase, therefore the discussion on these phosphates will be kept brief and a general overview is given below by reviewing few main prominent studies carried out to date.

One of the early studies on germanium-zirconium phosphates (Ge-ZrP) was carried out by Galli *et al.* [66] in the mid 80's, where the product was synthesised by refluxing the stoichiometric amounts of zirconium and germanium chloride in phosphoric acid solution. The Ge-ZrP product obtained was poorly crystalline but X-ray diffraction patterns were not published, therefore it is unclear if a single phase product was obtained. It was stated that solid solutions with up to 20% germanium substitution for the zirconium were formed but substitution higher than 35% resulted in two phases.

A study in to the mixed titanium-tin phosphates was done by Trobajo *et al.* [67] who synthesised a crystalline product by using the chloride metal solutions and similar conditions as used in the synthesis of γ -ZrP. It was concluded from the x-ray

diffraction and differential scanning calorimeter (DSC) that almost 75% substitution of tin by titanium occurred in the α -SnP structure. Any higher substitution resulted in the mixed alpha, beta and gamma products. Another study performed by Anillo *et al.* [68] used the same synthesis method as Trobajo *et al.* [67] for synthesising titanium-tin phosphate and reported similar results. The synthesised Ti-SnP was then loaded with vanadium oxide and used for the oxidative dehydrogenation of ethane.

Whang *et al.* [69] successfully synthesised a mixed zinc-cobalt phosphate with the composition $\text{Zn}_2\text{Co}_4(\text{PO}_4)_4(\text{H}_2\text{O})_5 \cdot 2\text{H}_2\text{O}$ that has a layered structure by using hydrothermal methods. A mixture of zinc nitrate, cobalt nitrate, 85% phosphoric acid and NEt_4OH or sodium hydroxide was heated in an autoclave at 160°C for 3 days. The results indicated a single phase product with pale purple, plate shaped crystals. However, only refinement of the lattice parameters was carried out. A low temperature phase of layered $\text{LiHf}_2(\text{PO}_4)_3$ (lithium-hafnium Phosphate) was also successfully synthesised for use as an ion conductor and was found to possess sodium (Na) Super Ionic Conductor (NASICON) type rhombohedral structure. [88] The main difference between its structure as compared to the NASICON material is due to the change in location of the cation. Lithium cations in the $\text{LiHf}_2(\text{PO}_4)_3$ are displaced from the central position and are randomly disordered which results in enhanced ionic conductivity. HfO_6 octahedra containing orderly arranged lithium atoms are connected to PO_4 tetrahedra which are co-ordinated with the polyhedral oxygen atoms. The ordered arrangement of lithium ions in the low temperature phase restricts the lithium ion motion as opposed to the high temperature phase in which the lithium ions are disordered within the lattice leading to enhanced conductive properties. [89]

Recently, Preetha *et al.* [70] reported the synthesis of an amorphous mixed cerium-zirconium phosphate (Ce-ZrP) with the composition $\text{CeO}_2 \cdot 2\text{ZrO}_2 \cdot 1.25\text{P}_2\text{O}_5 \cdot 14\text{H}_2\text{O}$. Zirconyl oxychloride and ceric sulphate solutions were used with the product precipitated by sodium dihydrogen phosphate. The product was obtained as yellow transparent solid and was amorphous in nature. Ion-exchange reactions using group 2,3 and 4 metals were carried out and it was shown that the selectivity of Ce-ZrP for the selected metals were in the following order: $\text{Pb}^{2+} > \text{Cu}^{2+} > \text{Zn}^{2+} > \text{Mn}^{2+} > \text{Cd}^{2+} > \text{Y}^{3+} > \text{Bi}^{3+} > \text{Co}^{2+} > \text{Ni}^{2+} > \text{Ca}^{2+} > \text{Al}^{3+} > \text{Th}^{4+} > \text{Hg}^{2+}$.

Most recently in 2014, the same authors reported synthesising a novel cerium-zirconium phosphotungstate ^[71] by precipitating 1M solutions of the zirconium oxychloride, ceric ammonium nitrate and sodium tungstate in sodium dihydrogen phosphate. The product obtained was a bright yellow glassy solid with poor crystallinity. The ion-exchange properties were studied and it was found that the selectivity was of the following order: $\text{Li}^+ < \text{Na}^+ < \text{K}^+$ (for monovalent cations) and $\text{Mg}^{2+} < \text{Ca}^{2+} < \text{Ba}^{2+}$ (for divalent cations).

1.8. Aims of the study

The main aim of this study was to synthesise an inorganic ion exchanger which is efficient for the removal of radionuclides generated from the nuclear waste of fission and fusion products such as ⁹⁰Sr, ¹³⁷Cs and the activated corrosion product of ⁶⁰Co from their aqueous solutions. Non-radioactive forms of these cations of interest were used due to obvious safety considerations.

Principally the main focus of this study was to successfully synthesise substituted metal (IV) phosphates with the α -ZrP structure with the general formula $(\text{M1})_x(\text{M2})_{1-x}(\text{HPO}_4)_2 \cdot \text{H}_2\text{O}$, where M1 and M2 includes zirconium, yttrium, iron(III) and Ce(III) where $x = 1, 0.95, 0.9, 0.85, 0.8, 0.70$ and 0.60 . The resulting materials would be characterised to study the structure and then further used for ion-exchange reactions. The main reason for performing the study with these mixed metal layered phosphates is due to the unavailability of the novel trivalent inorganic ion exchangers since it is believed that the charge imbalance created in the structure of α -ZrP could lead to a fine tuning of the ion-exchange properties. The best known example of such a study is the microporous titanium silicate sitinakite ^[123], where when 25% on the titanium is substituted for niobium the resulting material has increased ion-exchange selectivity for caesium. The prepared products were primarily analysed with the X-ray diffraction studies (XRD) to analyse the structural changes if present, followed by X-ray Fluorescence Spectroscopy (XRF), Scanning electron microscopy (SEM), Nuclear magnetic resonance (NMR), Fourier transform-Infrared spectroscopy (FT-IR) and refinement of the structural parameters using Rietveld refinement thus providing a clear insight in to the type of lattice crystal system formed.

Ion-exchanges with strontium, caesium and cobalt along with the use of competitive ions like sodium, magnesium and calcium were carried out on the selected mixed metal phosphates which were successfully synthesised as single phase materials. The ion-exchanged products were characterised again using XRD, XRF and SEM to analyse the change in lattice structure and unit cell parameters and determine the degree of ion-exchange.

1.9. References

1. Goldberg. S.M and Rosner. R, Amcn. Acdmy of Arts and Sci. (2011)
2. Gullberg, A.T., Ohlhorst, D., Schreurs, M., Renwl. Eng., 68, 216 (2014)
3. Harjula, R., Lehto, J., Paajanen, A., Tusa, E., Yarnell, P., React. Funct. Poly., 60, 85 (2004)
4. Donald, I. W., Metcalfe, B. L., Taylor, R. N. J., J. Mat. Sci., 32, 5851 (1997)
5. Marples, J. A. C., J. Mat. Sci., 29, 230 (1988)
6. Lutze, W., Ewing, R. C., J. Mat. Sci., 32, 699 (1997)
7. Half-Life measurements of Radionuclides, NIST Website, Accessed on 01/07/2014 <http://www.nist.gov/pml/data/half-life.html.cfm>
8. Koukoulidou, V., In NATO Science for Peace and Security Series C: Environmental Security; Springer, Netherlands: Vienna, Austria, 3 (2010)
9. DeMuth, S., Remdtn. Win. John Wiley & Sons, Inc.(1999)
10. Dyer, A. Keir. D., Zeolites, 4, 215 (1984)
11. Dyer, A., Aboujamous, J. K., J. Radioanal. Nucl. Chem., 183, 225 (1994)
12. Gerontopoulos, P., Arcangeli, G., Fava, R., Traverso, D.M., Nuclear Science and Technology, Comm. Eur. Comm. Report (1988)
13. Clearfield, A., Stynes, J. A., J. Inorg. Nucl. Chem., 26, 117 (1964)
14. Clearfield, A., Bortun, L. N., Bortun, A. I., React. Funct. Polym., 43, 85 (2000)
15. Clearfield, A., Nancollas, G. H., Blessing, R. H., In Ion Exchange and Solvent Extraction; Marcus, Y., SenGupta, A. K., Marinsky, J. A., Ed.; Dekker: New York, 5 (1973)
16. Kraus, K. A., Phillips, H. O., Carlson, T. A., Johnson, J. S., In Proc. Int. Conf. Peaceful Uses At. Energy: 2nd, Geneva, 15 (1985)
17. Santamaria Gonzalez, J., Martinez Lara, M., Banares, M. A., Martinez-Huerta, M. V., Rodriguez-Castellon, E., Fierro, J. L. G., Jimenez Lopez, A., J. Cat., 181, 280 (1999)
18. Farfan-Torres, E. M., Sham, E. L., Martinez-Lara, M., Jimenez-Lopez, A., Mat. Res. Bull., 27, 1255 (1992)
19. Alberti, G., Costantino, U., Allulli, S., Tomassini, N., J. Inorg. Nucl. Chem., 40, 1113 (1978)
20. Alberti, G., Cardini-Galli, P., Costantino, U., Torracca, E., J. Inorg. Nucl. Chem., 29, 571 (1967)
21. Merz, E., Z. Electrochem., 63, 288 (1959)

22. Bruque, S., Aranda, M. A. G., Losilla, E. R., Olivera-Pastor, P., Maireles-Torres, P., *Inorg. Chem.*, 34, 893 (1995)
23. Costantino, U., Gasperoni, A., *J. Chromatog.*, 51, 289 (1970)
24. Patrono, P., La Ginestra, A., Ferragina, C., Massucci, M. A., Frezza, A., Vecchio, S., *J. Therm. Anal.*, 38, 2603 (1992)
25. Peters, L., Evans, J. S. O., *J. Solid State Chem.*, 180, 2363 (2007)
26. Alberti, G., Torracca, E., *J. Inorg. Nuc. Chem.*, 31, 1189 (1969)
27. Clearfield, A., Kullberg, L., Oskarsson, A., *J. Phys. Chem.*, 78, 1150 (1974)
28. Hodson, L.F., & Whittaker, D., *Chem. Commun.*, 2131 (1996)
29. Trobajo, C., Khainakov, S.A., Espina, A., Garcia, J.R., *Chem. Mat.*, 12, 1787 (2000)
30. Andersen, A.M.K., Norby, P., Hanson, J.C., Vogt, T., *J. Inorg. Chem*, 37, 876 (1998)
31. Yuan, C., Hong-juan, W., Zhi-ning, X., *Trans. Nonferrous Met. Soc. China* 19, s656 (2009)
32. Panda, A.B., Sinhamahapatra, A., Sutradhar, N., Roy, B., Pal, P., Bajaj, H.C., *Apld. Catys. B: Envntl.*, 103, 379 (2011)
33. Naik, A.H., Deb, S.B., Chalke, A.B., Saxena, M.K., Ramakumar, L.L., Venugopal, V., Dharwadkar, S.R., *J. Chem. Sci.*, 122, 80 (2010)
34. Troup, J.M., Medina, A.S., Landis, A.L., Clearfield, A., *J. Inorg. Nucl. Chem.*, 35, 1099 (1973)
35. Clearfield, A., Blessing, R., Stynes, J. A., *J. Inorg. and Nucl. Chem.*, 30, 2249 (1968)
36. Alberti, G., Bernasconi, M. G., Casciola, M., *Reactive Polymers*, 11, 245 (1989)
37. Poojary, D. M., Shpeizer, B., Clearfield, A., *J. Chem. Soc., Dal. Trans.*, 111 (1995)
38. Clearfield, A., Smith, G.D., *J. Inorg. Chem.*, 8, 431 (1969)
39. Albertsson, J., Oaskarsson, A., Tellgren, R., Thomas, J.O., *J. Phys. Chem.*, 81, 1574 (1977)
40. Troup, J.M., Clearfield, A., *J. Inorg. Chem.*, 16, 3311 (1977)
41. Burnell, V.A., Readman, J.E., Tang, C.C., Parker, J.E., Thompson, S.P., Hriljac, J.A., *J. Solid State. Chem*, 183, 2196 (2010)
42. Leigh, D., Dyer, A., *J. Inorg. and Nucl. Chem.*, 34, 369 (1972)
43. Alberti, G., Costantino, U., Millini, R., Perego, G., Vivani, R., *J. of Sol. Stat. Chem.*, 113, 289 (1994)
44. Torracca, E., Galli, P., Fabiani, G.M., *J. Inorg. nucl. Chem.*, 40, 93 (1978)
45. Clearfield, A., Djuric, Z., *J. Phys. Chem.*, 41, 885 (1979)
46. Clearfield, A., Cheng, S., *J. Phys. Chem.*, 42, 1344 (1980)

47. Dyer, A., Shaheen, T., Zamin, M., *J. Mater. Chem.*, 7, 1898 (1997)
48. Zhuravlev, I., Zakutevsky, O., Psareva, T., Kanibolotsky, V., Strelko, V., Taffet, M., Gallios, G., *J. Radioanlyt. Nucl. Chem.*, 1, 87 (2002)
49. Pan, B., Zhang, Q., Du, W., Zhang, W., Pan, B., Zhang, Q., Xu, Z., Zhang, Q., *Wat. Res.*, 41, 3103 (2007)
50. Nakayama, S., Itoh, K., *J. Eur. Cer. Soc.*, 23, 1047 (2003)
51. Sun, L., Boo, W.J., Browning, R.L., Sue, H.J., Clearfield, A., *Chem. Mat.*, 17, 5606 (2005)
52. Yazawa, Y., Eguchi, T., Takaguchi, K., Tomita, I., *Bull. Chem. Soc. Jpn*, 52, 2923 (1979)
53. Tomita, I., Iwase, K., Saito, K., Sugiyama, Y., *Bull. Chem. Soc. Jpn*, 54, 749 (1981)
54. Thakkar, R., Chudasama, U., *J. Hazard. Mat.*, 172, 129 (2009)
55. Jignasa, A., Rakesh, T., Uma, C., *J. Chem. Sci.*, 118, 185 (2006)
56. Amin, J., Thakkar, R., Chudasama, U., *J. Chem. Sci.*, 118, 185 (2006)
57. Shakshooki, S. K., Naqvi, N., Kowalczyk, J., Khalil, S., Rais, M., Tarish, F., *React. Poly.*, 7, 221 (1988)
58. Frianeza, T. N., Clearfield, A., *J. Catal.*, 85, 398 (1984)
59. Shakshooki, S. K., Szirtes, L., Khalil, S., Azzabi, O., Naqvi, N., Kowalczyk, J., *J. Radio. Nucl. Chem.*, 121, 175 (1988)
60. Thakkar, R., Chudasama, U., *J. Sci. Ind. Res.*, 68, 312 (2009)
61. Yazawa, Y., Eguchi, T., Takaguchi, K., Tomita, I., *Bull. Chem. Soc. Jap.*, 52, 2923 (1979)
62. Clearfield, A., Frianeza, T. N. *J. Inorg. Nucl. Chem.* 40, 1925 (1978)
63. Hassan, Saad. S.M., Marei, S.A., Badr, I.H, Arida, H.A., *Anal. Chim. Acta*, 427, 21 (2001)
64. Khan. A.A., Paquiza. L., *Desal.* 265, 242 (2011)
65. Shakshooki, S. K., Hassan, M. B., El-Nowely, W. K., El-Belazi, A., Abed, S. M., Al-Said, M. M., *phys. Mat. Chem.*, 2, 7 (2014)
66. Galli, P., La Ginestra, A., Berardelli, M. L., Massucci, M. A., Patrono, P. *Thermo. Acta*, 92, 615 (1985).
67. Trobajo, C., Rodriguez, M. L., Suarez, M., Garcia, J. R., Rodriguez, J., Parra, J. B., Salvado, M. A., Pertierra, P., Garcia-Granda, S. *J. Mat. Res.* 13, 754 (1998).
68. Anillo, A., Rodriguez, M. L., Llavona, R., Rodriguez, J., Martinez-huerta, M. V., Banares, M. A., Fierro, J. L. G. *Inter. J. Inorg. Mat.* 2, 177 (2000).

69. Whang, D., Hur, N. H., Kim, K., *Inorg. Chem.*, 34, 3363 (1995)
70. Preetha B., Janardanan C., *J. Ind. Chem. Soc.*, 8, 1377 (2011)
71. Preetha B., Janardanan C., *Res. J. Chem. Sci.*, 4, 43 (2014)
72. Souka, N., Abdel-Gawad, A. S., R. Shabana, Farah, K., *Radiochim. Acta*, 22. 180 (1975)
73. Clearfield, A., Kalnins, J. M., *J. Inorg. Nucl. Chem*, 38. 849 (1976)
74. Alberti, G., Bernasconi, M. G., Costantino, U., Gill, J. S., *J. Chromat.*, 132. 477 (1977)
75. Peeters, K., Carleer, R., Mullens, J., Vansant, E. F., *Microporous Mater.* 4. 475 (1995)
76. Costantino, U., *J. Chem. Soc. Dalton Trans.*, 2. 402 (1979)
77. Trchova, M., Capkova, P. Matejka, P., Melanova, K., Benes, L., *J. Solid State Chem.*, 145. 1 (1999)
78. Costantino, U., Vivani, R., Zima, V., Benes, L., Melanova, K., *Langmuir*, 18. 1211 (2002)
79. Yamanaka, S., Tanaka, M., *J. Inorg. Nucl. Chem.*, 41, 45 (1979)
80. Clayden, N. J., *J. Chem. Soc., Dal. Trans.*, 1877 (1987)
81. Poojary, D. M., Zhang, B., Dong, Y., Peng, G., Clearfield, A., *J. Phy. Chem.*, 98, 13616 (1994)
82. Clearfield, A., Garces, J. M., *J. Inorg. Nucl. Chem.*, 41, 879 (1979)
83. Clearfield, A., Kalnins, J. M., *J. Inorg. Nucl. Chem.*, 40, 1933 (1978)
84. Nilchi, A., Maragheh, M. G., Khanchi, A., Farajzadeh, M. A., Aghaei, A. A., *J. Radioanal. Nucl. Chem.*, 261, 393 (2004)
85. Clearfield, A. (1977). Modified zirconium phosphates. Patent No. 4,059,679, accessed on 20th August 2014 from <https://www.legionpatent.com/patents/4059679/>
86. Andersen, A. M. K., Norby, P., *Acta Cryst.*, B56, 618-625 (2000)
87. Segawa, K.-I., Nakajima, Y., Nakata, S.-I., Asaoka, S., Takahashi, H., *J Cataly.*, 101, 81 (1986)
88. Aono, H., Sugimoto, E., Sadaoka, Y., Imanaka, N., Adachi, G., *Sol. Stat. Ion.*, 62, 309-316 (1993)
89. Losilla, E. R., Aranda, M. A. G., Martínez-Lara, M., Bruque, S., *Chem. Mater.*, 9, 1678-1685 (1997)
90. Alberti. G., *Atti. Accad. Nazl. Lincei, Rend., Classe Sci. Fis., Mat. Nat.* 31. 427 (1961)

91. Costa, M. J. N., Jeronimo. M. A. S., J. Chromatog. 5. 456 (1961)
92. Clearfield, A., Smith. G. D., J. Inorg. Nucl. Chem. 30. 327 (1968)
93. Alberti, G., Costantino, U., Pelliccioni. M., J. Inorg. Nucl. Chem. 35. 1327 (1973)
94. Alberti, G., Costantino, U., Gupta. J. P., J. Inorg. Nucl. Chem. 36. 2109 (1974)
95. Alberti, G., Costantino, U., Alluli, S., Massucci. M. A., J. Inorg. Nucl. Chem. 37. 1779 (1975)
96. Allulli, S., La Ginestra, A., Massucci, M. A., Pelliccioni, M., Tomassini. M., Inorg. Nucl. Chem. Lett. 10. 337 (1974)
97. Palmer, B. R., Fuerstenau M. C.. Proc. Int. Miner. Process. Congr., 10th. 1123 (1974)
98. Smits, R., D. L., et al. Massart. Anal. Chem. 48. 458 (1976)
99. Clearfield, A., Hunter. R. A., J. Inorg. Nucl. Chem. 38. 1085 (1976)
100. Alberti, G., Bertrami, R., Costantino, U., Gupta. J. P., J. Inorg. Nucl. Chem. 39. 1057 (1977)
101. Allulli, S., Ferragina, C., La Ginestra, A., Massucci, M. A., Tomasinni. N., J. Chem. Soc., Dalton Trans. 19. 1879 (1977)
102. Clearfield, A., Hagiwara. H., J. Inorg. Nucl. Chem. 40. 907 (1978)
103. Massucci, M. A., La Ginestra, A., Ferragina. C., Gazz. Chim. Ital. 110. 73 (1980)
104. Kullberg, L., Clearfield, A., J. Phys. Chem. 85. 1578 (1981)
105. Kullberg, L., Clearfield. A., J. Phys. Chem. 85. 1585 (1981)
106. Shaheen, T., Zamin, M., Khan. S., Main. Grou. Met. Chem. 24. 351 (2001)
107. Kim, C. H., Kim. H. S., Synth. Met. 71. 2051 (1995)
108. Y. Yuan, P., et al. Wang. Anal. Bioanal. Chem. 372. 712 (2002)
109. Yamanaka, S., Horibe, Y., Tanaka. M., J. Inorg. Nucl. Chem. 38. 323 (1976)
110. Kijima, T., Ueno, S., Goto. M., J. Chem. Soc., Dalton Trans. 2499 (1982)
111. Kijima, T., Sekikawa, Y., Ueno. S., J. Inorg. Nucl. Chem. 43. 849 (1981)
112. Kornyei, J., Szirtes, L., Costantino. U., J. Radioanal. Nucl. Chem. 89. 331 (1985)
113. Tindwa, R., Ellis, D. K., Peng, G. Z., Clearfield. A., J. Chem. Soc., Faraday Trans, Clearfield, A., Tindwa. R. M., J. Inorg. Nucl. Chem. 41. 871 (1979)
114. Costantino, U., Massucci, M. A., La Ginestra, A., Tarola, A. A., Zampa. L., J. Inclusion Phenom. 4. 147 (1986)

115. Alberti, G., Costantino, U., Marmottini, F., Perego, G., J. Inclusion phenom. Mol. Recognit. Chem. 7. 549 (1989)
116. Ferragina, C., Massucci, M. A., Mattogno, G., J. Inclusion Phenom. Mol. Recognit. Chem. 7. 529 (1989)
117. Giannoccaro, P., Nobile, C. F., Moro, G., La Ginestra, A., Ferragina, C., Massucci, M. A., Patrono, P. J., Mol. Catal. 53. 349 (1989)
118. Kumar, C. V., Tolosa, L. M., J. Phys. Chem. 97. 13914 (1993)
119. Capkovi, P., Benes, L., Melanova, K., Schenk, H., Appl Crystallog. 31. 845 (1998)
120. Kaneno, M., Yamaguchi, S., Nakayama, H., Miyakubo, K., Ueda, T., Eguchi, T., Nakamura, N., Int. J. Inorg. Mater. 1. 379 (1999)
121. RAJEH, A. O., SZIRTES, L., J. Radio. and Nucl. Chem., Art., 195, 2. 319 (1995)
122. Kotov, V., Stenina, I. A., Yaroslavtev, A. B., Solid State Ionics. 125. 55 (1999)
123. Celestian, A. J., Kubicki, J. D., Hanson, J., Clearfield, A., Parise, J. B. J., Am. Chem. Soc., 130, 11689 (2008)

CHAPTER 2: EXPERIMENTAL METHODOLOGY

2.1 Introduction

The work described in this thesis is divided into two main sections. The first section mainly deals with the synthesis of the mixed metal inorganic phosphates based on the α -zirconium phosphate (α -ZrP) using different preparation routes. The second section deals with the ion-exchange chemistry and subsequent analysis of the materials. The main characterisation techniques used for these materials include powder X-ray diffraction (XRD), X-ray fluorescence spectroscopy (XRF), scanning electron microscopy (SEM), energy dispersive X-ray analysis (EDAX), atomic absorption spectroscopy (AAS), inductively coupled plasma mass spectrometry (ICP-MS), fourier transform infra-red spectroscopy (FT-IR) and solid state nuclear magnetic resonance (SS-NMR).

2.2 Synthesis procedure

The synthesis of the metal substituted α -ZrP materials was carried out using two main synthetic routes: sol-gel and hydrothermal methods (Figure 2.1). The sol-gel method uses a similar approach as stated by Clearfield and Frianeza ^[1], where the initial metal chloride or nitrate salt solutions are mixed together in the desired stoichiometric concentrations and then precipitated in the phosphoric acid solution. The gel like product is either, dried and obtained as amorphous gel which is later refluxed in concentrated phosphoric acid (10-12 M). The hydrothermal method is used as an alternative to the reflux step for crystallisation where the gel like product is mixed with concentrated phosphoric acid (10-12 M) in Parr acid digestion autoclaves (pressure vessels) which are then placed in a hot air oven at the desired temperature for a set period of time. The use of these pressure vessels allows the synthesis mixtures to reach higher temperatures of up to 200°C under elevated pressures which allows phases to be produced at temperatures lower than those required at near ambient pressure ^[10].



Figure 2. 1 Photographs of conventional reflux set-up (left) and autoclave (right)

A third route of microwave assisted refluxing was also used in order to further reduce the reaction time however due to inconsistent pressure regulations and the small amount of sample produced, this method could not be extensively used. The most viable reaction conditions using this approach involved a power of 150 W with a pressure of 180 Pa and temperature between 150-180 °C for 14-18 hours and produced 1.5 g of the sample.

2.2.1 Synthesis of α -zirconium phosphate

The experimental procedure for synthesis of α -zirconium phosphate (α -ZrP) was based on that reported by Clearfield and Frianeza ^[1]. First, a 1 M solution of $\text{ZrOCl}_2 \cdot 8\text{H}_2\text{O}$ was prepared by dissolving 8.056 g (0.025 mol) of $\text{ZrOCl}_2 \cdot 8\text{H}_2\text{O}$ powder in 1M HCl/de-ionised water to make 25 ml of an oily solution. A crude gel was prepared by drop wise addition of this solution to 50 ml of 4 M phosphoric acid solution. This resulted in a white gel which was stirred continuously using a magnetic stirrer over night at room temperature. The crude product was then recovered using vacuum filtration and washed with copious amounts of deionised water to remove excess chloride ions. The product was then dried at 50°C for 24 hours and was obtained as a white powder (8-12 g). X-ray powder diffraction showed that this crude powder was poorly crystalline. In order to produce a crystalline product, three different methods were used:

- a. Conventional reflux: Crude zirconium phosphate was placed in a round bottom Pyrex flask and 50mL of H_3PO_4 (12 M) was added with a magnetic stirrer bar to aid stirring. Either an oil bath or heating mantle were used to heat the mixture with continuous stirring at the boiling point of the solution. The reaction was refluxed for 7 days and the product subsequently washed with 0.1M H_3PO_4 and copious de-ionised water to remove excess of acid present. It was then dried at 50°C for 24 hours in a hot air oven.
- b. Hydrothermal method: About 5 g of the zirconium phosphate was placed in a Teflon liner together with 5-10 mL of the 12 M H_3PO_4 . The pressure vessel is then securely sealed and kept in an oven at 200°C for 7 days. The product was worked up using the method described above.
- c. Microwave reflux: 2g of the zirconium phosphate was placed in a Pyrex glass vessel with 5-10 mL of 12 M H_3PO_4 . The tube is then capped and placed inside the microwave cavity.

The following parameters were used:

Microwave Power = 150 W

Temperature = $150\text{-}180^\circ\text{C}$

Pressure = 180 Pa

Time duration = 6 to 14 hours

The product was worked up using the method described above.

2.2.2 Synthesis of yttrium-zirconium phosphate

Yttrium-zirconium phosphate (Y-ZrP) was synthesised using the sol-gel method described previously as in the case of α -ZrP synthesis. The method involves preparing Zr(IV) solution using varying molar ratio (5%, 10%, 15%, 20%, 30%, and 40% Y/Zr) of $\text{ZrOCl}_2 \cdot 8\text{H}_2\text{O}$ powder in 1 M HCl/de-ionised water to make 25 ml of oily solution. A calculated amount of yttrium chloride ($\text{YCl}_3 \cdot 6\text{H}_2\text{O}$) in 1 M HCl / de-ionised water was added to produce a mixed metal chloride solution (50mL) using the quantities of zirconium and yttrium as shown in the Table 2.1 below. A crude gel was then prepared by drop wise addition of this solution to 50 ml of 4 M phosphoric acid solution and worked up in similar way as described for α -ZrP and characterised.

Table 2. 1 Quantities of reagents used for synthesis of yttrium-zirconium phosphate

Product	Moles of Zr (mol)	Volume of 1M $ZrOCl_2 \cdot 8H_2O$ (mL)	Moles of Y (mol)	Volume of 1M $YCl_3 \cdot 6H_2O$ (mL)
$Zr(HPO_4)_2 \cdot H_2O$	3.32×10^{-2}	33.20	0	0
$Y_{0.05}Zr_{0.95}(HPO_4)_2 \cdot H_2O$	2.28×10^{-2}	22.80	0.12×10^{-2}	1.20
$Y_{0.1}Zr_{0.9}(HPO_4)_2 \cdot H_2O$	2.16×10^{-2}	21.60	0.24×10^{-2}	2.40
$Y_{0.15}Zr_{0.85}(HPO_4)_2 \cdot H_2O$	2.04×10^{-2}	20.40	0.36×10^{-2}	3.60
$Y_{0.2}Zr_{0.8}(HPO_4)_2 \cdot H_2O$	1.92×10^{-2}	19.20	0.48×10^{-2}	4.80
$Y_{0.3}Zr_{0.7}(HPO_4)_2 \cdot H_2O$	1.68×10^{-2}	16.80	0.72×10^{-2}	7.20
$Y_{0.4}Zr_{0.6}(HPO_4)_2 \cdot H_2O$	1.44×10^{-2}	14.40	0.96×10^{-2}	9.60

The synthesis of two different crystalline mixed metal phosphates were attempted consisting of mixed iron-zirconium phosphate and cerium-zirconium phosphate using the same procedure described for the synthesis of yttrium-zirconium phosphate. Iron(III) chloride and cerium(III) chloride were used as the starting materials respectively. Both the products were characterised and were found to be biphasic and no further characterisation or synthesis of these materials for ion-exchange reactions were carried out. A detailed explanation of characterisation of the reaction products is provided in the forthcoming sections of this thesis.

2.3 Acid stability test

A considerable amount of work has previously been carried out on the acid stability of α -ZrP [2 - 4] so as to test its potential use in the legacy radioactive waste pools that have very low pH conditions and hence are capable of oxidising the ion exchangers which can lead to decomposition. It is therefore believed that the mixed metal α -ZrP products presented here are acid stable too, since they have the same framework as that of α -ZrP with similar crystal structure and physio-chemical properties.

In order to determine acid stability of the as synthesised phosphates, 1g of the α -ZrP product was mixed with varying concentrations of 50mL nitric acid, example with 1M and 3M HNO_3 for different periods of time (24 hours to 7 days). The suspension

was allowed to stand at room temperature without stirring. The products were filtered, washed with deionised water to remove excess acid and dried at 50°C for 24 hours and characterised using XRD and XRF in order to determine any loss of crystallinity or framework ions.

2.4 Ion-exchange

To investigate the ion-exchange chemistry of the mixed metal phosphates towards some of the cations (strontium, cobalt and caesium) commonly present in the nuclear waste pools, a systematic study was carried out. About, 125 mL solution of 0.1 M metal salt solutions were prepared in deionised water. 0.5 g of the as synthesised phosphate was added to the flask. The mixture was stirred initially overnight and further experiments were carried out with increased reaction time. It was observed that maximum exchanged was observed at 72 hours. Therefore further ion-exchange reactions were carried out for 72 hours to maximise the degree of ion-exchange. Then samples were washed with de-ionised water so as to remove the excess ions and dried at 50°C for 24 hours in an oven, ground and characterised using the methods described previously. The pH of the metal solutions was measured before and after the ion-exchange.

Exchanges using water soluble salts such as acetates, hydroxides and nitrates were carried out using single cation solutions and experiments in which the solutions contained two competing cations were also carried out. The competing metal solutions were prepared by dissolving two metal salts (acetate, hydroxide and nitrate) in de-ionised water to form 0.1M each of metal salt solutions (Table 2.2). Not only were competitive ion-exchanges carried out using the cations of interest to the nuclear industry, but to ascertain the selectivity of the materials towards these ions in the presence of common cations (Ca, Mg and Na) present in aqueous solutions.

Table 2. 2 Competitive ion-exchange scheme

<u>Competing metal ions</u>			
General	Strontium/metal	Caesium/metal	Cobalt/metal
Sr/Cs	Sr/Na	Cs/Na	Co/Na
Sr/Co	Sr/Ca	Cs/Ca	Co/Ca
Cs/Co	Sr/Mg	Cs/Mg	Co/Mg
Sr/Cs/Co			

2.5 Characterisation techniques

The properties of the materials are a consequence of the nature and location of the atoms in the structure therefore to fully understand the properties of the synthesised materials, it is important that the crystal structures should be studied.

2.5.1 X-ray Diffraction (XRD)

Powder X-ray diffraction is the principal technique for characterisation of materials. Every material has a distinct X-ray diffraction pattern which is used as a 'fingerprint' for the identification of it by easily comparing it to the known patterns present in crystallographic databases. This technique is also used extensively to determine the atomic coordinates, bond angles and bond distances of the material. The basic principle of this technique deals with the use of X-rays which have wavelengths comparable to the distances between atoms in crystals, which is approximately 1Å. These X-rays are diffracted by the electron clouds which surround the atoms. This interference of the waves which are diffracted off the planes is explained by Bragg's law which makes use of the lattice planes to explain the phenomenon. The complete derivation and in depth explanation of the law is given elsewhere ^[11, 12], but only a basic insight to the principles is presented here.

Bragg's law demonstrates the law to find the interlayer distance between two planes with the help of two parallel X-rays which are incident at an angle θ on two planes in a crystal as shown below:

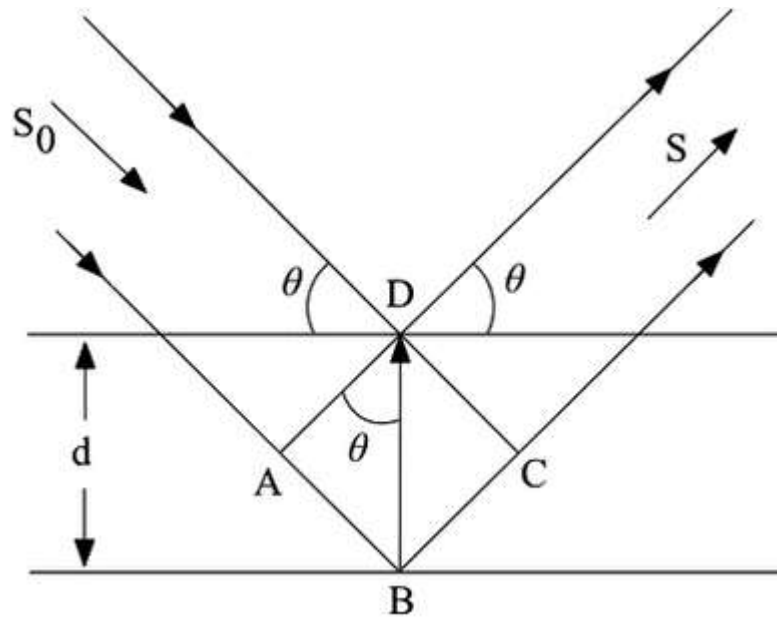


Figure 2. 2 Pictorial representation of Bragg's law description ^[5]

By using trigonometric equation to the schematic representation of the X-rays on crystal lattice, shown in figure 4,

$$\sin\theta = \frac{AB}{d} = \frac{BC}{d} \quad (1)$$

Therefore, the path difference which is present between the incident ray of first plane and that of the second ray is given by,

$$AB + BC = 2d \sin \theta \quad (2)$$

The 2 X-rays are in phase when the path difference of the scattered rays is a whole number, n , which leads to constructive interference and the formula is modified as:

$$n\lambda = 2d \sin \theta \quad (3)$$

The diffracted X-rays from the planes are then detected by the detector which produces a peak of certain intensity for every value of 2θ . But no peaks are observed from all non-integer values of ' n ' for destructive interference.

X-ray diffraction normally involves the use of a monochromatic source of X-rays which falls at an angle ' θ ' on a powdered sample that has random lattice planes.

The scattered radiation is detected by a position sensitive detector which measures the photon intensity at each angle (Figure 2.3).

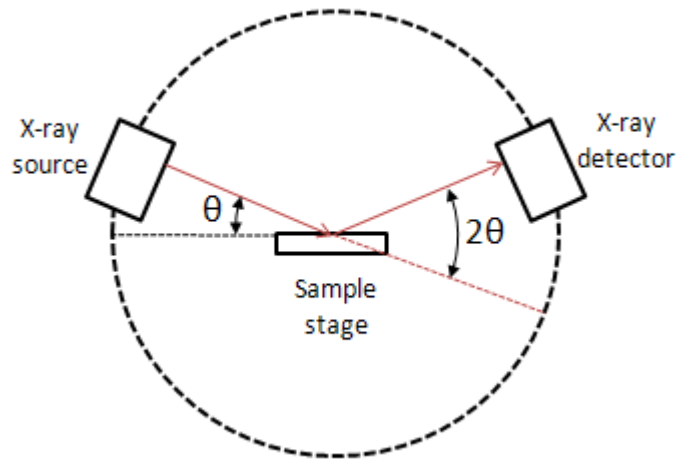


Figure 2. 3 Pictorial representation of the x-ray detection ^[13]

There are many types of detectors such as position sensitive and point detectors, which are used in X-ray diffraction, but the most common and fairly sensitive one is called a scintillation counter. This is a type of point detector which works by collecting the data at a single 2θ angle at one time when the X-rays hit the phosphorescent screen. This causes the emission of photons which are amplified and detected instantaneously. The intensity of the signal is directly related to the amount of the X-rays which hit the screen. On the other hand, position sensitive detectors collect data over a range of 2θ angles ^[13].

A diffraction pattern can be broken down into 4 main parts, each of which gives different information such as: peak shape, background noise, peak intensity and peak position. Background noise consists of instrumental noise and environmental interferences along with the sample effects such as fluorescence and incoherent scattering. Peak shape gives the information about the nature of the sample such as its grain size and crystallinity along with instrumental characteristics such as nature of incident beam. The peak position indicates the type of unit cell, space group and lattice parameters. Atomic positions and vibrations, phase fractions and preferred orientation of the planes can be extracted from the peak intensities ^[14].

The generation of X-rays in the lab based equipment uses an X-ray tube which consists of a tungsten filament that generates electrons in an evacuated space. These electrons are accelerated at about 30 KV voltage and then collide with a metal target which is typically copper or molybdenum. This incident beam of electrons then ionise the K-shell (1s orbital) electrons of the metal creating a vacancy (Figure 2.4) which is then filled by electrons from upper energy levels by emitting X-rays of characteristic wavelengths corresponding to the metal and the orbitals which are involved. In case of a copper target, the transition from 2p to 1s orbital leads to the generation of ($K\alpha$) X-rays with wavelength 1.5418 Å while transition from 3p to 1s leads to ($K\beta$) X-rays with wavelength 1.3922 Å. The most frequently observed transition is ' $K\alpha$ ' since it occurs as a doublet with $K\alpha_1 = 1.5401$ Å and $K\alpha_2 = 1.5433$ Å, and is the most common wavelength used in laboratory powder diffraction studies. The presence of a doublet is a result of slightly different energies associated with the two possible spin states of the electron in the 2p orbital [15].

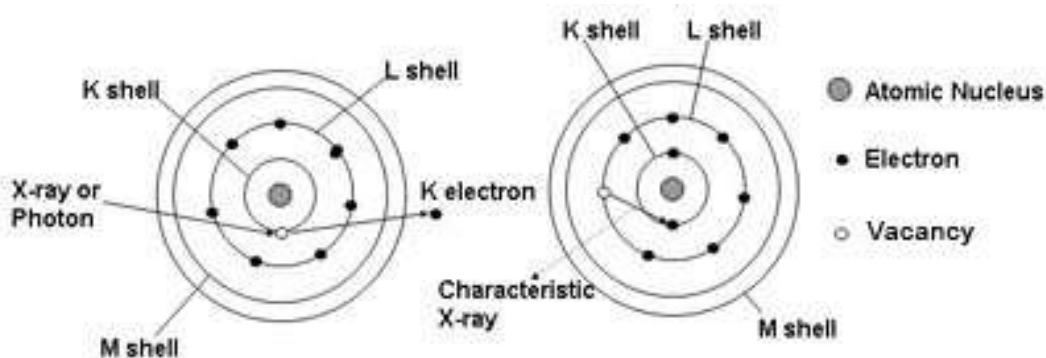


Figure 2. 4 Pictorial representation of X-rays generation mechanism [14]

Once the X-rays are generated, they travel through beryllium windows. These X-rays carry information about the metal target along with the background spectrum which is usually generated continuously due to Bremsstrahlung phenomenon (also called as 'braking radiation') of deceleration of electrons when the X-rays lose some of its energy into electromagnetic radiation. In order to minimize the background noises, a monochromatic source of X-rays is required by filtering out other wavelengths using a thin metal foil such as nickel which can effectively filter $K\beta$ component of the radiation allowing only $K\alpha$ to pass through. Crystal

monochromators can also be used for this purpose such as silicon or germanium crystals which are oriented in a particular position to allow rays of specific wavelengths to pass through using Bragg's equation ^[16].

The intensity of the diffracted X-ray is affected by some factors which are expressed as the following equation ^[17]:

$$I_{hkl} = K \times F_{hkl}^2 \times m \times A \times L \times P \quad (4)$$

Where,

K = Proportionality constant

m = Factor of multiplicity: It explains the total planes which contribute towards the same Bragg peak.

A = Absorption factor: It explains the amount of incident and diffracted rays which are absorbed by the sample and depends on the thickness of the sample, its composition and the diffraction angle used.

L = Lorentz factor: It explains the correction of diffractometer's geometry for varying the intensity of the rays in relation to the angle of diffraction.

P = Polarisation factor: it explains the polarisation of the X-ray beam so that it is strongly interacted with the sample by aligning the electric field vector of the rays parallel or anti-parallel to the sample.

F_{hkl} = Structure factor: It is one of the most important elements which affect the intensity of the peaks in a diffraction pattern. It in turn consists of a complicated mathematical expression that takes into account various factors such as atomic scattering factor, site occupancy of the atoms and fractional co-ordinates (x, y, z) for a particular reflection (h, k, l). An important component of the structure factor is the Debye-waller factor which takes into account the effect of temperature on the intensity of the Bragg peaks. It is a complex term which is expressed as the following equation ^[18]:

$$f_T = f \exp(-B \sin^2 \theta / \lambda^2) \quad (5)$$

Temperature effects differ from one atom to another in the structure since all the atoms are vibrating at some temperature and are not stationary as assumed classically. As the scattering angle (2θ) is increased, the destructive interferences also increase between the scattered X-rays from electron cloud. This leads to atomic scattering factor (f) which can cause the relative electron cloud broadening. In the above equation 5, the term B is called as the Debye-waller factor and is given by $B = 8\pi^2 u_{rms}^2$ which increases with temperature. Therefore as the structure factor is influenced by the Debye-waller factor which in turn is affected by the change in temperature of each atom, it causes relative changes in the intensity of the diffraction peaks. Simple multiplier methods often ignore this factor as it causes some systematic errors and distorts the intensities at higher 2θ values, but during refinement processes this factor is considered to list out missing intensities from the diffraction peaks, for example in Pair distribution function (PDF) analysis, as it carries some valuable information about the crystal lattice which might be of interest to the researchers.

Therefore, a complete structure factor equation including the Debye-waller factor is given by ^[18]:

$$\mathbf{F(S)} = \sum_n \mathbf{f_n N_n \exp\{2\pi i (hx + ky + lz)\} \exp(-B \sin^2\theta / \lambda^2)} \quad (6)$$

In this study, the powder diffraction patterns were recorded using a Bruker D2 Phaser diffractometer (Figure 2.5), The X-ray source is a copper tube with $K\alpha_1 = 1.54060 \text{ \AA}$ and $K\alpha_2 = 1.54439 \text{ \AA}$. A rotation of 30 rpm with a 2θ range between 5° to 80° was set. The DIFFRAC.SUITETM software ^[6] was set to Si PSD detector with the system operating at 30 kV and 10 mA using Ni-filtered Cu- $K\alpha$ radiation. The instrument parameters are listed below in the table 2.3.

Table 2. 3 Instrument parameter settings for D2 Phaser diffractometer [24]

INSTRUMENT PARAMETER	VALUE
Radiation Anode	Cu ($\text{Cu}_{\text{K}\alpha 1} = 1.5406 \text{ \AA}$)
Generator Settings	30kV, 10mA
Divergence slit	0.6mm
Axial Soller Slit Module	Primary 2.5mm, Secondary 2.5mm
Anti scatter screen	1.0 mm
Monochromatisation	0.5 Ni filter
Rotation	30 rpm
Scan type	Locked Coupled (Coupled θ - θ scan)
2θ range	Start 5.001855° , finish 80.001855° , increment 0.02019°
Time per step (s)	0.200 s

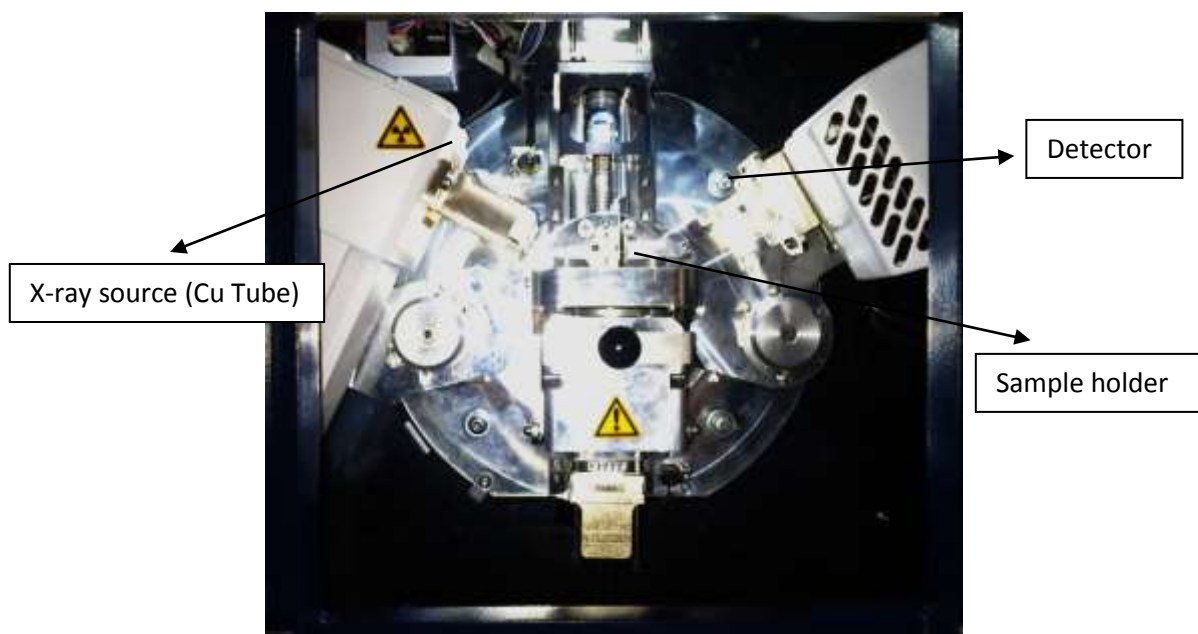


Figure 2. 5 Photograph of Bruker D2 Phaser Diffractometer used in this work

2.5.2 X-ray fluorescence (XRF) spectroscopy

XRF is an emission based technique which can provide reliable qualitative and quantitative data analysis for almost all inorganic materials. In this technique high energy X-rays bombard the sample which causes the ejection of the electrons from the core shells (K shell and L shell) to create vacancies or 'holes' which are subsequently filled by high energy electrons and the excess energy (i.e the energy difference between the two shells) is released as photons with energy in the X-ray region of the electromagnetic spectrum.

X-ray tubes as discussed earlier are the most widely used source for the generation of X-rays and for XRF measurements, the use of a high spectral throughput tube with a low electron back scatter is therefore a must requirement. Rhodium tubes are most widely used in XRF spectrometers as they provide a high spectral output and the electron back scatter is also moderate. ^[19] The fluorescence process itself is very inefficient as the radiation is much weaker than the primary beam therefore a collimator is used to improve the resolution by using scintillation detectors and gas filled proportional counters that has a metal tube filled with a readily ionisable gas which generates positive ions that travel to the cathode and the electrons move to the anode that creates a current proportional to the energy of the photon ionising the gas. This current is then converted to voltage and plotted on the x-axis on the XRF spectrum and represents the energy associated with each element.

Sometimes the atom returns to a stable state by using the emitted X-ray to reorganise the electrons in it and may knock out the electron from an outer shell and hence leads to the production of lower number of photons. This effect is termed as the 'Auger effect' ^[7] and is generally obtained in elements with low atomic number because the characteristic X-rays are more quickly absorbed as the electrons are loosely bound.

Unwanted errors in XRF spectrum is caused by two main phenomena: physical effects and elemental interactions. Physical effects include sample compositions, homogeneity, particle size and other surface orientations. To overcome this type of matrix effect, it is important to prepare a homogenous sample with uniform dispersion which can be achieved with the help of fused beads methods. Elemental interactions involves matrix effects generated due to the composition of the sample

such that the presence of an element in the matrix can scatter or absorb the fluorescence rays from another element of interest thus significantly reducing the number of photons reaching the detector. In a typical XRF spectrum there are multiple peaks which have different intensities and each peak can represent exclusively towards an element with a particular atomic number ^[20].

In this work, a Bruker TRACER IV-SD was used to acquire the XRF spectra. It is a hand-held XRF spectrometer and uses a rhodium tube to generate the X-rays to provide a qualitative and semi-quantitative analysis. The samples are in powdered form and are placed in sample holder with a Mylar film TF-125 with gauge thickness of 2.5 μ (0.10 mil) and dimensions of 3" x 300' (76mm x 91.4m). Data were acquired using the following parameters: 25.00 kV, 35 μ A and 10 seconds acquisition time. Qualitative analysis is possible for aluminium and other elements above in the periodic table along with a semi-quantitative analysis if careful calibration is carried out to compensate for the matrix effects as discussed above.

2.5.3 Scanning electron microscopy (SEM)

SEM works on the principle of surface scanning by using a high-energy focussed beam of electrons on solid samples to provide information about the particle composition, orientation of the elements and their external morphology (texture). Ideally, SEM can scan surface areas from 1cm to nanometer ranges with magnification of 20X to 50,000X and spatial resolution of 50 to 100nm ^[25]. Generally it is a 'non-destructive' technique since the electrons which are generated by the high energy beam do not lead to the loss of volume of the sample so the same sample can be analysed over and over again, except for some samples which can react in the beam and can be destroyed such as microporous silicates and phosphates. The beam of electrons interacts with the sample to produce secondary electrons, backscattered electrons and characteristic X-rays (the former two is used for providing images). A series of electromagnetic lenses are used in the SEM column to focus the electron into a small beam. These beams are then placed and positioned onto the sample surface with the help of scanning coils. One or more detectors can be used to collect the signals generated by these electrons which are then interpreted as 2-dimensional images on the computer screen (Figure 2.6).

The resolution of the images is the ability of the microscope to distinguish clearly between two closely spaced points in micron range. The resolution of the SEM depends on many factors such as interaction of the electron beam with the oriented sample, electron spot size, type of detector and magnification. The use of an Energy Dispersive X-ray Analyser (EDX) is often coupled with the SEM to provide the qualitative and quantitative information about the sample composition by scanning user specific areas of the sample under focus. The principle is based on the Auger effect as explained previously and utilises the energy of the Auger electrons to calculate the binding energy of the electrons which is specific for all the elements of the periodic table and hence provides a spectrum of peaks denoting possible elements which are present in the sample [26].

The FEI Quanta™ 200 SEM is used in this work to provide information about the sample morphology along with the EDX analysis for determining the elemental composition of the sample. It accommodates a sample size of approximately 80mm in depth and 200mm in diameter with a scanning area of 10mm x 10mm to 1µm x 1µm. The detection limit of this model is 100-0.1% on weight basis providing a resolution from few mm to nearly 50nm. The samples were placed on a sample stub with a sticky carbon tab to which the powder sample adheres. The sample was then coated using gold for enhancing the conductivity of the sample and minimising the ‘charging’ effects. An accelerating voltage of 20 kV was used at a vacuum pressure of $\sim 10^{-6}$ torr.

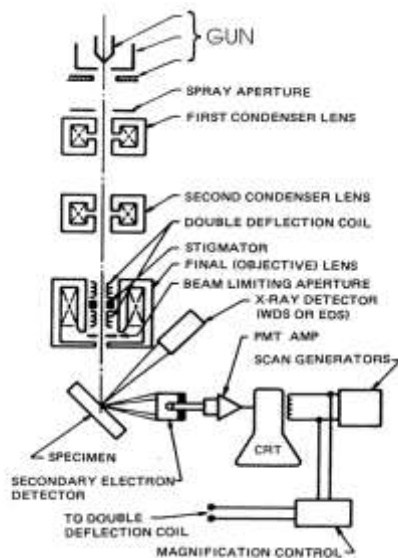


Figure 2. 6 Schematic diagram of working of scanning electron microscope [26]

2.5.4 Physical-adsorption study using BET

Brunauer-Emmett-Teller (BET) surface area adsorption studies are used to determine the surface area of the solids by using the multilayer physical adsorption of gas molecules on to the solid surface of the sample. It is an extended version of the Langmuir theory which can only be used when monolayer coverage occurs. The simplified mathematical expression ^[8] for the BET surface area calculations are as follows:

$$\frac{1}{V\left[\left(\frac{P_0}{P}\right)-1\right]} = \frac{C-1}{V_m C} \left(\frac{P}{P_0}\right) + \frac{1}{V_m C} \quad (7)$$

Where,

P = Equilibrium pressure of adsorbate at the temperature of adsorption

P₀ = Saturation pressure of adsorbate at the temperature of adsorption

V_m = Quantity of gas adsorbed at the monolayer in mL

V = Quantity of the gas adsorbed at STP in mL

C = BET constant given by $C = e^{\frac{E_1 - E_L}{RT}}$ where E₁ is heat of adsorption of first layer and E_L is the heat of adsorption for second and third layers.

The surface area of the sample is then calculated by using the correlation:

$$\mathbf{S_{total}} = \frac{V_m N s}{V a} \quad (8)$$

Where,

S_{total} = Total surface area

N = Avogadro's Number

s = Adsorption cross-section of sample

a = mass of the solid powder

In this work, the surface area measurements were carried out using a Micrometrics ASAP 2010 BET (Figure 2.7) which was operated in two step process of degassing and nitrogen adsorption. About 0.1g of the sample was weight and placed in a glass sample holder and placed under vacuum at about 150°C for approximately 4 hours. It was left overnight preferentially to allow the removal of complete moisture from the sample. In the second step, the vacuum dried sample was exposed to nitrogen at varying pressures to allow the absorption and desorption of nitrogen from the solid surface. The surface area in m^2/g and porosity of the sample could be calculated from the results obtained.

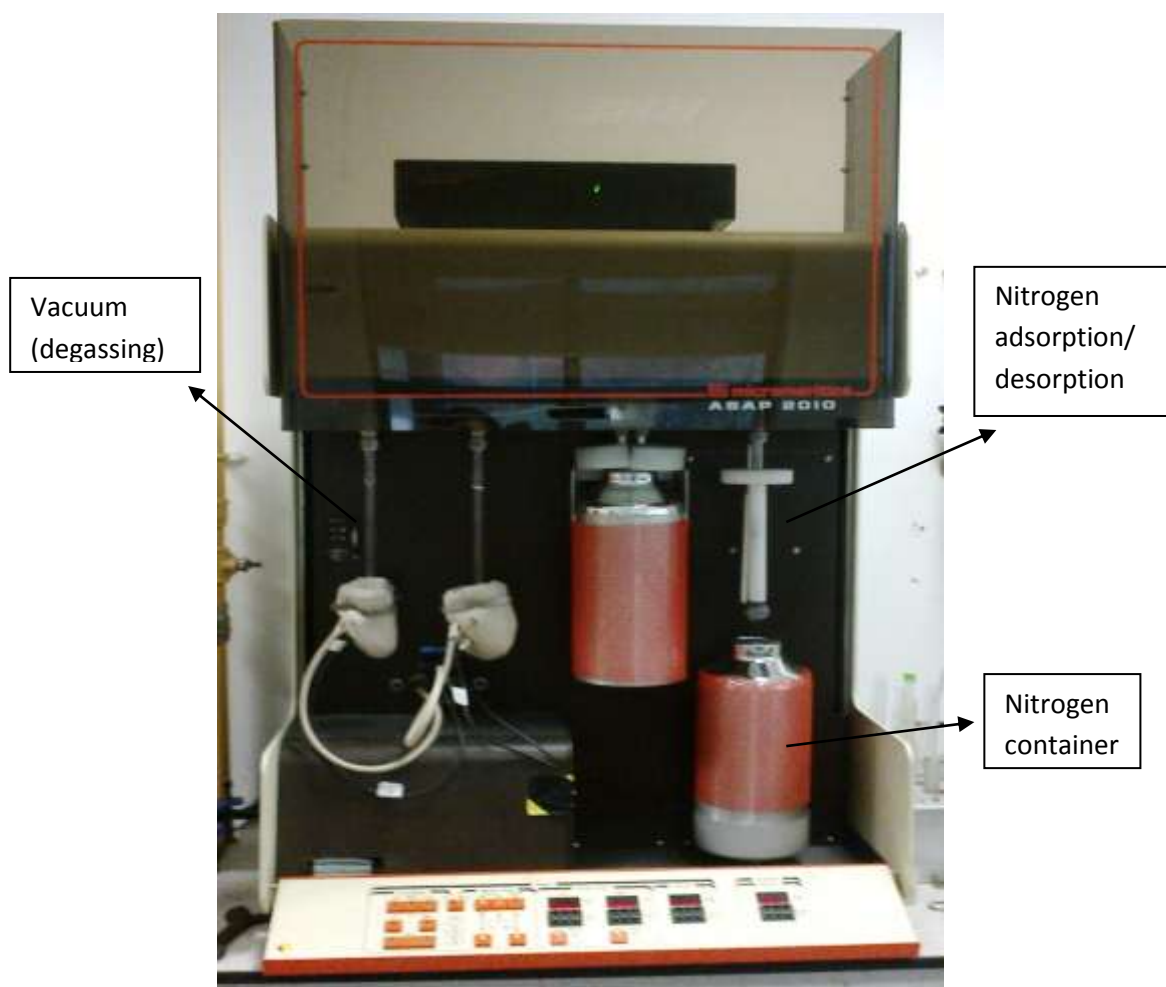


Figure 2.7 Photograph of Micrometrics ASAP 2010 used in this work

2.5.5 *Fourier transform infrared spectroscopy (FT-IR)*

FT-IR is a useful analytical technique which has been extensively used for over seventy years since it was first discovered. An FT-IR spectrum shows the characteristic and unique 'fingerprint' of a sample with the absorption / transmittance peaks which correspond to the vibration frequencies generated by the vibration of the atomic bonds present in the sample. As each material is uniquely different in the perspective of chemical composition and structure, there will be differences in the stretching and bending frequencies, thus producing a unique FT-IR spectrum for each sample ^[21]. FT-IR is used mainly as a qualitative technique to provide a screening or identification of the samples but the intensity of the peaks in the FT-IR spectrum can also indicate quantitative estimation about the amount components which is present in the sample. It is usually a non-destructive technique which can provide accurate identifications and quantification without using prior external calibration standards, except in case of complex sample preparations. It is very sensitive and very quick as a normal scan will take place over a period of few seconds. The working mechanism of the spectrometer is quite simple (figure 2.8) as it employs the use of an infrared emitting source which passes a beam of infrared radiation through an aperture which controls the emitted energy to the sample that enters the interferometer where the 'spectral encoding' takes place and the beam is split to allow it to reach the sample at slightly different times and transmitted or absorbed frequencies are then detected by the detector that measures the interferogram signal and sends to a computer process by Fourier transform ^[22].

In this work, FT-IR was used mainly to study the phosphorus groups and type of bonding present in the samples. A small amount of the sample (~0.1mg) was ground with spectroscopic grade potassium bromide (~1g) to attain a homogenous mixture which was then compressed into thin pellets using a force of approximately 8 tons under vacuum. Another method, attenuated total reflectance can also be carried out using diamond crystal cell onto which the sample is placed and compressed to ensure uniform contact. The resulting spectrum was recorded on a Thermo NICOLET IR200 spectrometer for the wavenumbers between 3800 cm^{-1} and 400 cm^{-1} using the settings for automated background noise cancellation for a total of 16 scans.

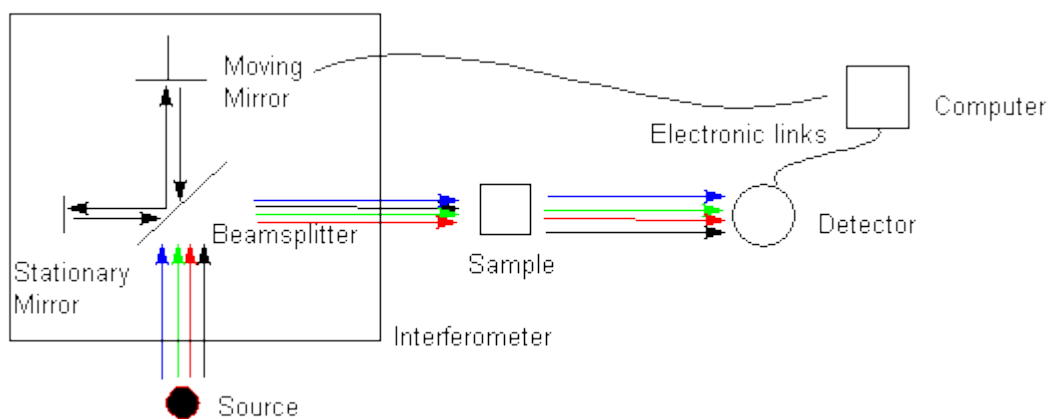


Figure 2. 8 Schematic diagram for FT-IR spectroscopy [22]

2.5.6 Solid state nuclear magnetic resonance (MAS-NMR)

Nuclear magnetic resonance (NMR) is one of the most extensively used techniques for the study of both organic and inorganic samples. It works on the principle of nuclear absorption and emission of electromagnetic radiation in the presence of magnetic field by all isotopes consisting of odd number of protons and/or neutrons [9]. This occurs at a specific resonant frequency which is dependent on the atomic isotopes present and the strength of the applied magnetic field. The presence of a non-zero spin state allows the generation of strong magnetic moment and angular momentum which leads to the polarization or alignment of the magnetic nuclear spins parallel or anti-parallel to the constant magnetic field when a radiofrequency pulse is applied. The total magnetisation of the nuclear spins and a nucleus in the higher energy will generate a magnetic field anti-parallel to that of the external magnetic field while a nucleus in the lower energy spin will create a magnetic field parallel to it causing a spin state splitting as shown in the Figure 2.9 below. The energy transfer occurs at specific wavelength and when the spins returns to its base level, energy is emitted at same frequency and the signal is generated which can be processed in terms of resonant frequency or chemical shift. The concept of chemical shift takes into account the nuclear shielding of the magnetic field as the differences in the electron cloud surrounding the atom of interest can prevent the total applied magnetic field acting on the nucleus which causes a shift in the peaks by few ppm. Therefore, the differences in the chemical environment can be resolved.

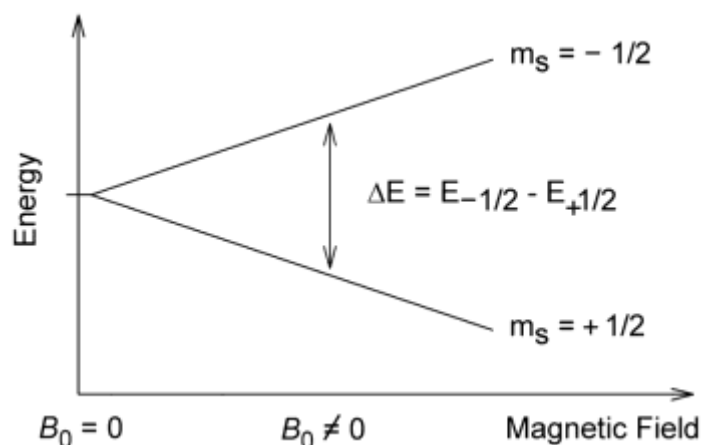


Figure 2. 9 Schematic representation of spin state splitting ^[23]

Splitting of spin states can often provide additional information about the chemical environment of the sample as it results from the magnetic effect of nuclei close enough in space to interact. For example in a proton NMR, a spin – spin splitting occurs when a peak from one or more equivalent hydrogen nuclei is split into two to produce a doublet because of the presence of one hydrogen on the adjacent carbon. Similarly a triplet is formed when the peak is split into 3 parts due to the two adjacent hydrogen atoms which are chemically equivalent. This phenomenon is more complex in the solid state NMR since the molecules are very rigidly held so even if the sample is very finely grounded, the fixed orientation of the samples will produce individual dipolar interactions between the corresponding atoms. This will cause them to flip and will in turn take several minutes to return to their original or ground state. This will produce line broadening that causes broad peaks for the solids as opposed to very fine and narrow peaks observed in more loosely held liquid samples. But certain practices such as dipolar decoupling, cross polarization and magic angle spinning (MAS) can cause the solid molecules to behave like that of a solution and hence help in reducing the line broadening ^[23].

In MAS-NMR the solid sample is spun at high frequencies (generally 4 - 7 kHz or even up to 35 kHz) at an angle of $\sim 54.74^\circ$ which is often referred to as the 'Magic Angle'. This minimises chemical shift anisotropy and dipolar coupling resulting in narrower peak shapes.

In this work, phosphorus MAS-NMR experiments were carried out on Bruker Advance II+ 400 MHz spectrometer with ammonium phosphate and 85% phosphoric acid as the shift reference. All ^{31}P experiments were performed using a 4 mm zirconia rotor in which the samples were packed. A single pulse excitation with a spinning speed of 6 kHz and 7 kHz and a recycle delay of 0.3 s were used. All spectra are recorded at room temperature. A ^{31}P 90° pulse of 6.0 ms and an attenuation level (PL1) of 8.60 dB was used with total number of scans of 512 and time domain of 2080 data points.

2.5.7 Inductively coupled plasma mass spectrometry (ICP-MS)

ICP-MS is an analytical technique which can detect a wide range of metals and non-metals at very low concentrations, close to parts per trillion in solutions. The technique involves ionising the sample by using heated plasma. In the majority of spectrometers, argon at a temperature of tens of thousands of Kelvin is used as source for plasma. When the sample is in contact with the plasma, it evaporates immediately and breaks down into individual atoms and the loosely bound electrons are subsequently lost which leads to the formation of charged ions (usually monovalent ions). These ions are then detected by mass spectrometer which separates the ions based on their mass to charge ratio.

In this work, ICP-MS was used as a complimentary technique to determine the extent of ion-exchange. The filtrate from the ion-exchange experiments were analysed for multi-ion quantification using the X-Series ICP-MS with the following parameters listed in table 2.4 below.

Table 2. 4 ICP-MS parameters

Parameters	Value
R _f power	1400W
Plasma gas flow rate	141/min
Nebulizer gas flow rate	0.81/min
Auxiliary gas flow rate	0.95/min
Sample introduction rate	11/min
Pole Bias	-3.1 V
Hexapole Bias	4.5 V
Extraction	-118 V
Focus	3 V
Analogue detector	2500 V
PC detector	3850 V
CCT gas (H ₂ :He) flow rate (7% H ₂ + 93% He)	5.9 ml/min
Integration time	0.1s
Stabilization time	35s
Sample pump tube (white/white)	1.02

2.5.8 Particle size measurement

The particle size measurement is a powerful technique that uses a laser diffractometer to measure the particle sizes of wide range of materials by dispersing it in a suitable solvent at appropriate concentration. It allows both wet and dry measurements for different type of materials such as pharmaceutical, coatings and building materials where the particle sizes may get affected due to hydration. There are three basic elements of a laser diffractometer, as shown in the figure below. The optical bench carries the dispersed sample across the measurement cell where the particles are illuminated by a laser beam (Figure 2.10). The intensity of the scattered light from the particles is then measured accurately using a series of detectors over a range of angles. The dispersion of sediments to ensure the delivery of particles to the measurement cell of the optical bench is carried out by sample dispersion

accessory. Finally, the software analyses the particle size distribution using the scattering data and controlling the measurement system. [34]

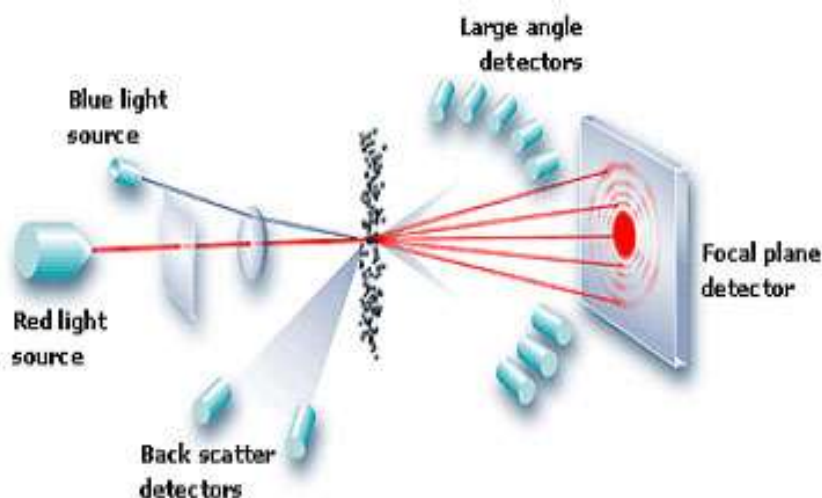


Figure 2. 10 Schematic diagram for a mechanism of laser diffractometer [34]

In this work, Malvern Mastersizer 2000 laser diffractometer with a HYDRO 2000SM pump is used. Samples of mixed metal phosphates were dispersed in water (0.05 g in 25 ml). Two light sources are used by the laser diffractometer, a red He-Ne laser at $0.632 \mu\text{m}$ and a blue LED laser at $0.466 \mu\text{m}$. A total of 52 sensors are used to measure the diffracted light from low angle laser light scattering and stored in 100 size fraction bins. Approximately 1000 measurements are taken per second and the particle sizes are reported as an average of the three laser diffraction runs successively.

2.6 Rietveld refinement

Rietveld refinement [28] is one of the most widely applied techniques for the 'whole-pattern fitting structural refinement' of the crystal data which is obtained from the diffraction studies. The Rietveld method [29] makes use of the least squares refinement approach to obtain a best fit between the entire calculated pattern and the observed powdered diffraction pattern. A structural model describing the unit cell shape and size along with the atomic positions, thermal parameters and occupancies of the atoms is used to generate a powder diffraction pattern. Also required are experimental parameters to describe the peak shapes and background.

The calculated pattern is compared to the observed pattern and various parameters are altered to obtain a good match between the two.

The calculated intensities of the peak, y_{ci} are calculated by using the structure factor equation along with the background factor, y_{bi} and is shown as follow:

$$y_{ci} = S \sum_K L_k |F_k|^2 \phi(2\theta_i - 2\theta_K) P_K A + y_{bi} \quad (9)$$

Where,

S = scale factor

K = miller indices (hkl) for a Bragg reflection

L_K = Lorentz, multiplicity and polarisation factors

F_K = structure factor for K^{th} Bragg reflection

ϕ = reflection profile function

θ_i = it is the 2θ position of the i^{th} diffraction point

θ_K = it is the calculated 2θ position of the K^{th} reflection

P_K = preferred orientation function

A = absorption factor

y_{bi} = background intensity at the i^{th} step

The application of the least squares method allows the reduction of the difference between the calculated and the observed diffraction patterns by trying to reach approximate equalisation of the y_i and y_{ci} values. This is done by consequent refinement of the different parameters which govern the y_{ci} value such as the experimental factors like zero point, absorption and background parameters and also sample specific factors like temperature factor, atomic coordinates, fractional site occupancies and lattice parameters ^[30]. All these factors are already summarised in the section 2.5.1 above. The nature of this technique demands that the initial modelling choice or the starting structural model phase should be close to the actual phase of interest.

The degree of refinement and its success can be observed from the Rietveld refinement plot, an example of which is shown below in Figure 2.11. The nature of the pattern of observed, calculated and difference plots can give an indication about the best fitting and high degree of refinement. In addition to the refinement plot, there are some mathematical terms which can provide an indication of the refinement progress such as the weighted profile R-value (R_{wp}) which is defined as the following equation:

$$R_{wp} = \left\{ \frac{\sum w_i (y_i - y_{ci})^2}{\sum w_i (y_i)^2} \right\}^{1/2} \quad (10)$$

The numerator is called as the residual (S_y) which has to be minimized so that the final R_{wp} value approaches the R_{exp} that is the statistically expected R value and is represented as follow:

$$R_{exp} = \left[\frac{N-P}{\sum_i^N w_i y_i (obs)^2} \right]^{1/2} \quad (11)$$

Where,

N is the number of observations

P is the number of parameters

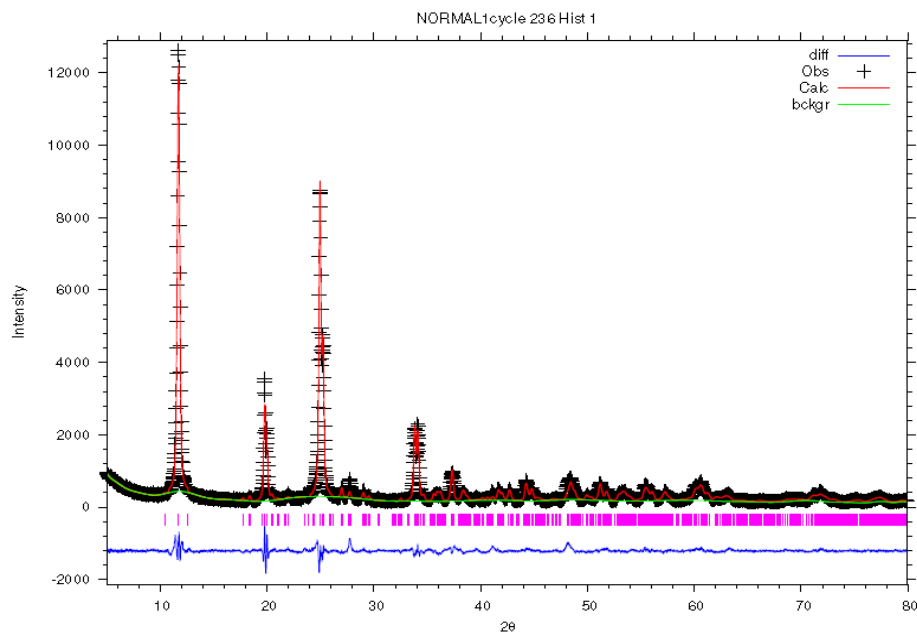


Figure 2. 11 Representation of the Rietveld refinement (achieved during this work)

The indication of a 'good fit' as explained widely in the literature is observed by the χ^2 which is the square of the ratio between the R_{wp} and R_{exp} values and is ideally desired to be 1 or as close to it as possible. The expression for this is given by:

$$\chi^2 = \left(\frac{R_{wp}}{R_{exp}}\right)^2 \quad (12)$$

Another generally used factor for structure refinement agreement is R_F^2 which is usually reported in the single crystal refinements. It is a comparison between the calculated and the observed intensity at the positions of Bragg reflections by predicting it from the unit cell of the structure model, hence it is biased towards the chosen phasic models for structural refinement. This is represented by the following equation:

$$R_F^2 = \frac{\sum |F_{obs}^2 - F_{calc}^2|}{\sum |F_{obs}^2|} \quad (13)$$

Other parameters such as the atomic bond distances, fractional occupancies and atomic bond angles are equally important for a successful refinement since it is important for the chemical model to also make sense in relation to the chemical composition of the sample. There can be certain circumstances where the numerical values and the plots which are obtained from the fit are impressive but the chemical model does not represent the actual composition of the sample. This is due to the non-model related effects which influence the numerical values of the fit, for example, R_{wp} can show higher values due to the misrepresentation of the background or when certain peaks are excluded. Also, very low values can be achieved as well due to a high well-fitted background because the intensity of the background is also significantly included by the background function ^[31]. Therefore, it is advised to consider both the numerical data and the graphical representation along with calculated structure value for defining a good structural refinement fit.

In this work, Rietveld refinements were carried out using the EXPGUI/GSAS software suite ^[32, 33] for the synthesised samples of yttrium–zirconium phosphates of varying composition and two different synthesis routes.

2.7 References

1. Clearfield, A., Frianeza, T. N. J. *Inorg. Nucl. Chem.* 40, 1925-1932 (1978)
2. Clearfield, A., Blessing, R., Stynes, J. A., *Journal of Inorganic and Nuclear Chemistry*, 30, 2249 (1968)
3. Troup, J. M., Medina, A. S., Landis, A. L., Clearfield, A., *J. Inorg. Nucl. Chem.*, 35, 1099 (1973)
4. Frianeza, T. N., Clearfield, A., *J. Catal.*, 85, 398-404 (1984)
5. Bragg, W.L. (1913). *The Diffraction of Short Electromagnetic Waves by a Crystal.* *Proceedings of the Cam. Philo. Soc.*, 17. 43
6. AXS, B. DIFFRAC.EVA, 3.0; Bruker Manual (2012)
7. Burhop, E. H. S., *The Auger Effect*; University Press: Cambridge (1952)
8. Brunauer, S., Emmett P. H., Teller, E., *J. Am. Chem. Soc.*, 60. 309 (1938)
9. J. Keeler (2005). *Understanding NMR Spectroscopy.* John Wiley & Sons.
10. Buisson, X., Arnaud. R., *J. de Phys. IV*, 04, C2-25 (1994)
11. West, A. R., *Solid State Chemistry and its Applications*; J. Wiley and sons; Chichester (1984)
12. A. K. Cheetham, P. D. *Solid State Chemistry Techniques*; Oxford University Press; Oxford (1990)
13. Jenkins, R., Snyder, R. L. (1996) *Introduction to X-ray Powder Diffractometry*, John Wiley & Sons, New York
14. Cullity B. D., (1977) *Elements of X-ray diffraction*, Addison- Wesley Publishers.
15. Rudolf P. R., Landes, B. G., *Spec.*, 9(6). 22 (1994)
16. Sulyanov, S. N., Popov A. N., Kheiker, D. M., *J. Appl. Cryst.* 27. 934 (1994)
17. Bunge H. J., Klein, H., *Z. Metallkd.* 87(6), 465 (1996)
18. Sirdeshmukh, D. B., Sirdeshmukh, L., Subhadra, K. G., *Mat. Sci.* 80. 77 (2006)
19. Glocker, R., Schrieber, H. *Ann. Physic.* 85, 1089 (1928)
20. Jenkins, R., Dale, G., Robert, W. G., *Quantitative X-ray spectrometry*, 2nd ed. *Practical Spectroscopy*, New York (1995)
21. Chatwal, G. R. Anand, S. K. *Instrumental methods of chemical analysis*, : 5th Edn, Himalaya publishing house, Mumbai, 2.50 (2004)
22. Braun, R. D. *Introduction to Instrumental Analysis, Infrared Spectroscopy*, Pharma Book Syndicate, Hyderabad: 371 (2006)

23. Malaney, M. E., "A Consumer's Guide to Archaeological Science: Analytical Techniques", Springer Science & Business Media, 470 (2010)
24. User Manual of Bruker D2 Phaser diffractometer (2012), accessed on 01/01/2015
25. Williams, T. J. (2005), Scanning electron microscopy and x-ray microanalysis, 3rd edition. By Joseph Goldstein, Dale Newbury, David Joy, Charles Lyman, Patrick Echlin, Eric Lifshin, Linda Sawyer, Joseph Michael Kluwer Academic Publishers, New York (2003)
26. Egerton, R. F. Physical Principles of Electron Microscopy: An Introduction to TEM, SEM, and AEM (2008)
27. Jones, R. H., Thomas, J. M., Huo, Q., Xu, R., Hursthouse, M. B., Chen, J, J. Chem. Soc., Chem. Commun, 1520 (1991)
28. Rietveld, H. M. Acta. Cryst. 22, 151 (1967)
29. Rietveld, H. M. J. Appl. Cryst. 2, 65-71 (1969)
30. Young, R. A. The Rietveld Method; Oxford University Press: Oxford, (2002)
31. Toby, B. R factors in Rietveld analysis: How good is good enough?, Pow. Diff., Vol. 21, No. 01., pp. 67-70 (2006)
32. Larson A.C., and Von Dreele, R.B., "General Structure Analysis System (GSAS)", Los Alam. Natinl. Lab. Rep. LAUR. 86 (2000)
33. Toby, B. H., EXPGUI, a graphical user interface for GSAS, J. Appl. Cryst. 34, 210-213 (2001).
34. Malvern Mastersizer Manual, MAN 0101: Malvern Instruments Ltd., Issue 1.3. (1997)

CHAPTER 3: RESULTS AND DISCUSSIONS FOR SYNTHESIS AND CHARACTERISATION OF MIXED METAL PHOSPHATES

This chapter consists of the results that were obtained from the synthesis of mixed metal phosphates (Y-ZrP, Fe-ZrP and Ce-ZrP), with a detailed characterisation of the yttrium-zirconium phosphate (Y-ZrP) using analytical techniques such as XRD, XRF, SEM, TEM, FT-IR and ICP-MS, etc. A discussion of all the results is done alongside to provide a comprehensive comparison of each set of results to highlight the similarities and deviations among different sample compositions. Finally a conclusion is made from these analyses about the most successful sample types which were taken further for ion-exchange applications, whose results are discussed in the following chapters.

3.1 Synthesised alpha zirconium phosphate

The general preparation of the α -ZrP was carried out by using a similar approach to that of by Clearfield and Frianeza ^[1]. The amorphous products obtained were refluxed in concentrated phosphoric acid (12M) for a period of 7 days for the two main synthetic routes: conventional reflux method and hydrothermal (autoclave) synthesis. Another route of synthesis involving the microwave irradiation for the refluxing stage was also attempted and the obtained samples were characterised and compared with those of the standard methods used.

3.1.1 X-ray diffraction (XRD) analysis

It is well known that the crystalline α -ZrP samples can differ slightly in their characteristic XRD patterns and in their physical and chemical properties such as the particle size, surface area, morphology, etc based on the reaction conditions, methodology and even on the type of apparatus used ^[2]. The evidence of this is also observed in the Figure 3.1 that compares the four most frequently used XRD patterns by different researchers over the last few decades.

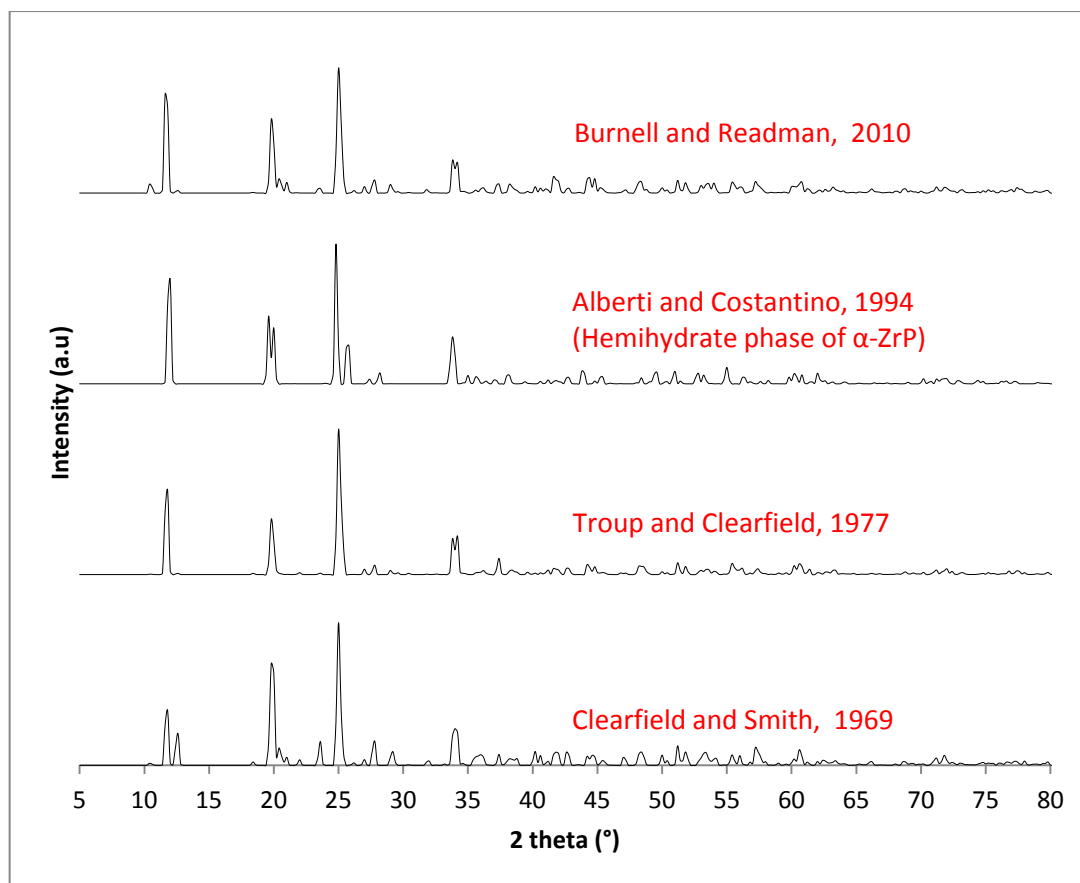


Figure 3. 1 Simulated powdered x-ray diffraction patterns of α -ZrP published by different research groups

It can be seen from the above figure that there are some slight changes in the number of peaks and relative intensities of the characteristic peaks of α -ZrP as synthesised by different researchers. For example, a couple of extra peaks are observed in the range of $2\theta = 21^\circ$ to 30° . There are some more peaks at higher 2θ ranges that differ but may be related to sample purity and other factors such as machine parameters and sample preparation. It is important to consider these differences and relate to the hypothesis that α -ZrP synthesis is governed by multiple factors, therefore there is no definite pure crystal phase with constant lattice parameters and fixed unit cell coordinates.

It can be seen here that there are 3 major characteristic peaks in the XRD pattern of α -ZrP. The first peak is at $2\theta = 11.7^\circ$ with a 002 reflection is actually a doublet but it is not evidently seen in most of the XRD patterns. It accounts for a d-spacing value of 7.56 Å. The second peak is of 110 reflection with $2\theta = 19.5^\circ$ and is again a

doublet while the third peak, also a doublet has a 112 reflection at $2\theta = 24.912^\circ$. It should be noted that there are some extra peaks that are observed in many of the synthesised α -ZrP by different researchers. For example, as seen in the α -ZrP pattern provided by Clearfield and Smith ^[3], there is an extra peak which is present at $2\theta = 12.5^\circ$ and for the α -ZrP pattern provided by Burnell and Readman ^[4], a significant peak is observed at $2\theta = 10.5^\circ$ which is normally not pronounced in other α -ZrP pattern since it has a very low signal to noise ratio. Finally, it is important to consider the similarities and differences between the hemihydrates phase of α -ZrP as provided by Alberti and Costantino ^[5] which clearly shows that it is isostructural to α -ZrP phase but has two significantly different peaks that are present at the $2\theta = 25.7^\circ$ and $2\theta = 35^\circ$ with a minor peak arising at $2\theta = 35.7^\circ$. These peaks of the hemihydrates phase of α -ZrP are important to our discussion, therefore are noted for explaining the results in the following sections.

The XRD diffraction patterns for the synthesised α -ZrP samples by all 3 synthesis routes are shown as below in Figure 3.2. The results of the synthesised α -ZrP are compared with that of reference materials from Clearfield and Smith ^[3] and Burnell and Readman ^[4] to confirm the identity. It can be seen from the XRD patterns that the synthesised α -ZrP is isostructural to that of the reference samples with all the peaks in the correct 2-theta positions.

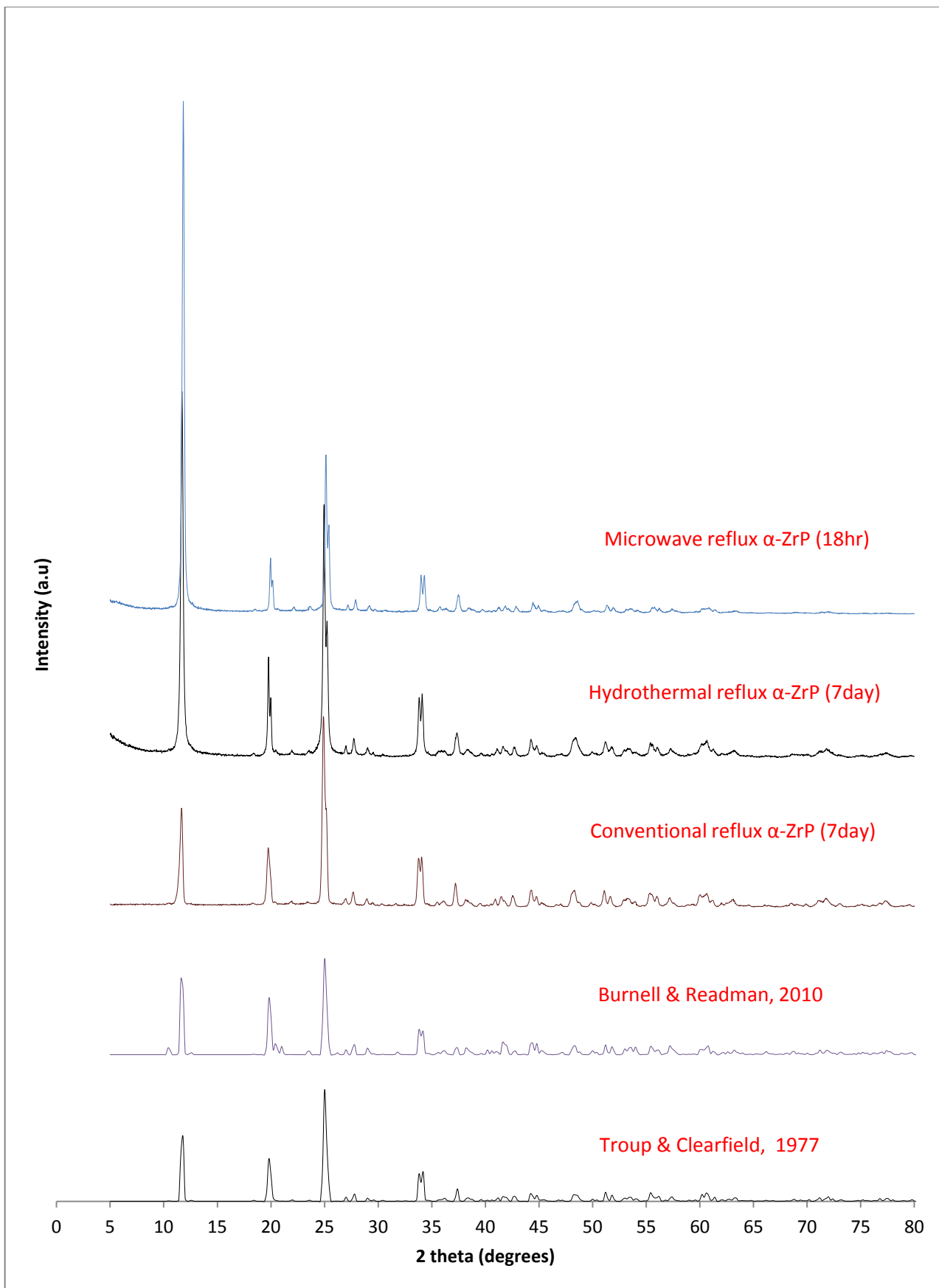


Figure 3. 2 XRD of the synthesised α -ZrP by all 3 synthesis methods

It can be seen that the synthesised α -ZrP by all the three routes of synthesis (hydrothermal, conventional and microwave reflux) is highly crystalline with sharp peaks. There is a slight change in the peak intensities among both the synthesised and reference α -ZrP with the major difference being observed in the first peak intensities (002 reflections). This is mainly due to various material preparation and instrumental factors (Structure factors) ^[6] as explained in Chapter 2. There can be other factors which are known to alter the peak intensities of known samples such as presence of mixed phases or non-uniform particle sizes ^[7] but since the synthesised and reference XRD patterns are isostructural with almost similar ratios of peak intensities, it can be assumed that there is no extra impurities or mixed amorphous phases present in the synthesised samples. However, it is reported recently by Shuai and Mejia ^[8] that the peak intensities are also affected by the concentration and amount of phosphoric acid which is used for refluxing the amorphous products for both conventional and hydrothermal methods.

Finally, it can be concluded from the XRD patterns shown in figure 2 above that crystallinity of the synthesised samples is higher for the microwave synthesised samples followed by hydrothermal and conventional refluxed samples respectively. Microwave synthesis produced a highly crystalline sample in just 18 hours as compared to the 7 day reflux time for the other two routes. Thus it is more convenient and efficient route of synthesis but it also has some limitations. The product yield is the lowest in the microwave synthesis as only 10mL samples can be used as opposed to about 20-40mL in autoclaves and about 150mL in a common Pyrex flask undergoing conventional reflux procedure. Additionally, the complexity and other technical issues arising of the sensitive microwave machine such as overheating, pressure sensor malfunction, etc can hinder the laboratory work often therefore this method was not preferred in this thesis.

3.1.2 X-ray fluorescence (XRF) analysis

The elemental composition of the synthesised α -ZrP samples are confirmed by the use of XRF analysis which confirms composition of samples as shown in the Figure 3.3 below.

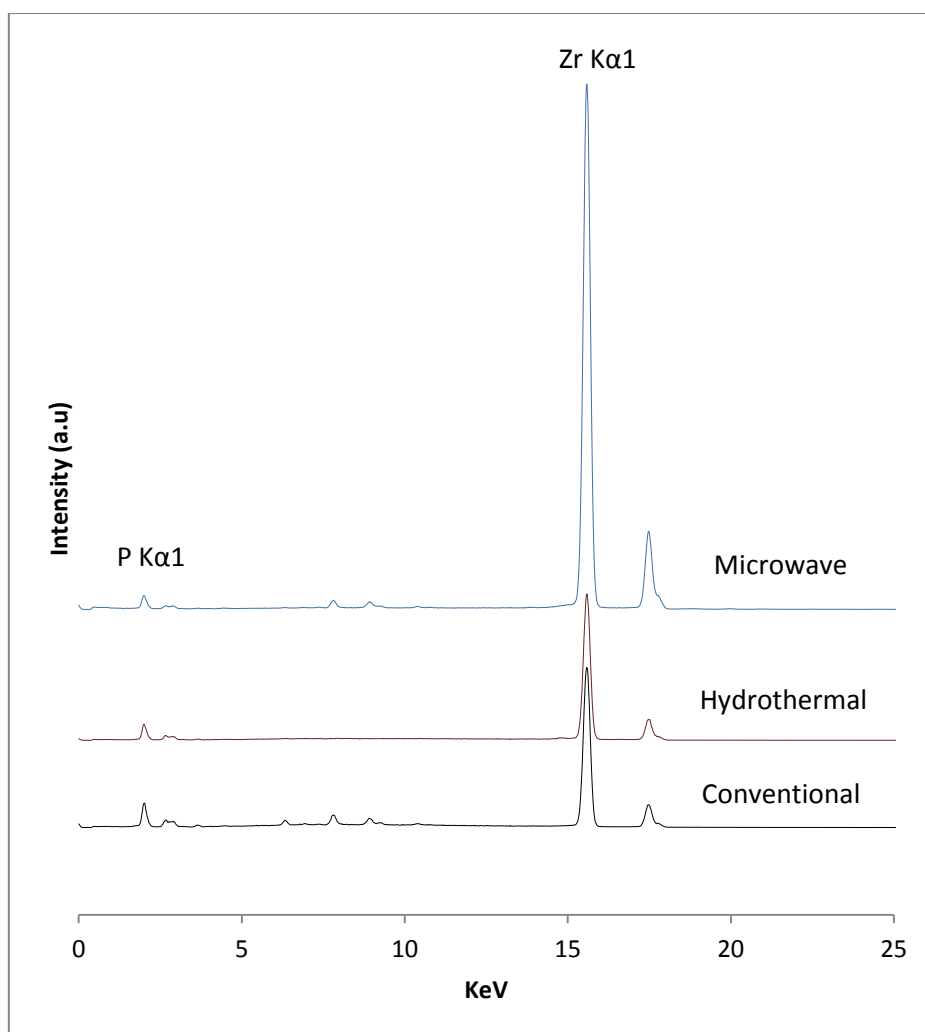


Figure 3. 3 XRF results for the α -zirconium phosphate synthesised by 3 routes

It can be seen from the above figure that the synthesised α -ZrP samples are almost pure except for the presence of a small peaks between 6 - 9 KeV which indicates the $L\alpha$ excitation for hafnium and iron impurity. The reason for this can be accounted to the use of $\geq 99\%$ pure $ZrOCl_2 \cdot 8H_2O$ chemical which is used for synthesis of α -ZrP samples. The presence of 1% impurities includes hafnium and other cations such as Mg, Co, Cr, Fe, etc. Therefore the presence of these impurities is most often associated with zirconium phosphate products. Also, there is a very minute peak observed at 2.69 KeV which is accounted for the $L\alpha$ excitation of rhodium source for x-ray tube and it is persistent in all the XRF analysis done in this research. Apart from the presence of these minute impurities, the synthesised α -ZrP samples are pure in composition otherwise.

3.1.3 Scanning electron microscopy (SEM) analysis

The sample morphology was analysed by using SEM analysis while the elemental compositional was obtained by EDX. A spot size of 3 nm with an accelerating voltage of 20 KV was used for studying the morphology of the samples while a spot size 6 nm with an approximate working distance of 10 mm was used for the EDX analysis. It was observed that the synthesised α -ZrP crystals are hexagonal shaped with a smooth surface and are arranged in a plate like morphology which is consistent with the previous findings for the α -zirconium phosphates [2, 5, 8, 9]. The crystals are approximately 1.5 μ m in length while about 1 μ m in width but it is evident from the results shown in Figure 3.4 below that there are some variations in crystal sizes. Also as suggested in the previous literature [2, 5] some crystals are arranged in a block like morphology due to the aggregation of few layers together and are therefore bound to have different particle sizes.

Individual SEM pictures of the synthesised samples from all the 3 routes are provided in figure 1 of Appendix 1.

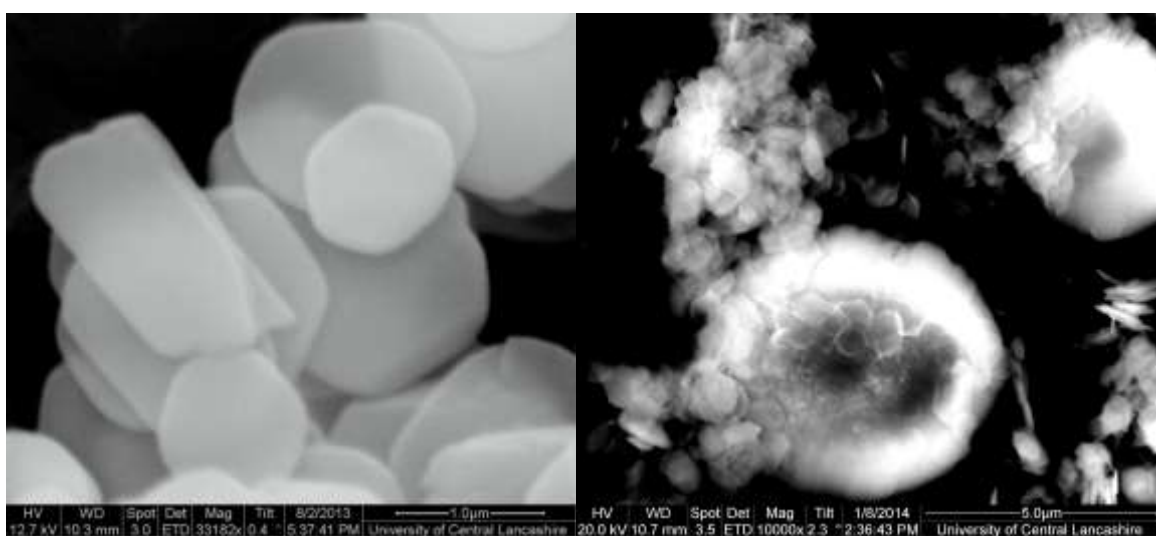


Figure 3. 4 SEM images for the synthesised α -ZrP showing plate (left) and block (right) like morphology

The elemental composition of the synthesised α -ZrP using the EDX analysis is summarised in Table 3.1 below. The estimated standard deviation (esd) errors are shown in the bracket as calculated from the 3 consecutive readings. The samples were prepared once but were scanned 3 times by focussing on alternative regions.

Table 3. 1 SEM/EDX analysis showing elemental composition of α -ZrP synthesised by different routes

Route of Synthesis	SEM/EDX Atomic %			P/Zr molar ratio
	O	P	Zr	
Conventional	84.4(1)	11.5(4)	4.10(1)	2.80(3)
Hydrothermal	76.3(5)	15.5(2)	8.2(8)	1.89(5)
Microwave	74.6(3)	17.6(2)	7.8(1)	2.25(3)
Theoretical $[\text{Zr}(\text{HPO}_4)_2 \cdot \text{H}_2\text{O}]$ ^[11]	75	16.7	8.3	2.01

It is observed here that EDX results for the synthesised α -ZrP were having some amount of error associated with it. This is due to the scatter and other factors such as instrumental errors, sample position, beam interactions and matrix effects, but the compositional ratios are comparable with that of the theoretical calculation and provide useful confirmation of the alpha phase of zirconium phosphate. An attempt was made to calibrate the SEM with the individual metal oxides and mono sodium phosphates, but the results obtained showed a high standard deviation from the theoretical weight percent. Therefore additional quantitative techniques were used to determine the elemental composition of the samples.

3.1.4 Mastersizer analysis

The particle size of the synthesised α -ZrP was analysed by using Mastersizer 2000SM which provides a quick result showing the average particle size and polydispersity index of the particles. The results shown in Table 3.2 below summarises the particle size information for the synthesised α -ZrP via 3 routes along with the particle size distribution graphs shown in Figure 3.5.

Table 3. 2 Summary of average particle size analysis using Mastersizer 2000SM for α -ZrP synthesised by different routes

Parameters	Route of Synthesis		
	Conventional reflux	Hydrothermal	Microwave
Obscuration	2.35(1) %	2.11(1) %	3.98(1) %
Span	2.839(3)	1.557(1)	1.413(1)
Uniformity	0.85(1)	0.647(1)	0.915(4)
Specific surface area (m ² /g)	0.97(2)	1.51(1)	1.64(1)
Surface weighted mean D[3,2]	6.188(1) μ m	3.972(1) μ m	3.179(3) μ m
Volume weighted mean D[4,3]	11.664(4) μ m	5.861(2) μ m	5.174(2) μ m
D(0.1)	2.7(2) μ m	2.33(1) μ m	2.446(1) μ m
D(0.5)	8.239(1) μ m	4.269(1) μ m	4.122(2) μ m
D(0.9)	26.09(2) μ m	8.161(2) μ m	6.245(1) μ m

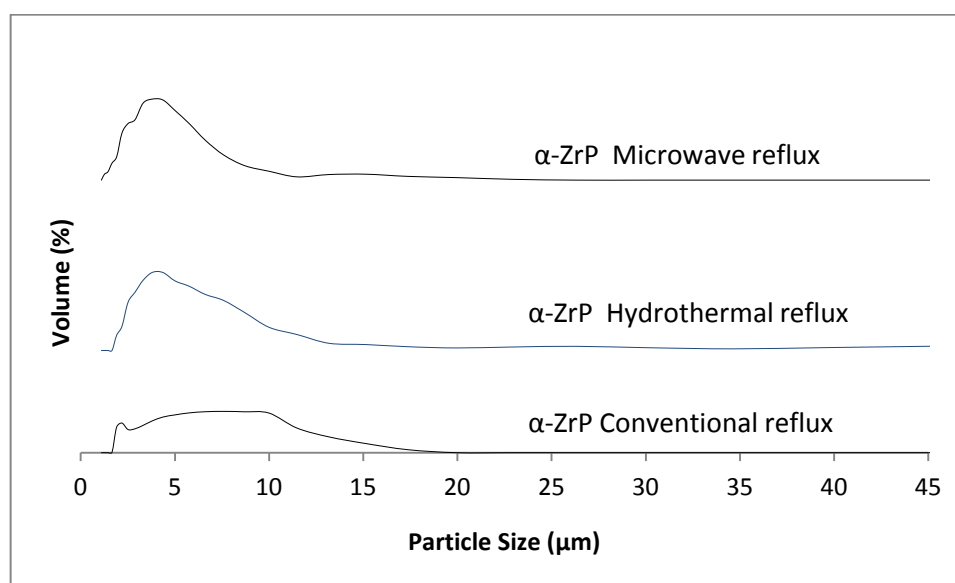


Figure 3. 5 Particle size distribution curves for α -ZrP synthesised by different routes

It can be seen from the above results that synthesised α -ZrP have a wide variation in the particle size as evident from the particle size distribution graph. The variation in the crystal sizes are more pronounced in conventional refluxed products as compared to the hydrothermal and microwave reflux. The presence of pressure and high temperature regulation in the latter techniques leads to a more uniform

synthesis of the crystals as compared to the conventional refluxed products. This can affect the physical and chemical properties of the product such as the surface area, catalytic and ion exchange activity [2, 14]. To confirm this, a BET surface area analysis was carried out for the synthesised α -ZrP. It was found that conventionally refluxed α -ZrP had a surface area of 24.18 m²/g, whereas hydrothermally refluxed α -ZrP was 18.92 m²/g and microwave refluxed α -ZrP had a surface area of 21.87 m²/g. These results imply that there is no direct correlation between the particle size and surface area for different routes of synthesis, but it is assumed as a general rule that if the particle size decreases, the surface area should increase for a given spherical particle.

3.1.5 FT-IR analysis

The synthesised α -ZrP samples were analysed by FT-IR in order to understand the type of chemical bonding present in the samples by producing the absorption or transmission IR spectrum. The FT-IR transmission spectrum for the synthesised α -ZrP samples via three routes is provided below in Figure 3.6.

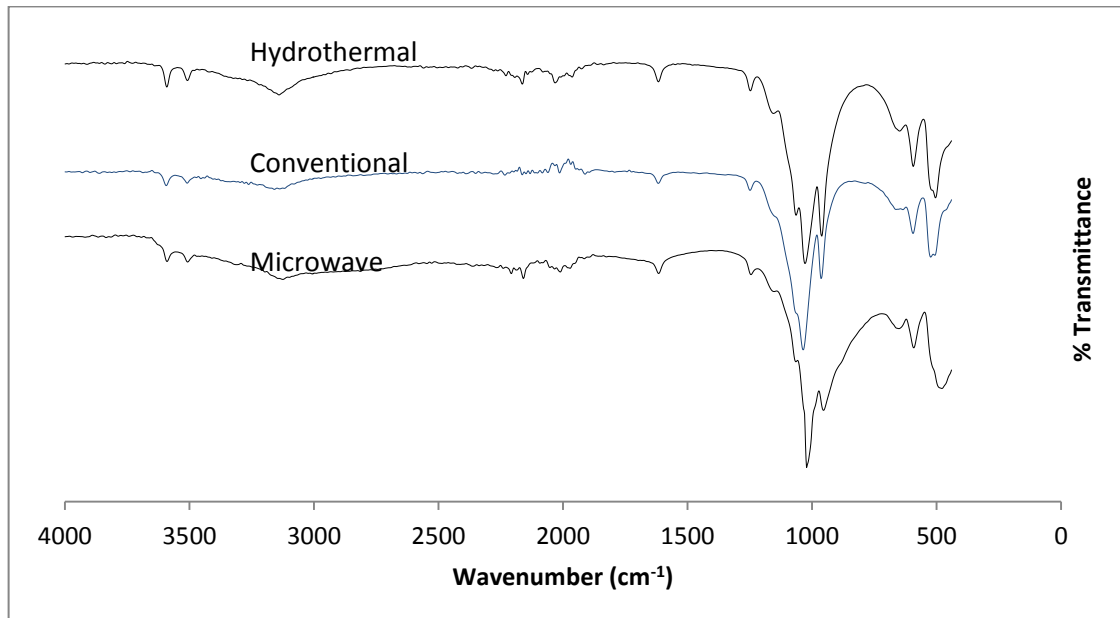


Figure 3. 6 FT-IT transmission spectrum for α -ZrP synthesised by 3 different routes

The characteristic peaks at different wavenumbers within the range of 400 to 4000 cm^{-1} represents the stretching or bending vibrations of the different chemical bonds present in the samples. A complete analysis of a typical FT-IR spectrum of α -ZrP as obtained from the literature sources ^[11-17] is shown in the Table 3.3 below.

Table 3. 3 Summary of the FT-IR results for a crystalline α -ZrP sample

Peak Wavenumber (cm^{-1})	Chemical bonds
525.01	O-P-O deformation
594.99	P-OH (out of plane)
658.54	O-H (out of plane)
964.11	P-O bending (in plane)
1027.93	P-O stretching (asym)
1247.50	P-O-H deformation
1621.46	O-H bending (asym)
2187.68	P-OH
2229.32	P-OH
3151.86	O-H stretching (sym)
3509.59	O-H stretching (asym)
3592.86	O-H stretching (asym)

The peaks occurring at 3100-3600 cm^{-1} and 1620 cm^{-1} are associated with the stretching and bending vibrations of the water molecule. The peak at 960 cm^{-1} is attributed to the in-plane bending of the P-O bond, whereas the peak at 1382 cm^{-1} is attributed to the vibration of P-O bond. The peaks occurring in the region of 450-600 cm^{-1} is associated with the presence of phosphate (PO_4) bonds along with the vibration of water molecule at 600 cm^{-1} . The peak at 525 cm^{-1} and 650 cm^{-1} corresponds to the O-P-O deformation of the PO_4 group and out of plane O-H bond respectively.

3.1.6 Nuclear magnetic resonance (NMR) analysis

NMR analysis for ^{31}P nuclei of the synthesised α -ZrP samples from all three routes of synthesis was carried out. The difference in the chemical shifts of the resonance peak is attributed to the type of external standard reference used for calibration at

different times. Three of the external standards were used in this research, namely triphenyl phosphine, 85% phosphoric acid and ammonium phosphate, of which ammonium phosphate (NMR spectrum shown in figure 2 of Appendix 1) was used extensively for calibration purposes. Hence the chemical shifts are relative to these external standards and the peaks represented here are shifted by almost 7.4 ppm upfield in regards to the ammonium phosphate. The ^{31}P NMR spectrum for the α -ZrP synthesised by all three routes of synthesis is shown in Figure 3.7 below.

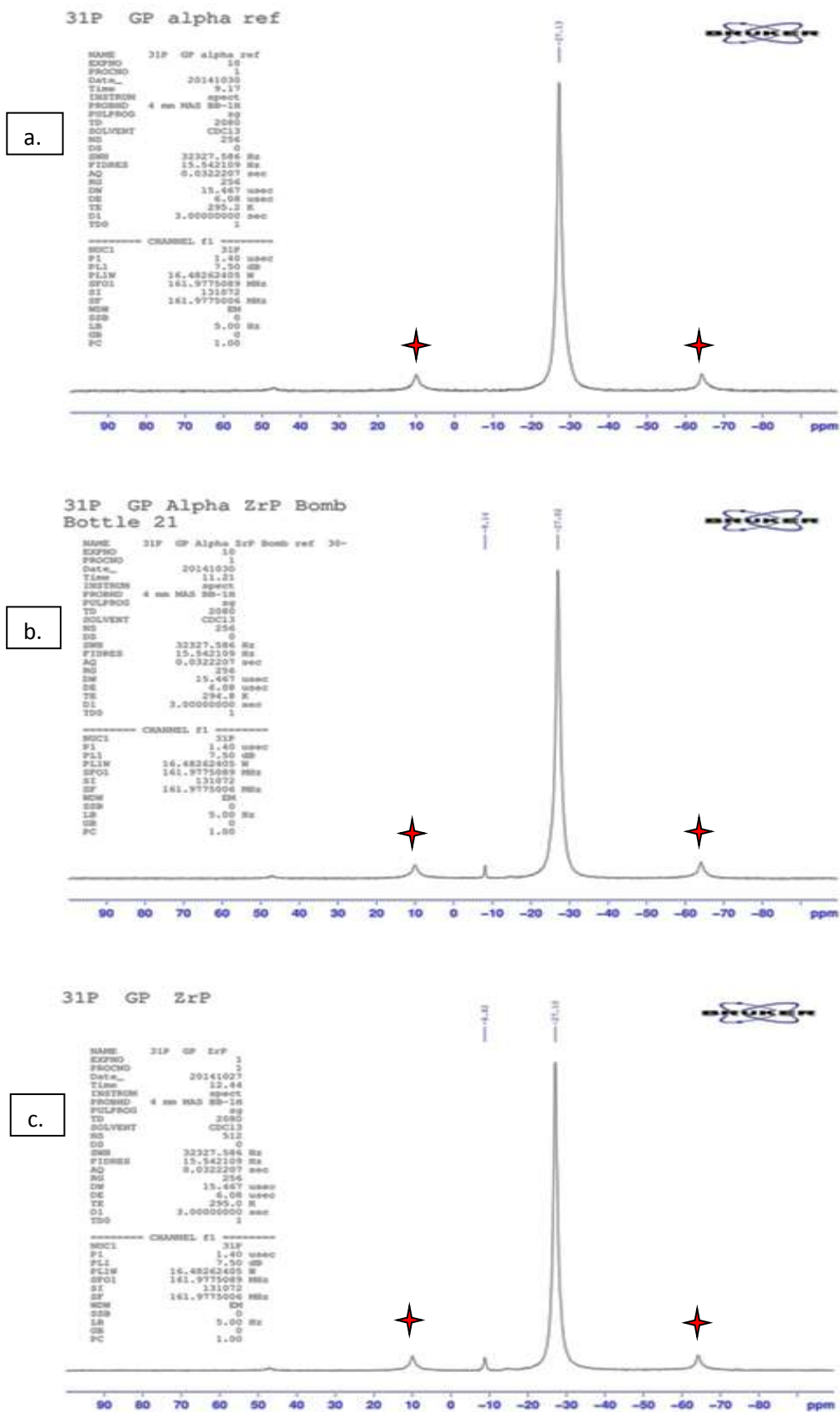


Figure 3. 7 ^{31}P NMR of Conventional (a), hydrothermal reflux (b) & Microwave reflux (c) α -ZrP (Spinning side bands are represented as \star)

The reported crystal structures have two phosphorus atoms which are crystallographically distinct. However, the spectra shown in Figure 3.7 have a single resonance peak present at -27.1 ppm. This indicates a single phosphorous environment representing the O₃-P-OH groups. This is in agreement with NMR studies on the alpha zirconium phosphate as reported by Clayden *et al.* [19] and Nakayama *et.al* [20]. It can be concluded that there is a similar electronic environment for phosphoric nuclei of crystallographically different phosphorus groups which accounts for one single peak instead of two distinct signals. Spinning sidebands can be observed on either side of the resonant peak with a low intensity which implies small chemical shift anisotropy as compared to that of the resonance peak.

However, the spectra recorded of the α -ZrP synthesised by hydrothermal and microwave refluxed methods have an additional peak at -8.14 ppm. It is understood from the previous studies [12-21] that this peak at -27.1 ppm corresponded to HPO₄²⁻ group but the peak at -8.14 ppm is unrecognised. It can be assumed here that a different phosphorus environment is present which is associated with this minor peak, possibly due to the paramagnetic interactions of the impurity phases of rare earth metal phosphates [34]. However, it is believed that the reason for this downfield peak resonance can be accounted to the Q⁰ connectivity of the phosphate group as suggested by Hudson *et.al* [21]. The Q⁰ structure is attributed to the presence of some protons surrounding the phosphorous group, but there might be some rotational motions of the spin nuclei which decrease the dipolar interactions between the surrounding protons and the phosphorous nuclei. This is the reason why the signal intensity from the Q⁰ structure of the phosphorus group diminishes strongly during the CPMAS NMR as opposed to the SPMAS where it remains unaffected. But an increase in contact time in CPMAS NMR and purely additive shielding of O-Zr groups can amplify this signal and provide a small peak at around -0.7 ppm as observed in this study.

It is concluded that the presence of a single sharp resonance peak at -27.1 ppm is indicative of the phosphorus environment where the phosphorus atom is connected via bridging oxygen to the three zirconium metal centres forming a HO-P-(O-Zr)₃ framework. By assigning the Q notations from the previous findings [21-22], it is seen that the phosphorus in the alpha type structure has Q³ connectivity. On the other

hand, the presence of another minor peak at around -8.14 ppm represents a proton rich region surrounding phosphorus group with a Q^0 connectivity that may indicate the presence of deshielded protons (possibly associated with the water molecule) in the lattice. This is most likely to be expected from the doping effect as the charge imbalance created will lead to the formation of $[H_2PO_4]^-$ groups, similar to those present in gamma-zirconium phosphate. The possibility of presence of an amorphous α -ZrP phase is overruled since the presence of sharper NMR peaks without the presence of other Q^n resonances and the XRD patterns indicate higher crystallinity of the hydrothermal and microwave refluxed products as compared to the conventional reflux. Therefore, it can be assumed that high pressure and temperature in a closed experimental apparatus like an autoclave or a microwave, lead to more crystalline and ordered lattice where the exchangeable proton sites are more compactly packed, hence exposing the deshielded phosphorus nuclei in the NMR analysis. Finally, the assumption of the presence of a different phase of α -ZrP such as the γ -ZrP is again disregarded as the peak ratios and the chemical shifts for such phases are not matching with the synthesised products.

3.1.7 Rietveld Refinement

The structure of the synthesised α -ZrP was refined using the structural model of Clearfield and Smith ^[23] for α -ZrP using the space group $P2_1/c$. It can be seen from the summary of the structural parameters in Table 3.4 below, that the α -ZrP samples from all the 3 routes of synthesis are in good agreement with refined structures of the literature. The details of the atomic coordinates and thermal parameters are given in the Tables 3.5-3.7 below along with the graphical fits in Figures 3.8-3.10. Each atom types were constrained to the same value of the isotropic temperature factor during the initial stages of the refinement. The details of the refined bond angles obtained from refinement results of products from all three routes of synthesis are summarised in table 1 of Appendix 2.

Table 3. 4 Refined structural parameters with estimated standard deviations for α -ZrP

Parameters	Conventional α -ZrP	Hydrothermal α -ZrP	Microwave α -ZrP	Reported α -ZrP ^[4]
a/Å	9.0759(7)	9.0593(9)	9.0700(8)	9.06336(2)
b/Å	5.2988(4)	5.2886(5)	5.2945(5)	5.29060(1)
c/Å	16.244(2)	16.255(2)	16.221(2)	16.24603(6)
β /deg	111.397(4)	111.397(5)	111.407(5)	111.4012(2)
V/Å ³	727.39(11)	725.12(13)	725.24(14)	717.16(3)
M-O(1)/Å	2.069(8)	2.056(11)	2.012(5)	2.085(5)
M-O(2)/Å	2.0986(1)	2.0999(2)	2.099(6)	2.090(6)
M-O(3)/Å	2.0609(1)	2.0922(2)	2.004(6)	2.086(6)
M-O(5)/Å	2.057(12)	2.040(14)	2.053(6)	2.084(6)
M-O(6)/Å	2.030(6)	2.070(10)	2.046(6)	2.105(6)
Avg. M-O/Å	2.0631	2.0716	2.0428	2.090
χ^2	4.404	11.46	6.028	2.844
R _p /%	7.43	11.21	8.86	5.51
R _{wp} /%	10.22	16.94	11.96	7.37
R _F ² /%	10.51	19.49	12.53	-

The Rietveld refinement results shown above are an indication of the high crystallinity and ordered crystal structure for the synthesised α -ZrP products. The crucial structure parameters with estimated standard deviations for R values such as the χ^2 , R_p, R_{wp} and R_F² are the governing factors which decide the validity and precision of the refinement results. However, there are no set rules to be considered while limiting these parameters to a certain value in order to consider the validity of the results since these factors vary according to the instrumental factors such as the signal to noise ratio, total number of counts per seconds recorded and peak properties. It is often noticed that as peak profiles become sharper, the observed structure factors can give increased χ^2 and R_{wp} values. The presence of asymmetry and irregular peak profiles can lead to discrepancies in the reflection based R factor (R_F). There can also be certain discrepancies between the calculated value based on the type of instrument used and the condition of the refinement parameters fixed

for a given set even for a high quality data set. However, these factors are relatively important while dealing with a Rietveld refinement as they proportionally indicate the 'goodness of a fit' by estimating the deviation in the calculated and observed variables [37]. Therefore, a satisfactory refinement result can be obtained by close monitoring and using the general mathematical hypothesis that for a good convergence of a data set to the reference or model structure, the estimated standard deviation should be minimized.

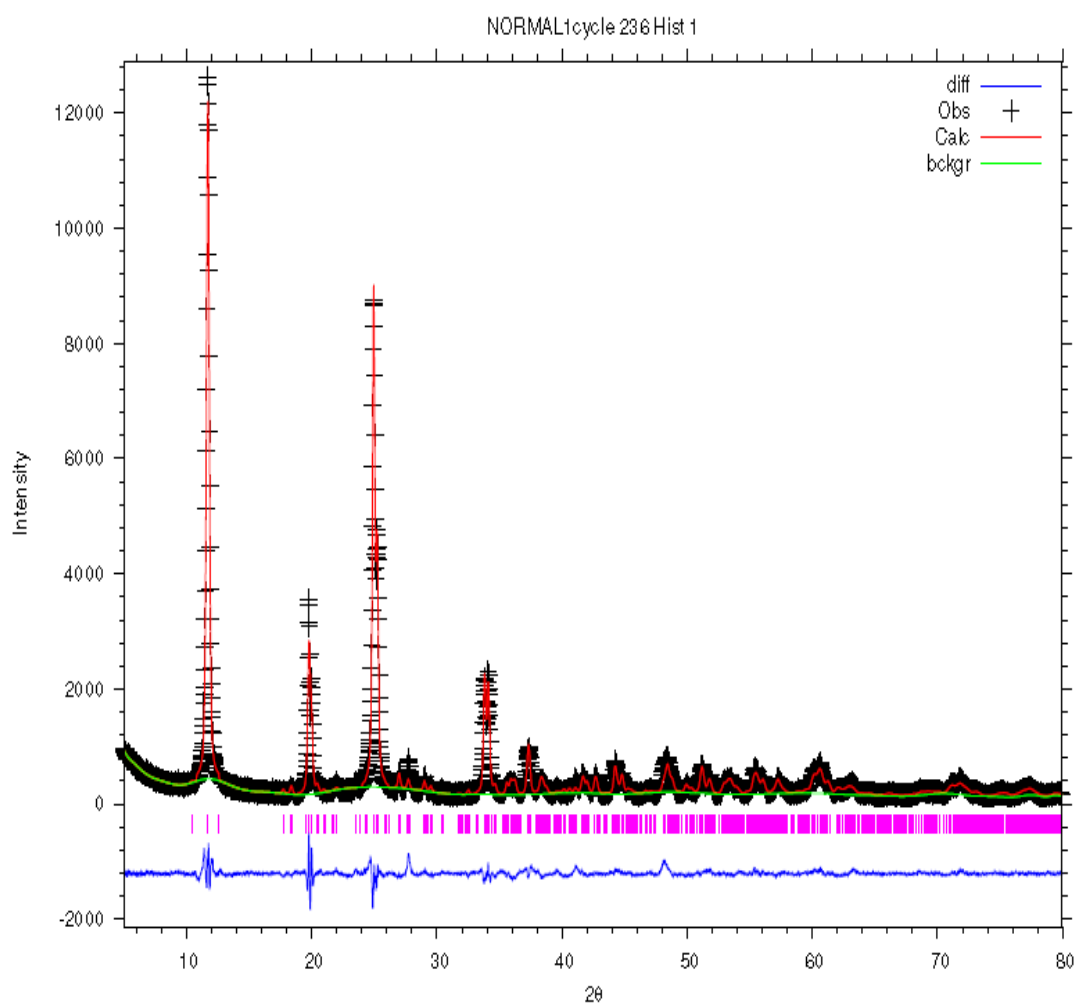


Figure 3. 8 Final observed (cross), calculated (red line) and difference (blue bottom) X-ray diffraction profiles obtained from Rietveld refinement for conventional α -ZrP

Table 3. 5 Refined fractional atomic coordinates and isotropic thermal displacement parameters for conventional α -ZrP

Atom	x	y	z	$U_{\text{iso}} (\times 10^2) / \text{\AA}$
Zr	0.7572(5)	0.2540(1)	0.5108(2)	0.31(1)
P(1)	0.0014(4)	0.7514(1)	0.6105(3)	2.96(8)
P(2)	0.4680(1)	0.2590(1)	0.1008(3)	8.53(9)
O(1)	0.1059(5)	0.8067(3)	0.5649(2)	14.11(7)
O(2)	0.9306(5)	0.4899(3)	0.5974(2)	0.17(6)
O(3)	0.8660(1)	0.9450(1)	0.5854(3)	1.65(1)
O(4)	0.0802(5)	0.7050(1)	0.7186(3)	3.93(4)
O(5)	0.3450(1)	0.4380(1)	0.5659(3)	16.18(8)
O(6)	0.4150(1)	0.5179(3)	0.0654(3)	10.84(5)
O(7)	0.5043(5)	0.2499(3)	0.2027(3)	8.01(5)
O(8)	0.3760(1)	0.8079(1)	0.9057(2)	4.63(3)
O(9)	0.2505(5)	0.2722(1)	0.2554(3)	13.54(7)

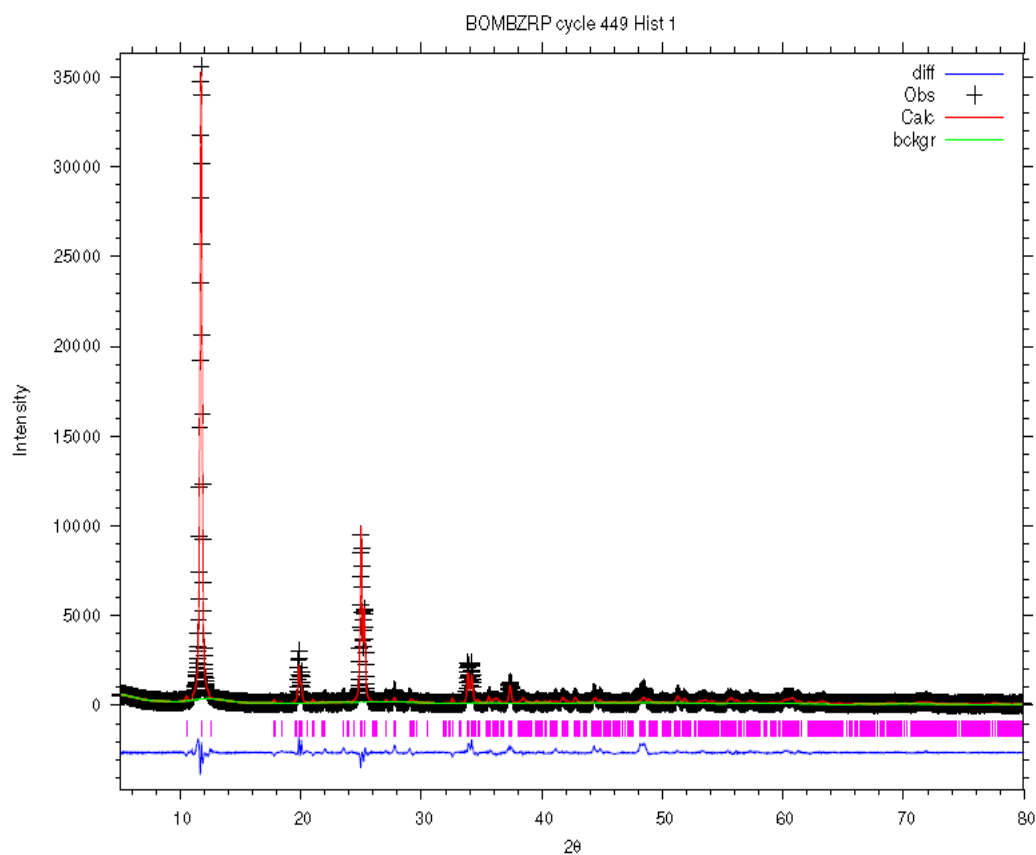


Figure 3. 9 Final observed (cross), calculated (red line) and difference (blue bottom) x-ray diffraction profiles obtained from Rietveld refinement for hydrothermal α -ZrP

Table 3. 6 Refined fractional atomic coordinates and isotropic thermal displacement parameters for hydrothermal α -ZrP

Atom	x	y	z	$U_{\text{iso}} (\times 10^2) / \text{\AA}$
Zr	0.7617(6)	0.253(2)	0.5135(2)	0.09(7)
P(1)	0.0007(6)	0.739(3)	0.6058(3)	10.78(5)
P(2)	0.461(1)	0.236(3)	0.0926(2)	0.62(5)
O(1)	0.101(1)	0.804(1)	0.5614(2)	38.08(5)
O(2)	0.937(1)	0.488(4)	0.6002(3)	2.42(8)
O(3)	0.869(5)	0.928(1)	0.5842(2)	1.16(2)
O(4)	0.104(5)	0.728(3)	0.6912(2)	1.92(2)
O(5)	0.346(7)	0.435(2)	0.5564(1)	40.12(1)
O(6)	0.414(1)	-0.0158(2)	0.5664(1)	39.61(5)
O(7)	0.626(6)	0.287(1)	0.5885(1)	58.76(9)
O(8)	0.501(1)	0.222(1)	0.6904(2)	38.33(8)
O(9)	0.254(6)	0.213(2)	0.7542(2)	3.06(2)

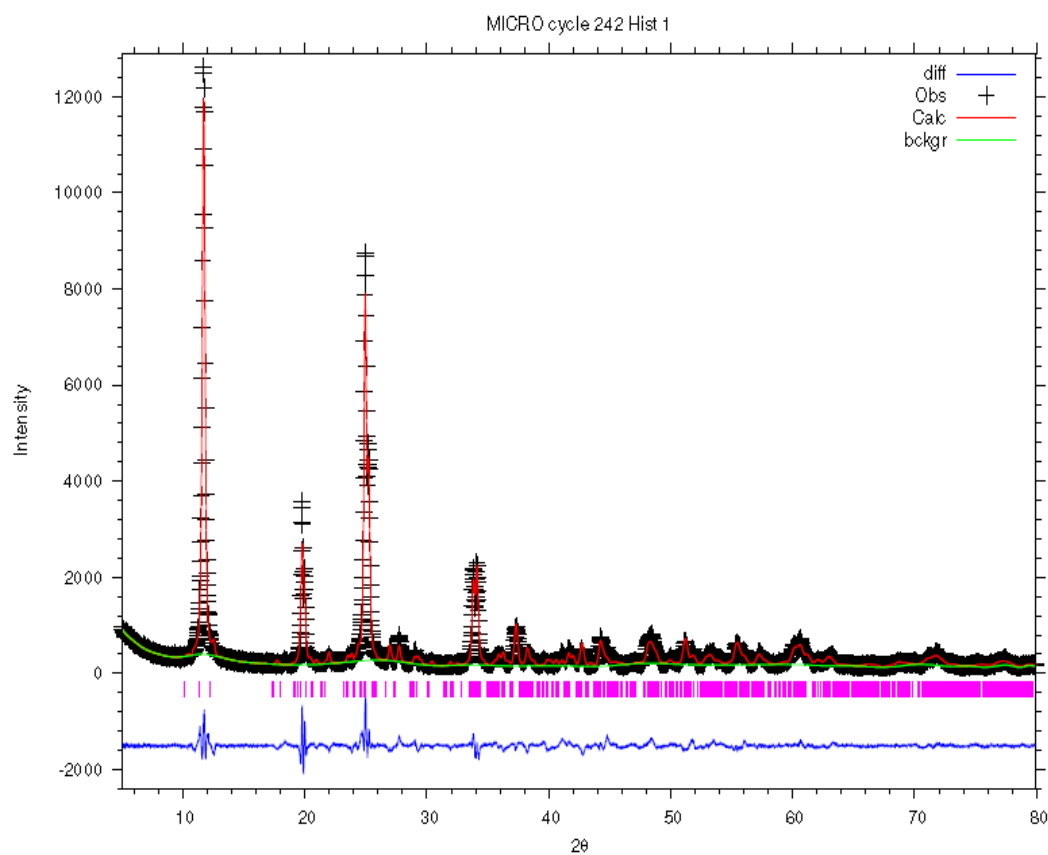


Figure 3. 10 Final observed (cross), calculated (red line) and difference (blue bottom) X-ray diffraction profiles obtained from Rietveld refinement for microwave α -ZrP

Table 3. 7 Refined fractional atomic coordinates and isotropic thermal displacement parameters for microwave α -ZrP

Atom	x	y	z	$U_{\text{iso}} (\times 10^2) / \text{\AA}$
Zr	0.7515(7)	0.2507(13)	0.51231(31)	1.97(1)
P(1)	0.000740(1)	0.746401(1)	0.599915(2)	2.75(4)
P(2)	0.517373(1)	0.224845(2)	0.100772(1)	3.19(3)
O(1)	0.110762(2)	0.781892(2)	0.560206(1)	4.29(3)
O(2)	0.970267(1)	0.432778(3)	0.541453(3)	8.96(8)
O(3)	0.898722(2)	1.018258(2)	0.602656(3)	3.40(7)
O(4)	0.07035(1)	0.808918(2)	0.714029(1)	1.84(3)
O(5)	0.301607(3)	0.085556(3)	0.056032(2)	5.52(3)
O(6)	0.410282(3)	-0.015560(1)	0.574840(2)	10.15(3)
O(7)	0.461745(1)	0.355468(1)	0.129588(1)	15.95(2)
O(8)	0.500823(2)	0.236507(1)	0.709091(1)	12.15(4)
O(9)	0.255002(2)	0.222857(2)	0.764617(1)	1.31(1)

It is seen from the refined structural parameters presented in table 4 that the average Zr – O octahedron is regular with an average bond distance of 2.0631 Å for the conventional α -ZrP, followed by 2.0716 Å for hydrothermal α -ZrP and 2.0428 Å for microwave α -ZrP. These Zr – O bond distances are within 3 esd's to the previously reported distance of 2.090 Å obtained from high resolution synchrotron x-ray data. ^[4] All the O – Zr – O bond angles shown in table 1 of Appendix 2 are close to 90° and for the phosphate groups (P-OH), where the oxygens are not bonded to zirconium, the P – O bonds are significantly longer, with an average of 105.2°.

Overall, on comparison of structural parameters of α -ZrP synthesised from 3 different routes shown in Table 3.8, it is seen that no significant differences were observed in the unit cell and all the three samples have $P2_1/c$ space group symmetry with an approximate unit cell volume of 725 Å³ and $\beta = 111.40^\circ$. The slight differences which were observed in the structural parameters are possible due to the differences in the degree of refinement of individual x-ray diffraction patterns, but are in well agreement with the reported values ^[4] in literature.

Table 3. 8 Comparison of the refinement parameters for α -ZrP from literature

Parameters	Conventional α -ZrP	Hydrothermal α -ZrP	Microwave α -ZrP	Reported α -ZrP ^[4]
a/Å	9.0759(7)	9.0593(9)	9.0700(8)	9.06336(2)
b/Å	5.2988(4)	5.2886(5)	5.2945(5)	5.29060(1)
c/Å	16.244(2)	16.255(2)	16.221(2)	16.24603(6)
β /deg	111.397(4)	111.397(5)	111.407(5)	111.4012(2)
V/Å ³	727.39(11)	725.12(13)	725.24(14)	717.16(3)

3.2 Synthesis of yttrium-zirconium phosphate (Y-ZrP)

The general preparation of the yttrium substituted α -ZrP samples was carried out by using the similar approach as that used for the synthesis of α -ZrP samples ^[1] with an extra step of using sonication for 20 minutes after precipitation of metal salts are completed with 4M phosphoric acid. It was found that the substitution of the yttrium into the α -ZrP framework was more homogenous after 20 minutes of sonication as previously reported in the literatures ^[24-25] and it lead to the preparation of more uniform particles which is discussed in the subsequent sections. A series of Y-ZrP samples were attempted according to the method mentioned in the experimental chapter, but it was observed that substitutions above 15% of zirconium with yttrium led to the formation of biphasic products, hence only 5, 10 and 15% yttrium substituted α -ZrP were used for ion exchange.

The obtained amorphous products were then refluxed in concentrated phosphoric acid (12M) for a period of 7 days using conventional method and hydrothermal (autoclave) synthesis. The final products are then washed, dried and finely ground for further characterisation.

3.2.1 X-ray diffraction of Y-ZrP samples

Two routes of synthesis were used for 4 compositions of the synthesised Y-ZrP samples and the results for the XRD analysis is shown below in Figures 3.11 and 3.12.

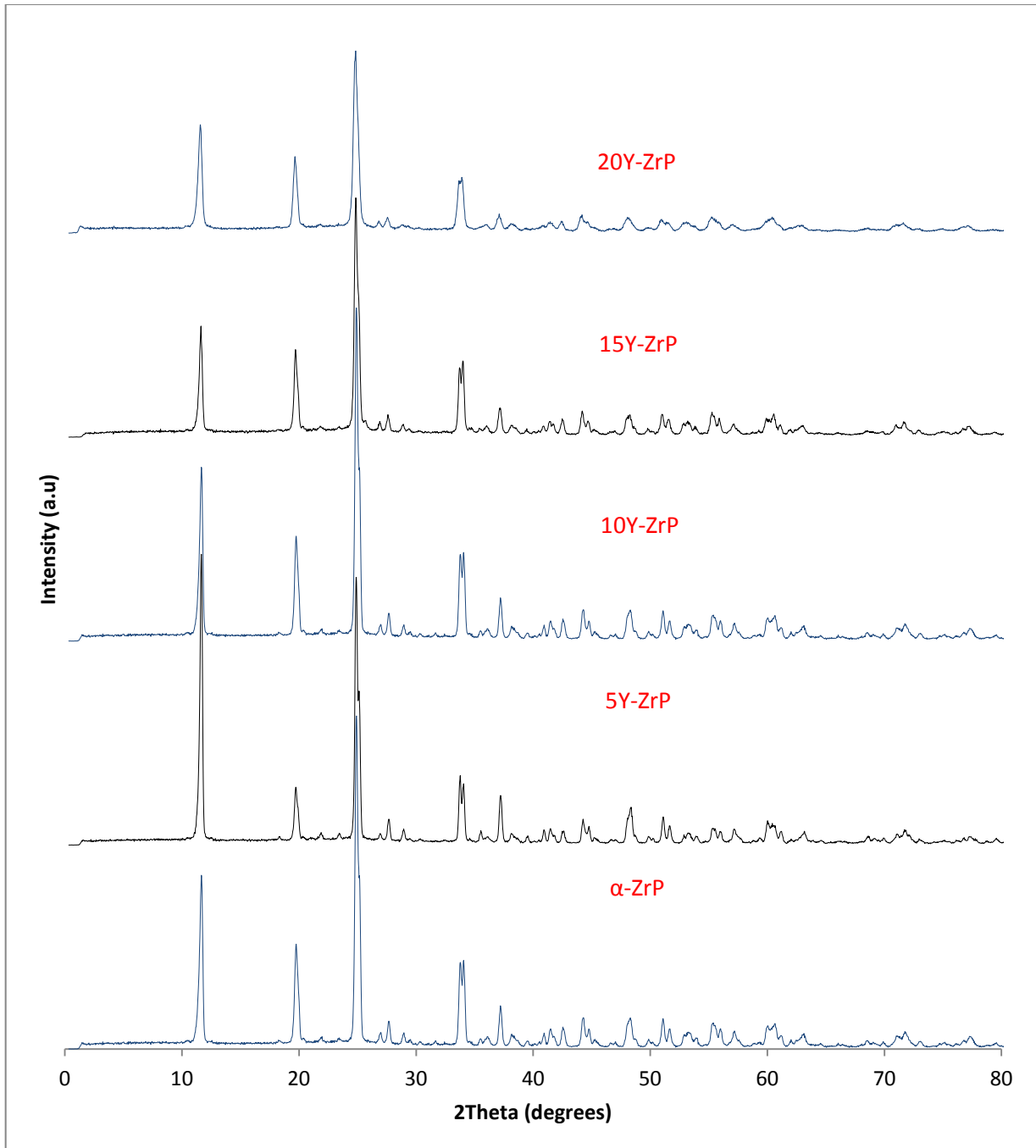


Figure 3. 11 Conventionally synthesised Y-ZrP samples

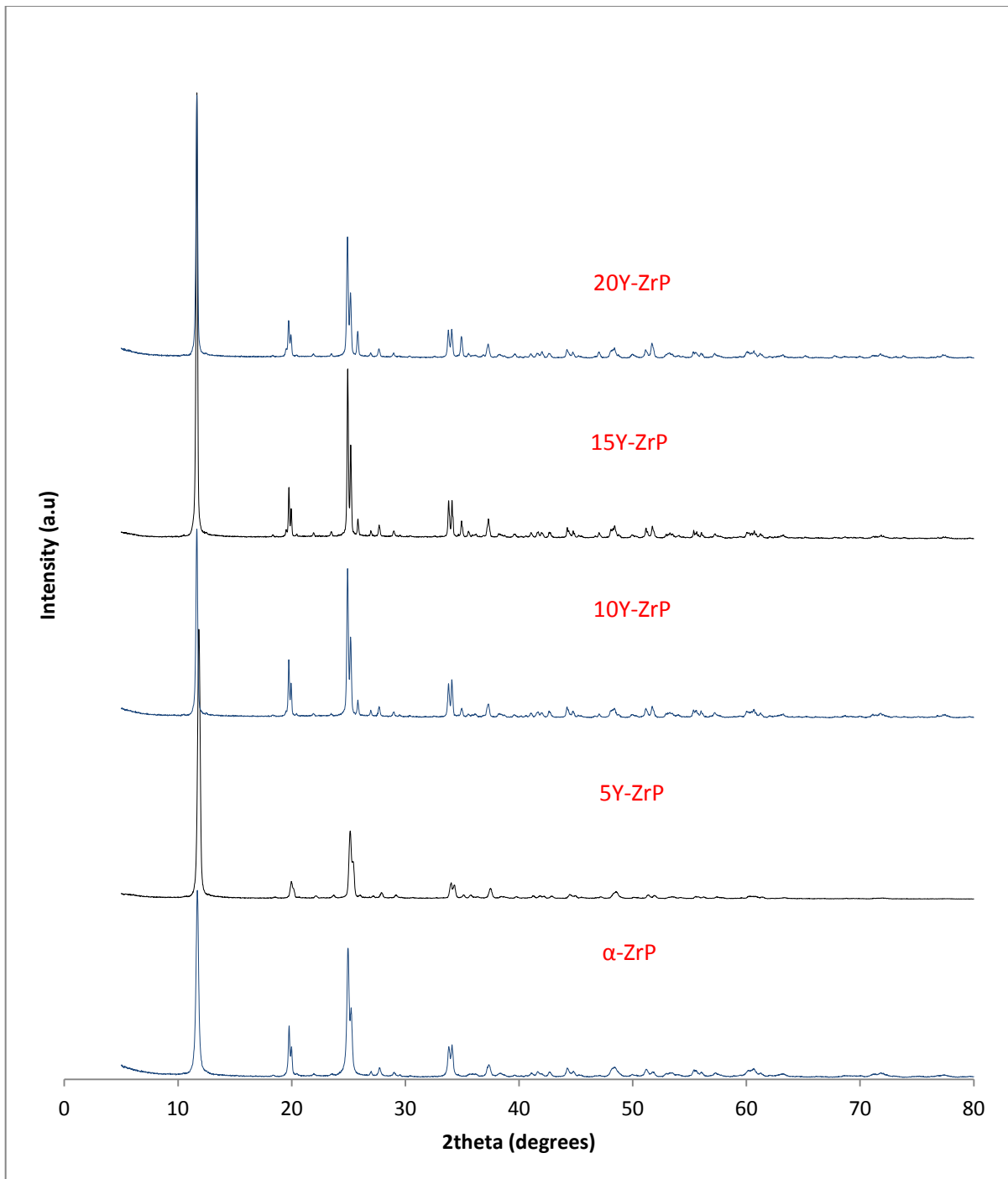


Figure 3. 12 Hydrothermally synthesised Y-ZrP samples

It can be observed from the Figure 3.11 above that the conventional route of synthesis was able to produce crystalline and isostructural products with regards to the α -ZrP. The samples obtained were single phase and no impurities were observed in the XRD patterns. Also, there is a slight variation in peak intensity as the substituted concentration of yttrium increased from 5% to 20% and therefore can

be correlated to the degree of crystallinity of the obtained products. The most crystalline and highly resolved XRD pattern among the batch can be attributed to 5% Y-ZrP as compared to the rest of the samples. This may be due to the variation in the temperature conditions along with the limitation of reaching higher temperatures in the conventional refluxing route. Also, it could be well possible that the substitution of yttrium into the α -ZrP lattice is straining the lattice and therefore producing lower crystallinity.

On the other hand, the hydrothermally refluxed Y-ZrP samples as shown in Figure 3.12 above lead to the formation of products with equal crystallinity. The first characteristic peak (002 reflection) is more pronounced as compared to the rest of the peaks and the products appear to be isostructural as compared to the α -ZrP. However, two extra peaks can be observed in products with yttrium substitution of 10% and above which do not match the database patterns for zirconium phosphate. The first peak occurs at $2\theta = 25.9^\circ$ and the second peak occurs at $2\theta = 35^\circ$ respectively, with a ratio of peak intensities of approximately 0.95. At first it was assumed that this could be due to the possibility of a two phase system where the formation of tetragonal yttrium phosphate or Xenotime (YPO_4) has occurred as the peaks were close to the published peak positions for yttrium phosphate. Therefore, YPO_4 was hydrothermally synthesised for comparison according to the procedure mentioned by Qiong and Yiguo ^[26] with the lattice parameters shown in Table 3.9 below. On inspection of the XRD pattern of Xenotime (as shown in Figure 3.13 below), it was found that there are 3 main peaks which are present at $2\theta = 19.5^\circ$, 25.9° and 35° that were also observed at approximately similar 2θ positions in Y-ZrP samples. However, the relative intensities of Xenotime do not match to those of the impurity phase in Y-ZrP. The difference in relative intensities implies that either the impurity phase is not YPO_4 or it is YPO_4 with preferred orientation.

Table 3. 9 Lattice parameters of Xenotime ^[26]

Space Group	a (Å)	b (Å)	c (Å)	Alpha (°)	Beta (°)	Gamma (°)
I41/amd	6.8947(6)	6.8947(6)	6.0276(6)	90	90	90

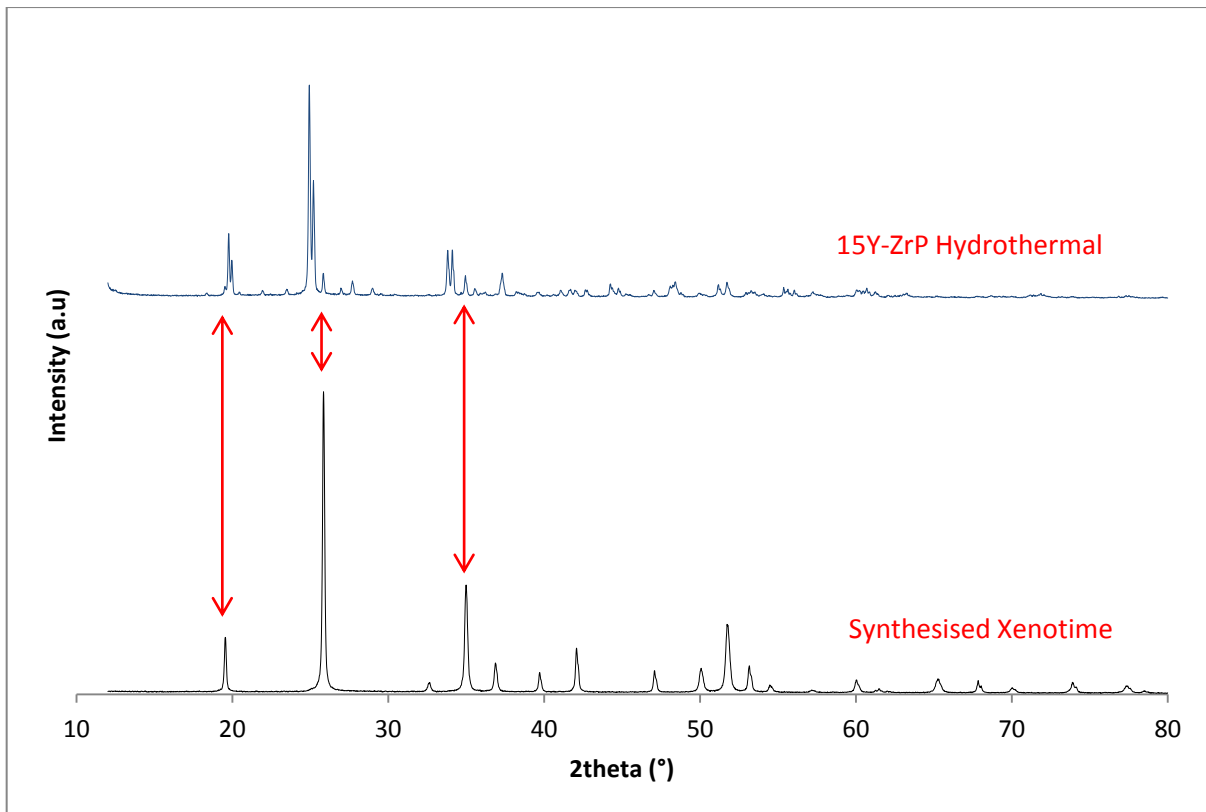


Figure 3. 13 Comparison of XRD patterns of synthesised YPO_4 and Y-ZrP samples

An online search using the PDF ICDD crystal database for possible match for these extra peaks was done and the results were compared to each other. The PDF resulting matches are shown as images in figures 3 and 4 in Appendix 1. The figure 3 shows that Xenotime (YPO_4) characteristic peaks appear shifted with regards to the unmatched peaks in the 20% Y-ZrP pattern. Also, there is no peak matching at $2\theta = 19.5^\circ$. Therefore, it can be concluded that the appearance of the extra peaks are not linked to the second phase of Xenotime. The PDF match in figure 5 of Appendix 1 shows a potential match of hydrogen form of α -ZrP for these extra peaks.

A blown up representation from mixed phase 40% Y-ZrP sample with a clear presence of extra biphasic peaks (at $2\theta = 19.5^\circ$, 25.9° and 35°) is matching with the PDF ICDD database search for rare-earth phosphates. It is observed that none of the individual rare earth phosphates match the peak intensities despite being isostructural hence there can be a presence of mixed rare-earth metal phosphates along with Xenotime that contribute to the enhanced peak intensities of all the peaks

at its respective 2θ positions. The absence of the peak at $2\theta = 19.5^\circ$ and the mismatch of the peak intensities for the synthesised Y-ZrP samples can indicate complex crystal chemistry of the products. It is therefore safe to conclude that the synthesised Y-ZrP samples are synthesised as single phase products up till 15% substitution with a possible rare-earth metal phosphate impurity along with the formation of a distinct Xenotime phase which increases with an increase in yttrium salt concentration.

3.2.2 X-ray fluorescence (XRF)

The use of XRF was carried out for semi-quantitative purposes by determining the Y/Zr ratio of the area under the peak. A calibration was carried out using the corn flour method as explained previously, for the molar composition of yttrium to zirconium and a graph is produced (as shown in Figure 3.14 below) from the scheme shown in table 1 of Appendix 1. Best fit linear regression was used for the calibration graph with a $R^2 = 0.9814$ after an average of 3 readings. The error bars are highlighted in the graph shows an average standard deviation of about 0.4%.

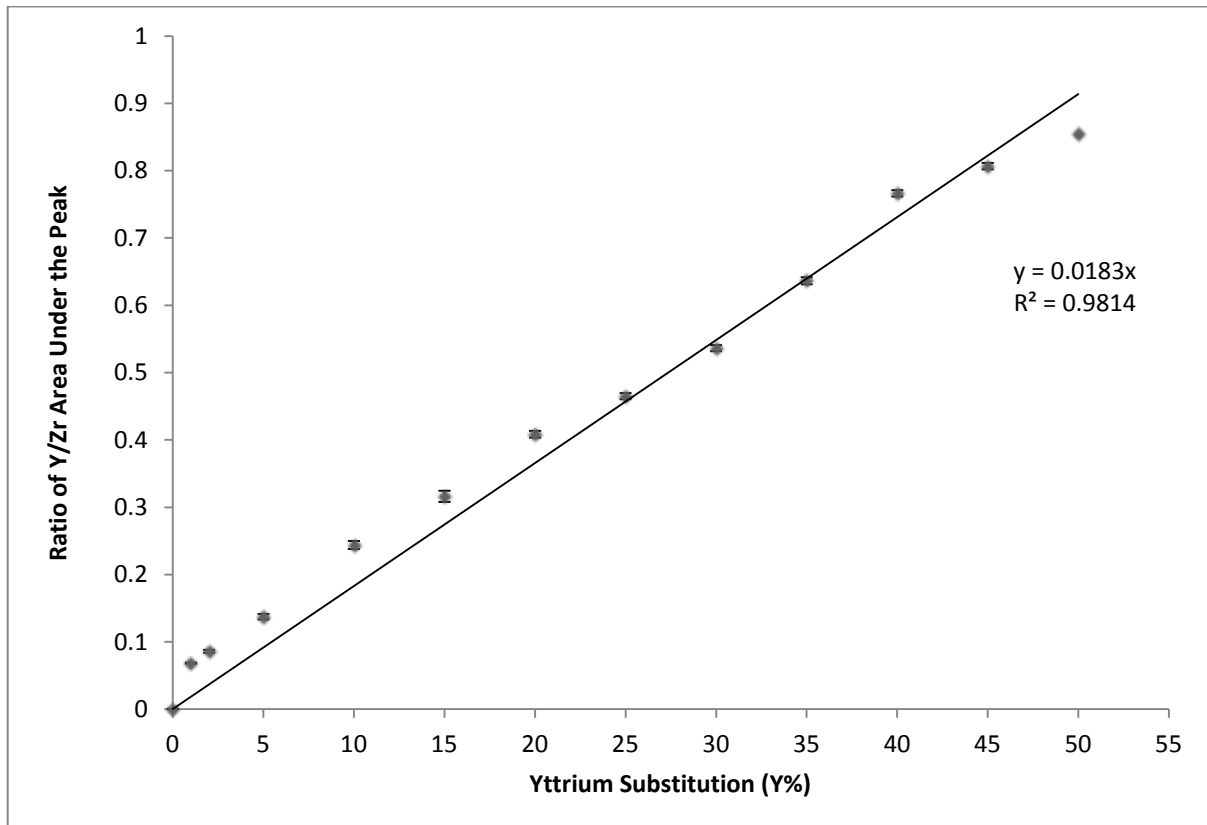


Figure 3. 14 XRF calibration graph for quantitative analysis of yttrium content

The ratio of the area under the peaks can provide a semi-quantitative analysis of the composition of samples. The equation of the best fit linear regression line which is obtained from the graph is shown below:

$$y = 0.0183x \quad (14)$$

This equation is used for calculating the exact yttrium substitution in the Y-ZrP samples by utilising the ratio of the area under the peaks of both yttrium and zirconium peaks and the results are summarised in Table 3.10 below. Graphical representation of the XRF peaks is provided in the figures 6 and 7 in appendix 1.

Table 3. 10 Substituted yttrium percentage in Y-ZrP samples as analysed from XRF

Sample	Theoretical yttrium %	Ratio of area under the XRF peaks (Y/Zr)	Calculated yttrium % from eq.1	Difference (Theoretical – Calculated)
5Y-ZrP Conventional	5%	0.04109157	2.25%	2.75%
5Y-ZrP Hydrothermal	5%	0.08911995	4.87%	0.13%
10Y-ZrP Conventional	10%	0.12445678	6.80%	3.2%
10Y-ZrP Hydrothermal	10%	0.19876593	10.86%	-0.86%
15Y-ZrP Conventional	15%	0.19171173	10.48%	4.52%
15Y-ZrP Hydrothermal	15%	0.29686151	16.22%	-1.22%
20Y-ZrP Conventional	20%	0.31839285	17.40%	2.6%
20Y-ZrP Hydrothermal	20%	0.4535712	24.79%	-4.79%

It is clear from the compositional analysis above that the conventionally refluxed Y-ZrP samples had a decreased yttrium substitution as compared to the theoretical molar percentages. A possible reason for this lower substitution of yttrium into the α -

ZrP structure can be again attributed to the low temperature synthesis for the conventional route, since the maximum temperature used was only up to 120°C. However, the formed Y-ZrP products were purely crystalline and were single phase.

On the other hand, the hydrothermally synthesised Y-ZrP samples generally had a good agreement between the theoretical and the calculated yttrium content as seen from the XRF analysis in Table 3.10 above. Most of the sample compositions were within 1.5% difference except for the 20% Y-ZrP product that showed an approximately 5% error.

3.2.3 Scanning electron microscopy (SEM) analysis

The morphology of the synthesised Y-ZrP products were analysed by SEM and its compositional information is obtained by EDX. Figure 3.15 below shows that the synthesised Y-ZrP sample crystals were arranged in a layered plate like morphology and were approximately 1-2 µm in size for both the conventional and hydrothermal refluxed samples.

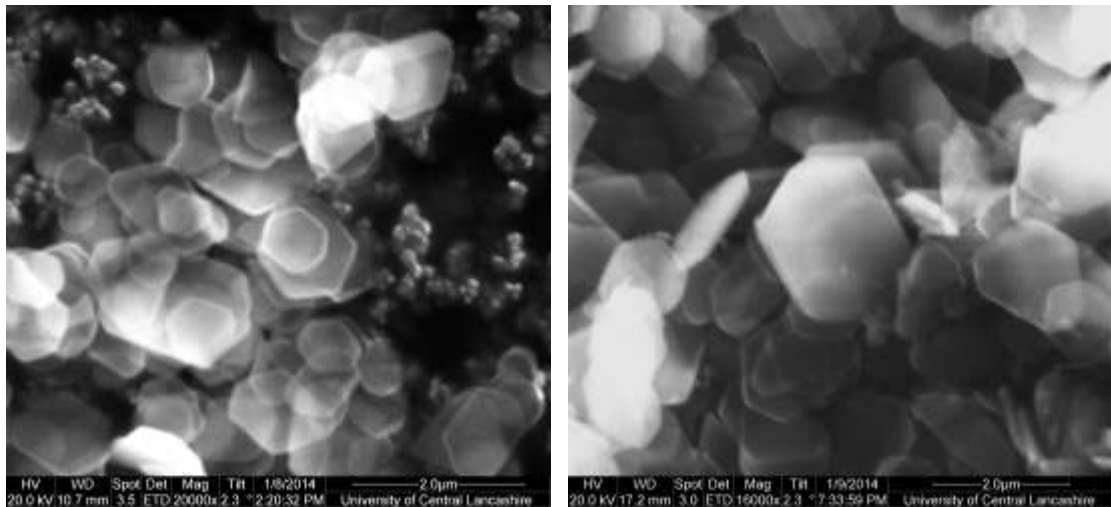


Figure 3. 15 SEM of conventional (left) and hydrothermal (right) reflux 5% Y-ZrP samples

The EDX analysis provided in the Table 3.11 below shows the composition of the synthesised Y-ZrP samples in the form of atomic percentages. These compositions obtained from the EDX are also compared with the XRF results as discussed in the previous section.

Table 3. 11 SEM/EDX analysis of Y-ZrP samples and comparison with XRF results

Samples	SEM EDX Atomic %		Y/Zr % from	Y/Zr % from
	Y	Zr	SEM	XRF
5Y-ZrP conventional	0.12(2)	6.20(2)	1.9%	2.25%
5Y-ZrP hydrothermal	0.22(5)	5.90(1)	3.7%	4.87%
10Y-ZrP conventional	0.29(1)	5.55(7)	5.22%	6.80%
10Y-ZrP hydrothermal	0.63(1)	7.19(2)	8.76%	10.86%
15Y-ZrP conventional	0.78(2)	7.55(3)	10.33%	10.48%
15Y-ZrP hydrothermal	0.93(2)	5.13(1)	18.13%	16.22%
20Y-ZrP conventional	1.55(4)	6.54(2)	23.7%	17.40%
20Y-ZrP hydrothermal	1.84(1)	6.24(2)	29.48%	24.79%

It can be seen from the above table that there is a significant amount of difference between the Y/Zr percentages of the synthesised Y-ZrP samples as obtained from the SEM/EDX and XRF analyses respectively. The SEM/EDX results are inconsistent with the theoretical molar ratios of the Y-ZrP composition as it gave increased values for the high end substituted Y-ZrP samples. This could be due to the EDX being not calibrated successfully for performing the compositional analysis. As discussed previously, factors such as sample preparations, spot size, beam interactions and other matrix effects may affect the SEM/EDX measurements and cause errors. Therefore it is concluded that the XRF results are more reliable than those obtained from the SEM/EDX since the latter scans a very small area and amount of sample against an intense background which can not only lead to interferences from absorption of detector signals but can also cause generation of matrix effects and high noise to signal ratio for some heavier elements like Zr, Y, Ti, Sn, Cs, etc.

3.2.4 Mastersizer analysis

The Malvern Mastersizer 2000SM was used for analysing the exact particle size of the synthesised Y-ZrP samples and the following graphical results were obtained, as shown in Figure 3.16 below.

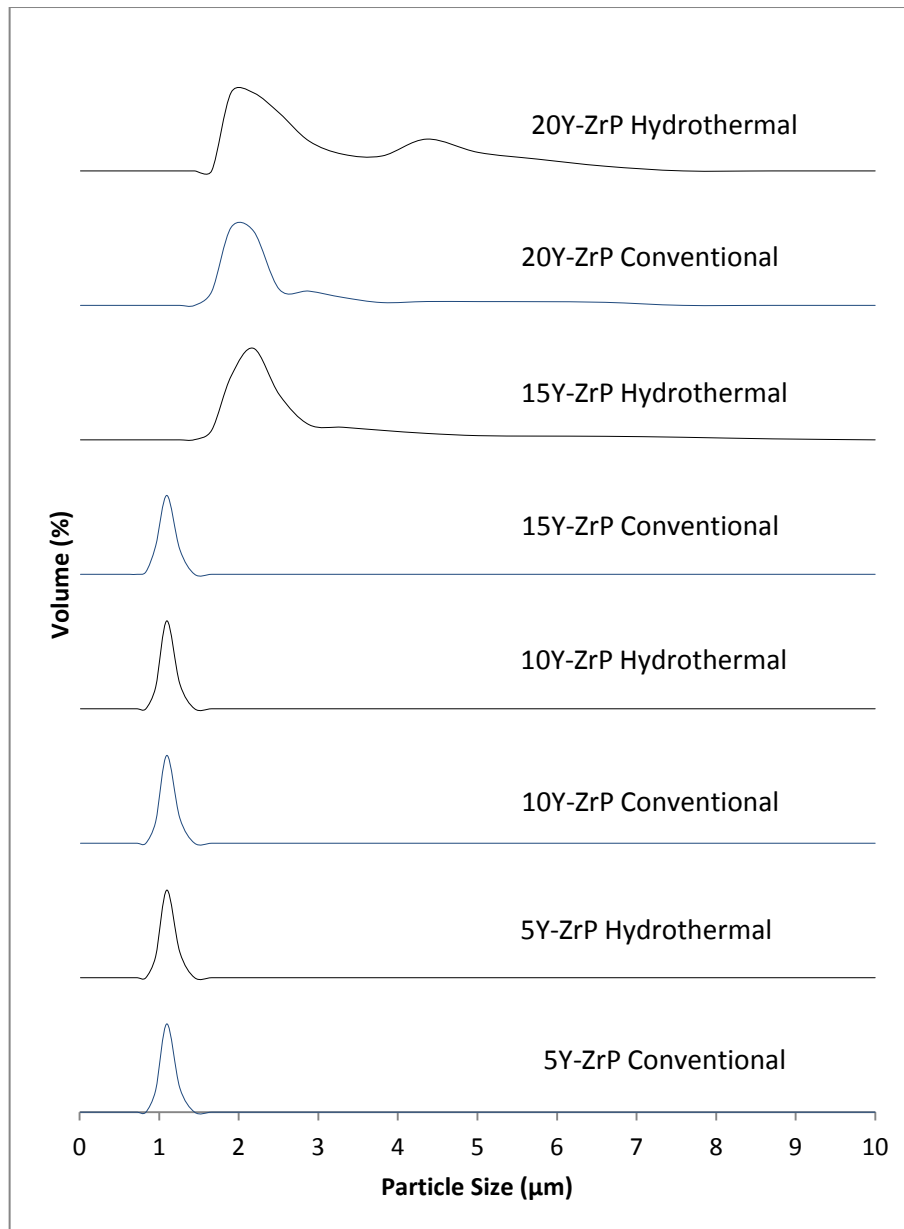


Figure 3. 16 Graphical representation of the particle size measurement by Mastersizer

The results of the Mastersizer analysis of the synthesised Y-ZrP samples are shown in Table 3.12 below and it shows that the synthesised Y-ZrP particles are within 1-2 μm .

Table 3. 12 Average particle size distribution data for synthesised Y-ZrP samples

Parameters	Conventional Y-ZrP Samples				Hydrothermal Y-ZrP Samples			
	5%	10%	15%	20%	5%	10%	15%	20%
Obscuration (%)	2.19(3)	2.23(1)	2.12(4)	2.12(1)	2.24(2)	2.16(1)	3.01(3)	2.1(1)
Span	0.18(2)	0.18(1)	0.21(1)	6.22(2)	0.18(3)	0.18(1)	1.23(1)	3.11(3)
Uniformity	0.07(1)	0.07(1)	0.08(2)	2.01(1)	0.07(1)	0.07(2)	0.38(1)	1.02(1)
Specific surface area (m^2/g)	5.11(1)	5.10(1)	5.17(3)	5.27(3)	5.10(1)	5.10(2)	5.17(1)	5.38(3)
Surface weighted mean $D[3,2]$ μm	1.17(1)	1.18(3)	1.16(1)	1.19(3)	1.18(2)	1.18(2)	1.9(2)	1.9(1)
Volume weighted mean $D[4,3]$ μm	1.18(3)	1.18(2)	1.17(1)	1.19(2)	1.18(3)	1.18(1)	1.9(2)	1.9(1)
$D(0.1)$ μm	1.07(5)	1.08(1)	1.05(2)	2.08(3)	1.08(1)	1.08(5)	1.95(1)	1.96(5)
$D(0.5)$ μm	1.17(1)	1.17(3)	1.16(5)	2.45(5)	1.17(3)	1.17(2)	2.48(4)	2.70(3)
$D(0.9)$ μm	1.29(1)	1.29(2)	1.29(1)	5.14(3)	1.29(1)	1.29(1)	5.06(5)	5.28(1)

The data shown in the Figure 3.16 and Table 3.12 above provides important details about the particle size distribution of the synthesised Y-ZrP samples. It can be observed from the data shown that most of the synthesised Y-ZrP samples have a uniform particle size ($D = 0.9$) in the range of 1 μm to 1.5 μm which is in correlation to the SEM analysis done before. However, there was an increase in particle size for both 15% and 20% Y-ZrP samples that were hydrothermally synthesised, along with the 20% Y-ZrP sample synthesised by a conventional reflux route.

The study from the use of particle size distribution gives a very important insight to the phase purity as it can list out all the different particles which may be present in a biphasic sample and can therefore yield distinct and separated peaks indicating the presence of two or more different types of crystals present. However, this hypothesis can be limited to samples that can have amorphous components which also provide different particle sizes as compared to crystals and give a high background in the XRD patterns, which was not present in our case. Also, the presence of different types of arrangement in crystals like the block type, plate type or the needle type, etc can also lead to the occurrence of different particle size peaks, as seen above in the synthesised α -ZrP samples. Further, the efficiency of sample preparation and other physical properties of the sample along with set machine parameters can greatly influence the particle size distribution and can therefore give erroneous results. But overall, it can be concluded from the analysis data presented above that most of the synthesised Y-ZrP samples are single phase in nature with a uniform particle size distribution of approximately 1.2 μm up till 15% yttrium substitution.

3.2.5 BET surface area analysis

It is of importance to analyse the surface area of the synthesised Y-ZrP products to note any changes in the morphology or arrangement of layers within the samples. A summary of results from all the synthesised Y-ZrP samples are shown in the Figure 3.17 below.

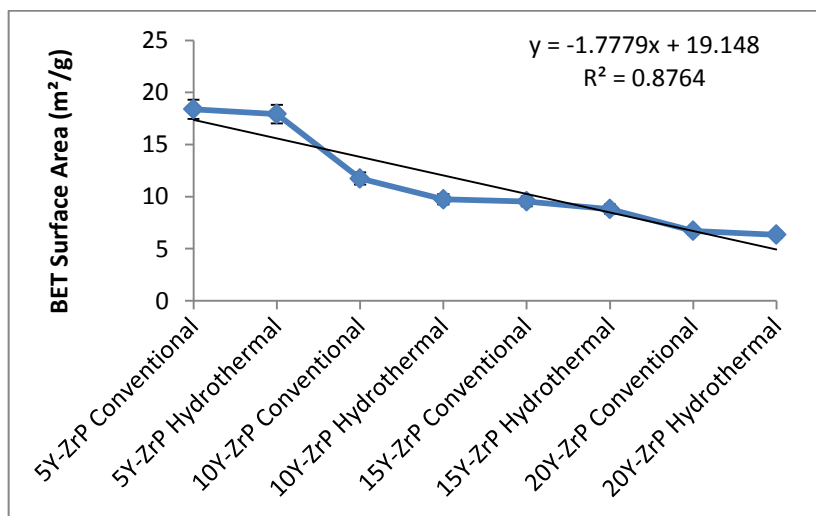


Figure 3. 17 BET surface area of the synthesised Y-ZrP samples

It can be seen from the Figure 3.17 above that there is a sharp decrease in the BET surface area of the synthesised Y-ZrP samples as the amount of yttrium substitution is increased from 5% to 15%, irrespective of the route of synthesis. However, there is little difference between the 15% and 20% Y-ZrP products. The reason for this can be accounted to more uniform and single phase particles as compared to the mixed phase products with different individual particle sizes that can affect the specific surface area. However, the general decrease in the surface area with respect to increasing yttrium substitution is accounted for the unit cell in one axis due to substitution of the larger Y^{3+} ion (ionic radius = 1.04 Å) in place of smaller Zr^{4+} ion (ionic radius = 0.86 Å). The resulting phenomenon is consistent with a similar research done for Ru substitution in strontium titanate perovskite lattice, where the increasing Ru substitution caused a decrease in the BET surface area [31-33]. Also as shown previously that the 5% and 10% Y-ZrP samples consists of more regular sized particles of 1-2 µm and the products are single phased as compared to the 15% and 20% Y-ZrP samples that consists of larger particle sizes (5 µm), probably due to biphasic components. Hence the surface area for the 15% and 20% Y-ZrP consisting of larger particles is expected to be lesser as compared to the smaller particles present in the 5% and 10% Y-ZrP samples, as shown in the figure above.

3.2.6 FT-IR of synthesised Y-ZrP

The changes in the Y-ZrP samples as a result of the yttrium substitution such as the decrease in surface area and uniformity of the particle size, etc. calls for a study into the chemical environment and types of bonding present in these samples. Therefore, an FT-IR analysis was done to investigate any changes in the chemical bonding of the synthesised Y-ZrP samples and the results are shown in Figure 3.18.

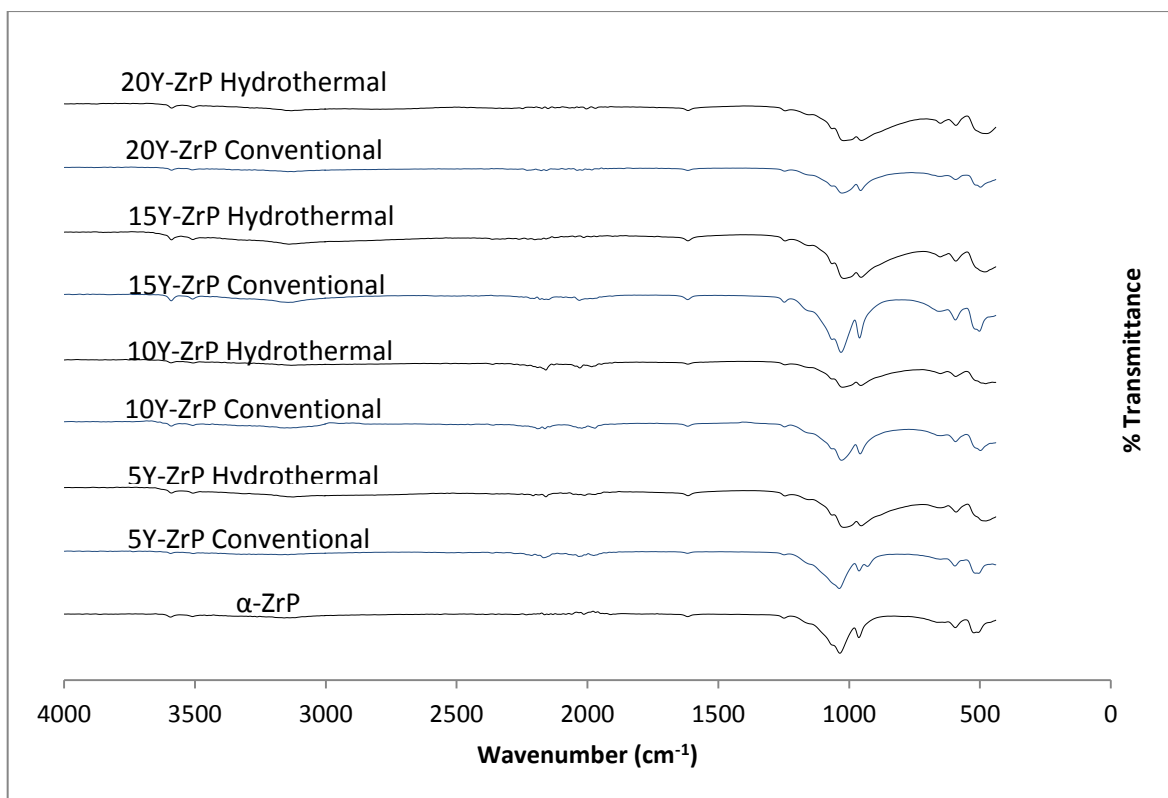


Figure 3. 18 FT-IR of the synthesised Y-ZrP samples

The assignment of the peaks observed in the FT-IR spectrum of a typical Y-ZrP sample is given in the Table 3.13 below.

Table 3. 13 Assignment of peaks in FT-IR spectrum

Peak Wavenumber (cm ⁻¹)	Chemical bonds
502.73	O-P-O deformation
594.09	P-OH (out of plane)
655.33	O-H (out of plane)
960.31	P-O bending (in plane)
1031.03	P-O stretching (asym)
1247.65	P-O-H deformation
1617.22	O-H bending (asym)
2181.50	P-OH
2204.70	P-OH
3143.68	O-H stretching (sym)
3508.99	O-H stretching (asym)
3590.70	O-H stretching (asym)

The FT-IR analysis of the synthesised samples shown in Figure 3.18 above shows a changing pattern in the FT-IR pattern for different routes of Y-ZrP synthesis. It was observed that the intensity of two peaks at 960 cm^{-1} and 1027 cm^{-1} decreases with yttrium substitution of zirconium in the α -ZrP structure. The decreasing intensity of the peak at 1027 cm^{-1} is more profound in the hydrothermal refluxed Y-ZrP samples as compared to the conventional reflux route. This observation is made even for the synthesised α -ZrP samples, but since the difference in peak intensities for the Y-ZrP series were quite small, it is not noticed.

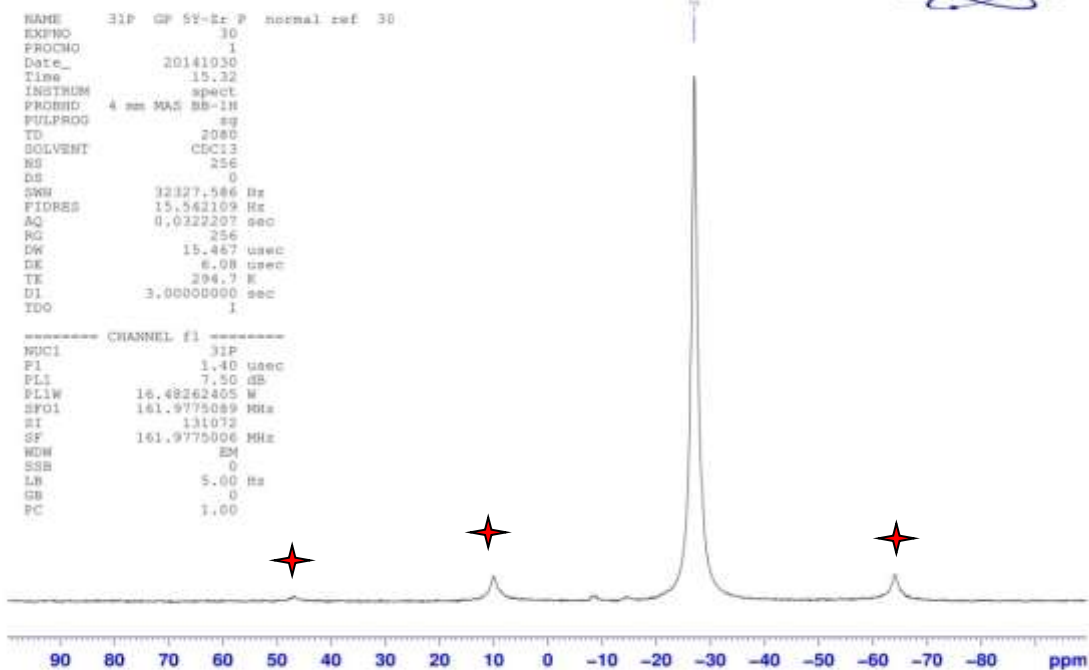
It is observed in the synthesised Y-ZrP samples that as the yttrium substitution percentage increases, the intensity of the two peaks at 960 cm^{-1} and 1027 cm^{-1} starts decreasing. Noticeably, the intensity of the peak at 1027 cm^{-1} is higher than that of the peak at 960 cm^{-1} (approximately 60% higher in conventional reflux and 30% higher in hydrothermal reflux). But this difference in the peak intensities narrows down gradually for the conventionally refluxed Y-ZrP samples and almost becomes close to 0.1% for the hydrothermally refluxed Y-ZrP samples, as the yttrium substitution increases. This explains that the phosphate bond's stretching is reduced which is indicative of possible lattice distortion. Also there is a very slight shift in the peak positions of these two peaks in the range of $1\text{-}10\text{ cm}^{-1}$ but it is difficult to provide an exact correlation of the shift with regards to the yttrium substitution.

3.2.7 Solid State ^{31}P MAS-NMR of Y-ZrP samples

The synthesised Y-ZrP from both the routes of synthesis were analysed by the solid state ^{31}P MAS-NMR and the resulting spectra are shown in figures 8-10 in Appendix 1. All the resonant peaks in this study are shifted by approximately 7.4 ppm upfield, relative to the ammonium phosphate reference.

The results obtained a single peak present at approximately -27.1 ppm for the conventional Y-ZrP products, while two peaks at approximately -8.1 ppm and -27.1 ppm were present for hydrothermal samples, as shown in Figure 3.19 below.

31P GP 5Y-Zr P normal



31P GP 5Y-Zr P Bomb 1
 Bottle 25

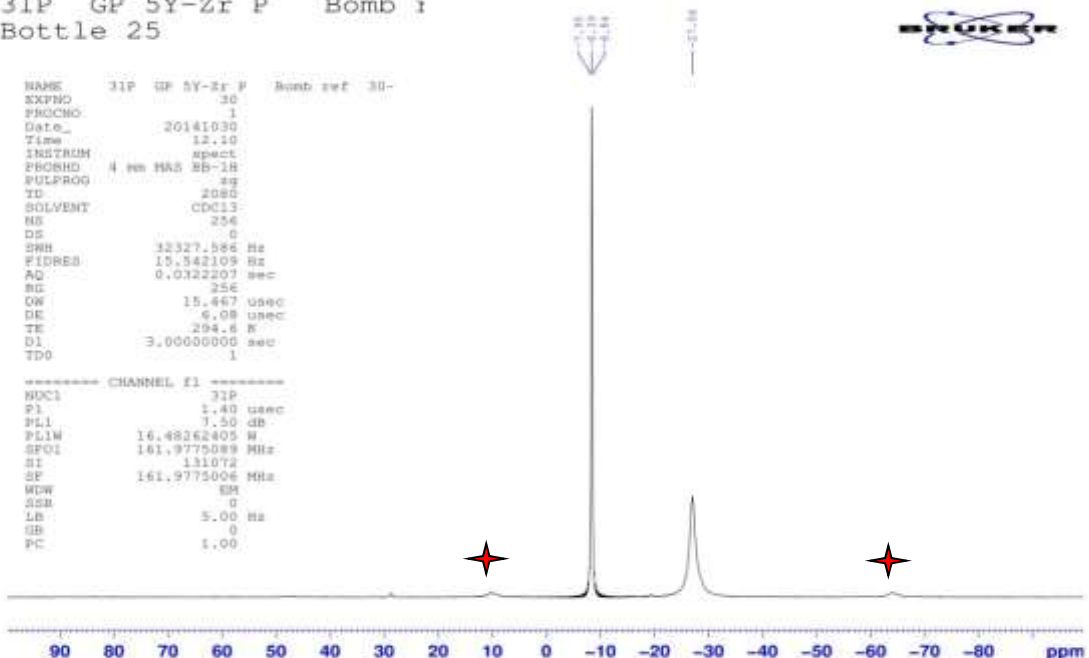


Figure 3. ^{31}P NMR for 5% Y-ZrP via conventional (top) & hydrothermal (bottom) route (spinning side bands shown as \star)

The results obtained from the NMR study clearly indicate that the synthesised Y-ZrP samples are single phase products consistent with α -ZrP. However, it is observed from the NMR spectrums that conventionally refluxed Y-ZrP samples gave a single narrow peak at -27.1 ppm approximately, whereas the hydrothermally synthesised Y-ZrP products gave an intense peak at -8.1 ppm along with a smaller peak at -27.1 ppm with a ratio of 3:1 respectively. This pattern is consistent with all the conventionally and hydrothermally synthesised Y-ZrP samples.

The presence of a strong peak at -8.1 ppm can be attributed to the minor peak which was also present in the hydrothermally refluxed pure α -ZrP at a very low intensity, as shown in figure 3.19 above. Therefore it can be understood that most of the yttrium substitution took place at the O-Zr sites which were having some unshielded protons from the phosphate groups that increased the dipolar interactions between the protons and the phosphorus nuclei and hence increased the peak intensity due to cross polarisation. The narrow and sharp appearance of this peak as compared to the relatively broader peaks of the parent α -ZrP might be due to the line broadening effect caused by fast decay of the nuclei signal. In order to determine if a two-phase product had been formed, YPO_4 was synthesised and the ^{31}P NMR spectrum obtained for comparison (as shown in figure 11 in Appendix 1). The spectrum consisted of an intense peak with a chemical shift of -19.34 ppm which is consistent with the previous findings [34-36]. Two minor peaks were also present at -8.29 ppm and -15.54 ppm which might be attributed to the paramagnetic interactions of the doped impurities of rare-earth metals present along with pure YPO_4 crystals, as found in literature [35-36]. It should be noted here that the peak at -8.29 should not be confused with the peak at -8.1 as the latter was also present in the hydrothermal and microwave refluxed α -ZrP, so it cannot be assigned to the YPO_4 phase.

Therefore, the analysis of the ^{31}P MAS-NMR spectrum reveals that the possibility for the presence of a second YPO_4 phase in 5-15% Y-ZrP samples is overruled since there was no characteristic chemical shift present at -19.34 ppm. However, it can be well possible that the increased intensity of the peak at -8.1 ppm is due to the increased presence of $[\text{H}_2\text{PO}_4]^-$ groups in addition to HPO_4^{2-} groups due to the charge imbalance created by yttrium doping. The integrated peak areas show that the peak at -27.1 ppm is 1.5 times that at -8.1 ppm. This is a supporting evidence to

prove that there are fairly good amount of $[\text{H}_2\text{PO}_4]^-$ groups giving resonance intensity at -8.1 ppm together with HPO_4^{2-} groups at -27.1 ppm. However, the 20% substituted products shows an emergence of a peak at -19.34 ppm which is characteristic of YPO_4 phase. This clearly shows that all mixed phase products will have a distinct peak at -19.34 ppm irrespective of the other characteristic peaks of $\alpha\text{-ZrP}$. Hence it can be confidently concluded that the synthesised batch of Y-ZrP products are single phase up to 15% yttrium substitution and exhibit similar chemical environment as compared to the parent $\alpha\text{-ZrP}$. But a detailed study of the crystal structure is required to get a further insight about the sites of yttrium substitution.

3.2.8 Rietveld Refinement of Y-ZrP

XRD data was obtained for all Y-ZrP synthesised to perform the Rietveld refinement using the GSAS/EXPGUI software package. ^[39, 40] Samples up to 15% yttrium substitution were deemed to be single phase therefore these samples were successfully refined using the structural model of Clearfield and Smith ^[23] for $\alpha\text{-ZrP}$ using the space group $P2_1/c$. The synthesised Y-ZrP samples were refined according to values for their molar compositions and so the fractional occupancies were also set likewise. The temperature factors for each atom type were constrained to the same value during the initial stages of the refinement. The compositions were also fixed according to the XRF results and the refinement for phase fractions were done. The results for the structural parameters and lattice coordinates are presented below along with the final Rietveld plots. The refined bond angles are shown in the table 2 and table 3 of Appendix 2.

Samples with 20% yttrium substitution had a presence of YPO_4 impurity phase and therefore, these samples were excluded from Rietveld refinement. Also the microwave route was not applied for the synthesis of Y-ZrP products, hence only conventional and hydrothermal refluxed samples were refined.

Table 3. 14 Refined structural parameters with esd's for conventional Y-ZrP

Parameters	5% Y-ZrP	10% Y-ZrP	15% Y-ZrP
a/Å	9.0537(4)	9.0660(4)	9.0546(3)
b/Å	5.2860(2)	5.2921(3)	5.2860(2)
c/Å	16.2372(9)	16.2501(10)	16.2380(6)
β /deg	111.400(3)	111.404(3)	111.397(2)
V/Å ³	723.52(7)	725.88(8)	723.633(5)
M-O(1)/Å	1.975(6)	2.039(6)	1.988(3)
M-O(2)/Å	2.13747(7)	2.09051(8)	2.08(5)
M-O(3)/Å	2.00883(7)	2.06067(8)	2.041(6)
M-O(5)/Å	2.113(3)	2.056(4)	2.006(7)
M-O(6)/Å	2.088(5)	2.113(5)	2.046(5)
M-O(8)/Å	2.104(6)	2.059(6)	2.105(3)
Avg. M-O/Å	2.07105	2.06969	2.04433
χ^2	7.295	2.880	4.039
R _p /%	9.41	7.13	8.18
R _{wp} /%	13.42	9.97	10.92
R _F ² /%	11.18	7.95	10.98

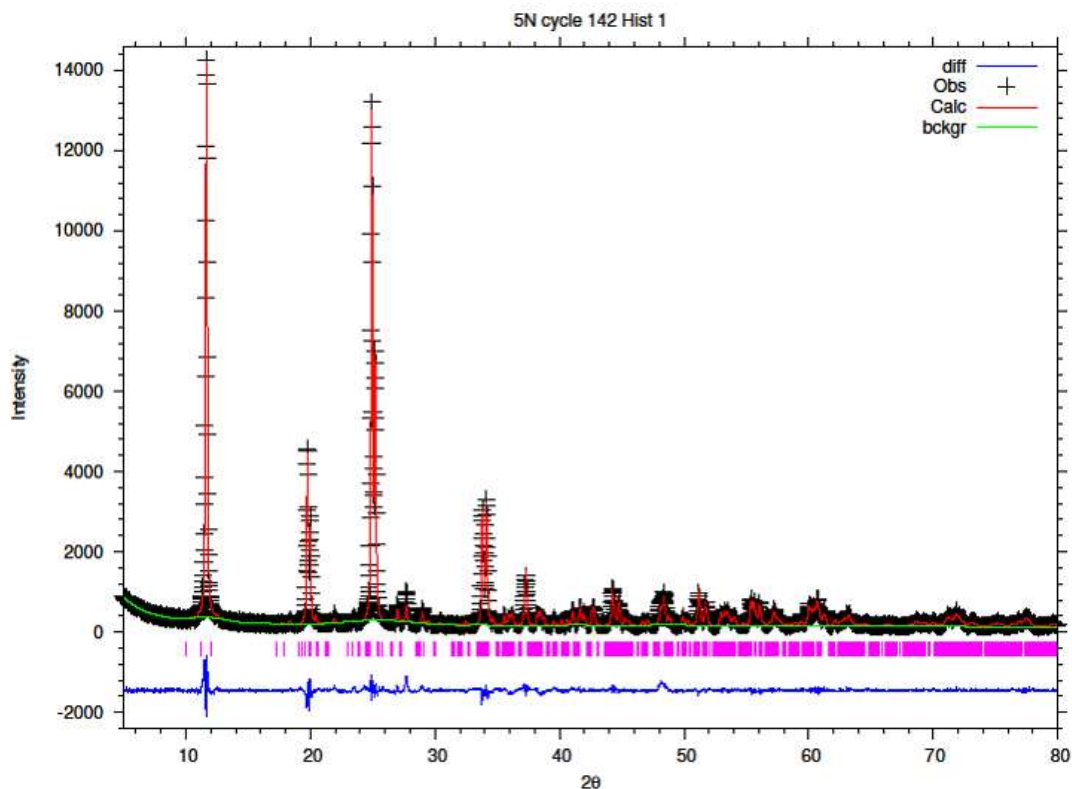


Figure 3. 20 Final observed (cross), calculated (red line) and difference (blue bottom) X-ray diffraction profiles from Rietveld refinement for conventional 5% Y-ZrP

Table 3. 15 Refined fractional atomic coordinates and isotropic thermal displacement parameters for conventional 5% Y-ZrP

Atom	x	y	z	$U_{\text{iso}} (\times 10^2) / \text{\AA}$	Occupancy
Zr	0.7620(4)	0.234(1)	0.5147(2)	1.40(3)	0.947(6)
P(1)	0.0039(3)	0.7438(1)	0.6119(2)	0.51(9)	
P(2)	0.4742(3)	0.2558(2)	0.1034(1)	0.32(9)	
O(1)	0.1086(4)	0.8068(2)	0.5590(1)	1.28(4)	
O(2)	0.9376(4)	0.4868(1)	0.6000(2)	2.42(3)	
O(3)	0.8726(3)	0.9318(1)	0.5880(1)	1.15(7)	
O(4)	0.1076(2)	0.7508(2)	0.7150(1)	1.91(7)	
O(5)	0.3476(2)	0.0578(1)	0.0610(2)	1.66(4)	
O(6)	0.4216(3)	0.5048(1)	0.0680(1)	1.15(7)	
O(7)	0.51248(3)	0.2578(1)	0.2040(2)	2.04(3)	
O(8)	0.3755(1)	0.8148(2)	0.9090(2)	1.53(7)	
O(9)	0.2545(2)	0.2658(1)	0.2580(1)	3.05(7)	
Y(13)	0.7620(4)	0.234(1)	0.5147(2)	1.41(6)	0.053(4)

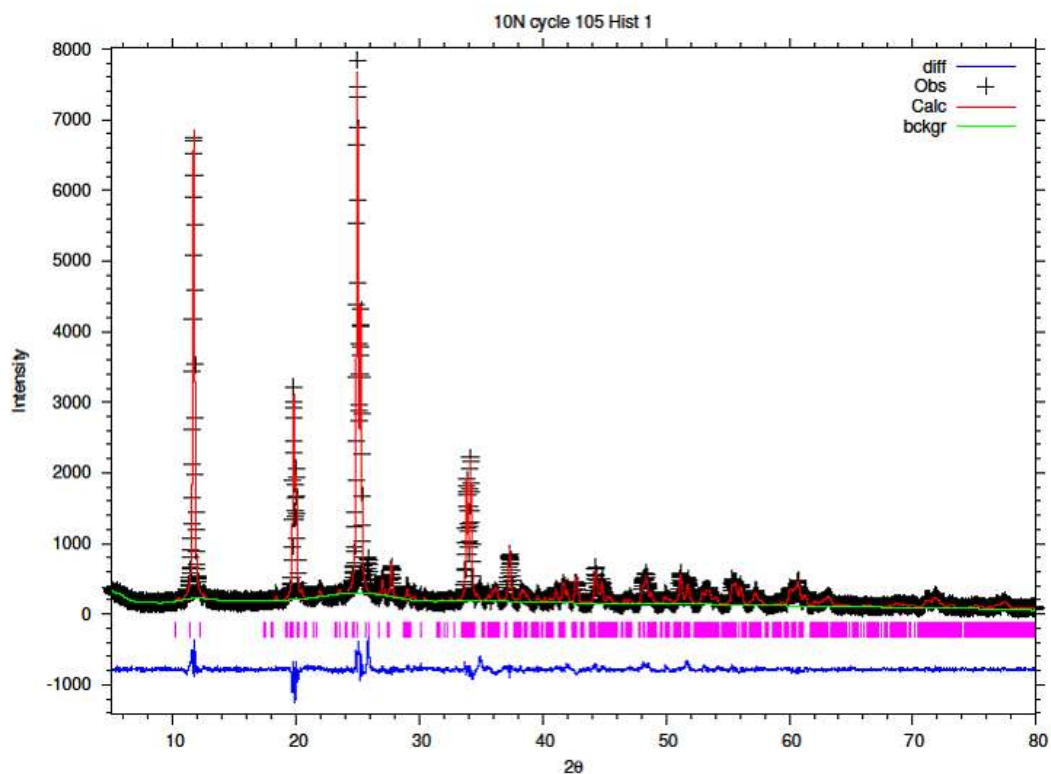


Figure 3. 21 Final observed (cross), calculated (red line) and difference (blue bottom) X-ray diffraction profiles from Rietveld refinement for conventional reflux 10% Y-ZrP

Table 3. 16 Refined fractional atomic coordinates and isotropic thermal displacement parameters for conventional refluxed 10% Y-ZrP

Atom	x	y	z	$U_{iso} (x10^2) / \text{Å}$	Occupancy
Zr1	0.7612(4)	0.258(1)	0.5149(2)	2.05(9)	0.900(2)
P1	0.0014(3)	0.760(1)	0.6133(2)	2.68(9)	
P2	0.4717(4)	0.263(1)	0.1048(2)	2.5(1)	
O1	0.1055(4)	0.813(1)	0.5601(2)	1.91(1)	
O2	0.934(2)	0.493(1)	0.60105(1)	3.05(6)	
O3	0.869(2)	0.948(2)	0.58904(1)	1.79(9)	
O4	0.104(1)	0.767(1)	0.71605(2)	2.54(8)	
O5	0.3445(4)	0.064(1)	0.06205(2)	2.29(6)	
O6	0.4185(4)	0.521(1)	0.06905(1)	2.67(6)	
O7	0.512(1)	0.264(1)	0.2051(1)	2.17(9)	
O8	0.375(1)	0.821(2)	0.9100(2)	3.68(8)	
O9	0.2545(4)	0.272(1)	0.2590(1)	1.61(1)	
Y13	0.7612(4)	0.258(1)	0.5149(2)	2.05(9)	0.100(9)

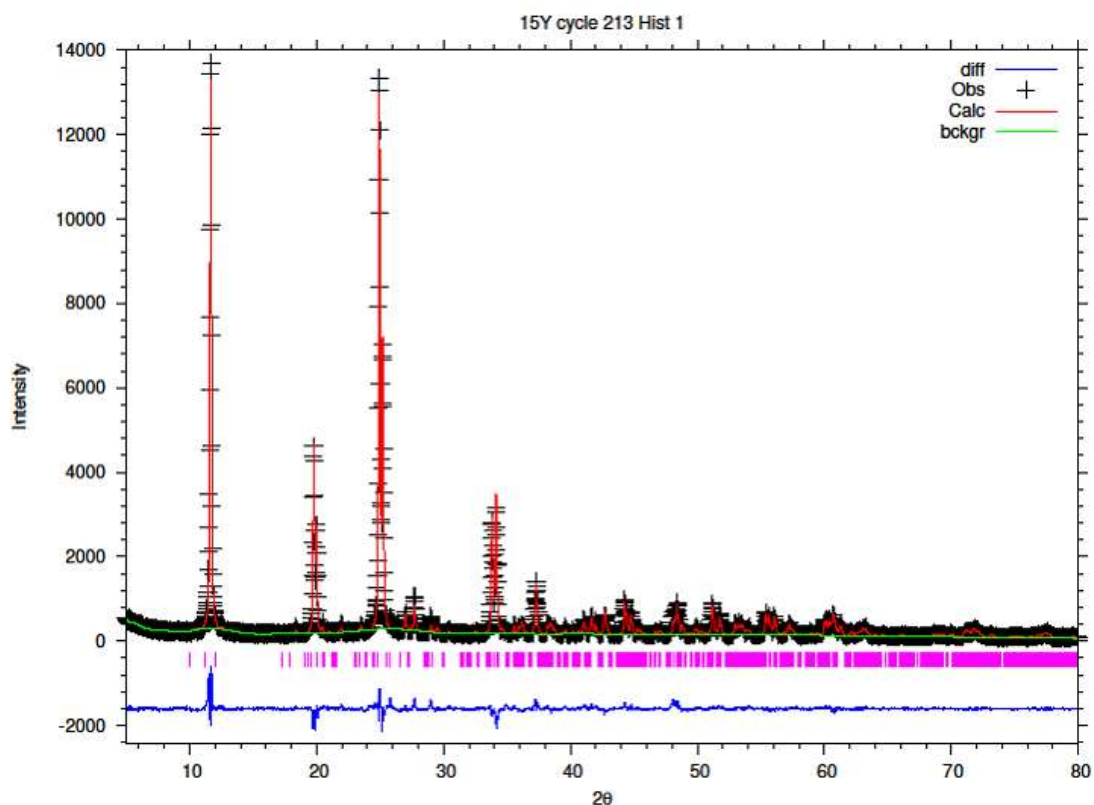


Figure 3. 22 Final observed (cross), calculated (red line) and difference (blue bottom) X-ray diffraction profiles from Rietveld refinement for conventional reflux 15% Y-ZrP

Table 3. 17 Refined fractional atomic coordinates and isotropic thermal displacement parameters for conventional 15% Y-ZrP

Atom	x	y	z	$U_{\text{iso}} (\times 10^2) / \text{\AA}$	Occupancy
Zr1	0.7591(7)	0.2553(4)	0.5124(7)	3.08(5)	0.701(1)
P1	0.006(3)	0.758(2)	0.6092(2)	3.66(8)	
P2	0.4691(4)	0.2606(2)	0.1007(1)	3.47(9)	
O1	0.1031(3)	0.8116(2)	0.5562(1)	4.39(8)	
O2	0.9320(3)	0.492(2)	0.5972(2)	5.52(3)	
O3	0.8670(4)	0.9466(2)	0.5852(2)	4.36(3)	
O4	0.1021(4)	0.7656(1)	0.71228(2)	5.02(8)	
O5	0.3420(2)	0.063(2)	0.05828(2)	4.76(6)	
O6	0.4160(2)	0.5196(2)	0.06528(1)	4.26(3)	
O7	0.5100(4)	0.2626(1)	0.20128(1)	5.14(9)	
O8	0.3731(3)	0.819(1)	0.9063(2)	4.64(4)	
O9	0.2521(3)	0.271(2)	0.2553(2)	5.16(3)	
Y13	0.7591(7)	0.2553(4)	0.5124(7)	3.08(5)	0.21(7)

Table 3. 18 Refined structural parameters with estimated standard deviations for hydrothermal Y-ZrP

Parameters	5% Y-ZrP	10% Y-ZrP	15% Y-ZrP
a/Å	9.0654(6)	9.0665(5)	9.0537(8)
b/Å	5.2943(4)	5.2927(3)	5.2861(5)
c/Å	16.2519(13)	16.2471(11)	16.2274(20)
β /deg	111.411(4)	111.409(3)	111.412(5)
V/Å ³	726.19(9)	725.83(8)	723.03(13)
M-O(1)/Å	1.971(8)	1.990(6)	1.944(11)
M-O(2)/Å	2.10842(10)	2.11268(9)	1.9429(2)
M-O(3)/Å	2.05864(10)	2.05222(8)	2.0564(2)
M-O(5)/Å	2.048(5)	2.054(4)	1.915(5)
M-O(6)/Å	2.107(6)	2.096(5)	1.993(8)
M-O(8)/Å	2.151(8)	2.118(6)	2.222(10)
Avg. M-O/Å	2.07401	2.07048	2.01222
χ^2	10.20	5.825	14.28
R _p /%	11.10	8.29	12.67
R _{wp} /%	15.93	12.34	18.68
R _F ²	15.08	11.70	17.64

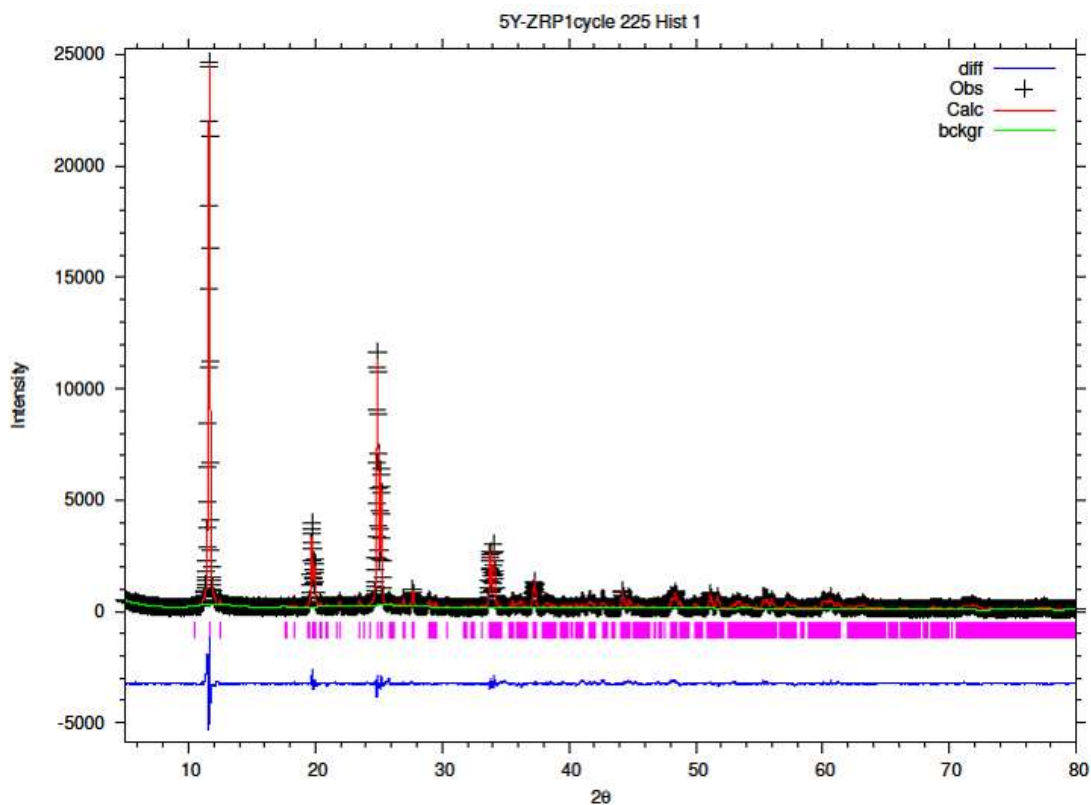


Figure 3. 23 Final observed (cross), calculated (red line) and difference (blue bottom) X-ray diffraction profiles from Rietveld refinement for hydrothermal 5% Y-ZrP

Table 3. 19 Refined fractional atomic coordinates and isotropic thermal displacement parameters for hydrothermal 5% Y-ZrP

Atom	x	y	z	$U_{\text{iso}} (\times 10^2) / \text{\AA}^2$	Occupancy
Zr1	0.7626(5)	0.266(1)	0.5126(2)	1.36(1)	0.943(1)
P1	0.0046(5)	0.769(1)	0.6110(2)	1.94(3)	
P2	0.4749(6)	0.272(1)	0.1025(2)	1.75(3)	
O1	0.1088(7)	0.823(1)	0.5581(3)	2.66(5)	
O2	0.9378(7)	0.503(1)	0.5991(3)	3.80(4)	
O3	0.8728(6)	0.958(2)	0.5871(3)	2.53(8)	
O4	0.1078(6)	0.777(2)	0.7141(2)	3.29(8)	
O5	0.3478(5)	0.0744(1)	0.0601(2)	3.04(4)	
O6	0.4218(5)	0.5314(1)	0.0671(1)	2.53(8)	
O7	0.5158(7)	0.274(1)	0.2031(1)	3.42(4)	
O8	0.3788(6)	0.831(1)	0.9081(2)	2.91(8)	
O9	0.2578(5)	0.2824(10)	0.2571(2)	4.43(8)	
Y13	0.7626(5)	0.266(1)	0.5126(2)	1.36(1)	0.057(1)

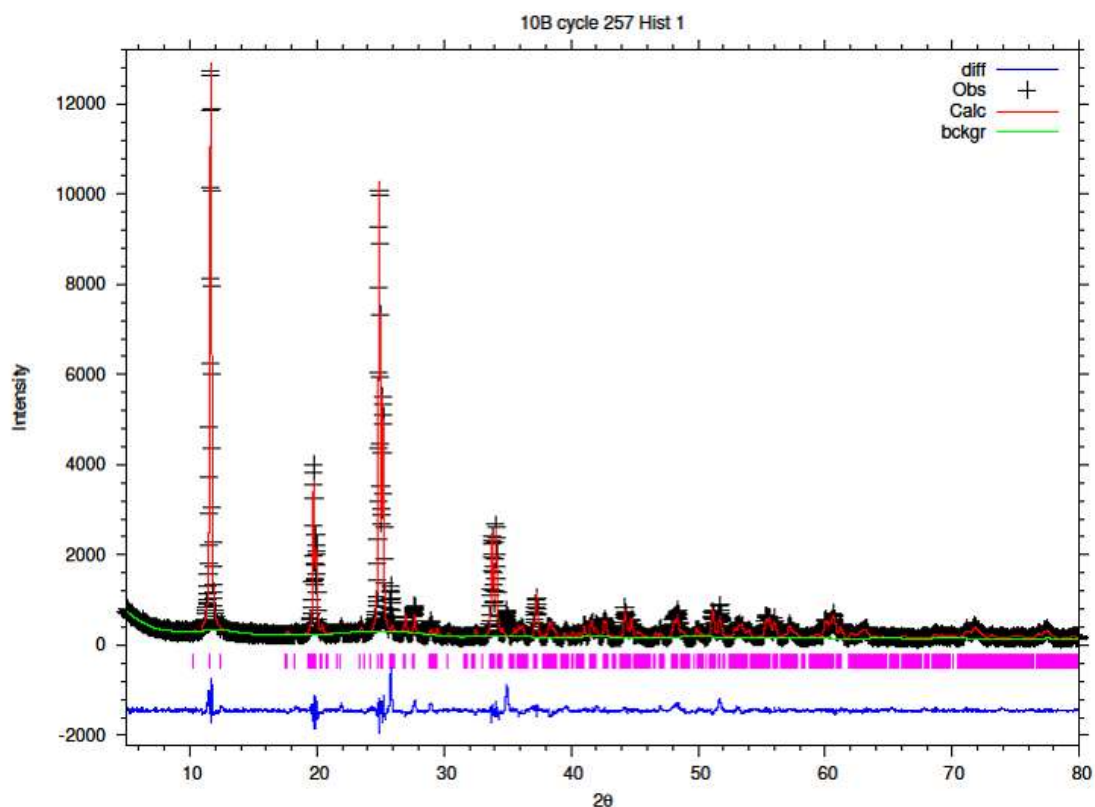


Figure 3. 24 Final observed (cross), calculated (red line) and difference (blue bottom) X-ray diffraction profiles from Rietveld refinement for hydrothermal 10% Y-ZrP

Table 3. 20 Refined fractional atomic coordinates and isotropic thermal displacement parameters for hydrothermal 10% Y-ZrP

Atom	x	y	z	$U_{iso} (x10^2) / \text{\AA}$	Occupancy
Zr1	0.7609(4)	0.259(1)	0.5134(2)	0.54(9)	0.900(5)
P1	0.0037(4)	0.7641(12)	0.6114(1)	1.50(9)	
P2	0.4740(4)	0.2670(2)	0.10287(2)	1.31(8)	
O1	0.10544(3)	0.8132(1)	0.5596(1)	2.23(1)	
O2	0.93444(4)	0.4932(2)	0.60064(2)	3.36(9)	
O3	0.86944(2)	0.9482(2)	0.58864(3)	2.10(1)	
O4	0.10444(3)	0.7672(2)	0.71564(1)	2.86(3)	
O5	0.34444(3)	0.0642(1)	0.06164(1)	2.61(9)	
O6	0.41844(2)	0.5212(1)	0.06864(2)	2.10(3)	
O7	0.5149(4)	0.2642(2)	0.20464(2)	2.99(9)	
O8	0.37544(4)	0.8212(2)	0.90964(1)	2.48(3)	
O9	0.2544(3)	0.272(1)	0.2586(1)	4.01(1)	
Y13	0.7609(4)	0.259(1)	0.5134(2)	0.54(9)	0.100(4)

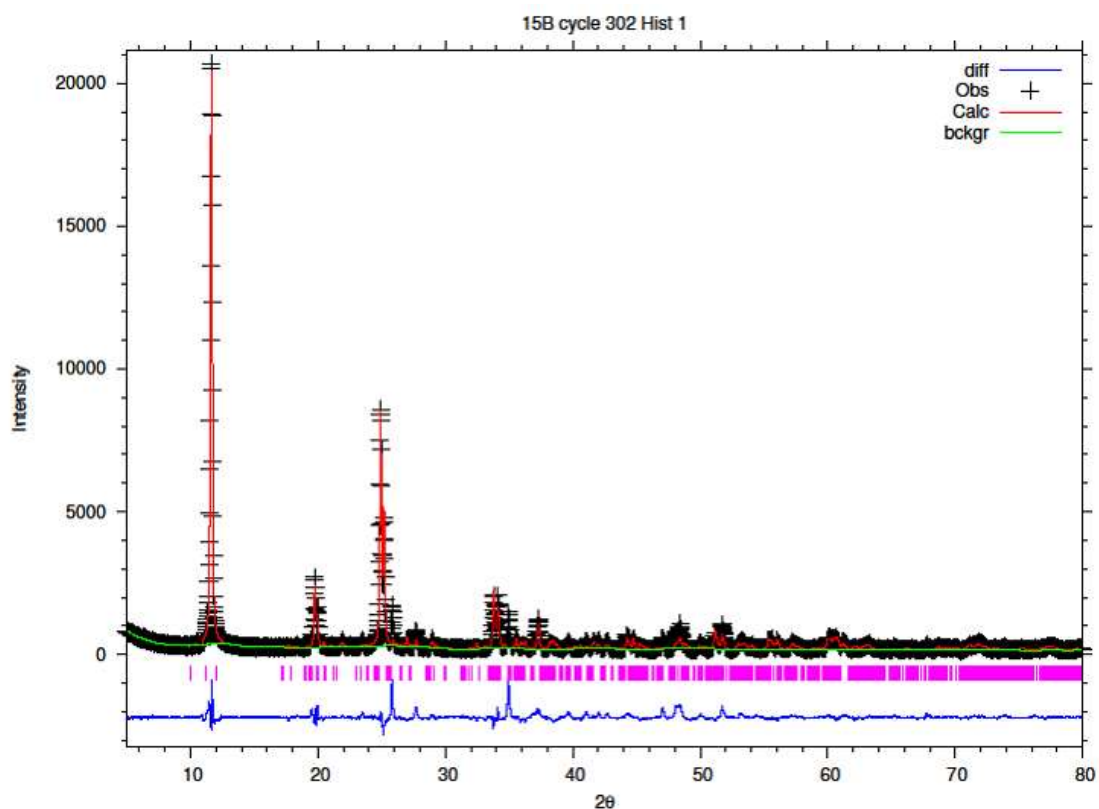


Figure 3. 25 Final observed (cross), calculated (red line) and difference (blue bottom) X-ray diffraction profiles from Rietveld refinement for hydrothermal 15% Y-ZrP

Table 3. 21 Refined fractional atomic coordinates and isotropic thermal displacement parameters for hydrothermal 15% Y-ZrP

Atom	x	y	z	$U_{\text{iso}} (\times 10^2) / \text{\AA}$	Occupancy
Zr1	0.7587(7)	0.259(2)	0.5089(3)	0.96(5)	0.828(5)
P1	0.0003(7)	0.767(2)	0.6167(3)	2.73(7)	
P2	0.4780(6)	0.299(1)	0.0883(3)	2.73(7)	
O1	0.1033(5)	0.808(3)	0.5564(2)	2.66(3)	
O2	0.9223(8)	0.478(3)	0.5874(4)	2.66(3)	
O3	0.8573(7)	0.933(4)	0.5754(4)	2.66(3)	
O4	0.0923(6)	0.751(2)	0.7024(3)	2.66(3)	
O5	0.3323(5)	0.069(2)	0.0484(3)	2.66(3)	
O6	0.4063(5)	0.506(2)	0.0554(2)	2.66(3)	
O7	0.5000(6)	0.255(2)	0.1900(4)	2.66(3)	
O8	0.3633(5)	0.826(4)	0.8964(2)	2.66(3)	
O9	0.2423(7)	0.257(1)	0.2454(3)	2.66(3)	
Y13	0.7587(7)	0.259(2)	0.5089(3)	0.96(5)	0.171(5)

The refinement results presented above for the synthesised Y-ZrP via two routes of synthesis are compared and analysed with regards to the model structure of α -ZrP as provided by Clearfield and Smith [3]. It can be observed from the conventionally refluxed Y-ZrP results shown in Table 3.14 that the refinement had a fairly good convergence fit for all the Y-ZrP products with almost similar structural parameters and atomic coordinates as compared to the synthesised α -ZrP. However, the 15% Y-ZrP sample showed a significant decrease in the average bond distance (2.04433 Å) as compared to 2.0631 Å for conventionally synthesised α -ZrP, showing a difference of 0.02 Å. This is accounted mainly due to the Zr – O(1) distance that was reduced by approximately 0.08 Å, in addition to other M – O bonds. On the other hand, 5% and 10% conventional refluxed Y-ZrP samples showed a slight increase in average bond distances as compared to synthesised α -ZrP, but followed a decreasing trend as the yttrium substitution increased.

The hydrothermally synthesised Y-ZrP products also followed a similar trend as that of conventionally synthesised samples but the decrease in the average bond distance for 15% Y-ZrP hydrothermally synthesised sample (2.01222 Å) was higher as compared to 15% conventional Y-ZrP (2.04433 Å). This is again accounted to the reduced Zr – O(1) distance which is lowered by approximately 0.11 Å.

Therefore, it is of interest to analyse the dimensions of unit cell in order to determine if the substitution of zirconium with yttrium follows the Vegard's law. The unit cell constants (a, b, c) along with the volume and average bond distances are plotted for both conventional and hydrothermal Y-ZrP samples as shown in Figures 3.26 and 3.27 below.

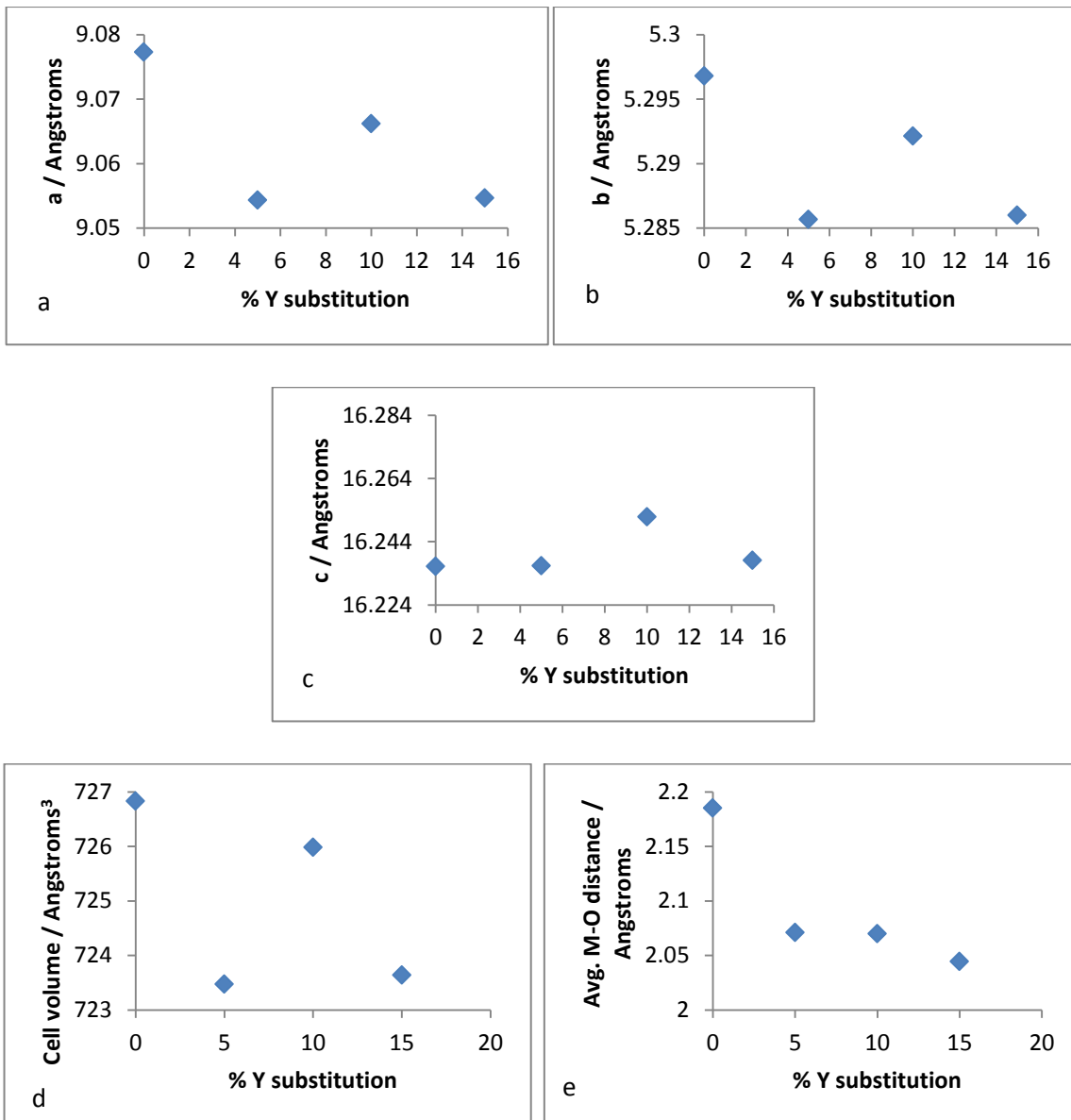


Figure 3. 26 Unit cell parameters for: (a) *a*-axis; (b) *b*-axis; (c) *c*-axis; (d) volume and (e) mean M-O distance versus % Y substitution for conventional Y-ZrP

It is observed from the above figure that the *a*-axis and *b*-axis are following a general decrease, whereas the *c*-axis is increasing slightly, with an increase in yttrium substitution. Also, the cell volume and average bond distances are decreasing in comparison to the synthesised α -ZrP. These results suggest that yttrium substituted samples were not following the Vegard's law, as principally the substitution of a smaller radius cation ($Zr = 0.86 \text{ \AA}$) with a larger radius cation ($Y = 1.04 \text{ \AA}$) will increase the lattice constants. The reason for deviation from Vegard's law can be attributed to many factors such as valence state, electron affinity and

percentage substitution of cation that can affect the bond lengths. This is confirmed from the results shown in Figure 3.26(e) that shows that the average bond length is reduced on yttrium substitution.

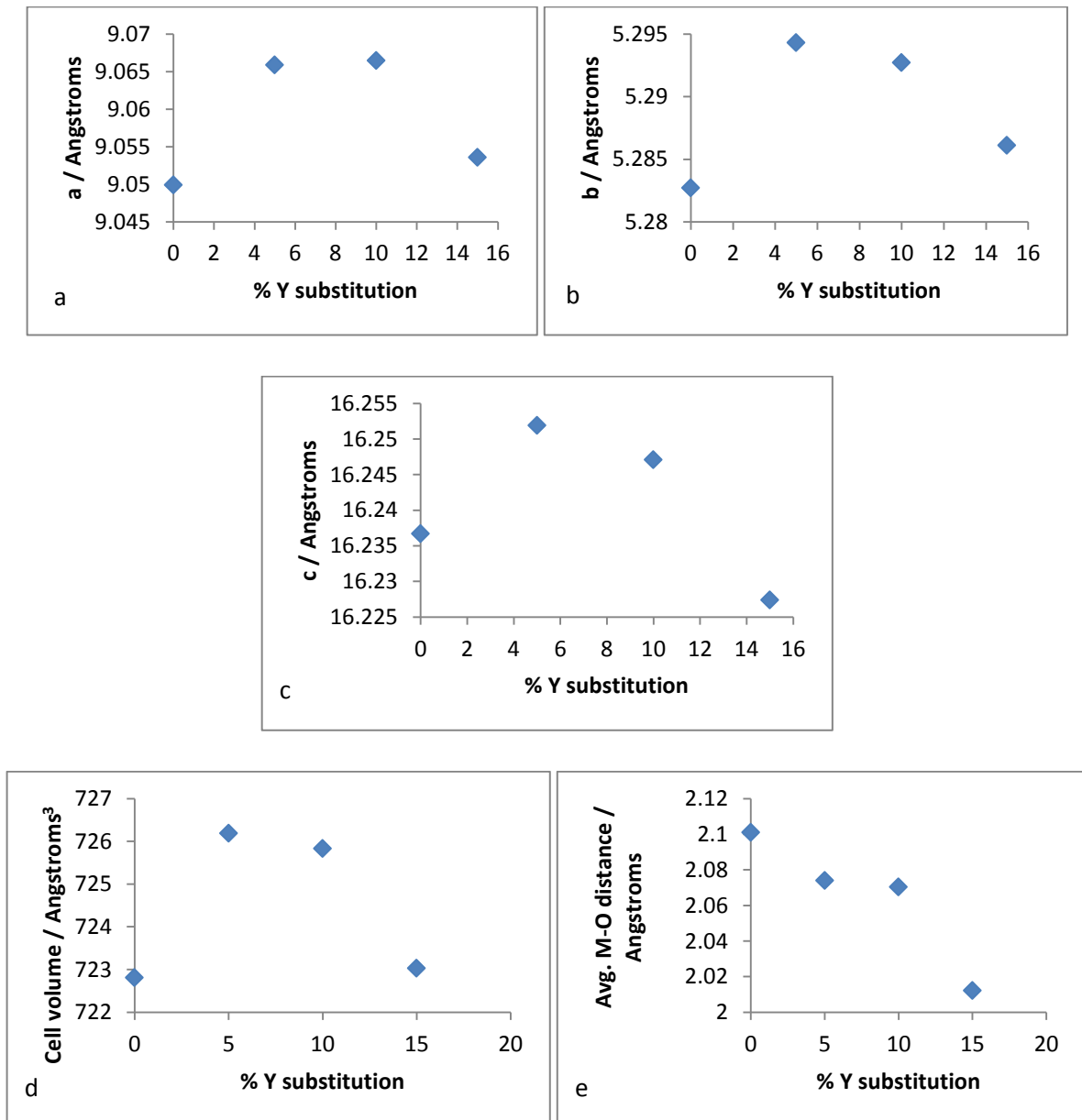


Figure 3. 27 Unit cell parameters for: (a) *a*-axis; (b) *b*-axis; (c) *c*-axis; (d) volume and (e) mean M-O distance versus % Y substitution for hydrothermal Y-ZrP

The results shown for hydrothermal Y-ZrP samples in Figure 3.27 shows an overall increase in the cell parameters (*a*, *b*, *c*) and cell volume of 5% and 10% Y-ZrP compared to α -ZrP, whereas, 15% Y-ZrP samples showed a subtle increase in *a*-axis and *b*-axis, but *c*-axis was reduced. However, the average bond distances were

reduced for Y-ZrP samples with an increase in yttrium substitution that indicates the deviation from Vegard's law. This might suggest that the substituted yttrium cations are clustered together accompanied by loss of zirconium cations which could result in vacancies in the metal sub-lattice. This may affect the stability of the system and hence could be the reason that is preventing the formation of solid solutions beyond 15% cationic substitution.

3.2.9 Acid Stability test

α -ZrP has been widely recognised as acid stable even at very low pH. [4, 38] Since Y-ZrP exhibits similar structural and chemical properties therefore it is likely that these samples will also be stable at low pH or in acidic medium. Acid stability tests were carried out for 5% and 10% Y-ZrP samples at 3M HNO₃ acid for 24hrs and powder XRD was used to analyse the samples. It was seen from the Figure 3.28 below that no structural damage occurred. Crystallinity was also not degraded as the peak intensities and background levels were similar to the crystalline α -ZrP.

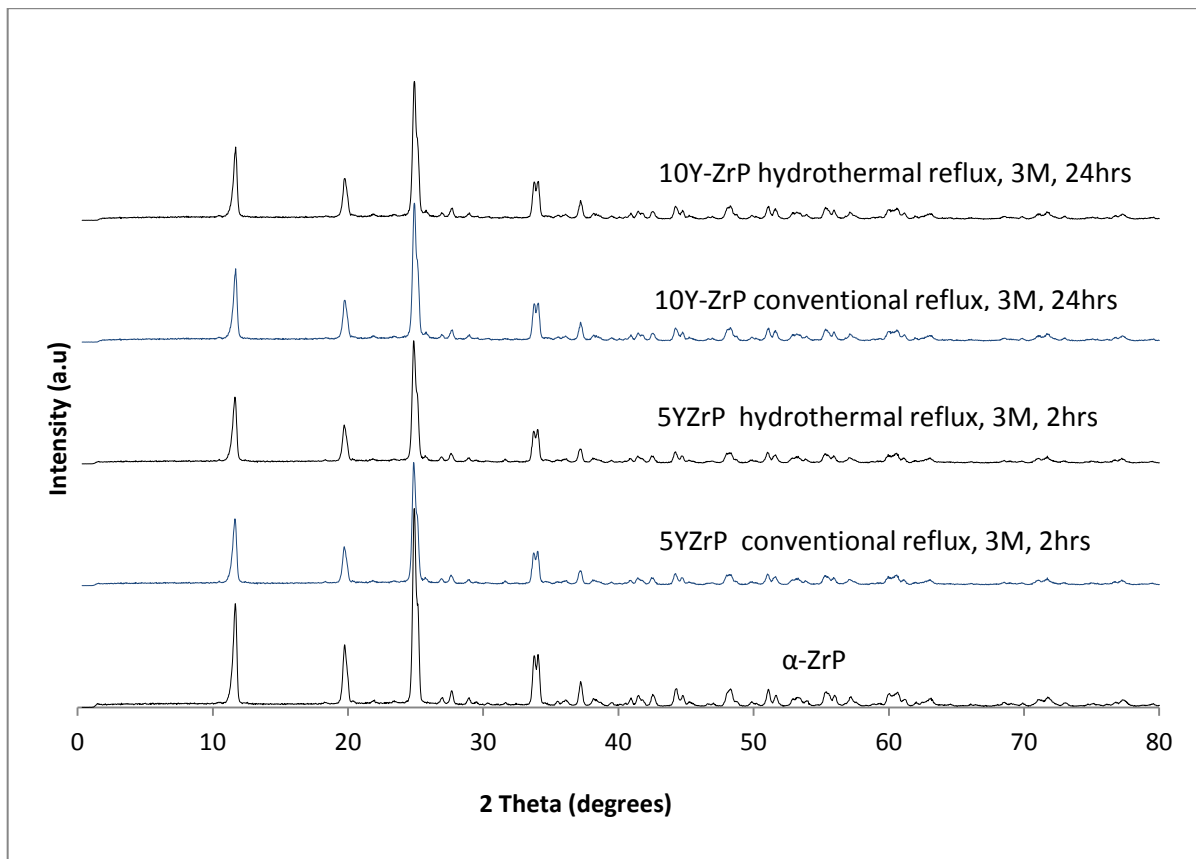


Figure 3. 28 Powder XRD results for acid stability test of 5% and 10% Y-ZrP products

The XRF analysis of the peak areas was also carried out to analyse any changes in the elemental composition of the Y-ZrP products after the acid treatment. The Table 3.22 below analyses the Y/Zr ratio of the 5% and 10% yttrium substituted products before and after the acid treatment. It is clear from the comparison shown that there seem to be no significant change in the composition of the samples after the acid treatment. Hence, it can be concluded that the synthesised Y-ZrP products are acid stable just like the parent α -ZrP.

Table 3. 22 XRF compositional analysis of the acid treated Y-ZrP products

Samples	Y/Zr % before acid treatment	Y/Zr % after acid treatment	Difference (before – after)
5Y-ZrP Conventional	2.25(2)	2.245(1)	0.005(1)
5Y-ZrP hydrothermal	4.87(1)	4.88(3)	-0.01(2)
10Y-ZrP Conventional	6.80(2)	6.78(3)	0.02(1)
10Y-ZrP hydrothermal	10.86(2)	10.80(5)	0.06(3)

3.3 Mixed phase Y-ZrP products

The substitution of yttrium beyond 20% into the α -ZrP lattice resulted in the formation of mixed phase products, irrespective of the route of synthesis employed in this work. An YPO_4 phase impurity was found in the XRD patterns and NMR spectra for a doping level of 20% and greater. Interestingly, they also formed separate pure tetragonal YPO_4 rich particles that were observed in the SEM/EDX analysis as discussed later. This suggests that there is a solution limit for yttrium substitution into the α -ZrP structure. Therefore, synthesis of Y-ZrP products beyond 20% substitution was abandoned and only few characteristic studies were done to confirm the presence of mixed phases.

3.3.1 X-ray diffraction (XRD) analysis

The results from some of the synthesised Y-ZrP samples with 25% and 30% yttrium substitution via both routes of synthesis is shown in the Figure 3.29 below.

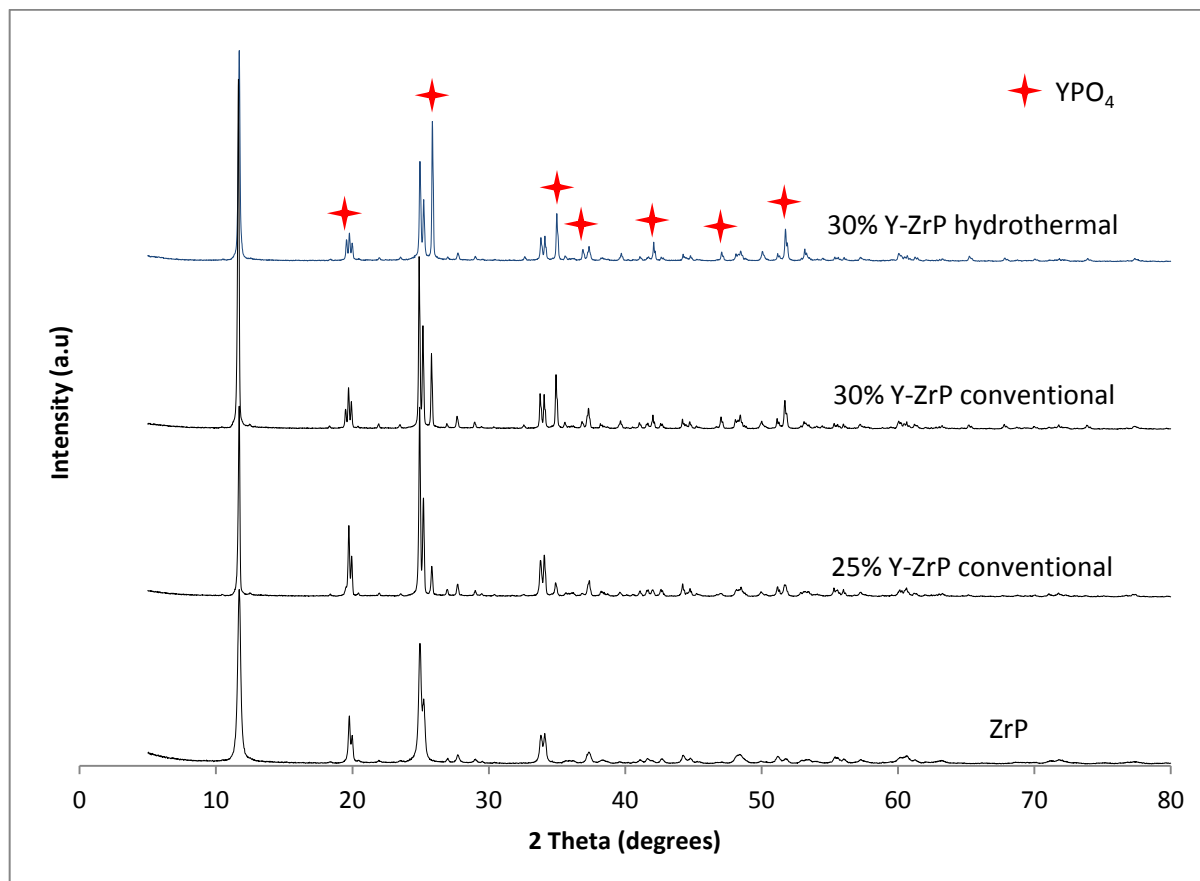


Figure 3. 29 XRD of mixed phase Y-ZrP synthesised via hydrothermal and conventional reflux

As discussed before, it can be seen from the above figure that the substitution of more than 20% yttrium resulted in the formation of an extra YPO₄ phase as evident from the observed characteristic peaks emerging alongside the α -ZrP pattern (shown as red stars). It can be seen that Y-ZrP samples above 20% yttrium content were formed of two separate crystalline phases consisting of either a distinct α -ZrP or partially exchanged Y-ZrP phase and a distinct YPO₄ phase products. The peak intensity of the YPO₄ rich phase increases with an increase in yttrium concentration above 20%. Thus, it is believed that some sort of solution chemistry is preventing the formation of a single phase product beyond 15% yttrium substitution, but nevertheless, all mixed phase products formed showed a high degree of crystallinity. So, it is concluded here that the possibility of synthesising single phase Y-ZrP is

restricted to less than 20% yttrium substitution for zirconium and the products formed are nearly isostructural to that of α -ZrP.

3.3.2 X-ray fluorescence analysis

The XRF analysis of the mixed phase Y-ZrP samples with 25% and 30% yttrium substitution from both synthesis routes are shown in Figure 3.30 below.

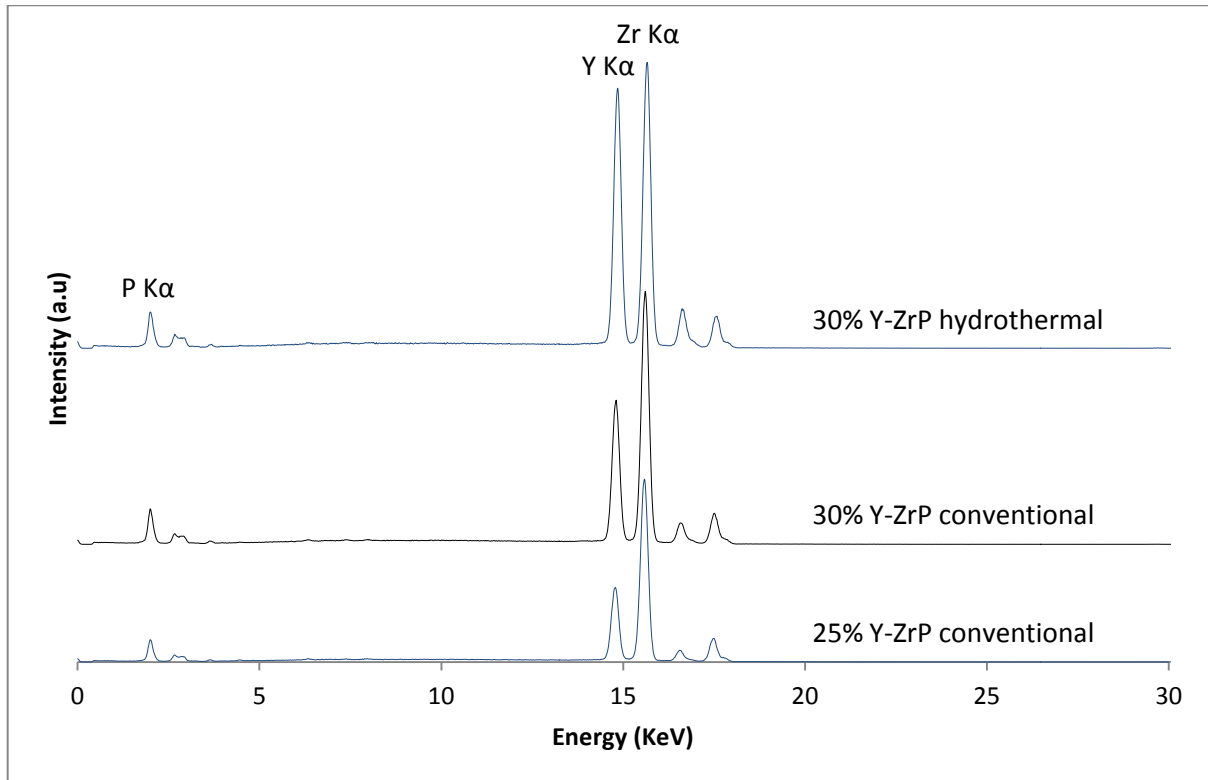


Figure 3. 30 XRF of mixed phase Y-ZrP synthesised via hydrothermal and conventional methods

It can be observed from the XRF results shown above that there seems to be high amount of yttrium content present in the synthesised samples. This is consistent with the XRD results shown in section 3.3.1 indicating two phase products where one of the phases is believed to be YPO_4 rich. The semi-quantitative results are shown in the Table 3.23 below to analyse the composition of these mixed phase products.

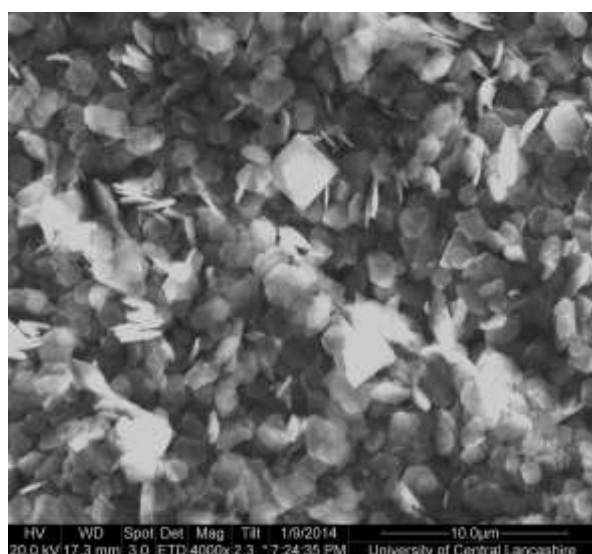
Table 3. 23 XRF compositional analysis for mixed phase Y-ZrP products

Sample	Theoretical yttrium %	Ratio of area under the XRF peaks (Y/Zr)	Calculated yttrium % from eq.1
25% conventional Y-ZrP	25%	0.453571(2)	24.785%
30% conventional Y-ZrP	30%	0.57729(1)	31.546%
30% hydrothermal Y-ZrP	30%	0.60784(8)	33.215%

It is evident from the XRF quantification of the mixed phase Y-ZrP samples that there is a good correlation between the theoretical composition and the calculated composition of the samples. This shows that most of the yttrium content is retained in the final product and as per the XRD results are seen, the resulting products are formed as mixed phase but crystalline in nature. Therefore, there is a good probability that most of the yttrium has either formed a separate YPO_4 phase and/or another zirconium substituted YPO_4 phase.

3.3.3 SEM analysis of the mixed phase products

The morphology and composition of the synthesised mixed phase Y-ZrP products is analysed by the use of SEM/EDX. The SEM images are shown in below in Figure 3.31 and the EDX compositional analysis is presented in Table 3.24.



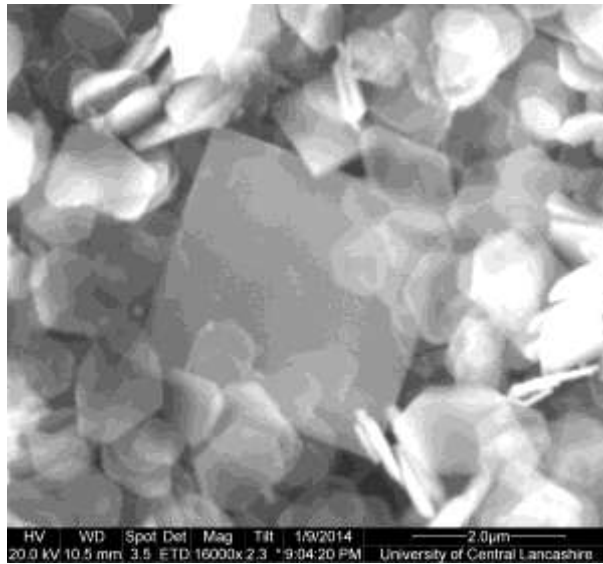
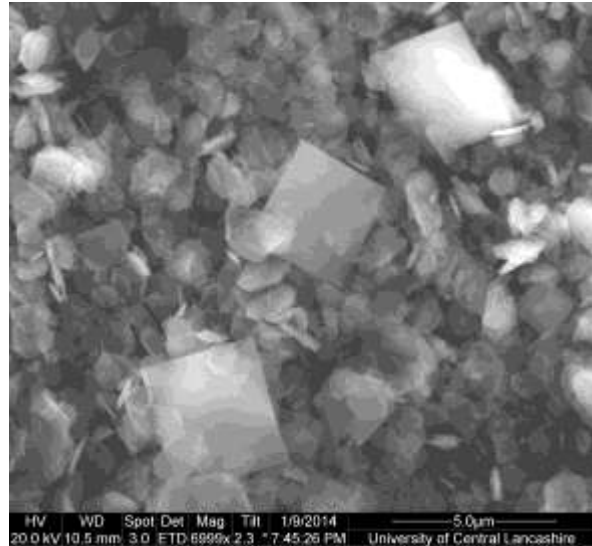


Figure 3. 31 SEM images for mixed phase 30% conventional Y-ZrP showing α -ZrP as hexagonal particles and tetragonal particles indicating a second phase of YPO_4

It can be seen from the SEM images that there are tetragonal particles alongside the well ordered hexagonal crystals characteristic of α -ZrP and Y-ZrP morphology. These tetragonal crystals are assumed to represent a pure YPO_4 crystal or a zirconium substituted YPO_4 crystalline product. In order to determine the actual composition of these two different crystal types present, EDX analysis was done at various regions and the compositional results are shown in the Table 3.24 below.

Table 3. 24 EDX analysis showing the compositions at different crystals in a mixed phase 25% Y-ZrP conventionally synthesised sample

Crystal type	Y atom%	Zr atom%	Y/Zr
Tetragonal	12.02	4.12	2.92
Tetragonal	12.54	4.12	3.04
Tetragonal	7.46	5.45	1.37
Hexagonal	2.96	7.26	0.41
Tetragonal	7.96	4.61	1.73
Tetragonal	11.24	3.02	3.72
Tetragonal	12.60	3.15	4.00
Hexagonal*	0.22	8.68	0.025
Tetragonal*	11.24	4.47	2.52
Hexagonal*	0.22	9.18	0.024
Hexagonal*	0.10	7.72	0.013
Hexagonal*	0.14	9.64	0.015
Tetragonal	12.08	6.57	1.84
Hexagonal*	0.52	7.43	0.070
Hexagonal	2.83	9.36	0.302
Hexagonal*	0.34	11.58	0.029
Hexagonal*	0.22	10.89	0.020
Hexagonal*	0.19	10.11	0.019
Hexagonal*	0.05	12.84	0.004
Hexagonal	0.97	9.98	0.097
Hexagonal	1.48	10.12	0.146
Hexagonal	0.87	8.69	0.100
Hexagonal*	0.20	9.94	0.020

Hexagonal* = purely α -ZrP crystals

The elemental analysis was carried out on multiple particle sites and it was attempted to narrow down the scanning area to a single particle type at a time. Single particles from both the hexagonal and tetragonal morphology were analysed for multiple acquisitions. However, it is understood that the actual area which is scanned is much bigger than a single crystal size even though a small spot size is used, due to the interaction of the sample with the incident beam at various orientations. Therefore, the presence of crystals below and neighbouring to the focussed area can affect the results.

But overall, the results from multiple EDX acquisitions as shown in the Table 3.24 above clearly depict the presence of three different types of phases in the sample. One phase is a hexagonal phase (shown as Hexagonal*) clearly marks the presence of pure α -ZrP crystals without any yttrium substitution because the ratio of Y/Zr atomic percent is very low (≤ 0.07). The second distinct phase consists of tetragonal crystals which clearly show yttrium rich content as with high Y/Zr atomic ratio (≥ 1). The tetragonal phase with Y/Zr atomic ratio of more than 2 can be classified as a pure YPO_4 phase, whereas those with Y/Zr atomic ratio of 1 – 2 can either be zirconium substituted YPO_4 or pure YPO_4 crystals. Finally, the third phase consists of hexagonal crystals which have a Y/Zr atomic ratio between 0.1 and 0.4 and can be assigned as single phase Y-ZrP crystals. Therefore, any further experiments and characterisation on the mixed phase samples with more than 20% yttrium content was not carried out and the work was focussed on applying the obtained single phase products for ion exchange purposes.

3.4 Other attempted mixed metal phosphates

Attempts were made to synthesise two other mixed metal phosphates based on the α -ZrP, namely iron (III)-zirconium phosphate and cerium (III)-zirconium phosphate respectively. These metals (Fe and Ce) were chosen as a form of trivalent (+3) ions for doping of the α -ZrP so that a charge imbalance can be created which is balanced by excessive protons that can improve the ion-exchange efficiency or selectivity of the exchangers. The synthesis of these metals was attempted using the chloride and nitrate metal salts and following the experimental procedure as outlined in Chapter 2. However, it was observed from the XRD studies that there

was no definite substitution of Ce^{3+} or Fe^{3+} ions into the α -ZrP lattice for the different synthetic routes.

3.4.1 XRD analysis of Ce-ZrP and Fe-ZrP

The XRD results for the Fe(III)-ZrP products are shown in the Figure 3.32 below.

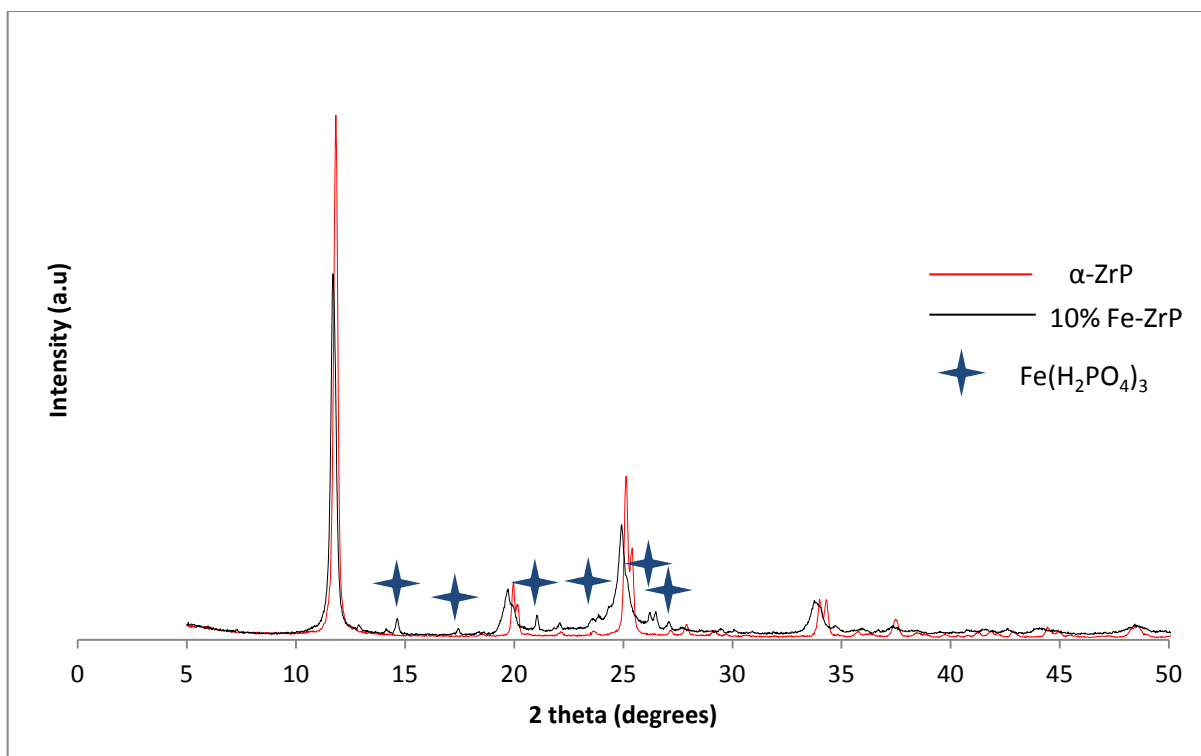


Figure 3. 32XRD patterns showing the mixed phase nature of 10% Fe(III)-ZrP

It is evident from the results shown above that Fe(III)-ZrP formed a mixed phase product with a clear presence of $\text{Fe}(\text{H}_2\text{PO}_4)_3$ (iron phosphate) peaks along with sharp characteristic peaks of α -ZrP, marked by blue stars. A single phase XRD pattern was not obtained for any synthesis with varying Fe:Zr ratio.

The XRD results for the Ce(III)-ZrP products are shown in the Figure 3.33 below. It is clear from the XRD patterns and the comparison with PDF ICDD database that there are additional peaks present in both the 5% and 10% cerium substituted α -ZrP, irrespective of the synthetic route. The peaks shown as red stars in the Figure 3.33 below indicate the presence of a cerium phosphate (CePO_4) or Monazite phase.

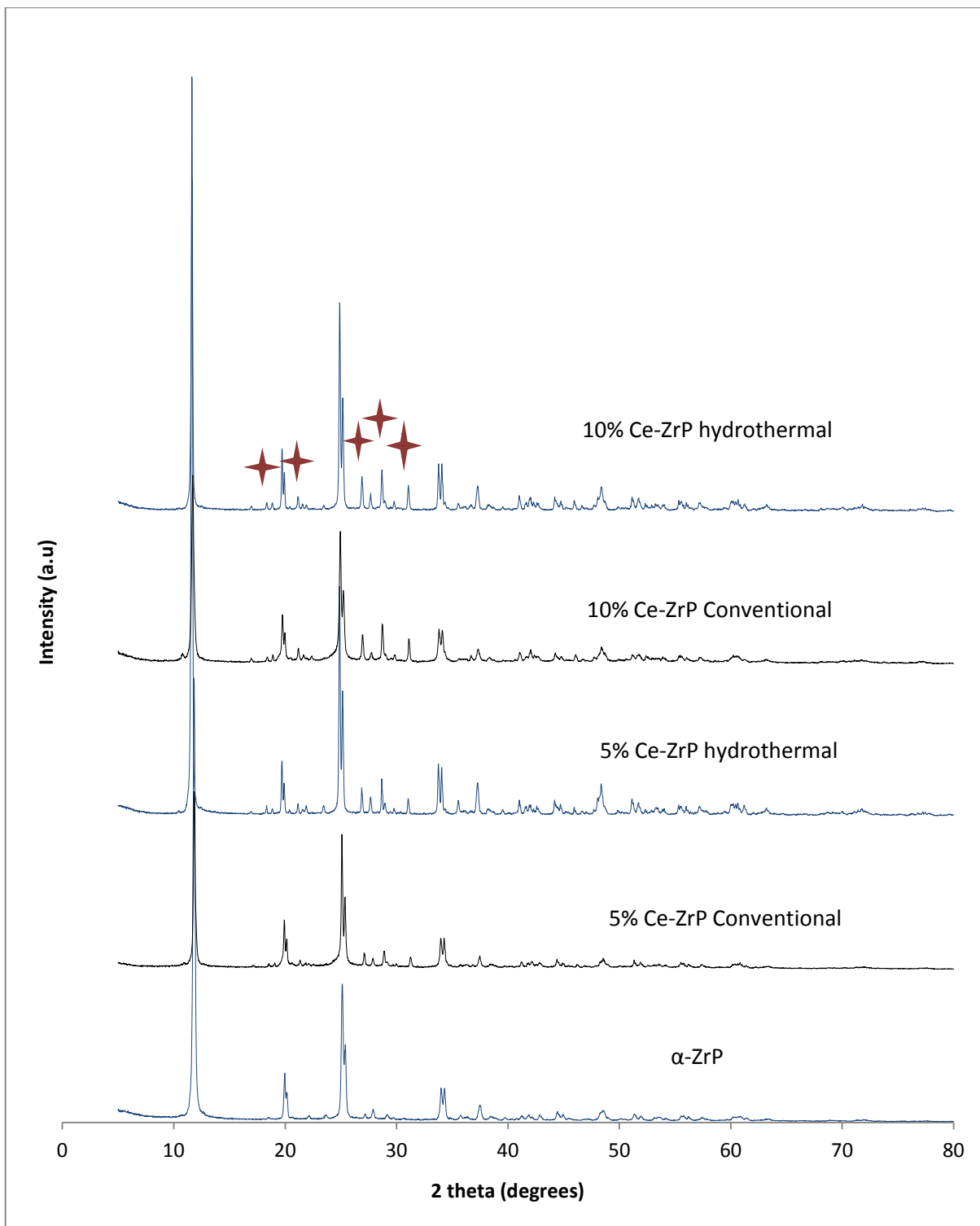


Figure 3. 33 XRD patterns for the 5% and 10% Ce-ZrP

3.4.2 XRF analysis of the mixed phase products

The XRF results for the mixed phase Fe(III)-ZrP are shown below in terms of peak profiles. No calibration was carried out to determine the iron composition, but the results can be estimated from the peak ratios of the principal components.

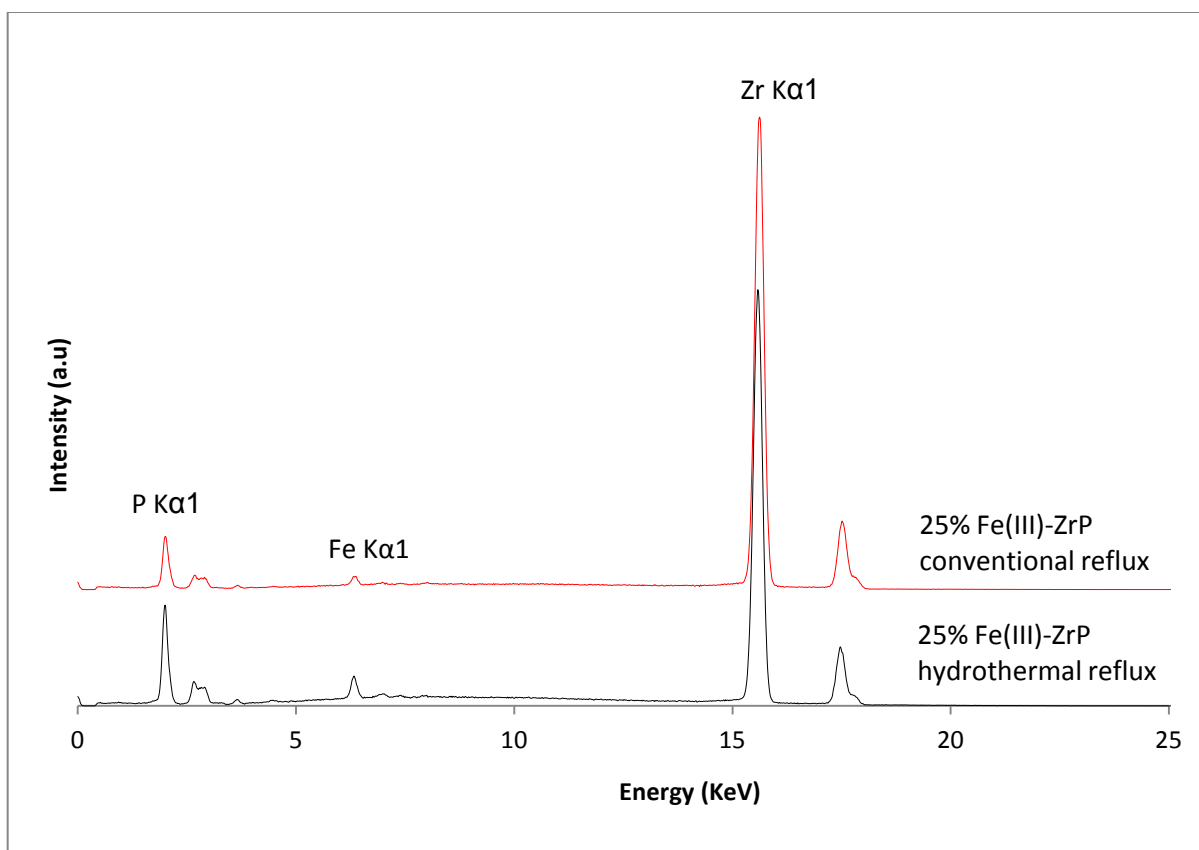


Figure 3. 34 XRF analysis for 25% Fe(III)-ZrP synthesised via two routes

The XRF results shown above indicate the presence of iron in the synthesised 25% Fe(III)-ZrP, however, since the XRD patterns shown in figure 3.33 indicates a two phase system, therefore no further analysis was done.

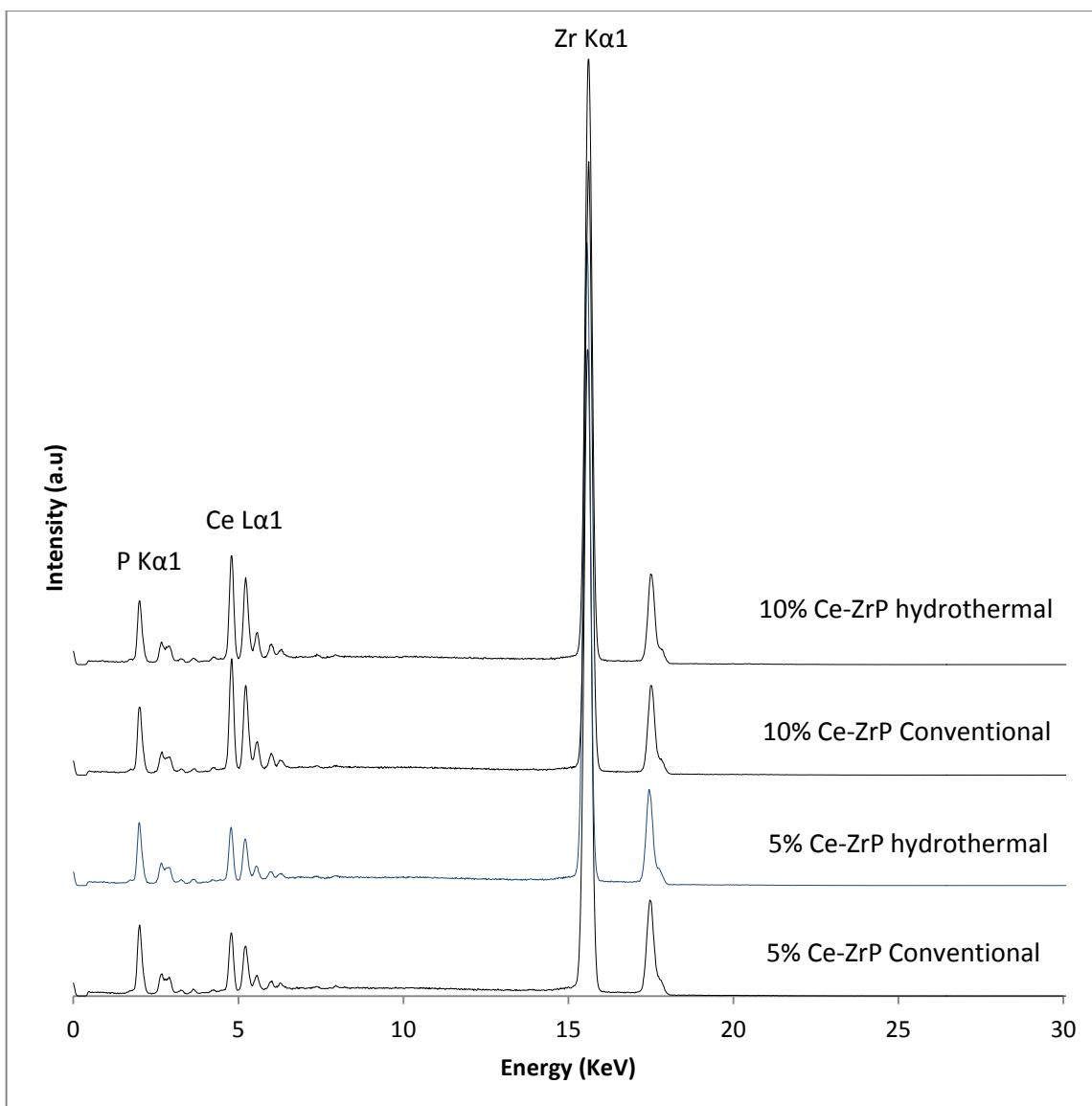


Figure 3. 35 XRF analysis for 5% and 10% Ce-ZrP products

The XRF results shown in Figure 3.35 above indicate the presence of cerium in the synthesised Ce-ZrP samples, however, as the XRD shows presence of two phase system no further analysis was done to determine the exact amount of cerium present in the samples.

As the aim of the project was to synthesise a single crystalline phase of α -ZrP doped with a trivalent (+3) ion, no further attempts were made to synthesise Ce/Fe doped α -ZrP products.

3.5 References

1. Clearfield, A., Frianeza, T. N., *J. Inorg. Nucl. Chem.* 40, 1925-1932 (1978)
2. ATIK, M. PAWLICKA, A. AEGERTER, M. A. *J. Mat. Sci. Lett.*, 14. 21. 1486 (1995)
3. Clearfield, A., Smith, G.D., *J. Inorg. Chem.*, 8, 431 (1969)
4. Burnell, V.A., Readman, J.E., Tang, C.C., Parker, J.E., Thompson, S.P., Hriljac, J.A., *J. Solid State. Chem*, 183, 2196 (2010)
5. Alberti, G., Costantino, U., Millini, R., Perego, G., Vivani, R., *J. of Sol. Stat. Chem.*, 113, 289 (1994)
6. Bunge H. J., Klein, H., *Z. Metallkd.* 87(6), 465 (1996).
7. Inoue, M., Hirasawa, I., *J. Crys. Grow.*, 380, 169 (2013)
8. Shuai, M., Mejia, A. F., Chang Y. W., Cheng, Z. *Cryst. Eng. Comm.*, 15, 1970 (2013)
9. Sun, L., Boo, W. J., Sue H. J., Clearfield, A., *New J. Chem.*, 31, 39 (2007)
10. Mrad, O., Abdul-Hadi, A., Arsan, H., *J. Radioanal. Nucl. Chem.*, 287, 1, 177 (2011)
11. Horsley, S.E., Nowell, D.V., Stewart, D.T., *Spectrochimica. Acta*, 30A, 535 (1974)
12. Busca, G., Lorenzelli, V., Galli, P., La Ginestra, A., Patrono, P., *J. Chem. Soc. Faraday Trans. I*, 83, 853 (1987)
13. Slade, R.C.T., Knowels, J.A., Jones, D.J., Rozière, J. *Sol. Stat. Ion.*, 96, 9 (1997)
14. Rajeh, A. O., Szirtes, L., *J. Radioanal. Nucl. Chem.*, 241, 1 83 (1999)
15. Genoveva, G. R., Enrique, O. R., Teresita, R. G. E., Eduardo, O. R., *J. Min. & Mat. Charac. & Engg.*, 6, 1, 39 (2007)
16. CLEARFIELD, A., *Inorganic ion exchange materials*, CRC Press, Florida (1982)
17. Rapôso, C. M. de Oliveira., Eon, J. G., *Mat. Res.* 5, 4 (2002)
18. Turner, G. L., Smith, K. A., Kirkpatrick, R. J., and Oldfield, E., *J. Magn. Reson.* 70, 408, (1986)
19. Clayden, N. J., *J. Chem. Soc., Dal. Trans.*, 1877 (1987)

20. Nakayama, H., Eguchi, T., Nakamura, N., Yamaguchi, S., Danjyo, M., Tsuhako, M.,
J. Mater. Chem., 7, 1063(1997)
21. Hudson, M.J., Workman, A.D., Adams, R.J.W., Sol. Stat. Ion., 46 (1–2), 159 (1991)
22. Chabé, J., Bardet, M., Gébel, G., Sol. Stat. Ion., 229, 20 (2012)
23. Clearfield, A.; Smith, D. Inorg. Chem., 8, 431 (1969)
24. I. Yu. Pinus, A. E. Baranchikov, A. G. Veresov, A. B. Yaroslavtsev, Russ. J. of Inorg.
Chem., 53, 8, 1163 (2008)
25. Clearfield A., and Costantino, U., in “Comprehensive Supramolecular Chemistry” (G.
Alberti and T. Bein, eds.), 7, Chap. 4, p107, Pergamon, Oxford (1996)
26. Qiong, L. Yiguo, S. Hongsheng, Y. Wei, H., J. Rar. Eart., 26, 4, 495 (2008)
27. Product impurities for yttrium chloride hexahydrate, accessed on 20/01/2015 from
http://www.gowealth.com.tw/files/rare_earth_table.pdf
28. Melnikov, P. P., Komissarova, L. N., Butuzova, T. A., Izv. Akad. Nauk. SSSR Neorg.
Mater., 17(11), 2110 (1981)
29. Bagieu M (1980) PhD report, Grenoble, France
30. Cannas, M., Manca, E., Pinna, G., Bettinelli, M., Speghini. A Z Naturforschung. A.
Hys. Sci. 53(10), 919 (1998)
31. Matsumoto, H., Murakami, D., Shimura, T., Hashimoto, S-I. & Iwahara, H., J.
Electro. Ceram., 7, 107 (2001)
32. Oswald, H. R., & Felder-Casagrande, S., Sol. Stat. Ion. 63, 565 (1993)
33. Gurav, H. R., Bobade, R., Das, V. L., & Chilukuru, S., Ind. J. Chem. 51A, 1339
(2012)
34. Palke, A. C., Stebbins, J. F., Amer. Mineral., 96, 1343 (2011)
35. Turner, G. L., Smith, K. A., Kirrpatrick, R. J., Oldfield, E., J. Magn. Reson., 70, 408
(1986)

36. Bose, M., Bhattacharya M., Ganguli, S., Phys. Rev. B 19, 72 (1979)
37. Young, R. A. The Rietveld Method; Oxford University Press: Oxford, (2002)
38. Troup, J.M., Medina, A.S., Landis, A.L., Clearfield, A., J. Inorg. Nucl. Chem., 35, 1099, (1973)
39. Larson A.C., Von Dreele, R.B., Los Alam. Nation. Lab. Rep. LAUR 86 (1994)
40. Toby, B. H., J. Appl. Cryst. (2001). 34, 210-213.

CHAPTER 4: SINGLE ION-EXCHANGE STUDIES

4.1. Introduction

In this chapter the ion exchange behaviour of the synthesised Y-ZrP samples are investigated and compared with the parent α -ZrP of particular interest in the removal of cations (Sr^{2+} , Cs^{2+} and Co^{2+}) which are present in the nuclear wastes. In order to immobilise these metal isotopes of radionuclides it is important to successfully trap them using efficient ion exchangers. An in-depth discussion about the efficiency of α -ZrP as an ion-exchanger is provided in the Chapter 1. However, the literature search shows very little evidence about the ion exchange studies of strontium ^[1-4], caesium ^[1, 5, 6, 7, 8] and cobalt ^[9] carried out using the crystalline layered phosphates.

In this chapter, synthesised single phase Y-ZrP samples with 5% to 15% yttrium substitution together with un-doped α -ZrP are exposed to nitrate, hydroxide and acetate salts of Sr^{2+} , Cs^{2+} and Co^{2+} ions as a part of single ion-exchange study. All ion exchange studies are performed at room temperature with extended periods of reaction time along with constant stirring to allow the exchangers to reach maximum ion exchange capacity. The ion exchanged materials were then characterised by XRD, XRF, FT-IR and ICP-MS.

4.2. Strontium ion exchanges of Y-ZrP samples

About 0.5 g of 5%, 10% and 15% Y-ZrP samples together with α -ZrP synthesised by hydrothermal and conventional reflux methods were treated with the 0.1M solution of strontium nitrate, strontium hydroxide and strontium acetate salts at room temperature for a period of 72 hours with constant stirring to allow maximum exchange. The volume of the exchange solution was kept constant at 125 mL and the obtained products were characterised to analyse both qualitative and quantitative changes in the crystal structure.

4.2.1 XRD analysis of strontium exchanged products

The XRD patterns for the $\text{Sr}(\text{NO}_3)_2$ ion exchanged products are shown in Figure 4.1 below.

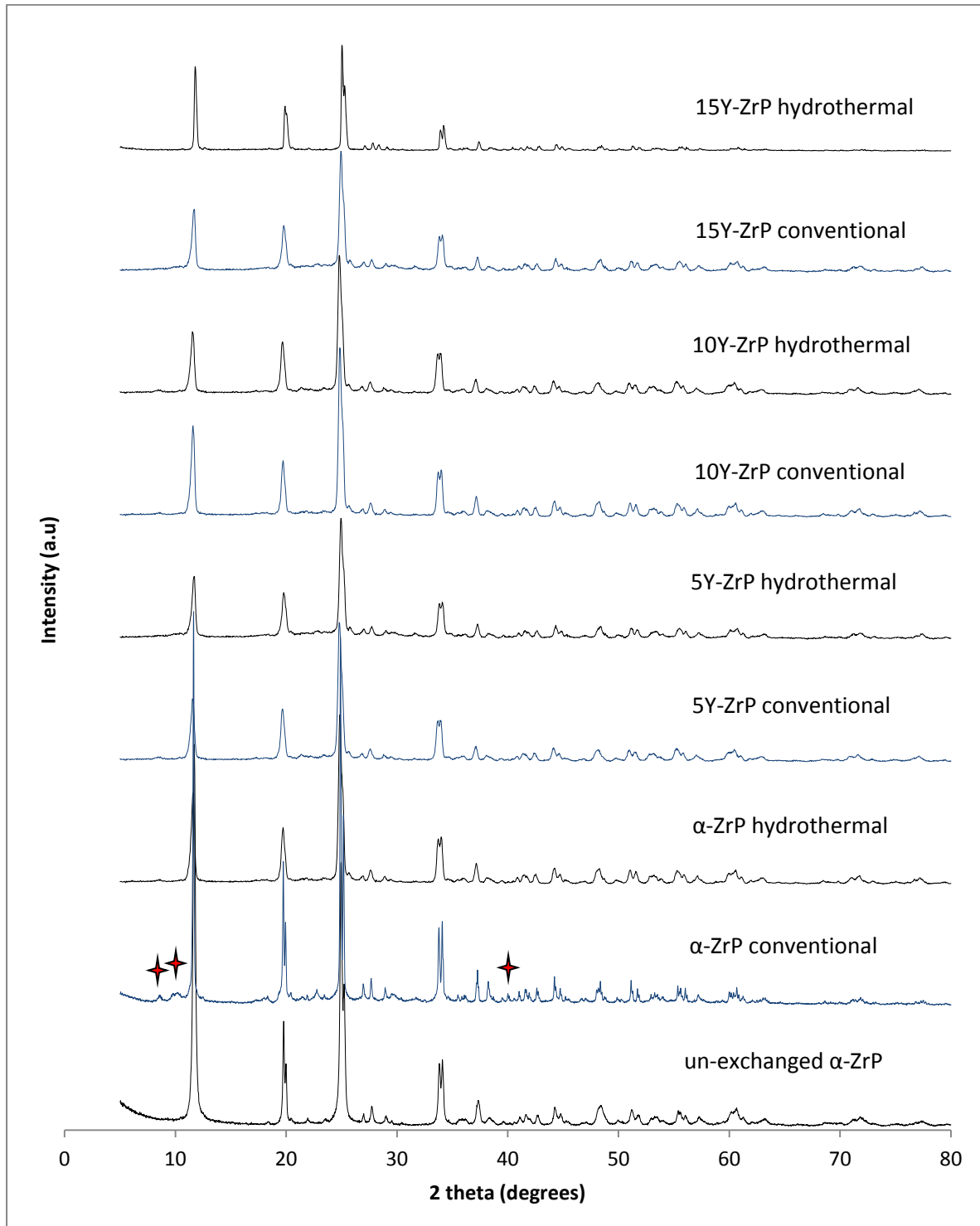


Figure 4. 1 XRD of $\text{Sr}(\text{NO}_3)_2$ ion exchange for Y-ZrP products

It can be observed from the Figure 4.1 above that there are extra low intensity peaks present at $2\theta = 8^\circ$ - 11° for the exchanged products along with few other minor peaks as marked with the red star. These could be the result of slight change in symmetry of the lattice due to the occurrence of extra inorganic ions into the structure, as explained in a similar literature ^[10] where the Sr^{2+} ions exchanged in the zirconium phosphate structure led to the decrease in intensities of characteristic peaks and also caused replacement of XRD singlets into doublets.

Similarly, it was observed that for the ion exchanged products that the intensity of these extra peaks and that of the other characteristic peaks after the ion exchange were altered for each product and is possibly indicative of the degree of Sr^{2+} ions exchanged. But interestingly, the signal noise for both the α -ZrP and Y-ZrP samples did not seem to be affected by the ion exchange and the peaks are distinctly resolved even at higher 2θ ranges, indicating a low decrease in crystallinity. However the literature search shows that this new peak at $2\theta = 8.62^\circ$ is assigned to the formation of $\text{ZrHSr}_{0.5}(\text{PO}_4)_2 \cdot 3.6\text{H}_2\text{O}$ as a result of the strontium ion exchange of α -ZrP at slightly acidic or neutral pH. ^[3, 10] Also, an online crystal structure database search using the PDF software shows the formation of a possible alpha strontium zirconium phosphate [α - $\text{SrZr}(\text{PO}_4)_2$] phase for a peak matching at $2\theta = 8.62^\circ$, as shown in figure 13 of appendix 3.

The XRD patterns for the $\text{Sr}(\text{OH})_2$ ion exchanged products are shown in Figure 4.2 below.

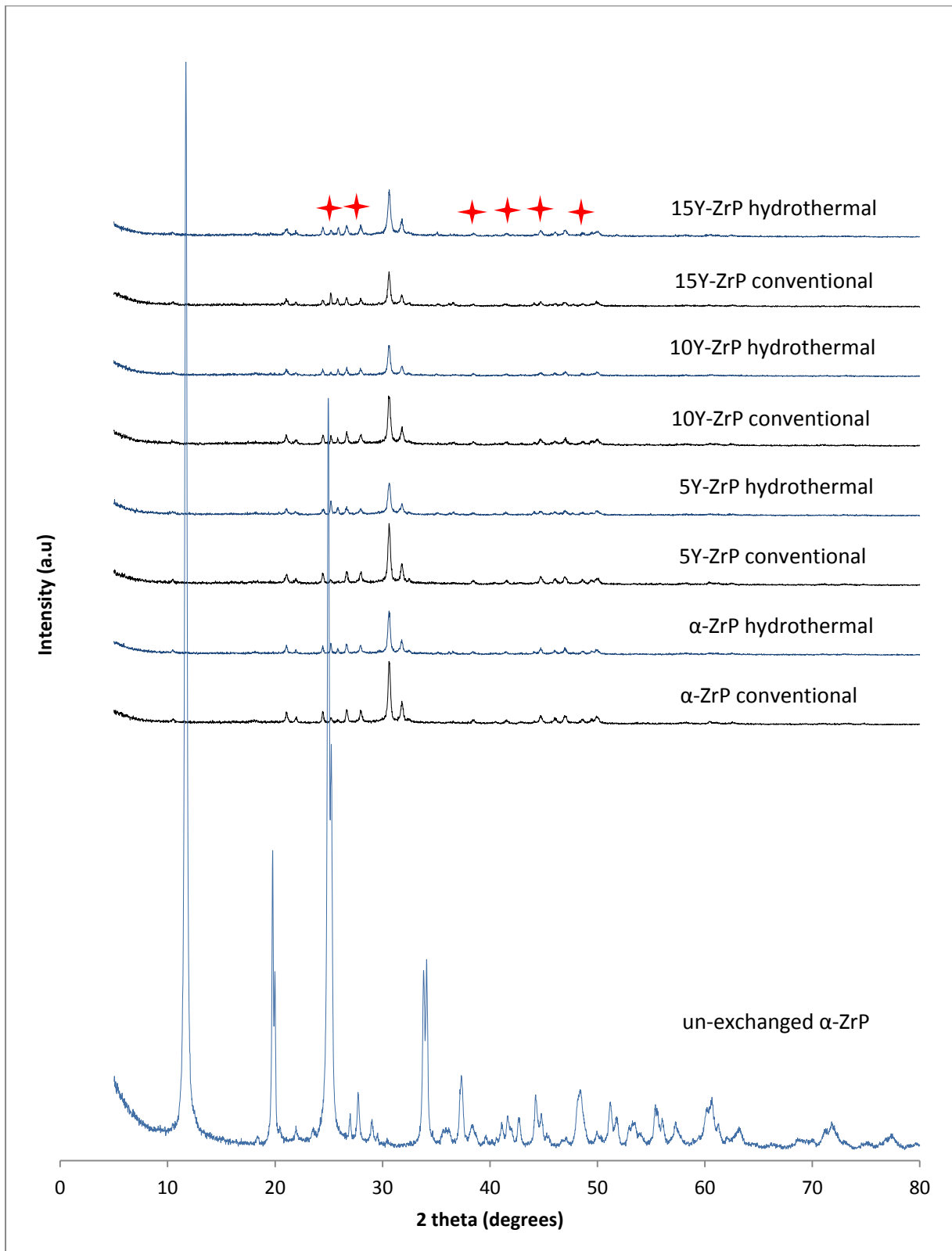


Figure 4. 2 XRD of $\text{Sr}(\text{OH})_2$ exchanged Y-ZrP products

It is interesting to observe from Figure 4.2 above that the peak intensities of all the characteristic peaks of α -ZrP structure are greatly reduced, especially that of the peak at d_{002} reflection which has nearly disappeared from the XRD patterns. Some of the visible α -ZrP peaks in the exchanged products are marked with red stars as shown in the Figure 4.2 above. However, two extra strong intensity peaks at $2\theta = 30.64^\circ$ and 31.79° arise that are not characteristic of α -ZrP structure. These peaks along with the other minor peaks between the $2\theta = 20^\circ - 28^\circ$ indicate from the literature search [3, 4, 11] to be representative of $\text{Sr}_5(\text{PO}_4)_3\text{OH}$ and $\text{Sr}_{10}\text{O}(\text{PO}_4)_6$. This is also confirmed from the PDF database search for the crystal structure that matches the 5%Y-ZrP $\text{Sr}(\text{OH})_2$ exchanged sample with the $\text{Sr}_5(\text{PO}_4)_3\text{OH}$ structure, as shown in figure 14 of appendix 3. Hence, it can be concluded that the precipitation of strontium-zirconium phosphate must have occurred from the $\text{Sr}(\text{OH})_2$ solution along with some mixed strontium phosphate phases due to the sample breakdown of both α -ZrP and Y-ZrP products.

The XRD patterns for the $\text{Sr}(\text{CH}_3\text{CO}_2)_2$ ion exchanged products are shown in Figure 4.3 below that clearly indicates the emergence of a new strontium phase.

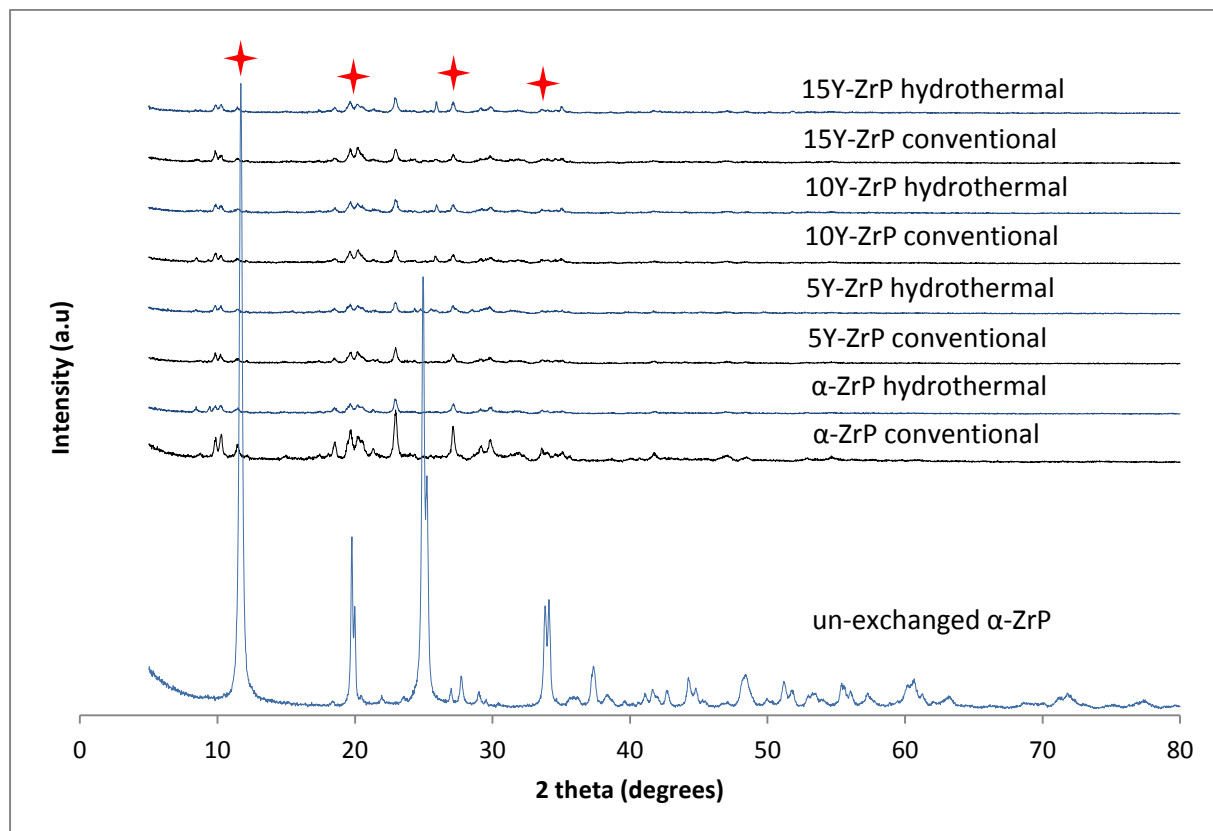


Figure 4. 3 XRD of $\text{Sr}(\text{CH}_3\text{CO}_2)_2$ exchanged Y-ZrP products

The XRD pattern from the strontium acetate ion exchange clearly show a decreased crystallinity of both α -ZrP and Y-ZrP samples, as evident from reduced signal to noise ratios of the peaks, especially for the reflections at $2\theta = 11.7^\circ$ and 24.95° . Also, it can be observed from the figure 4.3 above that there are some extra dominant peaks present in the XRD patterns at $2\theta = 8.77^\circ$, 9.78° , 10.27° and 22.95° and few other minor peaks at higher 2θ ranges along with few characteristic peaks of parent α -ZrP. All the products clearly show the presence of a mixed phase and no clear evidence or information is available in literature to match these patterns. But the presence of few extra peaks are indicating the formation of a possible β -strontium hydrogen phosphate, as shown in the PDF match presented in figure 15 in appendix 3. However, not all the peaks from these XRD patterns show a possible match in the PDF software but there are strong indications for the formation of α -strontium zirconium phosphate and other mixed phases of strontium along with the parent α -ZrP types structure in these $\text{Sr}(\text{CH}_3\text{CO}_2)_2$ exchanged Y-ZrP samples. Alternatively, it is also possible that the space group symmetry of the ion exchanged material is changed from monoclinic and therefore caused a different arrangement of ions or layers within the structure. This could also result in distortions within the tetrahedral and polyhedral units as some of the atoms are constrained within the layers, as shown by Poojary *et.al* ^[17] for complete sodium exchange of α -ZrP. This also causes change in diffraction patterns of the exchanged products as compared to the parent samples.

4.2.2 pH analysis of strontium exchanged solutions

The pH analysis was done before and after the ion exchange reactions to further understand the uptake rate of strontium in regards to the hydrogen ion being exchanged. The results are shown in Table 4.1 below.

Table 4. 1 Summary of pH analysis of strontium ion exchanged samples

Samples	pH of solutions		
	Sr(NO ₃) ₂ Stock pH = 6.78	Sr(OH) ₂ Stock pH = 13.1	Sr(CH ₃ CO ₂) ₂ Stock pH = 7.63
α-ZrP conventional	5.10	10.80	5.69
α-ZrP hydrothermal	4.94	10.80	5.48
5Y-ZrP conventional	4.89	10.78	5.55
5Y-ZrP hydrothermal	4.72	10.75	5.30
10Y-ZrP conventional	4.90	10.77	5.60
10Y-ZrP hydrothermal	4.89	10.79	5.60
15Y-ZrP conventional	4.93	10.80	5.62
15Y-ZrP hydrothermal	4.93	10.80	5.62

It is evident from pH results shown in the Table 4.1 above that Sr²⁺ ion exchange led to a decrease in the pH values for the solutions after the exchange. It can be seen that the hydroxide and the acetate salt solutions showed more reduction in the pH values as compared to the nitrate solution. This indicates that the extent of Sr²⁺ ion exchange is expected to be higher for the hydroxide and acetate salts, as established in previous studies ^[1, 4].

4.2.3 XRF analysis of strontium exchanged products

The XRF analysis of the strontium nitrate, strontium hydroxide and strontium acetate ion exchanged with the α-ZrP and Y-ZrP samples was carried out after calibrating the instrument using the corn flour method for the ions of interest, as per the scheme shown in table 1 along with the calibration graphs presented in figures 1 to 5 of Appendix 3.

The compositional analysis of the strontium ion exchanged products is done by analysing the peak areas of strontium, yttrium and zirconium ions from the XRF spectrum and calculating the molar ratios of which the results are summarised in the Table 4.2 below.

Table 4. 2 XRF compositional analysis for the strontium exchanged products

Samples	Extent of Exchange Ratio of Sr / (Y+Zr)		
	Sr(NO ₃) ₂	Sr(OH) ₂	Sr(CH ₃ CO ₂) ₂
α-ZrP conventional	0.1376(3)	1.1119(1)	0.4067(9)
α-ZrP hydrothermal	0.2400(1)	1.1254(4)	0.4406(2)
5Y-ZrP conventional	0.1844(1)	1.2610(6)	0.4949(3)
5Y-ZrP hydrothermal	0.2664(5)	1.2813(9)	0.5695(1)
10Y-ZrP conventional	0.1457(6)	1.1763(1)	0.4508(6)
10Y-ZrP hydrothermal	0.2495(1)	1.2136(1)	0.4915(4)
15Y-ZrP conventional	0.1389(8)	1.1458(2)	0.4169(6)
15Y-ZrP hydrothermal	0.2474(6)	1.1593(6)	0.4474(7)

It can be seen from the above compositional analysis that there is a higher strontium ion ratio for both α-ZrP and Y-ZrP samples from the hydroxide salt followed by the acetate and nitrate salts respectively. The extent of Sr²⁺ uptake from hydroxide salt for both α-ZrP and Y-ZrP samples is seen to be surpassing the theoretical maximum capacity. This is explained by the XRD results discussed above which clearly explains the formation of strontium phosphate product from the breakdown of the parent compounds resulting in strontium phosphate phases.

However, the acetate salts were able to reach about 57% of the total molar metal concentration (Y+Zr) followed by ca. 26% in case of strontium nitrate solutions. These products were analysed by XRD to successfully exchange Sr²⁺ ions into the lattice of the parent compounds and therefore led to the formation of about half exchanged phases as evident in the literature ^[3, 4].

In general, the hydrothermally refluxed samples were able to take up more strontium from all the three salt solutions as compared to the conventionally refluxed samples and this result holds true for both α-ZrP and Y-ZrP products. Finally, it can be observed from the Table 4.2 above that there is an increase of about 10–30% in the Sr²⁺ uptake for the 5% Y-ZrP samples via both routes, as compared to the parent α-ZrP. However, for the samples with 10% and 15% yttrium concentration, the Sr²⁺ uptake did not follow a definite trend in regards to the yttrium concentration and is

may be caused due to an increasing amount of disorder in the structure upon yttrium substitution. But it was observed that the exchange capacity of all the Y-ZrP products were still higher than the parent α -ZrP. This shows that there is an increased ion exchange capacity for the synthesised Y-ZrP toward the strontium ion. Also, the XRF analysis helps to explain the findings of the XRD analysis in such that almost 50% exchanged Sr-Y-ZrP samples are formed successfully from the nitrate and acetate salts of strontium, but as the extent of exchange is forced to reach the completion and beyond using the hydroxide salt solutions, there appears the formation of some unknown mixed strontium phosphate phases which deteriorates the structure for both α -ZrP and Y-ZrP samples.

4.2.4 FT-IR analysis of strontium exchanged products

In order to understand the changes in the chemical environment (precisely of the P-OH groups that are involved in the exchange) of the strontium exchanged samples an FT-IR analysis was attempted on all the samples and the results are shown in the Figures 4.4 – 4.6 below.

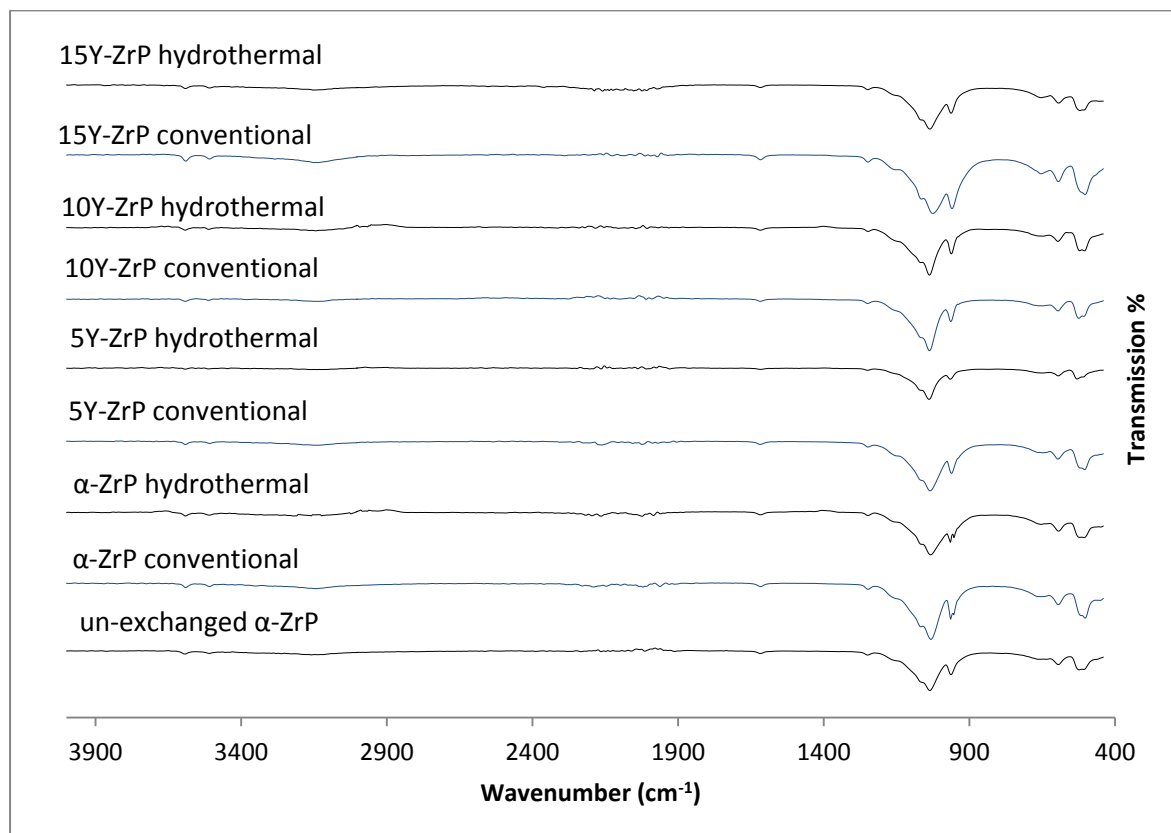


Figure 4. 4 FT-IR analysis for Sr(NO₃)₂ ion exchange

It can be seen from the above figure that the strontium exchanged products from the nitrate salt solution did not show any marked differences in the FT-IR spectrum as compared to the pristine α -ZrP. However, on close inspection it was found that there is a change in the peak intensities of the exchanged products especially for the peaks in the ranges of 900-1050 cm^{-1} and 3000-3500 cm^{-1} . These correspond to the change in the stretching and bending vibrations of the P-O and O-H bonds respectively. Therefore, it can be concluded that the FT-IR results are in accordance with the XRD and the XRF results shown above that the $\text{Sr}(\text{NO}_3)_2$ exchange showed an evidence of successful ion exchange in the structure despite the extent of exchange being minimum ($\leq 30\%$). But interestingly, the 5% Y-ZrP samples hydrothermally refluxed showed a marked increase in the Sr^{2+} ion exchange as compared to the rest of products which is also evident from the FT-IR results that shows a greater decline in the peak intensities of the O-H vibrational peaks. This shows that more of the H^+ ions were exchanged for incorporating a greater amount of Sr^{2+} ions as compared to the rest of the products. Also, there appears to be a shift in the peak wavenumbers for the low frequency peaks between the ranges of 400 – 600 cm^{-1} . This is due to the accommodation of the Sr^{2+} ions in the product which would change bond strength (force constant) and total mass of the atoms in the bond that would lead to the shift in the wavenumber. The metal-O vibrational peak at approximately 570 cm^{-1} is not observed due to the intense signal and peaks overlapping of the P-OH vibrations. But overall, most of the products produced very similar patterns as compared to each other indicating the limited exchange of Sr^{2+} ions as confirmed by XRD and XRF analysis before. Two minor peaks at ca. 1369 and 1439 cm^{-1} is not recognised in literature, hence remains unidentified. A summary of the typical peaks observed from the $\text{Sr}(\text{NO}_3)_2$ exchange is shown in the Table 4.3 below.

Table 4. 3 Summary of FT-IR results for Sr(NO₃)₂ ion exchange

Peak Wavenumber (cm ⁻¹)	Chemical bonds
521.22	P-O-P vibration
589.15	P-OH (out of plane)
644.14	O-H (out of plane)
961.32	P-O bending (in plane)
1033.45	P-O stretching (asym)
1247.92	P-O-H deformation
1617.10	O-H bending (asym)
2188.26	P-OH
3132.55	O-H stretching (sym)
3511.75	O-H stretching (asym)
3590.43	O-H stretching (asym)

The FT-IR spectrum for the Sr(CH₃CO₂)₂ exchanged products of both routes of reflux is shown in the Figure 4.5 below.

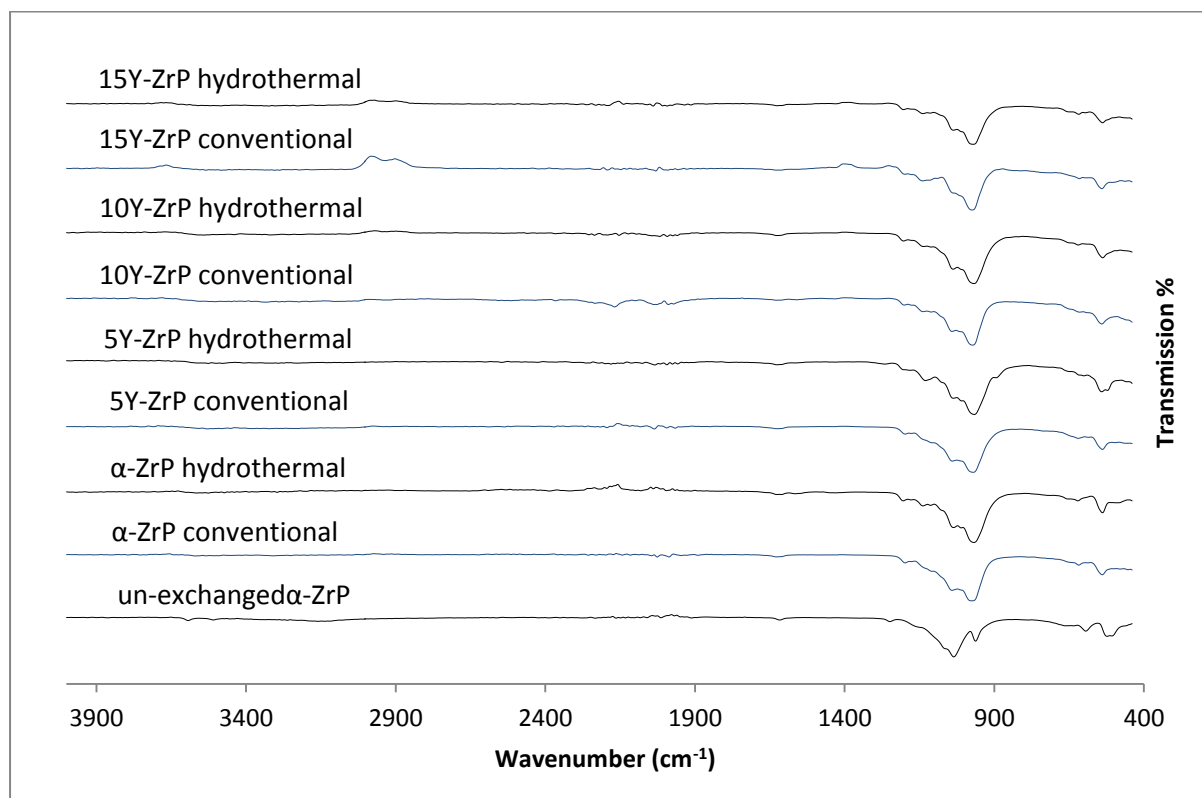


Figure 4. 5 FT-IR analysis for Sr(CH₃CO₂)₂ ion exchange

The spectra shown above indicate the changes upon ion exchanged when compared to the un-exchanged α -ZrP. The differences in the peaks can be observed in the regions 500-620 cm^{-1} and 900-1100 cm^{-1} . The characteristic α -ZrP P-O and O-H peaks at 502.73 cm^{-1} and 594.09 cm^{-1} were not present, instead these peaks were shifted to 539.56 cm^{-1} and 617.85 cm^{-1} and were assigned to the P-O-P bonds and P-OH out of plane bonds respectively. This is explained previously, as the result of change in the bond strength (force constant) and total mass of atoms within the bond due to the introduction of Sr^{2+} ions instead of the H^+ ions. Also, the peaks at 968.31 cm^{-1} and 1040.92 cm^{-1} showed a difference between the transmission percentages as the intensities of these peaks are changed. This explains that the in-plane P-O bending and asymmetrical P-O stretching vibrations are affected respectively. The P-O bending is more pronounced than the stretching and thus it explains that the exchanged strontium between the layers is causing the 'squeezing' of the in-plane phosphate bonds and in turn relaxes the asymmetrical P-O stretching vibrations. Further to enhance this effect, an absence of O-H stretching and bending vibrations was noticed in the regions of 3000-3500 cm^{-1} and 1600-1650 cm^{-1} . This is explained by the loss of hydronium ions due to the removal of hydrogen from the P-OH groups (evident from the very weak signals at 1247 cm^{-1} and 2100-2200 cm^{-1}) along with the cavity filling water molecules, thus allowing the exchange of larger radii strontium ions by pushing or breaking apart the structural layers. The metal-O vibrational peak is overlapped and is not observed at lower wavenumber (approximately 570 cm^{-1}). Therefore, the presence of strontium ions within the layer of α -ZrP and Y-ZrP samples caused the layers to swell and hence increasing the P-O bending and relaxing the P-O stretching vibrations. Also, the exchange causes the variation in the dipole of the bonds that can also affect the absorption/transmission intensities. Therefore, it explains the massive change in the transmission percentages of the P-O bending and stretching vibrations, with the former being increased and the latter being decreased with respect to increasing strontium ion uptake.

Overall, the FT-IR analysis confirms the XRD and XRF results to show that the acetate salt solution led to a structural change of the synthesised products due to the formation of certain strontium mixed phases causing the corrugation of the layers. A summary of the characteristic peaks from $\text{Sr}(\text{CH}_3\text{CO}_2)_2$ ion exchange is shown in Table 4.4 below.

Table 4. 4 Summary of FT-IR results for Sr(CH₃CO₂)₂ ion exchange

Peak Wavenumber (cm ⁻¹)	Chemical bonds
539.56	P-O-P vibration
617.85	P-OH (out of plane)
968.31	P-O bending (in plane)
1040.92	P-O stretching (asym)
1628.32	O-H bending (asym)

The FT-IR spectrum for the Sr(OH)₂ exchanged α-ZrP and Y-ZrP products of both routes of reflux is shown in the Figure 4.6 below.

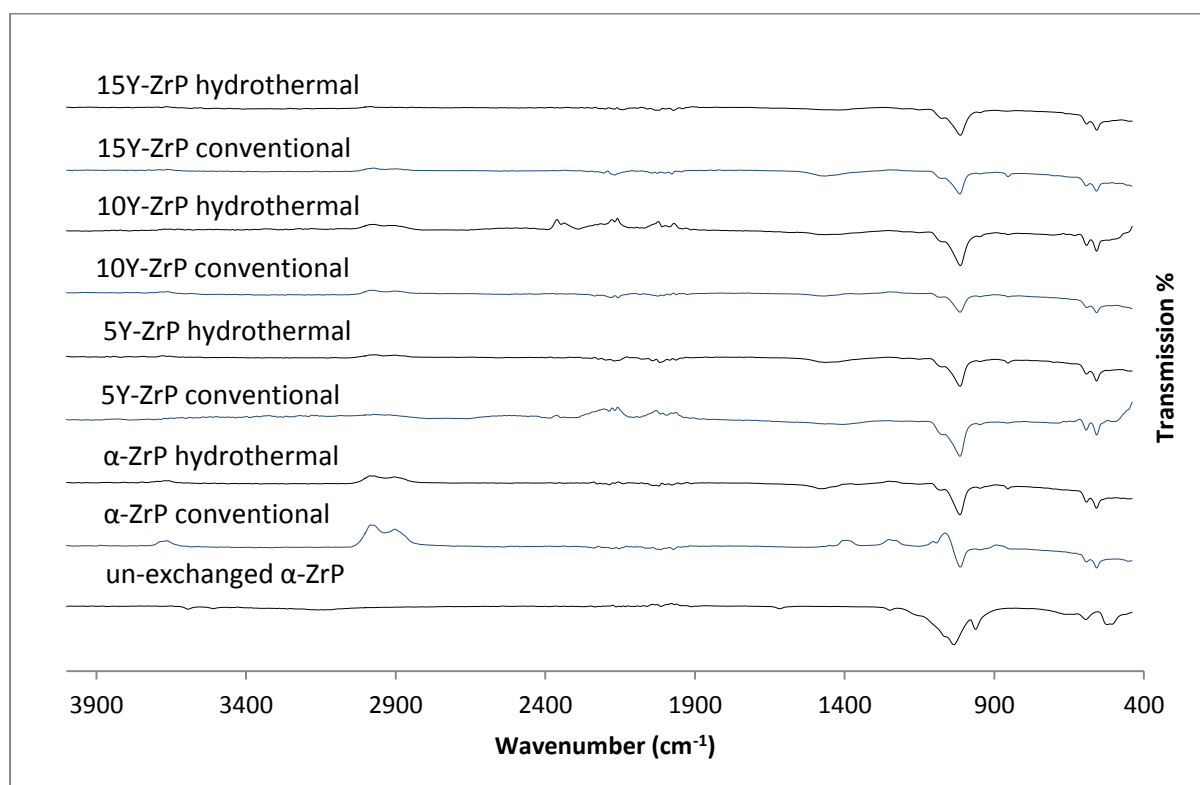


Figure 4. 6 FT-IR analysis for Sr(OH)₂ ion exchange

The results shown above for the Sr(OH)₂ ion exchange shows significant differences compared to those of Sr(NO₃)₂ and Sr(CH₃CO₂)₂ exchange (Figures 4.4 and 4.5). The P-O bending peak at 948 cm⁻¹ is disappeared from the FT-IR spectrum of all the Sr(OH)₂ exchanged products. A dominant sharp peak appearing at 1013 cm⁻¹ is characteristic of P-O stretching vibration which is accounted for the formation of

mixed strontium phosphate phases ^[11] as concluded from the XRD analysis above. It is evident from XRF results shown in Table 4.2 above that there is an exceptionally high strontium ion ratio obtained from exchange with hydroxide salts as compared to the half exchanged acetate salts and partially exchanged nitrate salts.. Also, there is a broad weak peak observed at 1464 cm⁻¹ which is assigned to the OH⁻ + H₂O deformation due to the hydration of the surface as a result of water adsorption mostly on the exposed Sr-O groups. The Sr-O bond appears shifted but is observed at ca. 560 cm⁻¹. These results therefore compliments the XRD and XRF analysis done before to conclude that the original α-ZrP structure of the exchanged products is lost during the Sr(OH)₂ ion exchange and instead a precipitate of mixed strontium phosphate phases are predominant.

A summary of the typical characteristic peaks of Sr(OH)₂ ion exchanged product is provided in the Table 4.5 below.

Table 4. 5 Summary of FT-IR results for Sr(OH)₂ ion exchange

Peak Wavenumber (cm ⁻¹)	Chemical bonds
558.34	Sr-O vibration
591.80	P-O (out of plane)
854.12	Zr-O stretching
948.35	P-O bending (in plane)
1013.82	P-O stretching (asym)
1464.81	O-H deformation

4.2.5 ICP-MS of the strontium exchanged products

ICP-MS analysis was carried out on the filtrate/supernatant collected post ion exchange. The solutions were diluted to 1000 times for preventing saturation of the detector.

The summary of the results from 0.1M ion exchanged filtrate solutions after multiplying the dilution factor (1000 times) is shown in the Table 4.6 below and the calibration graphs for the ions of interest (strontium, caesium, cobalt, yttrium and zirconium) are provided in figures 5-9 in Appendix 3.

Table 4. 6 Summary of ICP-MS results for strontium ion exchanged Y-ZrP samples

Samples	X = Amount of Sr ²⁺ remaining (ppm)			% of Sr ²⁺ incorporation $\frac{8800ppm - Xppm}{8800ppm \text{ of } 0.1M \text{ Sr}} \times 100$		
	Sr(NO ₃) ₂	Sr(OH) ₂	Sr(CH ₃ CO ₂) ₂	Sr(NO ₃) ₂	Sr(OH) ₂	Sr(CH ₃ CO ₂) ₂
α-ZrP conventional	6946(6)	2475(4)	5299(8)	21.06%	71.87%	39.78%
α-ZrP hydrothermal	6783(2)	2418(6)	5114(4)	22.92%	72.52%	41.88%
5Y-ZrP conventional	6816(8)	2267(6)	4748(2)	22.54%	74.23%	46.04%
5Y-ZrP hydrothermal	6717(6)	2259(4)	4484(8)	23.67%	74.32%	49.04%
10Y-ZrP conventional	6854(4)	2354(2)	4829(11)	22.11%	73.25%	45.13%
10Y-ZrP hydrothermal	6734(3)	2322(6)	4783(8)	23.47%	73.61%	45.64%
15Y-ZrP conventional	6904(2)	2488(4)	5168(6)	21.54%	71.72%	41.27%
15Y-ZrP hydrothermal	6711(8)	2426(1)	5092(4)	23.73%	72.43%	42.14%

It can be seen from the elemental analysis of strontium that there is approximately 24% uptake of Sr²⁺ from 0.1M strontium nitrate solution for both α-ZrP and Y-ZrP samples, followed by almost 49% uptake from the 0.1M strontium acetate and almost 74% uptake from the 0.1M strontium hydroxide solutions. These results complement the XRF results shown in Table 4.2 above. The pH measurements shown in Table 4.1 above are also in agreement with these results showing that there is a higher drop in the pH values for the hydroxide solutions as compared to the acetate and nitrate solutions since more H⁺ ions are removed from the materials. However, it is evident from the XRD analysis that the exchanged products from the acetate and hydroxide salt solutions tend to form mixed strontium phosphate phases at the expense of lattice distortion. Therefore, ICP-MS can confirm these results by

measuring the amount of leached yttrium and zirconium ions into the solution due to breakdown of parent structure. A summary of the leached Y^{3+} and Zr^{4+} ions is provided in the Table 4.7 below.

Table 4. 7 Summary of ICP-MS for the leached Y^{3+} and Zr^{4+} ions

Samples	$Sr(NO_3)_2$		$Sr(OH)_2$		$Sr(CH_3CO_2)_2$	
	Y^{3+} (ppm)	Zr^{4+} (ppm)	Y^{3+} (ppm)	Zr^{4+} (ppm)	Y^{3+} (ppm)	Zr^{4+} (ppm)
α -ZrP conventional	-	0.006(1)	-	13.75(1)	-	1.325(1)
α -ZrP hydrothermal	-	0.004(1)	-	9.985(2)	-	1.471(6)
5Y-ZrP conventional	0.002(1)	0.001(2)	0.140(3)	9.748(9)	0.109(1)	1.299(2)
5Y-ZrP hydrothermal	0.005(1)	0.003(2)	0.070(1)	9.960(6)	0.528(1)	0.137(1)
10Y-ZrP conventional	0.009(2)	0.003(1)	0.098(2)	5.070(8)	0.120(2)	1.160(4)
10Y-ZrP hydrothermal	0.006(2)	0.008(2)	0.103(1)	7.089(9)	0.073(1)	1.105(2)
15Y-ZrP conventional	0.004(1)	0.009(2)	0.349(4)	7.500(8)	0.777(5)	0.630(1)
15Y-ZrP hydrothermal	0.001(8)	0.007(7)	0.187(1)	3.581(2)	0.429(2)	0.064(1)

It can be seen from the results shown above that yttrium and zirconium leaching from the materials during exchange with $Sr(NO_3)_2$ was almost negligible. This suggests that the structure of the ion exchangers were maintained after the exchange. However, the $Sr(OH)_2$ exchanged samples showed the highest leaching of Zr^{4+} ions but the Y^{3+} ions were leached in averaged amounts. But overall, the leaching from $Sr(OH)_2$ exchange solution decreased as the yttrium substitution percentage is increased from 5% to 15% for their respective synthesis routes. Contrarily, the $Sr(CH_3CO_2)_2$ exchanged samples showed mixed results for the

leached ions but it was observed that the Y^{3+} and Zr^{4+} ions were leached highest for the conventionally refluxed samples as opposed to the hydrothermally refluxed samples which showed relatively lower leaching. This is believed to be caused due to the differences in the surface areas and particles sizes of the conventional and hydrothermally refluxed samples as previously discussed. But overall these results compliment the XRD, XRF and ICP-MS results indicating that higher efficiency of Y-ZrP samples as strontium ion exchangers.

From all the above analysis it can be concluded that the strontium uptake by the synthesised Y-ZrP samples is higher compared to that of the parent α -ZrP but follows the similar trend. The highest amount of strontium can be exchanged from the hydroxide ions (ca. 75%) followed by acetates (ca. 50%) and nitrates (ca. 25%) for both α -ZrP and Y-ZrP. But as the uptake of strontium ions increases, the crystallinity of the samples decreases, the parent structure becomes unstable and the presence of new strontium exchanged phase starts to appear.

4.3. Caesium ion exchange

0.5g of the synthesised Y-ZrP samples (5%, 10% and 15%) together with α -ZrP synthesised by conventional and hydrothermal reflux methods were exposed to 125 mL of 0.1M caesium salt solutions (nitrates, acetates and hydroxides) ion exchange for extended reaction times (72 hours). The exchanged products were then characterised by XRD, XRF, FTIR and ICP-MS.

4.3.1 XRD analysis of caesium exchanged products

The XRD patterns of the $CsNO_3$ ion exchanges are shown in the Figure 4.7 below and it indicates the change in the physio-chemical properties of the products as compared to the un-exchanged α -ZrP.

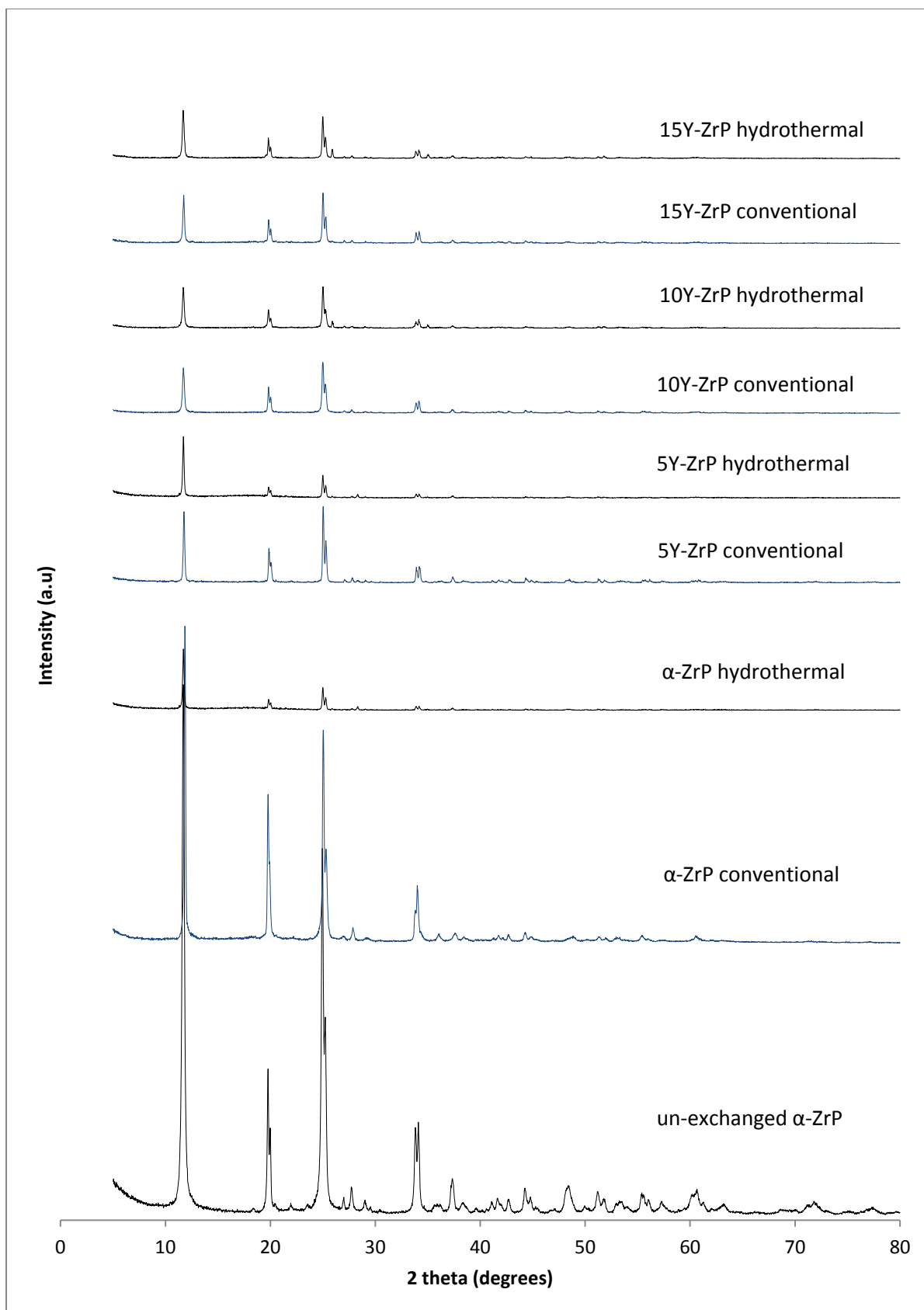


Figure 4. 7 XRD of CsNO_3 exchanged Y-ZrP products

The above results show that the structures of both the α -ZrP and Y-ZrP samples is conserved after caesium ion exchanged from the nitrate salt indicating that either no exchange or very limited exchange had taken place. Previous studies ^[5, 7, 12] show that α -ZrP exhibits ion-sieving effect in case of Cs^+ ion exchange due to the relatively large diameter of the Cs^+ ion to get accommodated into the layers of α -ZrP with a relatively smaller interlayer distance (7.6 Å). Therefore the Cs^+ ions are forced to exchange at high temperatures or alkaline pH conditions into the water-filled zeolite-type cavities due to the size (2.64 Å) present in the structure of α -ZrP. Excess energy is required for replacing the lattice water or spreading the layers apart to facilitate the uptake of the larger Cs^+ ions ^[5, 7], which is not possible at slightly acidic nitrate salt solutions.

But it is observed from the current results that there is a decrease in the peak intensities which is related to the compromised crystallinity of the exchanged products, hence it is understood that due to the possible adsorption or incorporation of caesium ions there was a decreased signal to noise ratio. This suggests that both the α -ZrP and Y-ZrP might have exchanged Cs^+ ions even though in very low amounts. The presence of a small peak at $2\theta = 28.5^\circ$ for all exchanged products indicates the possibility of exchange or formation of another phase. A PDF database search was conducted that matched this peak to cesium phosphate (CsPO_4) as shown in figure 16 of appendix 3, but no other peaks corresponding to CsPO_4 were found to match the XRD pattern.

The XRD patterns for the CsOH are shown in Figure 4.8 below and clearly show the change in the structure and crystallinity of the exchanged products as compared to that of the un-exchanged α -ZrP.

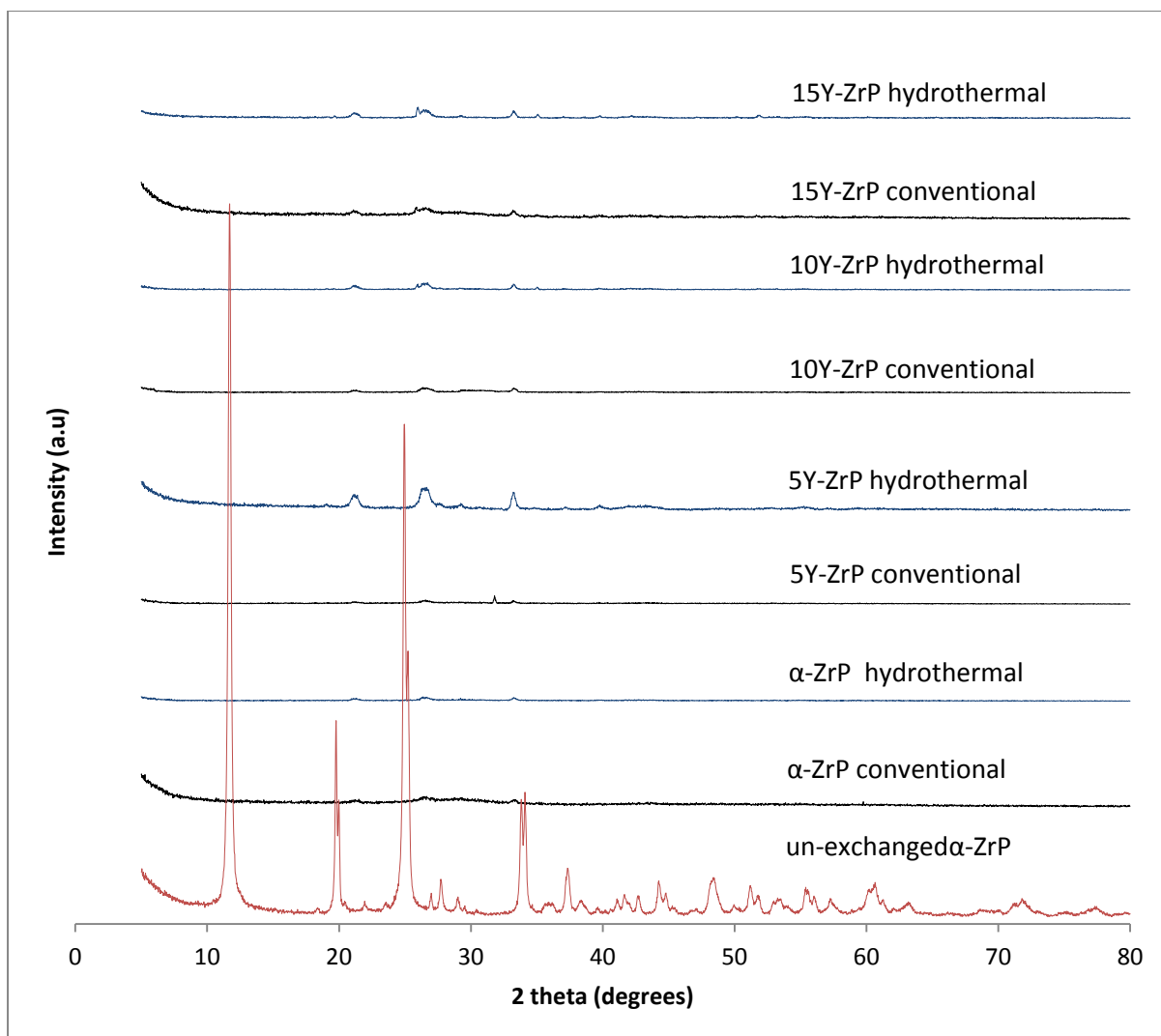


Figure 4. 8 XRD of CsOH exchanged Y-ZrP products

The results shown above for CsOH exchanged products indicate a significant decrease in the crystallinity for both α -ZrP and Y-ZrP samples. However the Y-ZrP products exhibited a better degree of crystallinity as compared to an almost amorphous α -ZrP product. Also, the hydrothermally refluxed samples in general were found to conserve some degree of order after the CsOH exchange compared to the conventionally refluxed samples that a poor degree of crystallinity. The characteristic peaks of α -ZrP structure ($2\theta = 11.5^\circ$) were missing and extra peaks were observed at $2\theta = 21.1^\circ$ and 28° . These peaks are not identified in the literature but a PDF database match for the crystal structure indicated the presence of α -caesium phosphate phase (α -CsP₂O₇), as shown in figure 17 of appendix 3.

However in previous studies [6, 8, 13] it was found that high pH conditions from the hydroxide salt solutions can provide sufficient energy to spread the layers and can lead to the formation of a single phase Cs⁺ exchanged products depending on the extent of loading. But, since no detailed characterisation of these Cs⁺ exchanged structures are present in the literature, the XRD pattern shown in the Figure 4.8 above cannot be deduced to a particular structure. However, since it is evident from one of the study [14] that approximately 80% exchange is observed for alkaline solutions above pH 10.3 which leads to the formation of dicaesium phase [Zr(CsPO₄)₂·6H₂O] with an interlayer spacing of 14.2Å. However, since the crystallinity of the exchanged products is extremely low, it was not possible to distinctly observe the peak corresponding to d-spacing of 14.2Å to confirm this phase.

The XRD patterns for the CsCH₃CO₂ exchanged Y-ZrP products are shown in the Figure 4.9 below.

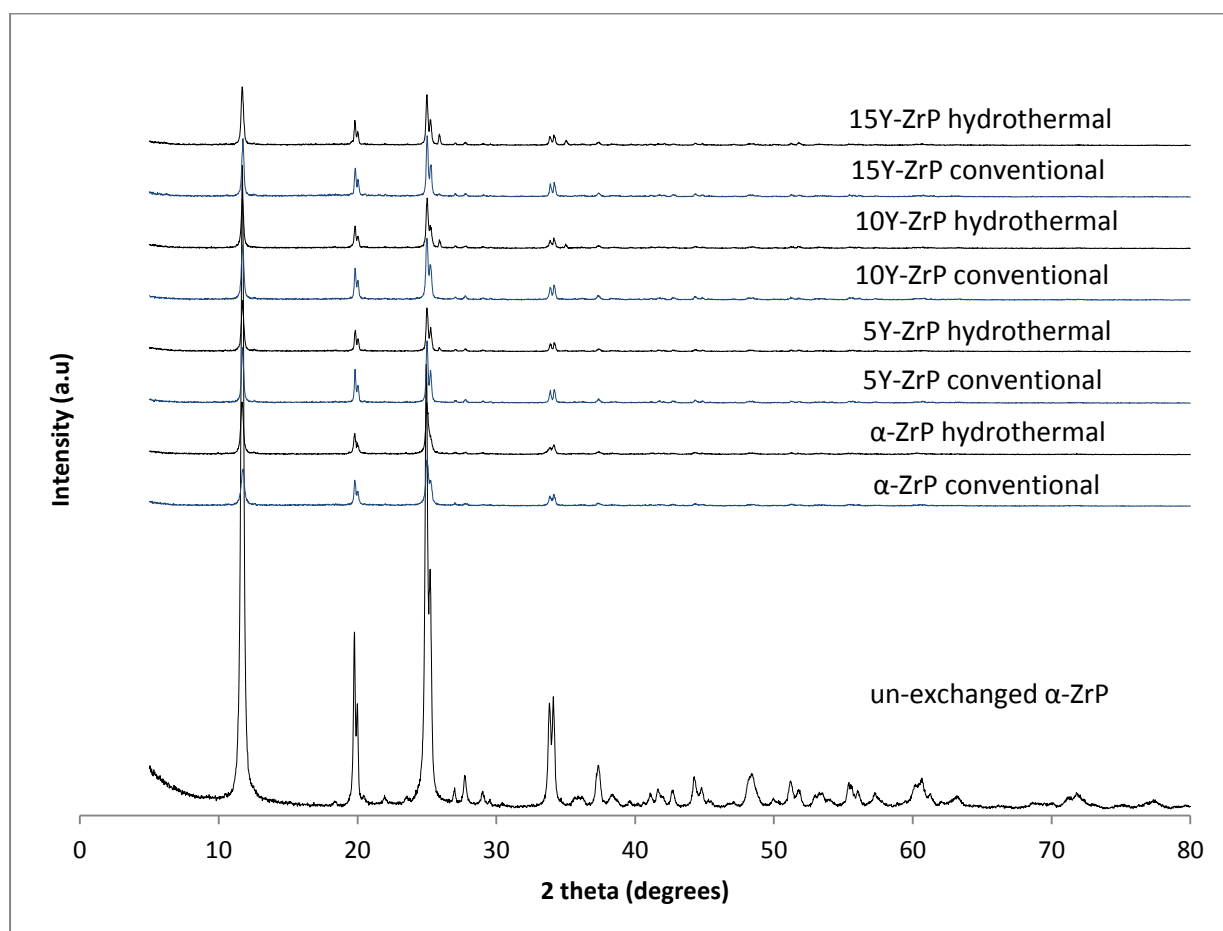


Figure 4. 9 XRD of CsCH₃CO₂ exchanged Y-ZrP products

It is observed from the XRD patterns shown in the Figure 4.9 above that the exchange with caesium acetate solution maintains the crystallinity of the samples. However, there is a decrease in peak intensities for all the products which can be attributed to the decrease in the crystallinity of the samples due to the alkaline pH conditions of the exchange solution. There are no peaks indicative of a phase transformation and little changes in the relative intensities of the peaks across all samples, suggesting that the Cs⁺ ion exchange was negligible or very limited. But the literature search suggests that slightly alkaline solutions (ca. pH = 8) were able to exchange minimum 30% Cs⁺ ions into the α -ZrP^[14] and therefore produces a single phase Cs-exchanged form [ZrHCs(PO₄)₂·2H₂O]. The patterns for caesium acetate exchange are similar to those from exchange with caesium nitrate (Figure 4.7) suggesting similar behaviour.

4.3.2 pH analysis of caesium exchanged products

The pHs of the ion exchanged solutions are analysed and the results are presented in the Table 4.8 below.

Table 4. 8 Summary of the pH analysis of caesium exchanged solutions

Samples	pH of solutions		
	CsNO ₃ Stock pH = 5.93	CsOH Stock pH = 12.59	CsCH ₃ CO ₂ Stock pH = 8.75
α -ZrP conventional	4.19	12.55	7.05
α -ZrP hydrothermal	4.76	12.53	6.89
5Y-ZrP conventional	4.52	12.53	7.15
5Y-ZrP hydrothermal	4.55	12.50	6.85
10Y-ZrP conventional	4.96	12.40	6.98
10Y-ZrP hydrothermal	5.12	12.51	6.81
15Y-ZrP conventional	4.43	12.50	7.13
15Y-ZrP hydrothermal	4.97	12.52	6.97

It is seen from the above results that no definite trend can be observed for the pH results of the CsNO₃ exchanged samples. However all the Y-ZrP samples showed similar pH results as compared to the hydrothermally refluxed α -ZrP but the

conventionally refluxed α -ZrP showed the highest decline in the pH. Therefore it can be concluded that conventionally refluxed α -ZrP showed the highest Cs^+ uptake. This might be again due to the difference in the surface areas and particle sizes of the conventional and hydrothermally refluxed samples as discussed previously. Overall, similar trend was observed for the CsCH_3CO_2 exchanged Y-ZrP samples too since they showed comparable results to that of α -ZrP for both routes of reflux. However, for CsOH exchanged samples, Y-ZrP products showed a lower pH measurement as compared to the α -ZrP for both routes of reflux indicating that the synthesised Y-ZrP samples may be uptaking more Cs^+ ions as compared to the parent α -ZrP.

4.3.3 XRF analysis of caesium exchanged products

XRF analysis was carried out for the Cs^+ exchanged products to quantify the extent of exchange occurring in the samples. The summary of the XRF results is shown in Table 4.9 below.

Table 4. 9 XRF compositional analysis for the caesium exchanged products

Samples	<u>Extent of Exchange</u>		
	Ratio of Cs / (Y+Zr)		
	CsNO ₃	CsOH	CsCH ₃ CO ₂
α -ZrP conventional	0.0522(5)	0.1909(1)	0.0267(6)
α -ZrP hydrothermal	0.0160(8)	0.2178(2)	0.0279(7)
5Y-ZrP conventional	0.0236(2)	0.2197(7)	0.0151(8)
5Y-ZrP hydrothermal	0.0233(6)	0.2813(4)	0.0176(1)
10Y-ZrP conventional	0.0175(3)	0.2059(6)	0.0148(8)
10Y-ZrP hydrothermal	0.0144(6)	0.2324(3)	0.0165(7)
15Y-ZrP conventional	0.0295(1)	0.1923(3)	0.0148(5)
15Y-ZrP hydrothermal	0.0170(3)	0.2188(6)	0.0160(4)

It can be seen from the above elemental analysis of the caesium exchanged Y-ZrP products that caesium hydroxide was able to exchange the highest caesium ions (ca. 28% molar concentration) for both α -ZrP and Y-ZrP samples as compared to acetate (ca. 2.8% molar concentration) and nitrate salts (ca. 2.9% molar concentration). Y-

ZrP products synthesised via both methods exchanged more caesium than the α -ZrP samples from the CsOH solution which clearly indicates that Y-ZrP shows higher exchange capacity for caesium ions at alkaline conditions. However, there was little difference (approximately 10%) observed between the uptake of caesium from the nitrate and acetate salts and the exchange capacity for Y-ZrP samples was seen to be lower than α -ZrP for the caesium acetate solution. It can be seen that the conventionally refluxed α -ZrP as compared to the hydrothermal refluxed α -ZrP exchanged more caesium from the nitrate salt solution than from the acetate salt solutions. This result shows that the Cs^+ ion exchange does not follow a definite trend for α -ZrP type structure possibly due to the large size of Cs^+ ions.

But the Y-ZrP samples from both routes of synthesis showed a slight increase (approximately 8%) in the caesium ion exchange from the nitrate salt solution as compared to the hydrothermally synthesised α -ZrP but the results are not consistent with respect to the yttrium concentration, hence no definite relation can be outlined from these results. Also, the conventionally refluxed α -ZrP showed a heightened exchange from the nitrate solution. This might be a result of some error during the exchange reaction, possibly due to temperature or pH variation.

In summary, the synthesised Y-ZrP samples in comparison with the α -ZrP samples via both refluxing routes showed a better exchange capacity of Cs^+ ions from the CsOH solution as compared to the CsCH_3CO_2 and CsNO_3 solution. These results are in consistency with the previous findings in the literature [5, 8, 14].

4.3.4 FT-IR analysis of caesium exchanged products

A FT-IR analysis was done on the caesium exchanged products so as to analyse any change in the chemical environment of these products which might be related to their ion exchange behaviour.

A FT-IR spectrum for the CsNO_3 exchanged products is shown in the Figure 4.10 below and indicates the similarity of the bonding environments of the exchanged samples as compared to α -ZrP.

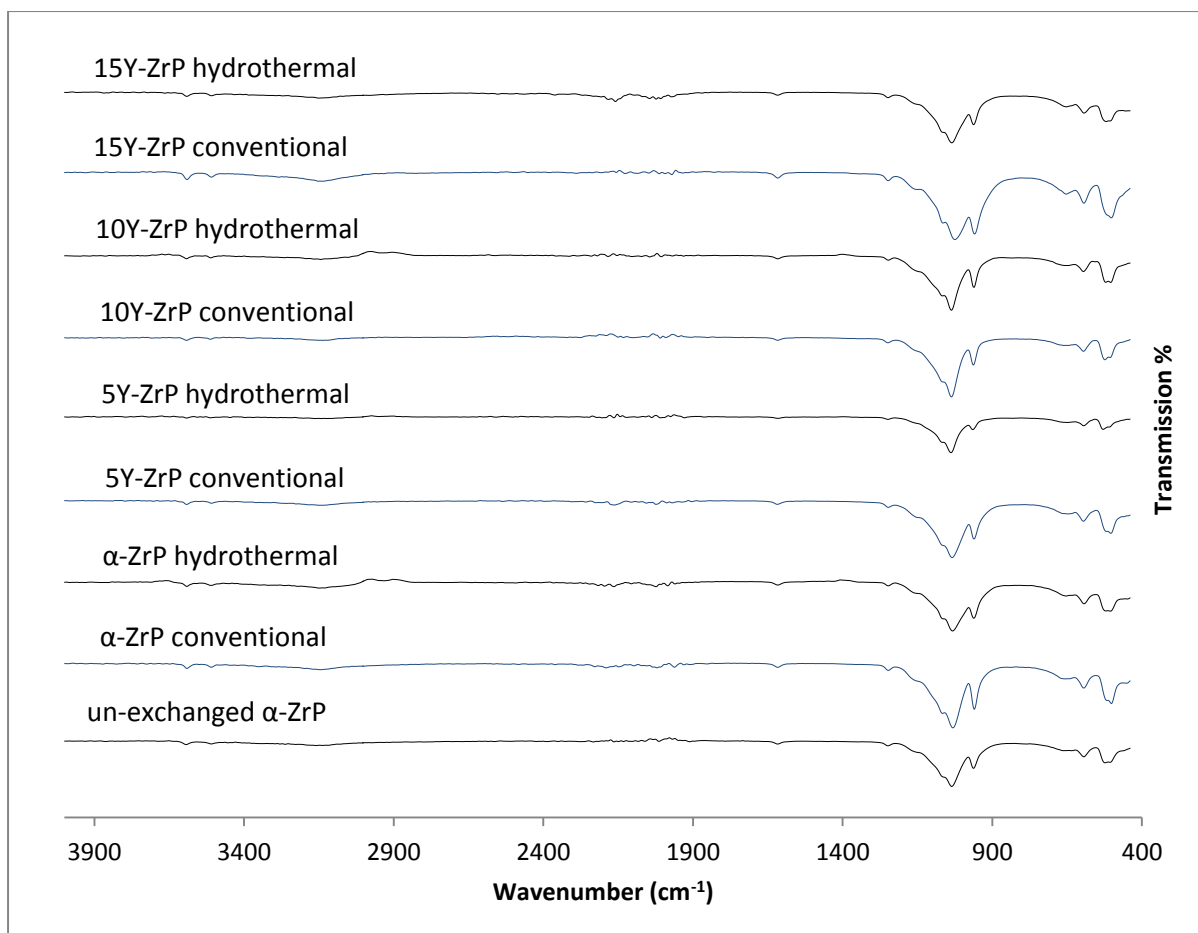


Figure 4. 10 FT-IR of CsNO₃ exchanged Y-ZrP products

It can be observed from the FT-IR spectra shown in the figure above that no distinctive changes had occurred for the CsNO₃ exchanged Y-ZrP as well as α-ZrP samples from both synthesis methods. However, low frequency peaks (400-550 cm⁻¹) appear to be shifted slightly towards lower wavenumber with few subtle changes that can be observed in the peak intensities at ca. 960, 3509 and 3586 cm⁻¹. But these changes are not consistent within the exchanged products to deduce a firm conclusion about the exchange. Therefore, it can be concluded that Cs⁺ ions might be only adsorbed to the surface of the samples. Hence it can be concluded that these results are complimenting the XRD and XRF analysis done above. A summary of the major identified peaks is provided in the Table 4.10 below.

Table 4. 10 Summary of FT-IR results for CsNO₃ ion exchange

Peak Wavenumber (cm ⁻¹)	Chemical bonds
523.74	P-O-P vibration
595.52	P-OH (out of plane)
647.54	O-H (out of plane)
963.35	P-O bending (in plane)
1036.75	P-O stretching (asym)
1248.83	P-O-H deformation
1617.16	O-H bending (asym)
2190.06	P-OH
3137.15	O-H stretching (sym)
3512.35	O-H stretching (asym)
3591.90	O-H stretching (asym)

The FT-IR spectrums for CsOH exchanged products are shown in the Figure 4.11 below and indicate the significant chemical changes in all the exchanged samples as compared to un-exchanged α -ZrP.

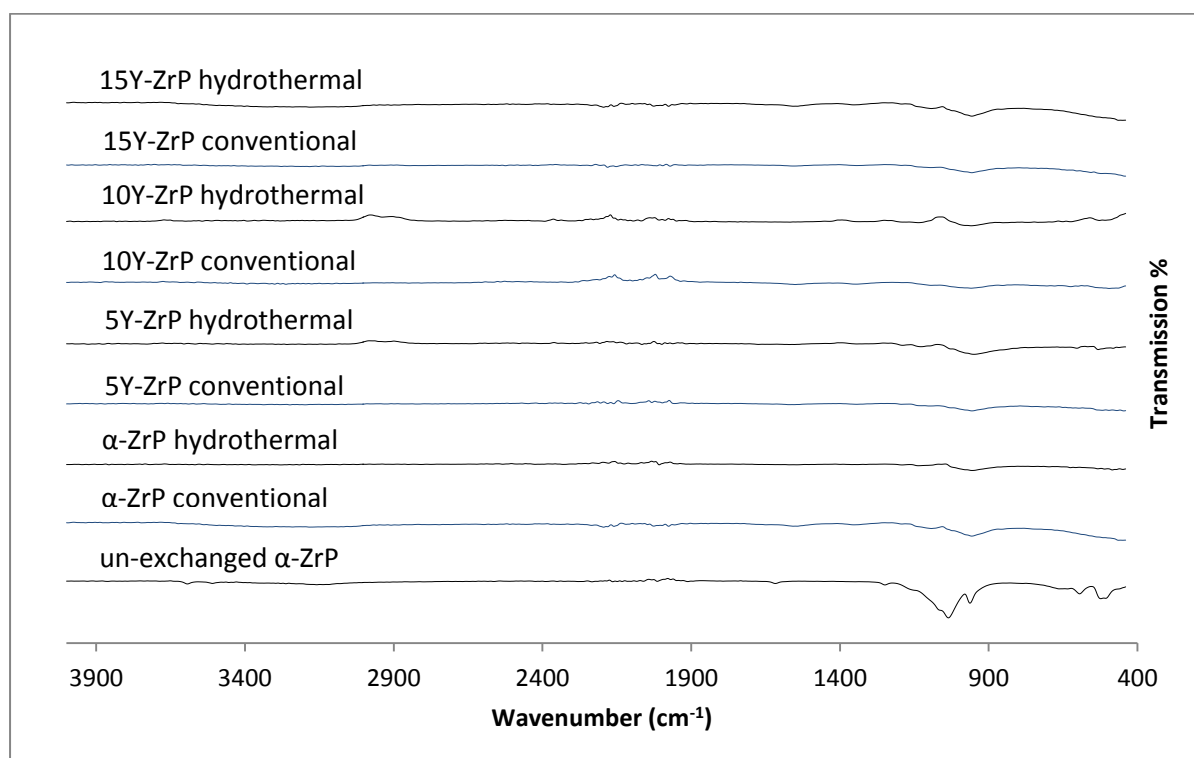


Figure 4. 11 FT-IR of CsOH exchanged Y-ZrP products

It can be seen from the above results that the FT-IR spectrums of the CsOH exchanged products differ greatly with respect to that of parent α -ZrP. A Few extra but relatively weaker peaks were seen in the region of 450 – 500 cm^{-1} and 700-850 cm^{-1} which could correspond to the vibration of the Cs-Cs or Cs-O bonds [5, 14]. The characteristic bending and stretching modes for P=O bonds at ca.955 and 1030 cm^{-1} are absent and instead a broader peak is present in that region. It can be seen that the peak at ca.1030 cm^{-1} is very weak, while the peak at ca.955 cm^{-1} appeared to be dominant. This suggests that P-O bonds were more bent and the P-O stretching was relaxed due to the possible exchange of the Cs^+ ions into the cavities of layers and hence pushing them apart. Also the vibrational peaks for O-H bending and stretching were not observed in the region of ca.1620 cm^{-1} and 3000-3500 cm^{-1} respectively, again indicating that no OH^- groups of H_2O molecules remain in the materials post ion-exchange. Hence it is again concluded that the CsOH exchanged products are structurally very different from the α -ZrP type products due to the presence of different chemical environments and types of chemical bonds. These results are complimenting the XRD and XRF analysis done above indicating the possible exchange of Cs^+ ions into the lattice leading to deformation of the parent α -ZrP type structure.

A summary of the key peaks from a typical Cs^+ exchanged product is shown in the Table 4.11 below.

Table 4. 11 Summary of FT-IR results for CsOH ion exchange

Peak Wavenumber (cm^{-1})	Chemical bonds
518.01	P-O-P vibration
713.02	Cs-Cs or Cs-O (unknown)
955.41	P-O bending (in plane)
1036.75	P-O stretching (asym)

The FT-IR spectrum of the CsCH_3CO_2 exchanged products are shown in the Figure 4.12 below and indicate a similarity in the spectra of the exchanged samples as compared to α -ZrP.

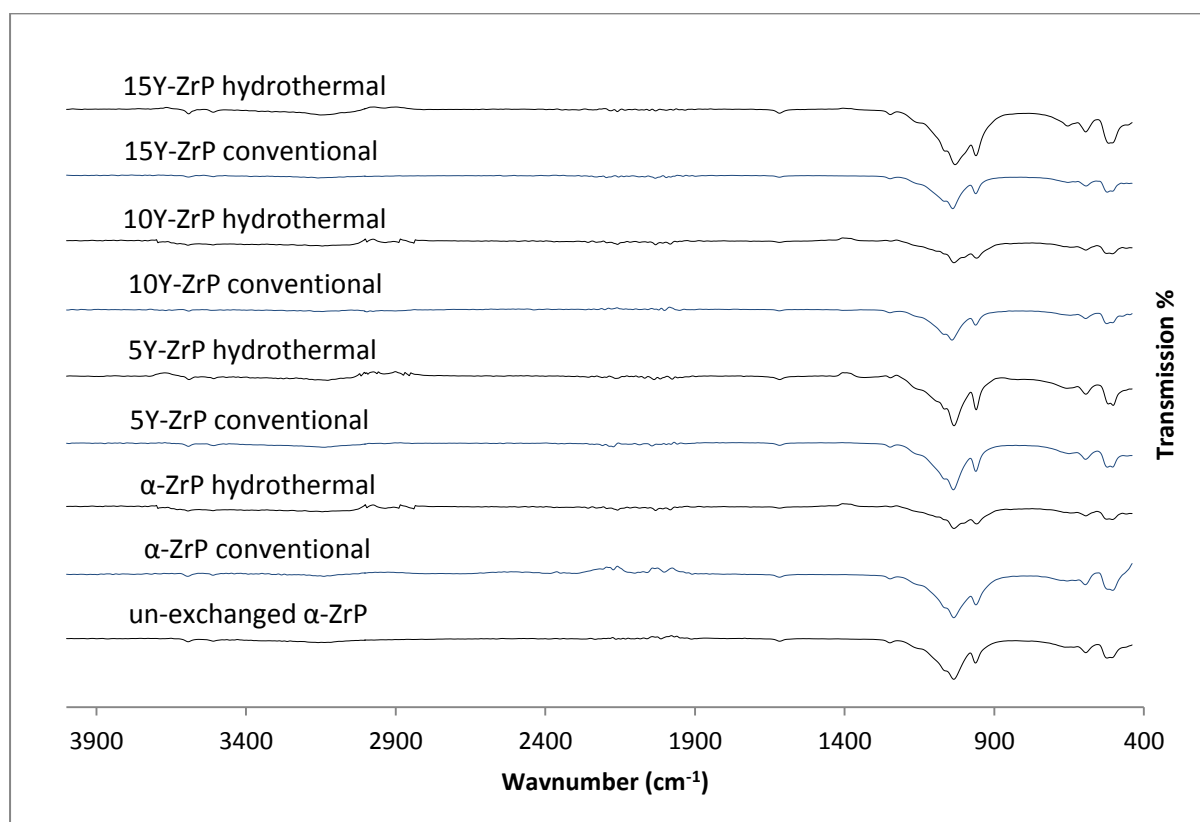


Figure 4. 12 FT-IR of CsCH_3CO_2 exchanged Y-ZrP products

It is seen from the above results that the FT-IR spectrums of the CsCH_3CO_2 exchanged products are very similar to that of un-exchanged α -ZrP. However, subtle changes can be observed in the P-O bending and stretching vibrations from the difference in the peak intensities at 960 cm^{-1} and 1030 cm^{-1} . Similar changes can be observed through the intensity difference of the vibrational peaks for O-H bending and stretching in the region of $\text{ca.}1620\text{ cm}^{-1}$ and $3000\text{-}3500\text{ cm}^{-1}$ respectively. However, apart from these minute changes in peak intensities, few very weak peak signals were observed in the region of $1800\text{-}2200\text{ cm}^{-1}$ but no clear evidence of any of these peaks can be found in the literature to reach a clear conclusion about the nature of exchange. Hence it can be again concluded that the CsCH_3CO_2 exchanged products were successful as opposed to mere adsorption from CsNO_3 solution but the amount of Cs^+ exchange seems very limited, as seen from the XRF analysis above.

A summary of the typical peaks from the CsCH₃CO₂ exchanged products are shown in Table 4.12 below.

Table 4. 12 Summary of FT-IR results for CsCH₃CO₂ ion exchange

Peak Wavenumber (cm ⁻¹)	Chemical bonds
517.01	P-O-P vibration
594.72	P-OH (out of plane)
654.63	O-H (out of plane)
961.38	P-O bending (in plane)
1030.96	P-O stretching (asym)
1247.31	P-O-H deformation
1617.73	O-H bending (asym)
2189.45	P-OH
3150.30	O-H stretching (sym)
3509.47	O-H stretching (asym)
3591.63	O-H stretching (asym)

4.3.5 ICP-MS analysis of caesium exchanged products

An analysis of the filtrate solution after caesium exchange was carried out using the ICP-MS in order to ascertain the extent of Cs⁺ ion exchange from different salt solutions and therefore confirm the XRF results of the exchanged solid products. In order to do so, the filtrate solutions were diluted 1000 times and were analysed by ICP-MS against the calibration curves (figures 4-6 in Appendix 3) to precisely determine the amount of Cs⁺ ions exchanged in the samples. A summary of the ICP-MS results is shown in the Table 4.13 below.

Table 4. 13 Summary of ICP-MS results for caesium ion exchanged Y-ZrP samples

Samples	X = Amount of Cs ⁺ remaining (ppm)			% of Cs ⁺ incorporation $\frac{13290.55ppm - Xppm}{13290.55ppm \text{ of } 0.1M \text{ Cs}} \times 100$		
	CsNO ₃	CsOH	CsCH ₃ CO ₂	CsNO ₃	CsOH	CsCH ₃ CO ₂
α-ZrP conventional	12275(6)	9099(2)	12789(3)	7.64%	31.53%	3.77%
α-ZrP hydrothermal	12950(5)	8876(7)	12710(2)	2.56%	33.21%	4.36%
5Y-ZrP conventional	12773(3)	8613(5)	12974(5)	3.89%	35.19%	2.38%
5Y-ZrP hydrothermal	12775(5)	7307(3)	12952(8)	3.87%	45.02%	2.54%
10Y-ZrP conventional	12921(4)	8789(6)	12982(5)	2.78%	33.87%	2.32%
10Y-ZrP hydrothermal	13000(3)	8314(4)	12969(6)	2.18%	37.44%	2.42%
15Y-ZrP conventional	12669(4)	8990(4)	12979(2)	4.67%	32.35%	2.34%
15Y-ZrP hydrothermal	12969(2)	8598(5)	12970(4)	2.42%	35.31%	2.41%

It is evident from the ICP-MS results shown above that the highest amount of caesium uptake is from the caesium hydroxide solution (45%) for the 5% Y-ZrP hydrothermally synthesised sample. Also, in general all the Y-ZrP samples take up more Cs⁺ ions from the CsOH solution compared to the α-ZrP samples but the same results could not be observed for the CsNO₃ and CsCH₃CO₂ exchanged samples as Y-ZrP products performed almost similar to α-ZrP. Also the XRD results show that the layered structure of all the samples were not preserved after the CsOH exchange as opposed to that present in the CsNO₃ and CsCH₃CO₂ exchanged samples. Therefore it is of interest to analyse the extent of lattice breakdown by measuring the amounts of zirconium and yttrium released due to the formation of these new

phases. A summary of the leached Y^{3+} and Zr^{4+} ions from the exchange solutions is measured by ICP-MS and is provided in the Table 4.14 below.

Table 4. 14 Summary of ICP-MS for the leached ions

Samples	CsNO ₃		CsOH		CsCH ₃ CO ₂	
	Y ³⁺ (ppm)	Zr ⁴⁺ (ppm)	Y ³⁺ (ppm)	Zr ⁴⁺ (ppm)	Y ³⁺ (ppm)	Zr ⁴⁺ (ppm)
α-ZrP conventional	-	0.347(2)	-	171.5(6)	0	28.36(4)
α-ZrP hydrothermal	-	0.178(5)	-	145.3(4)	0	25.21(2)
5Y-ZrP conventional	0.032(1)	0.685(4)	4.020(1)	172.5(3)	0.458(1)	28.70(4)
5Y-ZrP hydrothermal	0.012(1)	0.238(2)	1.770(1)	118.3(7)	0.511(2)	20.78(6)
10Y-ZrP conventional	0.035(2)	0.170(1)	6.840(1)	169.4(3)	1.034(4)	24.96(9)
10Y-ZrP hydrothermal	0.033(1)	0.295(3)	1.220(4)	153.2(5)	0.849(7)	16.64(3)
15Y-ZrP conventional	0.070(3)	0.580(6)	4.490(5)	196.1(3)	1.822(6)	18.45(5)
15Y-ZrP hydrothermal	0.087(4)	0.228(2)	5.800(2)	129.6(6)	1.113(3)	28.30(6)

It can be observed from the above table that there is no apparent trend for the leaching of Y^{3+} and Zr^{4+} ions from the CsNO₃ exchanged products. This shows that the samples showed a limited exchange due to the instability of the α-ZrP type structures on accommodation of the large caesium ions from the salt solutions. Similar results were observed for the CsOH solutions where the Y^{3+} and Zr^{4+} ions showed no apparent trends with regards to the percentage of yttrium substitution. However, the leached quantities of both these ions are very high which shows that breakdown of structures must have taken place. This explains the very low yield (< 0.1g) of the CsOH exchanged products. However, for the CsCH₃CO₂ exchange it

was observed that Y^{3+} and Zr^{4+} ions were leached in very little quantities as compared with the CsOH exchange which indicates higher stability of the products in the acetate salt solutions and therefore will favour a successful exchange. Overall, the total leached amounts of metal ions (Y^{3+} and Zr^{4+}) from Y-ZrP samples is lower than that of the total Zr^{4+} leached ions from α -ZrP samples. But in general conventionally refluxed samples leached more of the ions compared to the hydrothermally synthesised samples, again indicating some difference in the surface area and particle sizes/morphology which makes leaching more facile. Hence it can be concluded that the nitrate and acetate salt solutions are more likely to exchange Cs^+ ions as compared to the hydroxide salt solution which clearly show a breakdown of the structure indicating the formation of mixed phases leading to high amount of leaching for the parent ions. These results also compliment the XRD, XRF and ICP-MS analysis in previous sections.

In conclusion, the results for both α -ZrP and Y-ZrP samples towards caesium ion uptake showed no apparent trends, but generally showed a slightly higher stability for the Y-ZrP samples as compared to the α -ZrP. However no definite conclusion can be drawn from these results and hence it is clear that the caesium uptake by α -ZrP type structures is low.

4.4. Cobalt ion exchange

The α -ZrP and Y-ZrP materials produced via both synthesis routes were subjected to the cobalt ion exchange using both nitrate and acetate salt solutions at the room temperature for extended periods of time (72 hours). Cobalt hydroxide [$Co(OH)_2$] was sparingly soluble in water and appeared to be only suspended even after heating the solution to near boiling point. Therefore the separation of the exchanged products from the un-dissolved $Co(OH)_2$ was difficult and there was a high possibility of errors due to cobalt hydroxide impurity and so these results are not included. The cobalt exchanged products were characterised by XRD, XRF, FT-IR and ICP-MS.

4.4.1 XRD analysis of the cobalt exchanged products

The XRD pattern of the $Co(NO_3)_2$ exchange for both the α -ZrP and Y-ZrP via both routes of reflux is shown in the Figure 4.13 below.

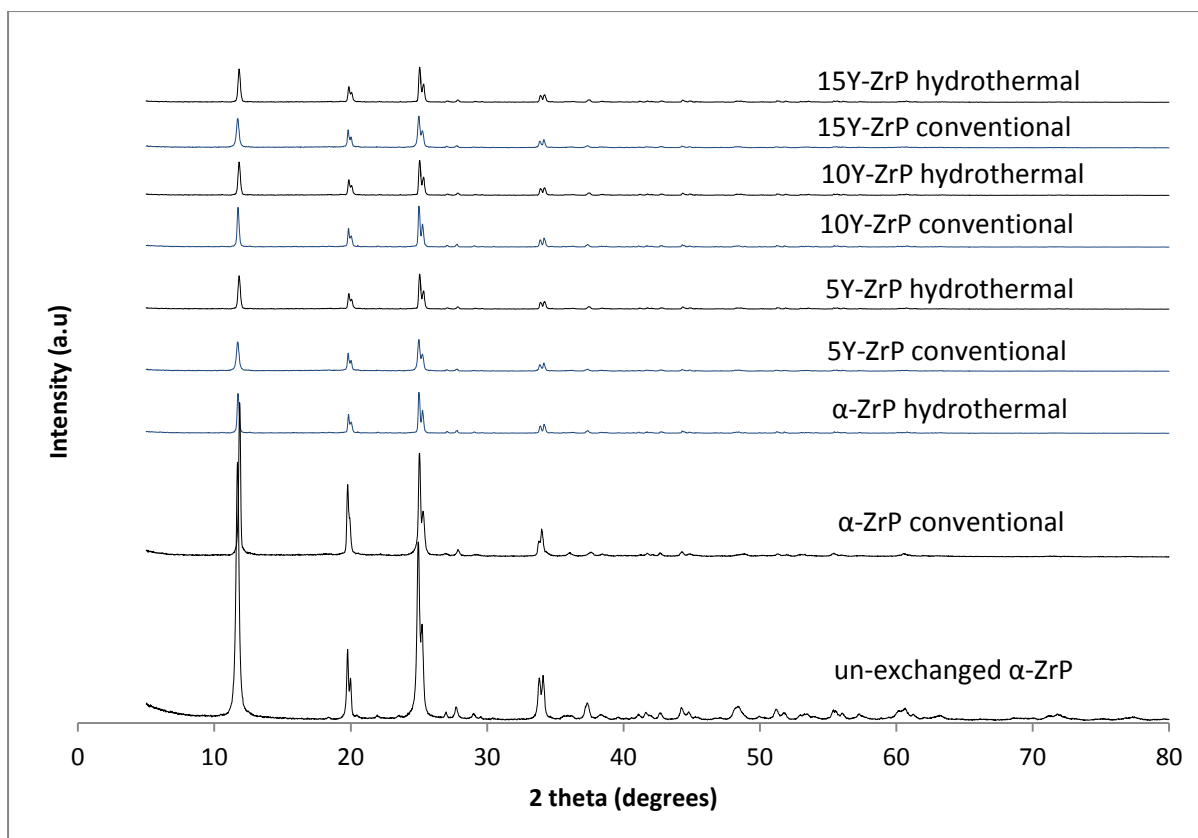


Figure 4. 13 XRD of $\text{Co}(\text{NO}_3)_2$ exchanged products

It can be seen from the above results that the crystalline structure of the Co^{2+} ion exchanged products remains intact as evident from the isostructural patterns. However, there is a change in the peak intensities which might be an indication of the decreasing crystallinity. Some extra peaks at $2\theta = 10.57^\circ$, 12.60° and 20.5° were observed in Y-ZrP samples but with a very low intensity. These peaks were not identified in the literature search and also did not show a potential match in the PDF database search. But the existence of these extra peaks suggests a possible Co^{2+} ion exchange into the structure from the nitrate salt solution.

The XRD pattern for the cobalt acetate exchanged products from both synthesis routes are shown in the figure 14 below.

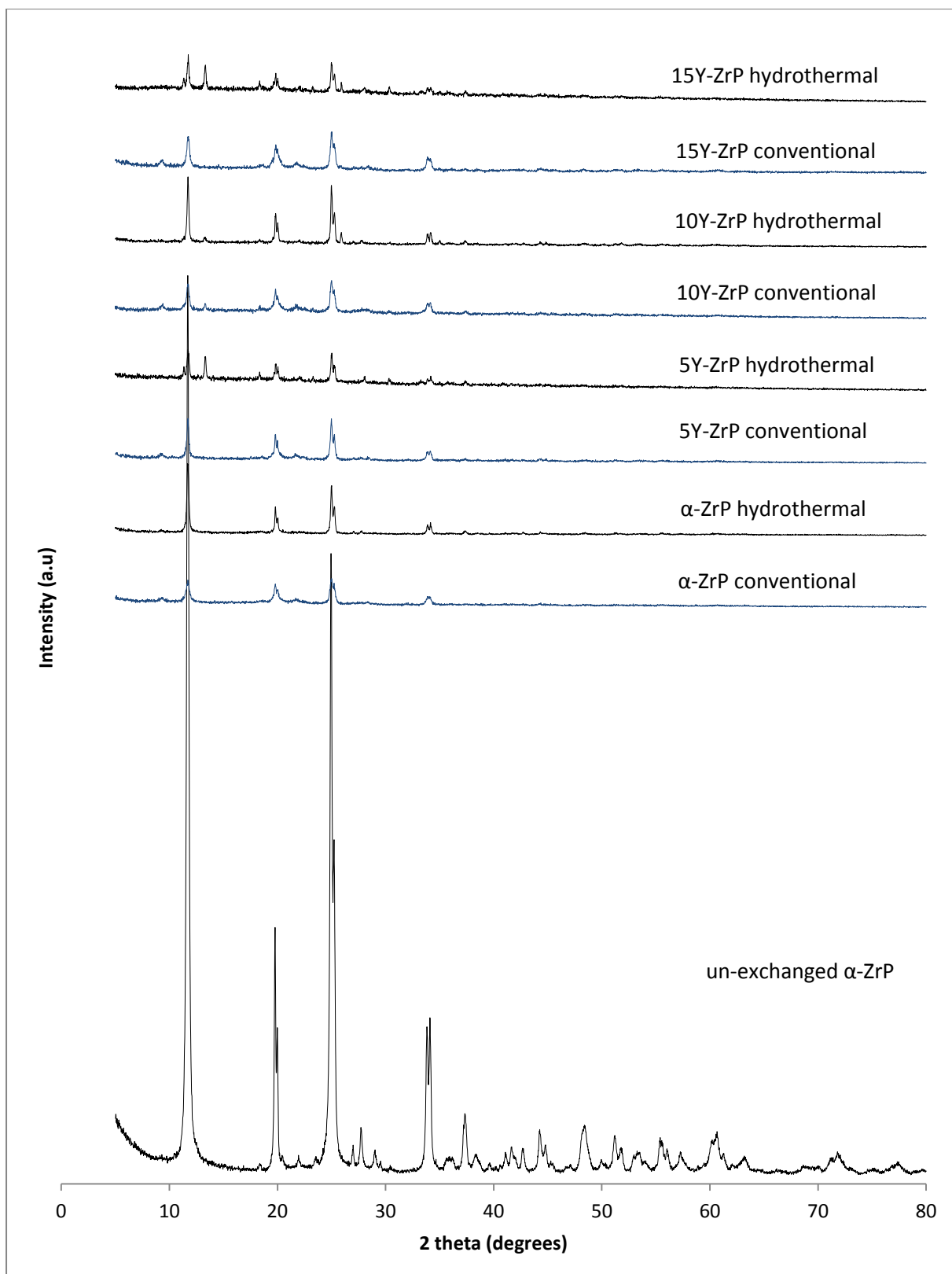


Figure 4. 14 XRD of $\text{Co}(\text{CH}_3\text{CO}_2)_2$ exchanged products

It is evident from the above results that there is a change in the XRD patterns of the exchanged products for both α -ZrP and Y-ZrP samples. This indicates that the

acetate salt solutions were able to exchange Co^{2+} ions in substantial amounts into the α -ZrP type structure. This result is consistent with the previous findings [14, 15] where it was concluded that more than 33% exchange is observed for Co^{2+} ions from the acetate solution.

It is observed here that the peak intensities are affected and the products appear to lose their crystallinity and become semi-crystalline. The XRD patterns of the conventional refluxed samples showed a higher loss of crystallinity as compared to the sharper peaks of the hydrothermally synthesised samples indicating a more crystalline structure. Some extra peaks were observed at $2\theta = 9.2^\circ$, 11.36° , 13.27° and 30.36° . These peaks were not identified from the literature since the Co-exchanged ZrP patterns are not characterised yet. But it is suggested in one of the studies [15] that a phase with composition $\text{ZrCo}_{0.33}\text{H}_{1.34}(\text{PO}_4)_2 \cdot 2.4\text{H}_2\text{O}$ is formed at around 33% cobalt exchange. A PDF database search shows a match for some of these peaks suggesting a possible formation of Pakhomovskyite [$\text{Co}_3(\text{PO}_4)_2 \cdot 8\text{H}_2\text{O}$] phase [16], as shown in the figure 18 of appendix 3.

Therefore It is understood from these results of $\text{Co}(\text{CH}_3\text{CO}_2)_2$ exchange shown in Figure 4.14 above that the cobalt is successfully exchanged into the synthesised samples from the acetate solution but it is important to further analyse the exchanged products to understand the extent of exchange and extent of structure deformation due to this exchange.

4.4.2 XRF analysis of cobalt exchanged products

Elemental analysis was carried out on the Co^{2+} exchanged products using XRF. The analysis of $\text{Co}(\text{OH})_2$ exchanged products were not carried out since the exchanged products could not be separated from the un-dissolved $\text{Co}(\text{OH})_2$ impurity. The results of the XRF analysis are presented in the Table 4.15 below.

Table 4. 15 XRF elemental analysis for the cobalt exchanged products

Samples	Extent of Exchange Ratio of Co / (Y+Zr)	
	Co(NO ₃) ₂	Co(CH ₃ CO ₂) ₂
α-ZrP conventional	0.0123(2)	0.1025(2)
α-ZrP hydrothermal	0.0140(1)	0.1035(6)
5Y-ZrP conventional	0.0199(1)	0.1213(7)
5Y-ZrP hydrothermal	0.0254(9)	0.4915(3)
10Y-ZrP conventional	0.0181(2)	0.2514(9)
10Y-ZrP hydrothermal	0.0242(3)	0.1178(9)
15Y-ZrP conventional	0.0139(9)	0.1345(4)
15Y-ZrP hydrothermal	0.0184(3)	0.5045(6)

The results shown above indicate that the extent of Co²⁺ ion uptake was higher for Y-ZrP products compared to α-ZrP produced by both synthesis routes. It is evident that 5% Y-ZrP hydrothermally synthesised was able to uptake approximately 2.5% Co²⁺ ions as compared to only 1.4% by α-ZrP from Co(NO₃)₂ solutions. It is understood from the above analysis and past studies ^[9, 14] that the low uptake of α-ZrP from nitrate solution could be due to surface adsorption rather than an exchange inside the structure. However, almost twice the uptake was achieved by the Y-ZrP samples which indicate a possible low amount of exchange into the structure. However, no definite trend was observed for the Co²⁺ ion exchange with respect to the yttrium concentration of the Y-ZrP products.

Also, the Co(CH₃CO₂)₂ solutions gave higher Co²⁺ uptake as compared to the nitrate solution. The synthesised Y-ZrP products again showed an increased uptake (minimum ca. 11.7%) for the Co²⁺ ions as compared to the capacity of α-ZrP (ca. 10%). However, the appearance of certain unusually high Co% (ca. 50%) indicates that cobalt is precipitated out either as Co(OH)₂ or CoPO₄ phases as discussed before, due to the breakdown of α-ZrP type structures with loss of zirconium and yttrium ions. An estimation of yttrium and zirconium ions in the filtrate solutions using ICPM-MS was required to confirm this. Overall, it was observed that Y-ZrP

exchanged products performed better than parent α -ZrP for successfully exchanging the Co^{2+} ions.

4.4.3 pH analysis of the cobalt exchanged products

The summary of the pH results of the ion exchanged solutions from each of the products are shown in the Table 4.16 below.

Table 4. 16 Summary of the pH analysis of cobalt exchanged solutions

Samples	pH of solutions	
	$\text{Co}(\text{NO}_3)_2$ Stock pH = 4.2	$\text{Co}(\text{CH}_3\text{CO}_2)_2$ Stock pH = 7.20
α -ZrP conventional	3.89	6.30
α -ZrP hydrothermal	3.78	6.32
5Y-ZrP conventional	3.42	5.98
5Y-ZrP hydrothermal	3.30	5.22
10Y-ZrP conventional	3.56	5.57
10Y-ZrP hydrothermal	3.38	5.92
15Y-ZrP conventional	3.82	5.89
15Y-ZrP hydrothermal	3.55	5.25

The pH results shown in the table above indicate that there is decrease in the pH after the Co^{2+} ion exchange for both α -ZrP and Y-ZrP samples of both synthesis routes. Also, the acetate salt solutions showed greater decrease in the pH compared to the nitrate solutions indicating that the extent of exchange is higher with the acetate solution. However, no definite trend could be observed in the pH values in regards to the yttrium concentrations but it was generally seen that the Y-ZrP samples on comparison with the parent α -ZrP were able to exchange more H^+ ions into the solutions for Co^{2+} ions, thereby reducing the pH more.

4.4.4 FT-IR analysis of the cobalt exchanged products

The FT-IR results for the $\text{Co}(\text{NO}_3)_2$ exchanged products are shown in the figure 15 below and indicate a similar nature of chemical environment of the exchanged products as compared to α -ZrP.

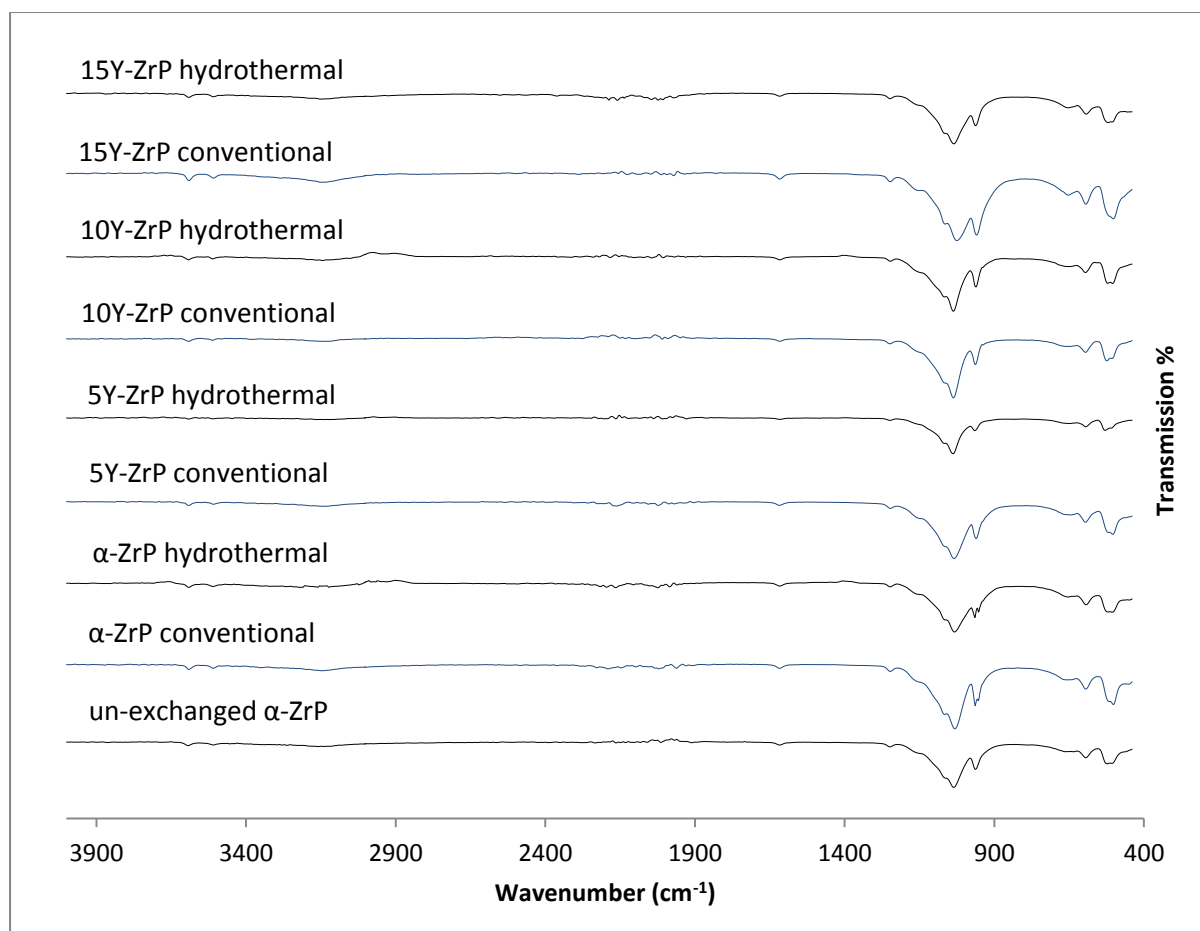


Figure 4. 15 FT-IR of $\text{Co}(\text{NO}_3)_2$ exchanged products

The results above for the exchanged samples did not show any major differences compared to the un-exchanged α -ZrP, indicating no major structural changes had occurred. However there are some differences in the O-H and P-O vibrations. However, as suggested in a few of the previous studies ^[14, 15] that the exchange of cobalt into the α -ZrP type structure led to an increase in number of moles of water present in the unit crystal. Therefore, the appearance of sharper peaks of O-H vibrations at ca. 1620 cm^{-1} and $3000\text{-}3500\text{ cm}^{-1}$ range could be accounted to the total change in the dipole of the O-H molecules. These peaks were sharper and more pronounced for the Y-ZrP samples as compared to the α -ZrP exchanged products, indicating again that more Co^{2+} ions were exchanged in the Y-ZrP. These

results are in consistency with the XRF and XRD results discussed above. The summary of the peaks observed in the FT-IR spectrum of $\text{Co}(\text{NO}_3)_2$ exchanged products is provided in the Table 4.17 below.

Table 4. 17 Summary of FT-IR results for $\text{Co}(\text{NO}_3)_2$ ion exchange

Peak Wavenumber (cm^{-1})	Chemical bonds
504.41	P-O-P vibration
594.67	P-OH (out of plane)
646.24	O-H (out of plane)
960.33	P-O bending (in plane)
1027.26	P-O stretching (asym)
1248.86	P-O-H deformation
1617.29	O-H bending (asym)
2159.20	P-OH
3163.29	O-H stretching (sym)
3507.00	O-H stretching (asym)
3590.60	O-H stretching (asym)

The FT-IR results for the $\text{Co}(\text{CH}_3\text{CO}_2)_2$ exchanged products are shown in the Figure 4.16 below and indicate the changes in the chemical environment of the exchanged products as compared to α -ZrP.

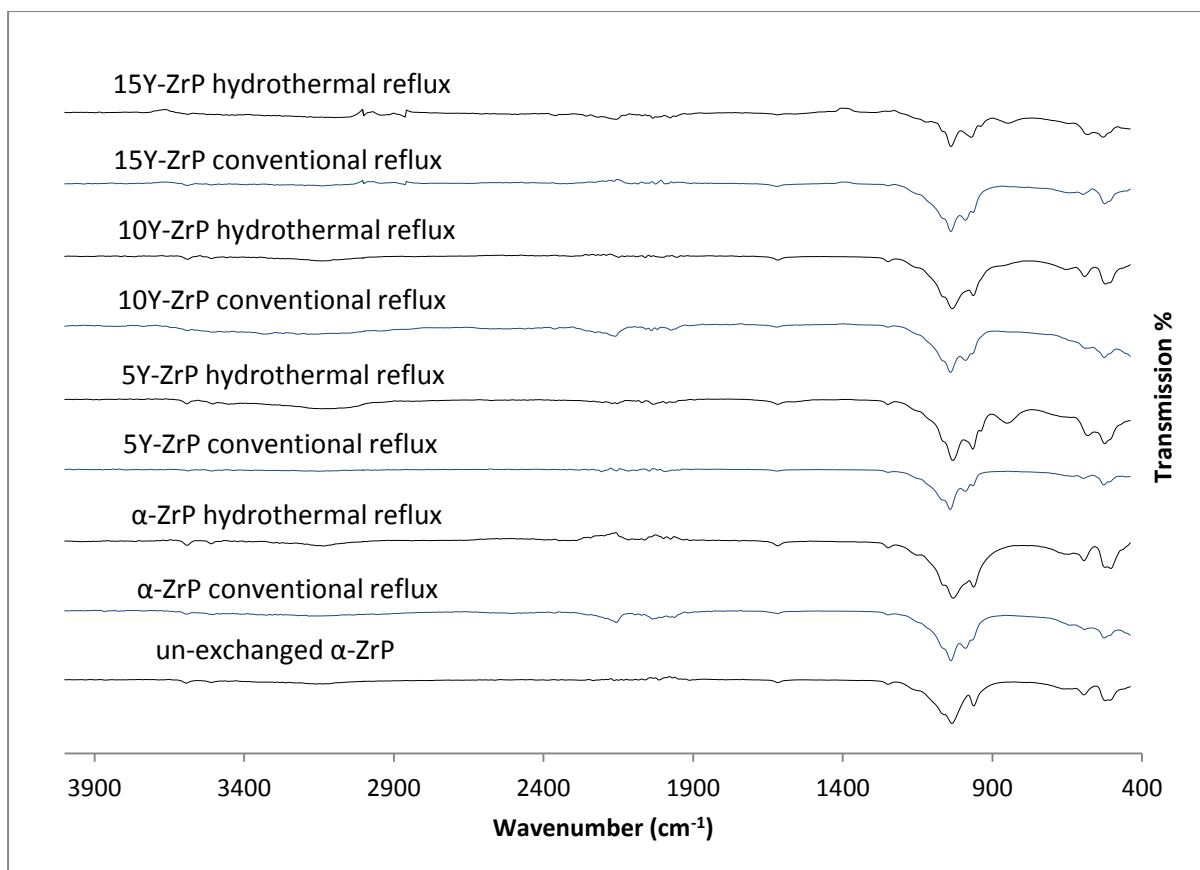


Figure 4. 16 FT-IR spectrum for the $\text{Co}(\text{CH}_3\text{CO}_2)_2$ exchanged products

It can be seen that the majority of the spectra of the exchanged products are similar to the un-exchanged α -ZrP apart from the occurrence of an extra peak of medium intensity seen at ca. 850 cm^{-1} . This peak is assigned to the Co-O stretching vibration for most cobalt containing compounds ^[15]. Hence it is evident that the saturation of layers with cobalt atoms together with the additional incoming water molecules must have taken place to provide a medium intensity peak distinctly in the low frequency region of the FT-IR spectrum.

Also the reduced intensities of the P-O vibrations peaks at ca. 960 cm^{-1} and 1030 cm^{-1} along with that of O-H vibrations in the region of $3000\text{-}3500\text{ cm}^{-1}$ for some of Y-ZrP samples (5% and 15% hydrothermally synthesised) indicate that lattice structure is more or less disordered with layers being pushed apart due to incoming cobalt ions and new possible cobalt phases were formed. The reduced P-O vibrations in these samples explains that cobalt must have precipitated as $\text{Co}_3(\text{PO}_4)_2 \cdot 8\text{H}_2\text{O}$ as discussed before together with the reduced O-H vibrations which occurred due to the

loss of crystal water from the cobalt exchanged phases. Hence, these results indicate that mixed phases must be present in the exchanged products that gave exceptionally high cobalt concentrations as analysed by the XRF and showed the extra peaks in the XRD results discussed above.

However, FT-IR spectrum from other Y-ZrP products were observed to depict sharper O-H vibrations in the ca. 1620 cm^{-1} and 3000-3500 cm^{-1} range complimenting the XRD and XRF analysis of a single phase cobalt exchanged product, possibly of the composition as $\text{ZrCo}_{0.33}\text{H}_{1.34}(\text{PO}_4)_2 \cdot 2.4\text{H}_2\text{O}$ as discussed in one of the studies [14].

A summary of the FT-IR results for the $\text{Co}(\text{CH}_3\text{CO}_2)_2$ exchanged products is provided in the Table 4.18 below.

Table 4. 18 Summary of FT-IR results for $\text{Co}(\text{CH}_3\text{CO}_2)_2$ ion exchange

Peak Wavenumber (cm^{-1})	Chemical bonds
524.96	P-O-P vibration
581.45	P-OH (out of plane)
850.86	Co-O stretching
965.81	P-O bending (in plane)
1032.39	P-O stretching (asym)
1249.03	P-O-H deformation
1617.47	O-H bending (asym)
2170.95	P-OH
3137.85	O-H stretching (sym)
3504.89	O-H stretching (asym)
3591.55	O-H stretching (asym)

4.4.5 ICP-MS analysis of the cobalt exchanged products

ICP-MS analysis was carried out on the filtrate solutions from the Co^{2+} ion exchanged products to analyse the extent of exchange between the solutions and the solids. A summary of the results are presented in the Table 4.19 below.

Table 4. 19 Summary of ICP-MS results for the cobalt ion exchanged Y-ZrP samples

Samples	X = Amount of Co ²⁺ remaining (ppm)		% of Co ²⁺ incorporation $\frac{5893.32ppm - Xppm}{5893.32ppm \text{ of } 0.1M \text{ Co}} \times 100$	
	Co(NO ₃) ₂	Co(CH ₃ CO ₂) ₂	Co(NO ₃) ₂	Co(CH ₃ CO ₂) ₂
α-ZrP conventional	5599(7)	2829(8)	4.99%	50.99%
α-ZrP hydrothermal	5510(2)	2946(4)	6.50%	50.01%
5Y-ZrP conventional	5365(4)	2504(3)	8.96%	57.51%
5Y-ZrP hydrothermal	5192(2)	103(9)	11.88%	98.25%
10Y-ZrP conventional	5392(4)	233(8)	8.50%	96.04%
10Y-ZrP hydrothermal	5145(1)	2651(3)	12.69%	55.01%
15Y-ZrP conventional	5505(3)	2209(9)	6.58%	62.50%
15Y-ZrP hydrothermal	5387(1)	92(3)	8.59%	98.43%

The above ICP-MS results indicate that the cobalt nitrate solution was able to exchange a maximum of ca.13% Co²⁺ ions in the Y-ZrP products as compared to ca. 62.5% exchange from the cobalt acetate solution (neglecting the exceptionally high exchange of 98% due to impurity phases). In general, it was observed that the synthesised Y-ZrP products showed a higher extent of exchange as compared to the parent α-ZrP samples for both synthesis routes. Overall, it was observed that there was no definite trend for the exchange capacity in relation to the yttrium percentage for both nitrate and acetate solutions but the extent of exchange for different Y-ZrP samples was found to be higher than that of the parent α-ZrP. These results are consistent to the XRD, XRF, FT-IR and the pH results shown previously. Also, the appearance of relatively high exchange capacity (ca. 98%) for some of the Y-ZrP

products were investigated for the yttrium and zirconium ions and the results are shown in Table 4.20 below.

Table 4. 20 Summary of ICP-MS for the leached ions

Samples	Co(NO ₃) ₂		Co(CH ₃ CO ₂) ₂	
	Y ³⁺ (ppm)	Zr ⁴⁺ (ppm)	Y ³⁺ (ppm)	Zr ⁴⁺ (ppm)
α-ZrP conventional	-	1.150(2)	-	4.203(5)
α-ZrP hydrothermal	-	1.093(4)	-	4.114(7)
5Y-ZrP conventional	0.089(1)	1.130(2)	0.307(1)	3.108(3)
5Y-ZrP hydrothermal	0.177(3)	0.820(5)	1.098(1)	10.91(2)
10Y-ZrP conventional	0.145(1)	0.995(3)	1.509(2)	18.96(6)
10Y-ZrP hydrothermal	0.165(4)	0.922(2)	0.030(5)	2.076(3)
15Y-ZrP conventional	0.117(3)	0.846(5)	0.279(2)	1.943(2)
15Y-ZrP hydrothermal	0.126(1)	0.973(2)	1.210(4)	10.03(1)

It is observed from the leaching data of the Y³⁺ and Zr⁴⁺ ions of the cobalt exchanged samples from the nitrate and acetate solutions showed mixed results for the amount of leached Y³⁺ ions, whereas a more clear relationship of decreasing amount is seen for the leached Zr⁴⁺ ions. However, 5% and 15% Y-ZrP hydrothermally synthesised samples and 10% conventionally refluxed samples showed exceptionally high amount of leached ions. This explains that the high cobalt percentage in the XRF and ICP-MS of the products is due to the structure breakdown of the parent materials to facilitate the formation of new phosphate phases which were coexisting with the exchanged phase. But overall, it was observed that the total metal leaching (Y³⁺ and Zr⁴⁺) for the Y-ZrP sample was lesser than α-ZrP samples which concludes that Y-ZrP products were more stable in the acetate salt solutions. These results compliment the XRD, XRF and ICP-MS analysis concluding that the synthesised Y-ZrP samples are efficient cobalt ion exchangers as compared to the parent α-ZrP.

4.5. Summary of single ion-exchange results

This chapter consists of the single ion exchange results for both Y-ZrP and α-ZrP samples from the nitrate, acetate and hydroxide solutions of strontium, caesium and cobalt. The strontium ion exchanged samples showed good degree of stability and

crystallinity as observed from the XRD patterns from the nitrate solutions followed by reduced crystallinity and new mixed phases arising from the acetate solution and almost complete loss of structural framework from the hydroxide solutions. The results are further confirmed from the FT-IR analysis that also indicates almost similar spectra for the nitrate solution exchanged samples followed by few specific changes observed from the acetate exchange solution and almost loss of typical α -ZrP spectra from the hydroxide exchange solution. These results are related to the degree of strontium exchange in the samples as observed from the pH and XRF results which indicate the increasing order of exchange from the nitrate solution followed by acetate solution and highest for the hydroxide solution. The results are further confirmed by the ICP-MS analysis which shows approximately 22% strontium exchange from the nitrate solution, followed by 45% from the acetate solution and 73% from the hydroxide solution.

Similar results were observed for the caesium and cobalt exchanged products as well but the stability and degree of crystallinity was higher for the acetate solutions as opposed to that from the strontium acetate exchange as observed from the XRD and FT-IR results. However, the caesium exchange was limited to approximately 2.5% from the nitrate and acetate solutions and 35% from the hydroxide solution. The cobalt exchange on the other hand yielded about 6% exchange from the nitrate solution and up to 98% from the acetate solution.

Overall, it can be concluded from the above results that the Y-ZrP samples synthesised from both synthesis routes were showing higher degree of single ion exchanges as compared to α -ZrP samples. The extent of exchange for the Y-ZrP samples followed the order of $\text{Sr}^{2+} > \text{Co}^{2+} > \text{Cs}^+$ as opposed to that of α -ZrP that follows $\text{Sr}^{2+} > \text{Cs}^+ > \text{Co}^{2+}$. [3]

4.6. References

1. Dyer, A., Leigh, D, Ocon, F. T. J. *Inorg. Nucl. Chem.*, 33, 3141 (1971)
2. Clearfield, A., Nancollas, G. H., Blessing, R. H. In *Ion Exchange and Solvent Extraction*; Marcus, Y., SenGupta, A. K., Marinsky, J. A., Ed.; Dekker: New York; Vol. 5 (1973)
3. Clearfield, A., Hagiwara, H J. *Inorg. Nucl. Chem.*, 40, 907 (1978)
4. Alberti, A., Costantino, U., Pelliccioni, M J. *Inorg. Nucl. Chem.*, 35, 1327 (1973)
5. Clearfield, A. *Ann. Rev. Mater. Sci.*, 14, 205 (1984)
6. Clearfield, A., Stynes, J. A. J. *Inorg. Nucl. Chem.*, 26, 117 (1964)
7. Alberti, G., Giammari, G., Grassini-Strazza, G. J. *Chromatog.*, 28, 118 (1967)
8. Alberti, G., Cardini-Galli, P., Costantino, U., Torracca, E J. *Inorg. Nucl. Chem.*, 29, 571 (1967)
9. Parida, K. M., Sahu, B. B., Das, D. P. J. *Coll. Inter. Sci*, 270, 436 (2004)
10. Alberti, G., Bertrami, R., Casciola, M., Costantino, U., Gupta, J. P. J. *Inorg. Nucl. Chem.*, 38, 843 (1976)
11. Zheng, Y., Cheng, Y., Wang, Y., Yu, Y., Chen, D., Bao, F., *J. Crys. Grow.*, 280, 3, 569 (2005)
12. Clearfield A (1998) *Metal phosphonate chemistry*. In: Karlin KD (ed.) *Progress in Inorganic Chemistry*, Vol. 47. New York: John Wiley.
13. Le Van So, J. *Radioanal. Nucl. Chem.*, 99, 1, 7 (1986)
14. Alberti, G., Costantino, U., Allulli, S., Massucci, M. A., J. *Inorg. Nucl. Chem.*, 37, 1779 (1975)
15. Szirtes, L., Riess, L., Megyeri, J., Kuzmann, E., *Cen. Eur. J. Chem. CEJC* 5(2), 516 (2007)
16. Yakovenchuk, V., Ivanyuk, N., Yu.; Mikhailova, Y. A., *Cand. Mineral.*, 44, 117 (2006)
17. Poojary, D. M., Shpeizer, B., Clearfield, A., *J. Chem. Soc., Dal. Trans.*, 111 (1995)

CHAPTER 5: COMPETITIVE ION EXCHANGE

5.1. Introduction

It is of interest to see how the Y-ZrP samples exchange Sr^{2+} , Cs^+ and Co^{2+} ions as compared to the α -ZrP in the presence of other competitive ions. This aspect of competitive ion exchange is important in nuclear waste research since the isotopes of radionuclides are predominantly present in the nuclear waste effluents along with common alkali and alkaline metal ions such as Na^+ , K^+ , Mg^{2+} and Ca^{2+} .

The work in this chapter describes the competitive ion exchanges using Na^+ , Mg^{2+} and Ca^{2+} as the interfering ions to study the selectivity of the synthesised Y-ZrP samples to these ions using the scheme shown in Table 2.2. It also allows a study of the selectivity of these ions of interest against each other.

5.2. Strontium – caesium exchange

The synthesised Y-ZrP samples together with α -ZrP from both synthesis methods were subjected to competitive ion exchange using a mixture of 0.1M nitrate salt solutions of strontium and caesium. These reaction conditions were kept similar to single ion exchange experiments (72 hours, room temperature) and the products obtained were characterised using XRD, XRF/SEM, ICP-MS and FT-IR.

5.2.1 XRD analysis of strontium-caesium exchange

The XRD patterns are shown in Figure 5.1 below for both Y-ZrP and α -ZrP via both routes of synthesis and show a variation of the degree of crystallinity of Y-ZrP samples as compared to α -ZrP.

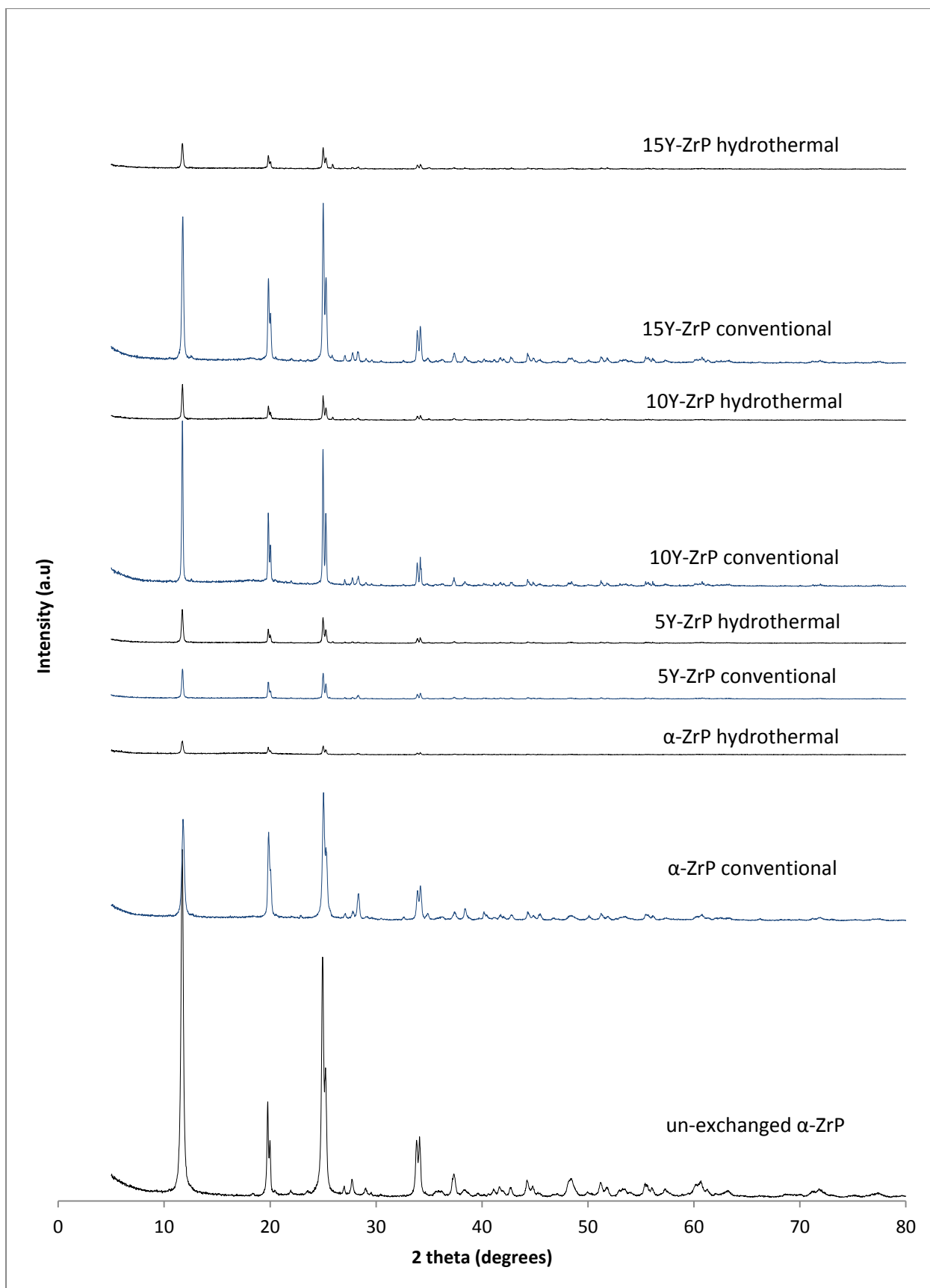


Figure 5. 1XRD of strontium-caesium exchanged products

It can be observed from the above figure that the crystallinity of the exchanged products is significantly decreased, especially for the hydrothermal refluxed samples. This is observed for both Y-ZrP and α -ZrP samples as the conventionally refluxed samples were found to be more crystalline as compared to the very low signal to noise ratio of the hydrothermally refluxed samples indicating a relatively amorphous product. But, the 5% Y-ZrP products via both routes of reflux showed similar decrease in crystallinity indicating a large transition to the amorphous state. However, the presence of characteristic peaks in the exchanged Y-ZrP and α -ZrP clearly point to a layered structure being held intact, although the variation in the crystallinity could be representing the extent or selectivity of exchange. Also, the increased caesium exchange is expected to cause structure breakdown due to restricted interlayer spacing, so further analysis of the exchanged solution by ICP-MS was also done, as discussed in the following sections.

Conclusively, it was observed from the XRD patterns of the exchanged products that the patterns were not identical to either of the single ion exchanges (Sr^{2+} and Cs^+) in terms of the order of crystallinity. The characteristic α -ZrP peaks in the range of $2\theta = 26^\circ$ - 29° appeared sharper and resolved in the exchanged samples and had slight variation in intensity which might be indicative of the exchange that occurred within the layers. Also it was observed that there were small peaks present at $2\theta = 8^\circ$ - 11° which might be due to the formation of $\text{ZrHSr}_{0.5}(\text{PO}_4)_2 \cdot 3.6\text{H}_2\text{O}$ as explained previously and consistent with the literature [1, 2]. However, these peaks were not highly resolved as compared with the background noise, therefore an online PDF database search did not return with a confident match. Further analysis is required to conclude the extent and site of exchange of either of the ions (Sr^{2+} and Cs^+) in order to understand the steps of exchange in a competitive ions solution.

5.2.2 XRF analysis of strontium-caesium exchange

The elemental analysis was carried out using the XRF after calibrating the instrument for ions of interest as per the scheme provided in Table 1 of Appendix 3 and analysing the peak areas to yield the calibration graphs as shown in figures 1-4 provided in the Appendix 3.

The Table 5.1 below provides the result for the strontium – caesium exchanged products for both Y-ZrP and α -ZrP samples and it can be seen that the extent of Sr^{2+} ion exchange is higher than Cs^+ ions.

Table 5. 1 XRF compositional analysis of the exchanged products (M = Sr or Cs ions)

Samples	Extent of Exchange Ratio of M / (Y+Zr)	
	Sr / (Y+Zr)	Cs / (Y+Zr)
α -ZrP conventional	0.0915(1)	0.0572(1)
α -ZrP hydrothermal	0.0913(3)	0.0514(4)
5Y-ZrP conventional	0.0964(2)	0.0576(1)
5Y-ZrP hydrothermal	0.0957(4)	0.0566(1)
10Y-ZrP conventional	0.0833(2)	0.0498(2)
10Y-ZrP hydrothermal	0.0888(1)	0.0486(2)
15Y-ZrP conventional	0.0872(1)	0.0409(1)
15Y-ZrP hydrothermal	0.0962(5)	0.0515(1)

The above results when compared with the XRF results of single ion exchanges present in Table 4.2 (for strontium) and Table 4.9 (for caesium) clearly show that the exchange capacity towards Sr^{2+} ions was reduced in the presence of larger radii Cs^+ ions. However the exchange of caesium ions was increased for both Y-ZrP and α -ZrP samples and the exchange followed a similar trend as observed in caesium exchange experiment discussed previously. Overall, the Y-ZrP samples showed a similar extent of exchange as that of α -ZrP samples of both routes of synthesis.

It can be concluded that the synthesised Y-ZrP followed a similar trend of exchange as seen in the caesium nitrate exchange experiment but the exchange capacity for caesium ions were increased at the expense of strontium ions. One possible reason for this is that the Sr^{2+} ions are exchanged first and this tends to increase in the interlayer spacing to accommodate some Cs^+ ions that normally occupies large size cavities. Therefore some of the Cs^+ ions were believed to have exchanged within the layers that causes the Sr^{2+} exchange to get competitively inhibited due to the limited sites of exchange present. Also, the possibility of structure breakdown due to increased amount of large Cs^+ ions is expected and therefore ICP-MS analysis was

done as discussed in the following sections. Additionally, further characterisation of the exchanged products is needed to establish the mechanism of exchange and repetitive experiments need to be done to establish similar results.

5.2.3 pH analysis of strontium-caesium exchange

The pH results before and after the competitive ion exchange reaction is shown in the Table 5.2 below to establish the success of exchange.

Table 5. 2 Summary of pH analysis for strontium-caesium exchange

Samples	pH of Solution
Strontium – caesium solution (0.2M)	Stock pH = 6.5
α -ZrP conventional	3.75
α -ZrP hydrothermal	3.98
5Y-ZrP conventional	3.65
5Y-ZrP hydrothermal	2.56
10Y-ZrP conventional	3.12
10Y-ZrP hydrothermal	3.00
15Y-ZrP conventional	3.58
15Y-ZrP hydrothermal	3.12

It is seen from the results shown in the table above that there is a gradual decline in the pH of the solutions after the ion exchange. On comparison with the results shown in Table 4.1 (for Sr^{2+}) and Table 4.8 (for Cs^+), it is observed that this decrease in pH is relatively more for the competitive solution. This indicates that more protons are exchanged from the products into the solution. This is consistent with the elemental analysis from the XRF results that indicates more caesium ions being exchanged but the extent of strontium ions were slightly reduced as compared to the single exchange experiment. Overall, the exchange capacity is increased and hence the pH decrease is also greater as expected that shows the extent of exchange for Y-ZrP samples to be higher as compared to the α -ZrP.

The change in the chemical environment of the competitive ion exchanged products is analysed using the FT-IR, in order to understand the nature of exchange occurring within the samples. The result of the FT-IR spectrums from exchanged products is shown in Figure 1 of Appendix 5 along with Table 1 that summarises the key peaks with their respective bonding environment for an ideal FT-IR pattern from the strontium-caesium exchange of α -ZrP type structures.

It was observed that ion exchanged products showed almost uniform α -ZrP type structure retaining a similar chemical bonding environment as compared to the un-exchanged α -ZrP. However, there were some distortions in the peak profiles which were noticed in the region of 1050-1250 cm^{-1} , but due to intense peak overlapping and extremely low intensities, these minor variations cannot be identified distinctly and assigned to a particular chemical bond, due to lack of literature sources. Also two additional peaks at 1369 and 1439 cm^{-1} is not recognised in literature but it was only observed in strontium ion exchange experiment and therefore is believed to be linked with the Sr-O-P bond.

Overall, it was observed that the patterns of exchanged products closely resembled the FT-IR patterns of the caesium acetate exchange, as provided in Figure 4.12. This compliments the XRF results indicating that the presence of strontium in the exchange solution slightly facilitates the uptake of Cs^+ ions at relatively acidic conditions similar to that observed during the exchange from alkaline caesium acetate solution.

5.2.4 ICP-MS analysis of strontium-caesium exchange

The exchange capacity of both Sr^{2+} and Cs^+ ions was determined by analysing the filtrate solutions using ICP-MS. The calibration graphs for the ions of interest are provided in figures 7-9 of appendix 3. The summary of the results obtained from the ICP-MS for the exchanged products is shown in the Table 5.3 below.

Table 5. 3 Summary of ICP-MS results for the strontium-caesium exchange

Samples	X = Amount of ions remaining (ppm)		% of ions incorporation $\frac{M_{ppm} - X_{ppm}}{M_{ppm} \text{ of } 0.1M} \times 100$	
	$X_1 = Sr^{2+}$	$X_2 = Cs^+$	$M_1 = Sr^{2+}$ (8800 ppm)	$M_2 = Cs^+$ (13290.55 ppm)
α -ZrP conventional	6963(5)	12342(4)	20.875	7.137
α -ZrP hydrothermal	7190(3)	12309(6)	18.295	7.385
5Y-ZrP conventional	6911(6)	12310(7)	21.465	7.377
5Y-ZrP hydrothermal	6953(3)	12220(3)	20.988	8.054
10Y-ZrP conventional	7124(1)	12443(1)	19.045	6.377
10Y-ZrP hydrothermal	7110(3)	12387(6)	19.204	6.798
15Y-ZrP conventional	6982(5)	12336(7)	20.659	7.182
15Y-ZrP hydrothermal	6935(4)	12290(4)	21.193	7.528

It can be seen that Y-ZrP showed a similar Sr^{2+} and Cs^+ uptake compared to α -ZrP samples with no clear trend in the exchange with increasing yttrium concentration. However, there appears to be slight increase in the exchange capacity of the 5% and 15% hydrothermally synthesised Y-ZrP for both cations. This result is consistent with the XRF and pH analysis discussed previously.

In addition to this, an ICP-MS analysis was done to evaluate the possibility of structure breakdown of the parent materials by determining the concentration of the Y^{3+} and Zr^{4+} leaching into the exchange solution. The results obtained are shown in the Table 5.4 below.

Table 5. 4 Summary of ICP-MS for the leached ions

Samples	Concentration of ions	
	Y ³⁺ (ppm)	Zr ⁴⁺ (ppm)
α-ZrP conventional	-	3.992(2)
α-ZrP hydrothermal	-	20.27(6)
5Y-ZrP conventional	0.497(2)	0.822(3)
5Y-ZrP hydrothermal	0.927(1)	0.110(1)
10Y-ZrP conventional	0.349(1)	21.86(4)
10Y-ZrP hydrothermal	0.514(4)	0.658(1)
15Y-ZrP conventional	1.411(1)	0.027(1)
15Y-ZrP hydrothermal	1.961(3)	4.019(5)

The results shown in the table above shows mixed results for both Y-ZrP and α-ZrP samples, however it was seen that there was a considerable amount of Y³⁺ ions which were leached from the 15% Y-ZrP samples from both synthetic methods which indicates a possible structural damage or loss of surface adsorbed ions. Also the presence of Zr⁴⁺ ions in relatively higher quantity also supports the possibility for a structural damage, although in low degrees. This complements the XRD, XRF and FT-IR results above and explains the expected damage which occurs to the α-ZrP type materials due to the incoming larger radii Cs⁺ ions within the structure, causing the breaking of intra and/or interlayer bonds.

5.3. Caesium-Cobalt exchange

A competitive ion exchange solution containing Cs⁺ and Co²⁺ ions was performed using a mixture of 0.1M nitrate salt solutions of caesium and cobalt for all Y-ZrP and α-ZrP samples. The experimental conditions were similar to that of the single ion exchange experiments (72 hours, room temperature). The exchanged products were filtered from the solutions and analysed using XRD, XRF, FT-IR and ICP-MS.

5.3.1 XRD analysis of the caesium-cobalt exchange

The XRD analysis of the exchanged Y-ZrP and α-ZrP products are shown in the Figure 5.2 below.

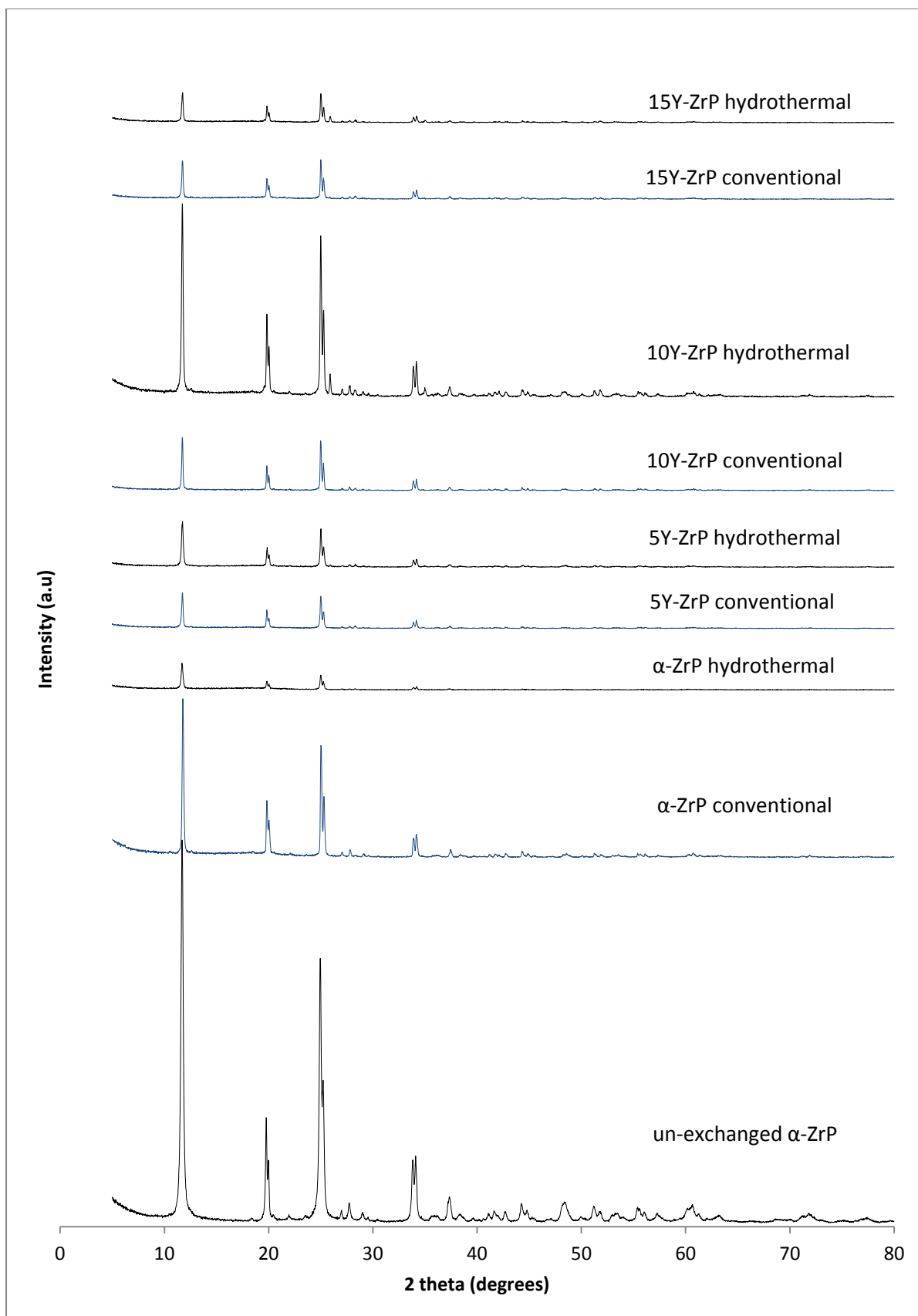


Figure 5. 2 XRD of caesium-cobalt exchange

The XRD patterns shown above clearly indicate a decrease in crystallinity of the exchanged products which is evident due to decline in peak intensities as compared with the parent samples. However, 10% Y-ZrP shows a higher crystallinity than the rest of the products, which might be representative of an incomplete or selective exchange, also with a possibility of experimental error.

In addition to this, a few minor but distinct peaks were observed at $2\theta = 20.4^\circ$, 25.9° and 28.3° which were matched using the PDF crystal database to cobalt phosphate (PDF 00-013-0503) and caesium phosphate (PDF 04-016-1910), as shown in figure 1 of appendix 4. This indicates the possible formation of a mixed phase products where some of the Cs^+ and Co^{2+} ions were precipitated as phosphate products alongside the exchanged samples. However, further characterisation of the exchanged products is needed to establish strong conclusions.

5.3.2 XRF analysis of caesium-cobalt exchange

An elemental analysis using XRF was carried out for the caesium-cobalt exchanged products to determine the extent of exchange and the results are shown in the Table 5.5 below.

Table 5. 5 XRF compositional analysis of exchanged products (M = Cs or Co ions)

Samples	Extent of Exchange	
	Ratio of M / (Y+Zr)	
	Cs / (Y+Zr)	Co / (Y+Zr)
α -ZrP conventional	0.0203(1)	0.0169(1)
α -ZrP hydrothermal	0.0267(3)	0.0219(2)
5Y-ZrP conventional	0.0379(2)	0.0322(1)
5Y-ZrP hydrothermal	0.0306(4)	0.0352(1)
10Y-ZrP conventional	0.0216(2)	0.0176(3)
10Y-ZrP hydrothermal	0.0282(4)	0.0240(2)
15Y-ZrP conventional	0.0380(1)	0.0289(4)
15Y-ZrP hydrothermal	0.0325(3)	0.0274(2)

On comparison with the XRF results for the single ion exchange experiments presented in Table 4.9 (for Cs^+) and Table 4.15 (for Co^{2+}), it can be seen that the

mixed solution led to a similar extent of caesium exchange but the capacity was increased for the exchange of cobalt ions. But as the extent of caesium exchange increased, the cobalt uptake was also improved. This is explained by the fact that first caesium exchange must have occurred in to cavities by replacing the water molecules, due to ion-sieving effect caused by large radii Cs^+ ions [3, 4] followed by very limited exchange within the layers causing them to spread slightly. This can enhance the uptake of the smaller radii Co^{2+} ions within the layers by exchanging more protons and occupying additional space. However, reliable literature sources are not present to confirm this mechanism of exchange and further characterisation is needed to establish the results.

In summary, the synthesised Y-ZrP samples showed a similar trend of exchange as that of α -ZrP but the synthesised Y-ZrP samples from both routes of reflux showed slightly higher exchange for both Cs^+ and Co^{2+} ions, with 5% Y-ZrP showing the highest exchange for both cobalt and caesium. However, no uniform trend was observed in terms of yttrium concentration but overall it was observed that Y-ZrP samples performed better as compared with the α -ZrP for cobalt ion removal in the presence of interfering caesium ions within the exchange solution. Also, the performance of synthesised Y-ZrP samples for caesium exchange showed a more or less uniform extent of exchange in the presence of Co^{2+} ions as opposed to a non-uniform exchange as observed during the single ion exchange experiment.

5.3.3 pH analysis of caesium-cobalt exchange

The pH analyses of the filtrate solutions recovered from both Y-ZrP and α -ZrP products were done and the results are presented in the Table 5.6.

Table 5. 6 pH results of caesium-cobalt exchange

Samples	pH of Solution
Caesium-cobalt solution (0.2M)	Stock pH = 6.6
α -ZrP conventional	3.77
α -ZrP hydrothermal	3.63
5Y-ZrP conventional	3.50
5Y-ZrP hydrothermal	2.55
10Y-ZrP conventional	3.60
10Y-ZrP hydrothermal	3.13
15Y-ZrP conventional	3.75
15Y-ZrP hydrothermal	3.40

It can be seen from the above results that the synthesised Y-ZrP samples showed a higher decline in pH as compared to the α -ZrP samples. It was seen that 5% Y-ZrP refluxed hydrothermally showed the highest decline in pH value which indicates that highest number of protons were exchanged for the cations of interest. This result is consistent with the XRF results which also show that the highest Co^{2+} uptake was achieved by 5%Y-ZrP samples. It is believed that the drop in pH is attributed exclusively to the Co^{2+} ions as Cs^+ ions usually resides within the zeolite-type cavities by replacing the water molecules, rather than accommodating within the layers by exchanging protons [4, 5]. However, the displacement of excess protons due to outgoing water molecules can cause further drop in the pH and allow enhanced exchange of Co^{2+} ions. Also as confirmed from the XRF results, the Cs^+ uptake did not increase for these samples in regards to the single ion exchange experiments which further confirms these pH results due to the fact that 2 exchangeable protons are exchanged for one divalent cation (Co^{2+} ions in this case) and Cs^+ ions are usually not exchanged at protonic sites due to the larger radii of these ions.

The FT-IR spectrums for both Y-ZrP and α -ZrP samples via both routes of reflux are analysed to understand any change in the chemical environment due to the nature of exchange from the competitive exchange solutions of caesium and cobalt nitrates. The resulting FT-IR spectrums are presented in the figure 2 of Appendix 5 along with

table 2 showing a summary of ideal FT-IR peaks from a caesium-cobalt exchanged product corresponding to its chemical bonds.

The results indicate a more or less uniform FT-IR spectrum for both α -ZrP and Y-ZrP as compared to the pristine α -ZrP. However, subtle changes were observed in the peak intensities at ca. 950-1050, 1800-2200 and 3000-3500 cm^{-1} . But these changes are not recognised distinctly to assign it to relevant chemical bonds. However, the change in the peak intensities for the O-H bonds at ca. 1620 and 3000-3500 cm^{-1} indicates the change in water content of the exchanged products which is representative of the caesium being exchanged into the cavities by displacing the lattice water. Hence, it can be concluded that FT-IR results clearly show a conserved structure of the exchanged products for both Y-ZrP and α -ZrP with few minute variations. Also the competitive ion exchanged products tends to exhibit a similar pattern of exchange as that of cobalt exchange shown in figure 15 of chapter 4, which compliment the results of XRD and XRF as discussed above.

5.3.4 ICP-MS of caesium-cobalt exchange

The filtrate solutions from the caesium-cobalt exchanged products were analysed by ICP-MS after diluting it to 1000 times for quantitatively analysing the extent of exchange for ions of interest. A summary of the ICP-MS results for caesium and cobalt ions are shown in the Table 5.7 below.

Table 5. 7 Summary of ICP-MS results for caesium-cobalt exchange

Samples	X = Amount of ions remaining (ppm)		% of ions incorporation $\frac{Mppm - Xppm}{Mppm \text{ of } 0.1M} \times 100$	
	X ₁ = Co ²⁺	X ₂ = Cs ⁺	M ₁ = Co ²⁺ (5893.32 ppm)	M ₂ = Cs ⁺ (13290.55 ppm)
α-ZrP conventional	5430(2)	12710(5)	7.861	4.368
α-ZrP hydrothermal	5360(5)	12740(4)	9.049	4.142
5Y-ZrP conventional	5040(3)	12693(1)	14.48	4.496
5Y-ZrP hydrothermal	5090(2)	12680(4)	13.63	4.593
10Y-ZrP conventional	5290(1)	12710(2)	10.23	4.368
10Y-ZrP hydrothermal	5130(2)	12720(3)	12.95	4.293
15Y-ZrP conventional	5170(1)	12700(3)	12.27	4.443
15Y-ZrP hydrothermal	5100(5)	12696(2)	13.46	4.473

It is evident from the above results and single ion exchange ICP-MS results present in Table 4.13 (Cs⁺ ions) and Table 4.19 (Co²⁺ ions), that the extent of exchange for both caesium and cobalt ions was increased slightly. However, no clear trend of exchange was observed for the caesium ions in regards to the yttrium concentration, but the cobalt exchange showed similar trend of exchange as that of single cobalt ion exchange experiment. Also the synthesised Y-ZrP samples showed a higher extent of exchange for both Cs⁺ and Co²⁺ ions as compared with the α-ZrP of both synthesis methods. These results are consistent with the XRF and pH findings which also clearly show enhanced uptake of these ions from the competitive exchange solution.

As before, the filtrate was analysed for Y³⁺ and Zr⁴⁺ leaching from the materials during the exchange process. The results are shown in Table 5.8 below.

Table 5. 8 Summary of ICP-MS for the leached ions

Samples	Concentration of ions	
	Y ³⁺ (ppm)	Zr ⁴⁺ (ppm)
α-ZrP conventional	-	0.174(3)
α-ZrP hydrothermal	-	0.292(2)
5Y-ZrP conventional	0.880(1)	2.014(1)
5Y-ZrP hydrothermal	0.548(2)	3.550(4)
10Y-ZrP conventional	1.592(4)	0.895(2)
10Y-ZrP hydrothermal	0.282(2)	0.320(1)
15Y-ZrP conventional	1.023(3)	5.898(4)
15Y-ZrP hydrothermal	1.593(1)	3.526(1)

The above results clearly indicate a small amount of leached Y³⁺ and Zr⁴⁺ ions from the parent samples into the solution due to breakdown of the structure. The leached amount is slightly higher for the 5% and 15% Y-ZrP samples, indicating a higher degree of structural damage compared with the other Y-ZrP and α-ZrP samples. Also, the Y³⁺ ions show a significant leaching as compared to the Zr⁴⁺ in regards to the relative abundance of these ions within the structure. However, the XRF and ICP-MS results shown in Table 5.6 and 5.9 above indicate that these samples have the highest Cs⁺ ion uptake. Therefore these results support the XRD, XRF and ICP-MS analysis which indicate a small amount of structural breakdown for the caesium-cobalt exchange products.

Overall, it can be concluded from these studies that the Y-ZrP samples are efficient exchangers for Co²⁺ ions in presence of larger Cs⁺ ions, compared to the α-ZrP for both synthesis methods. However, the exchanged products show a small degree of structure breakdown due to heavy loading of both Cs⁺ and Co²⁺ ions into the layers but despite this the products showed an improved performance for both these ions when present competitively, compared with the single ion exchange experiments.

5.4. Strontium - cobalt exchange

0.5 g of Y-ZrP and α -ZrP samples from both methods of synthesis were used for ion-exchange experiments using 0.1M strontium and cobalt nitrate solutions for 72 hours at room temperature, in order to study the selectivity and extent of exchange. All the reaction conditions were kept same to that of the single ion exchange experiments and the resulting products were also similarly analysed by XRD, XRF, FT-IR and ICP-MS.

5.4.1 XRD analysis of strontium-cobalt exchange

The exchanged products were analysed by XRD in order to determine any structural changes that occurred due to the exchange. The resulting XRD patterns for both Y-ZrP and α -ZrP are shown in Figure 5.3 below.

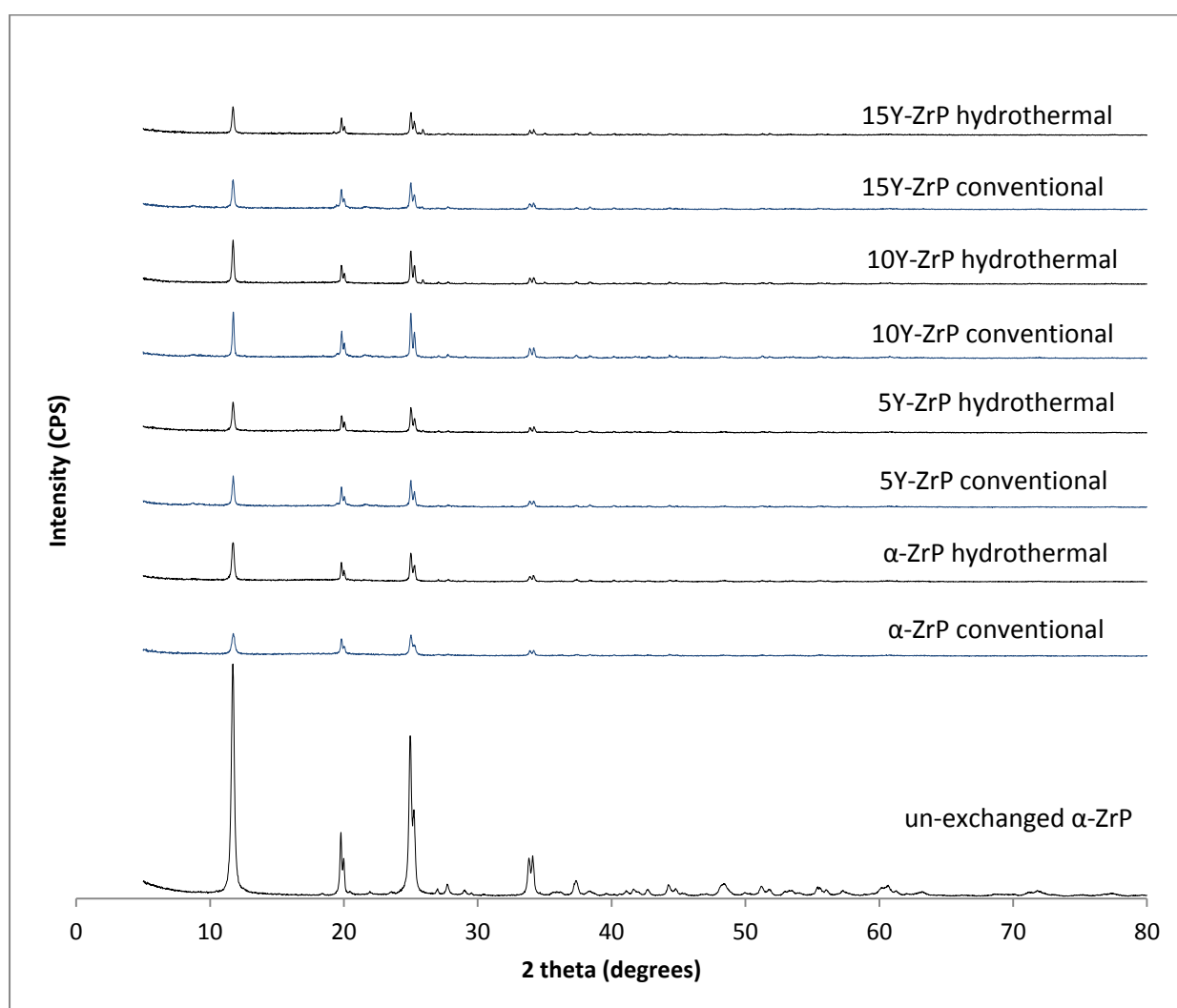


Figure 5. 3 XRD of strontium-cobalt exchange

The results shown in the figure above clearly demonstrates a reduced crystallinity uniformly for both Y-ZrP and α -ZrP products after a strontium-cobalt exchange. Also, subtle changes were observed in the XRD pattern in regards to the emergence of few extra peaks within the pattern. However, these extra peaks were not distinctly resolved due to very low signal to noise ratio and hence could not be confidently matched to any known structural lattice, even by the use of PDF crystal database.

Overall, the strontium-cobalt exchanged products showed a high degree of loss of crystallinity as evident from reduced signal to noise ratio of all the characteristic peaks. This in turn is related to the extent of ion exchange and structural breakdown which is expected to occur due to slightly alkaline reaction conditions. However, the presence of all the characteristic peaks of α -ZrP type structure at correct 2θ values shows that the samples retained the crystal lattice after the exchange. This indicates an unsaturated exchange of ions as observed from the single ion exchange experiments of nitrate salt solutions.

5.4.2 XRF analysis of strontium-cobalt exchange

The composition of the exchanged Y-ZrP and α -ZrP products was determined using the XRF after calibrating the machine for the ions of interest and obtaining the calibration graph as shown in figure 1 and 3 of Appendix 3. A summary of the XRF results is provided in the Table 5.9 below.

Table 5. 9 XRF elemental analysis of the exchanged products (M = Sr or Co ions)

Samples	<u>Extent of Exchange</u>	
	Ratio of M / (Y+Zr)	
	Sr / (Y+Zr)	Co / (Y+Zr)
α -ZrP conventional reflux	0.1258(1)	0.0563(2)
α -ZrP hydrothermal reflux	0.1011(1)	0.0443(2)
5Y-ZrP conventional reflux	0.1269(3)	0.0596(1)
5Y-ZrP hydrothermal reflux	0.1265(2)	0.0653(1)
10Y-ZrP conventional reflux	0.1005(1)	0.0527(1)
10Y-ZrP hydrothermal reflux	0.0979(3)	0.0586(3)
15Y-ZrP conventional reflux	0.1203(2)	0.0579(2)
15Y-ZrP hydrothermal reflux	0.1298(2)	0.0626(3)

The results show that the Y-ZrP and α -ZrP samples were able to exchange both Sr^{2+} and Co^{2+} ions from the mixed exchange solution. However on comparison with the XRF results of single ion exchanges shown in Table 4.22 (for Sr^{2+} ions) and Table 4.15 (for Co^{2+} ions), it was found that there is a decreased uptake of Sr^{2+} ions from the competitive exchange solution although the trend of exchange was similar to that single ion exchange experiment. But the results for the cobalt exchange showed an increased uptake (nearly twice) of Co^{2+} ions from the competitive exchange solution. This nature of exchange is believed to occur due to the strong cationic replacement ability of strontium compared with that of cobalt ions. But an overall competition for exchange occurs between the two ions because the hydrated radii of Co^{2+} ions (4.23 Å) and that of Sr^{2+} ions (4.12 Å) is similar. Therefore it is possible that first Sr^{2+} were exchanged into the structure according to their high affinity for replacing H^+ ions and slightly smaller hydrated ionic radii, but Co^{2+} ions being smaller in ionic radii are preferred for exchange within the layers. Hence the driving force for exchange is increased due to the high affinity of Sr^{2+} ions (ionic radii = 1.18 Å) that also causes an increased uptake of smaller radii Co^{2+} ions (ionic radii = 0.74 Å) until an exchange equilibrium is attained.

Overall it was found from the XRF analysis that all the Y-ZrP samples exchanged an almost similar amount of Sr^{2+} ions as that of α -ZrP but there was an overall decrease in strontium exchange as compared with the single ion exchange experiments. However the Co^{2+} exchange was increased from the competitive exchange solution and the synthesised Y-ZrP samples showed a higher cobalt exchange than α -ZrP, particularly the 5% Y-ZrP sample synthesised hydrothermally that showed the highest Co^{2+} exchange. Also, the increased amount of total cationic exchange within the samples is believed to cause a partial breakdown of structure and the XRD results shown above also indicates such possibility.

5.4.3 pH analysis of strontium-cobalt exchange

The summary of the pH results from the strontium-cobalt exchange of Y-ZrP and α -ZrP samples is shown in the Table 5.10.

Table 5. 10 Summary of pH results of strontium-cobalt exchange

Samples	pH of Solution
Strontium-cobalt solution (0.2M)	Stock pH = 5.23
α -ZrP conventional	2.75
α -ZrP hydrothermal	1.80
5Y-ZrP conventional	2.10
5Y-ZrP hydrothermal	1.40
10Y-ZrP conventional	1.95
10Y-ZrP hydrothermal	1.80
15Y-ZrP conventional	1.55
15Y-ZrP hydrothermal	1.50

The results shown in the above table indicate a significant decrease in the pH of the exchange solution. This confirms that a high level of exchange for both Y-ZrP and α -ZrP has taken place. However, for the Y-ZrP samples the decrease in the pH was larger compared to that of α -ZrP for both synthesis routes. Also the highest decline in the pH was observed for the 5% Y-ZrP refluxed hydrothermally and these results are in consistent with the XRF results for compositional analysis. However, it is of interest to note that the pH of the competitive solution is relatively acidic (pH = 5.23) and the final pH of all the samples also reached a highly acidic value. This compliments both the XRD and XRF results indicating that the structural damage due to alkaline pH conditions had not occurred and any breakdown of structure is contributed due to excessive straining of the structure due to incoming cations.

The analysis of any changes which had occurred in the chemical environment of the strontium-cobalt exchanged Y-ZrP and α -ZrP samples was done by using FT-IR. The resulting FT-IR spectrums are shown in the figure 3 of Appendix 5 along with a summary of the characteristic peaks respective to their chemical bond from a strontium-cobalt exchange is shown in the table 3 of Appendix 5.

It was seen from the results that the strontium-cobalt exchanged Y-ZrP and α -ZrP samples showed an almost similar chemical environment as that of pristine α -ZrP with most of the peaks occurring at almost similar wavenumber. However, slight changes are observed in the peak intensities in the region of 900-1050 cm^{-1} and 3000-3500 cm^{-1} which is attributed to the change in P-O bonding and O-H bonding environment. Two additional peaks at 1369 and 1439 cm^{-1} is not recognised in literature, but it is found in this study to be related to the strontium exchange and hence is present in all the exchanged products

5.4.4 ICP-MS analysis of strontium-cobalt exchange

The filtrate solutions from all the strontium-cobalt exchanged samples of Y-ZrP and α -ZrP samples were analysed using ICP-MS in order to quantify the extent of exchange for both cations. The results of ICP-MS for all the samples are shown in Table 5.11 below.

Table 5. 11 Summary of ICP-MS results for strontium-cobalt exchange

Samples	X = Amount of ions remaining (ppm)		% of ions incorporation $\frac{M_{ppm} - X_{ppm}}{M_{ppm} \text{ of } 0.1M} \times 100$	
	$X_1 = \text{Sr}^{2+}$	$X_2 = \text{Co}^{2+}$	$M_1 = \text{Sr}^{2+}$ (8800 ppm)	$M_2 = \text{Co}^{2+}$ (5893.32 ppm)
α -ZrP conventional	7428(2)	5120(1)	15.590	13.121
α -ZrP hydrothermal	7450(1)	5180(1)	15.340	12.103
5Y-ZrP conventional	7383(3)	4990(3)	16.102	15.327
5Y-ZrP hydrothermal	7297(2)	4820(2)	17.079	18.212
10Y-ZrP conventional	7449(3)	5070(1)	15.352	13.970
10Y-ZrP hydrothermal	7397(1)	5009(1)	15.943	15.005
15Y-ZrP conventional	7314(2)	4990(2)	16.886	15.327
15Y-ZrP hydrothermal	7308(1)	4910(1)	16.954	16.685

It can be seen from the above results that strontium uptake is reduced slightly for all samples as compared with the single ion exchange result presented in Table 4.6. On the other hand, the cobalt uptake was increased compared with the single ion

exchange result shown in Table 4.19. Also, the synthesised Y-ZrP samples showed a higher extent of exchange for both these cations compared with the α -ZrP samples, especially the 5%Y-ZrP synthesised hydrothermally that showed the highest uptake for both the ions. These results are consistent with the XRD, XRF and pH results shown above. However, it is of interest to also analyse the leached amount of framework ions (Y^{3+} and Zr^{4+}) in the filtrate solution in order to explain any breakdown of structure which may have occurred during the exchange. Hence a summary of results are shown in the Table 5.12 below which shows the amount of leached framework ions present in the filtrate solution from each exchange product.

Table 5. 12 Summary of ICP-MS for leached ions

Samples	Concentration of ions	
	Y^{3+} (ppm)	Zr^{4+} (ppm)
α -ZrP conventional	-	4.923(3)
α -ZrP hydrothermal	-	5.313(4)
5Y-ZrP conventional	1.791(2)	4.952(2)
5Y-ZrP hydrothermal	0.869(1)	3.718(1)
10Y-ZrP conventional	1.671(1)	3.210(1)
10Y-ZrP hydrothermal	1.900(2)	4.777(2)
15Y-ZrP conventional	1.867(2)	3.140(2)
15Y-ZrP hydrothermal	1.129(1)	5.411(3)

It is seen from the above results that both the yttrium and zirconium ions were present in considerable quantities for all the exchanged solutions. This suggests that a possible breakdown of structure is occurring for both Y-ZrP and α -ZrP samples in strontium-cobalt solution and in turn can affect the crystallinity of the samples. These results therefore confirm the results of XRD, XRF and FT-IR analysis which also points towards a partial breakdown of structure and loss of crystallinity.

Overall, it was seen that the strontium-cobalt exchange showed a slight decrease in the strontium uptake but an overall increase in the cobalt exchange was clearly evident. However a decrease in crystallinity was observed for all the Y-ZrP and α -ZrP samples which were believed to occur due to partial breakdown of lattice structure consequently of heavy cationic loading within the layers. But in summary,

the synthesised Y-ZrP samples performed efficiently as compared with the α -ZrP for uptake of both Sr^{2+} and Co^{2+} ions from the strontium-cobalt exchange solution.

5.5. Strontium-caesium- cobalt exchange

The synthesised Y-ZrP and α -ZrP samples were exchanged with a solution containing a mixture of Sr^{2+} , Cs^+ and Co^{2+} ions with a 0.1M concentration made from nitrate salts. The resulting products were separated from the filtrate solution and both the products and filtrates were analysed to determine the selectivity and extent of exchange using XRD, XRF, FT-IR and ICP-MS techniques.

5.5.1 XRD analysis of strontium-caesium-cobalt exchange

The resulting XRD patterns for the strontium-caesium-cobalt exchanged Y-ZrP and α -ZrP products are shown in the Figure 5.4 below.

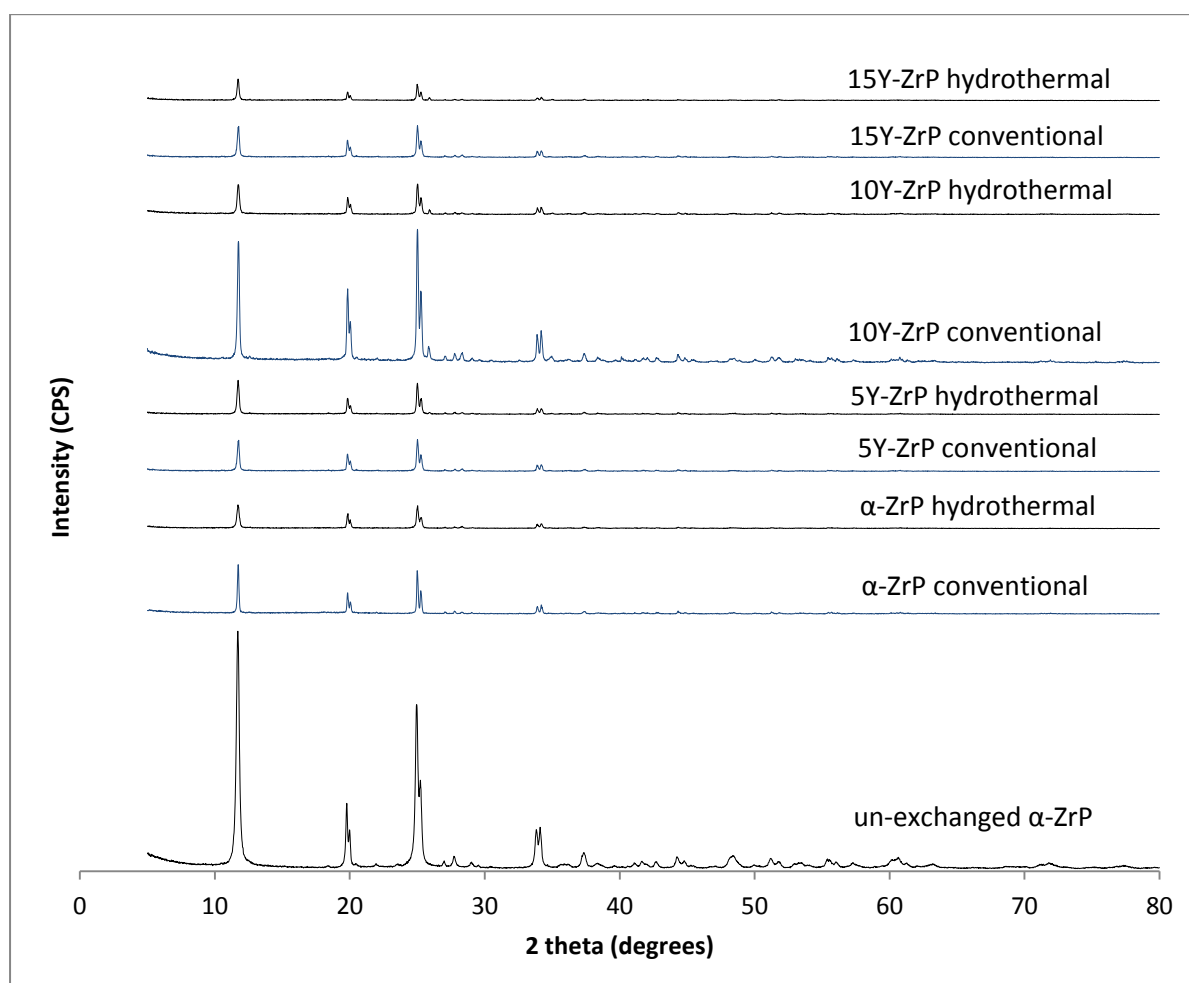


Figure 5. 4 XRD of strontium-caesium-cobalt exchange

The XRD results shown in the Figure 5.4 above indicates that the strontium-caesium-cobalt exchanged Y-ZrP and α -ZrP samples had an enormous loss in crystallinity in regards to the pristine α -ZrP, as evident from the reduced intensities of all the characteristic peaks. Also, an extra low intensity peak was observed at $2\theta=25.92^\circ$ which was persistent in all exchange experiments and cannot be attributed to any specific type of product. It is therefore believed to be linked with any interlayer cations exchanged within the α -ZrP type structure. However, the 10% Y-ZrP refluxed conventionally showed a higher crystallinity as compared to the rest of the samples which can be explained either due to limited exchange or experimental errors during the reaction. Overall, both the Y-ZrP and α -ZrP samples indicated a successful exchange of either or all the 3 cations (Sr^{2+} , Cs^+ and Co^{2+}) from the competitive exchange solution. Also the reduced signal to noise ratio indicates a loss of crystallinity due to a possible breakdown of structure.

5.5.2 XRF analysis of strontium-caesium-cobalt exchange

The exchanged products of Y-ZrP and α -ZrP from the competitive solution of Sr^{2+} , Cs^+ and Co^{2+} ions were analysed by XRF in order to determine the extent and selectivity of exchange. The results from the XRF analysis are shown in the Table 5.13.

Table 5. 13 XRF compositional analysis of exchanged products (M = Sr,Cs,Co ions)

Samples	Extent of Exchange		
	Ratio of M / (Y+Zr)		
	Sr / (Y+Zr)	Cs / (Y+Zr)	Co / (Y+Zr)
α -ZrP conventional	0.0361(1)	0.0223(3)	0.0174(1)
α -ZrP hydrothermal	0.0413(1)	0.0272(1)	0.0191(1)
5Y-ZrP conventional	0.0575(3)	0.0337(3)	0.0269(3)
5Y-ZrP hydrothermal	0.0865(4)	0.0382(2)	0.0403(2)
10Y-ZrP conventional	0.0333(2)	0.0303(1)	0.0271(1)
10Y-ZrP hydrothermal	0.0385(1)	0.0231(2)	0.0287(3)
15Y-ZrP conventional	0.0516(3)	0.0323(1)	0.0334(2)
15Y-ZrP hydrothermal	0.0608(1)	0.0369(3)	0.0377(1)

The above results indicate a successful uptake of all three cations (Sr^{2+} , Cs^+ and Co^{2+}) from the competitive exchange solution for both Y-ZrP and α -ZrP samples. It was seen that the uptake of strontium was reduced compared with the single ion exchange and other competitive exchange experiments. However, the caesium and cobalt exchange results showed an overall increase in the uptake compared with the single ion exchange experiments. This is explained by the fact that strontium is readily exchanged into the α -ZrP type structures due to its strong proton displacement ability but Co^{2+} ions being smaller in ionic radii (0.74 Å) compete strongly with the Sr^{2+} ions (1.18 Å). Hence equilibrium is maintained between these two ions to occupy an interlayer space in the parent structure, but since Cs^+ ions have larger ionic radii (1.67 Å) that restrict it from occupying the interlayer space and therefore reside in the water filled cavities by displacing water molecules.

It was also seen that that the uptake of strontium was highest compared with cobalt and caesium for both Y-ZrP and α -ZrP. However all Y-ZrP samples showed the order of exchange as $\text{Sr}^{2+} > \text{Co}^{2+} \geq \text{Cs}^+$, particularly the hydrothermally synthesised, whereas the α -ZrP showed higher exchange for caesium as compared with cobalt from the competitive exchange solution. [2] Further repetitive experiments are needed to confirm these results and establish the extent of exchange for these ions.

5.5.3 pH analysis of strontium-caesium-cobalt exchange

It is of interest to measure the pH changes in the competitive exchange solution due to proton exchange occurring from Y-ZrP and α -ZrP samples. A summary of the pH results are shown in the Table 5.14.

Table 5. 14 Summary of pH results of strontium-caesium-cobalt exchange

Samples	pH of Solution
Strontium-caesium-cobalt solution (0.3M)	Stock pH = 6.30
α -ZrP conventional	3.77
α -ZrP hydrothermal	3.50
5Y-ZrP conventional	3.04
5Y-ZrP hydrothermal	2.35
10Y-ZrP conventional	3.57
10Y-ZrP hydrothermal	3.35
15Y-ZrP conventional	3.20
15Y-ZrP hydrothermal	3.15

The above results for pH measurements shows that the synthesised Y-ZrP showed a greater decrease in pH upon ion exchange from competitive solution as compared with that of α -ZrP samples for both synthesis methods. However, the 5% Y-ZrP showed the greatest decrease in the pH which indicates the highest exchange of protons for cations from the solution. These results are consistent with the XRF findings that also points out a similar trend of exchange for both Y-ZrP and α -ZrP samples. However, further analysis of the filtrate solution is needed to confirm the XRD results for the possibility of any structure breakdown which would have also contributed to such pH measurements.

The FT-IR analysis of ion exchanged Y-ZrP and α -ZrP samples of both routes of reflux is done in order to study the type and nature of changes that had occurred due to incoming cations within the structure. The results for the FT-IR spectrums are provided in the figure 4 of Appendix 5 along with a summary of the typical FT-IR peaks corresponding to respective chemical bonds for a Sr-Cs-Co exchanged Y-ZrP product is shown in the table 4.

The FT-IR results presented in the figure above shows a very similar spectrum for the exchanged Y-ZrP and α -ZrP samples as compared with the pristine α -ZrP. It was observed that almost all the peaks present in the spectrums of the exchanged products match to that of a typical α -ZrP spectrum in regards to the wavenumber.

However there were subtle changes which were observed in the intensities of the corresponding peaks that might be related to the crystallinity or extent of exchange within the structures. Also, two additional peaks at 1369 and 1439 cm^{-1} were present in all the products which were previously discussed to be associated with all the strontium exchanged products from both single and competitive exchange experiments. Therefore, no clear conclusions about the extent or nature of exchange for the products can be deduced from these results apart from the confirmation that both Y-ZrP and α -ZrP products retained their original structure after the cationic exchange from the competitive ion exchange solution.

5.5.4 ICP-MS analysis of strontium-caesium-cobalt exchange

The filtrates from the competitive ion exchange solution containing Sr^{2+} , Cs^+ and Co^{2+} ions after separating the products were analysed by ICP-MS in order to determine the extent and selectivity of exchange. The samples were diluted 1000 times and calibrated against the standards (calibration curves provided in figures 5-9 of Appendix 3) for determining the concentration of the ions left in the solution and that incorporated within the samples. A summary of the ICP-MS results is shown in the Table 5.15.

Table 5. 15 Summary of ICP-MS results for strontium-caesium-cobalt exchange

Samples	X = Amount of ions remaining (ppm)			% of ions incorporation $\frac{M_{ppm} - X_{ppm}}{M_{ppm} \text{ of } 0.1M} \times 100$		
	X ₁ = Sr ²⁺	X ₂ = Cs ⁺	X ₃ = Co ²⁺	M ₁ = Sr ²⁺ (8800 ppm)	M ₂ = Cs ⁺ (13290.55 ppm)	M ₃ = Co ²⁺ (5893.32 ppm)
α-ZrP conventional	7624(3)	12740(5)	5650(4)	13.363	4.142	4.128
α-ZrP hydrothermal	7651(2)	12700(3)	5625(2)	13.056	4.443	4.552
5Y-ZrP conventional	7538(3)	12650(2)	5490(1)	14.340	4.819	6.843
5Y-ZrP hydrothermal	7422(1)	12660(4)	5270(1)	15.659	4.744	10.576
10Y-ZrP conventional	7611(1)	12720(4)	5510(2)	13.511	4.292	6.504
10Y-ZrP hydrothermal	7600(2)	12714(2)	5514(2)	13.636	4.338	6.436
15Y-ZrP conventional	7594(4)	12690(1)	5460(3)	13.704	4.518	7.352
15Y-ZrP hydrothermal	7554(3)	12680(3)	5420(2)	14.159	4.593	8.031

The above results of ICP-MS shows a decreased percentage of Sr²⁺ incorporation into the Y-ZrP and α-ZrP of both routes of reflux, as compared with that of the single ion exchange experimental results shown in Table 4.6. However, Cs⁺ ions showed a similar extent of exchange but there was a subtle improvement in Co²⁺ uptake as that of their single ion exchange experiments, seen from Table 4.19 and Table 4.13 respectively. Also it can be clearly observed that the synthesised Y-ZrP and α-ZrP samples showed the highest uptake of Sr²⁺ ions from the competitive solution but the order of uptake for Y-ZrP follows a trend of Sr²⁺ > Co²⁺ > Cs⁺, whereas α-ZrP shows almost similar extent of exchange for caesium and cobalt ions.

Therefore, these ICP-MS results compliment the XRF and pH results above which indicates a similar trend of exchange for both Y-ZrP and α -ZrP samples. However the XRD results indicate a possible breakdown of structure, therefore a further investigation of filtrate solution for analysing the presence of framework ions (Y^{3+} and Zr^{4+}) was done and the results are shown in the Table 5.16.

Table 5. 16 Summary of ICP-MS for leached ions

Samples	Concentration of ions	
	Y^{3+} (ppm)	Zr^{4+} (ppm)
α -ZrP conventional	-	3.197(2)
α -ZrP hydrothermal	-	5.070(4)
5Y-ZrP conventional	1.835(2)	1.937(1)
5Y-ZrP hydrothermal	0.386(1)	0.174(1)
10Y-ZrP conventional	1.036(2)	1.066(2)
10Y-ZrP hydrothermal	0.408(1)	0.439(3)
15Y-ZrP conventional	2.127(3)	0.110(1)
15Y-ZrP hydrothermal	2.936(4)	0.046(1)

It is seen from the above results that α -ZrP showed a moderate presence of Zr^{4+} ions in the analysed filtrate solutions which indicates a partial breakdown of structure. Also the synthesised Y-ZrP samples showed higher amount of Y^{3+} ions as opposed to the Zr^{4+} ions which indicates a possible breakdown of structure at the sites of yttrium substitution. This is believed to have occurred due to straining of the structure due to heavy loading of cations which distorts the structure further and releases yttrium ions to reduce steric hindrance and reach a more stable state. However, further investigation and repetitive experiments are required to establish similar results and provide a confirmed mechanism of exchange from the competitive solution for α -ZrP type samples

In summary, it was observed that both Y-ZrP and α -ZrP samples from both synthesis methods showed high efficiency to remove all the ions of interest (Sr^{2+} , Co^{2+} and Cs^+) from the competitive solution following the order of selectivity and extent as $Sr^{2+} > Co^{2+} \geq Cs^+$.

5.6. Competitive exchange with calcium

The synthesised Y-ZrP and α -ZrP samples were exchanged with solutions consisting of Sr^{2+} , Co^{2+} and Cs^+ ions together with calcium as an interfering cation. No previous studies are present in the literature on exchanging Ca^{2+} ions from such competitive solutions however two elaborate studies were conducted on exchanging calcium ions into α -ZrP [6, 7].

Therefore it is of interest to perform competitive exchanges with calcium on both Y-ZrP and α -ZrP samples in order to study the selectivity and extent of exchange for the cations of interest. Three sets of competitive exchanges using nitrate salt solutions were performed as follows: strontium-calcium, caesium-calcium and cobalt-calcium. As before, the exchanged samples were characterised by XRD, XRF, FT-IR and ICP-MS.

5.6.1 XRD analysis of competitive exchange with calcium

A series of competitively exchanged Y-ZrP and α -ZrP samples were analysed by XRD in order to determine any changes that occurred in the crystal structure of the parent samples due to incoming cations. The results of the XRD analysis are shown in the Figure 5.5 and indicate the changes in the XRD patterns of the exchanged products compared to un-exchanged α -ZrP.

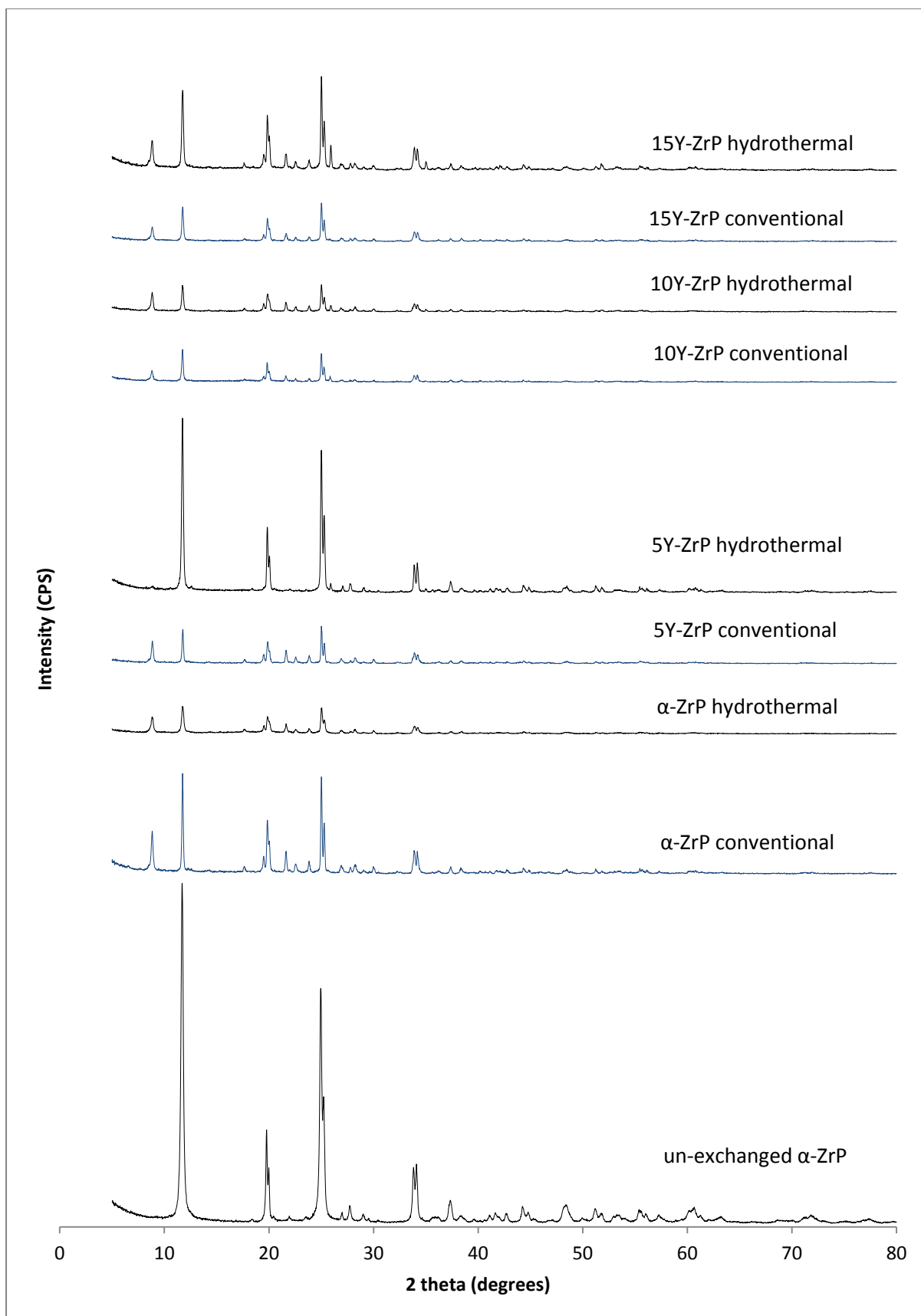


Figure 5. 5 XRD of strontium-calcium exchange

It is seen from the above XRD results for strontium-calcium exchange that there is decrease in crystallinity for both Y-ZrP and α -ZrP samples however the 5% Y-ZrP and 15%Y-ZrP refluxed hydrothermally showed a higher degree of crystallinity as compared to the rest of the exchanged products. However the presence of characteristic peaks of the parent samples indicate that the lattice structure of the products is conserved. But, the appearance of extra low intensity peaks were observed at $2\theta = 8.83^\circ$, 17.7° and 25.9° and were matched with the PDF online crystal database (shown in figure 2 of appendix 4) to strontium phosphate hydrate and calcium hydrogen phosphate.

There is a lack of literature data to match some of these peaks with regards to the calcium exchanged form of α -ZrP but the peak corresponding to $2\theta = 8.83^\circ$ is highly pronounced in this competitive exchange with calcium as compared with all other exchange experiments. This peak is previously assigned to the α -SrZr(PO₄)₂ of composition ZrHSr_{0.5}(PO₄)₂·3.6H₂O as explained in literature [3, 8]. Also few minor peaks were observed in some of the patterns that were not matched with the online crystal database and remained unknown. There is a possibility that these peaks arise due to the change in the space group symmetry of the samples upon exchange with cations. Therefore further characterisation of the XRD data is needed in order to understand the site of exchange and the changes that occurred in the crystal lattice.

The XRD pattern for caesium-calcium exchanged Y-ZrP and α -ZrP samples is shown in the Figure 5.6.

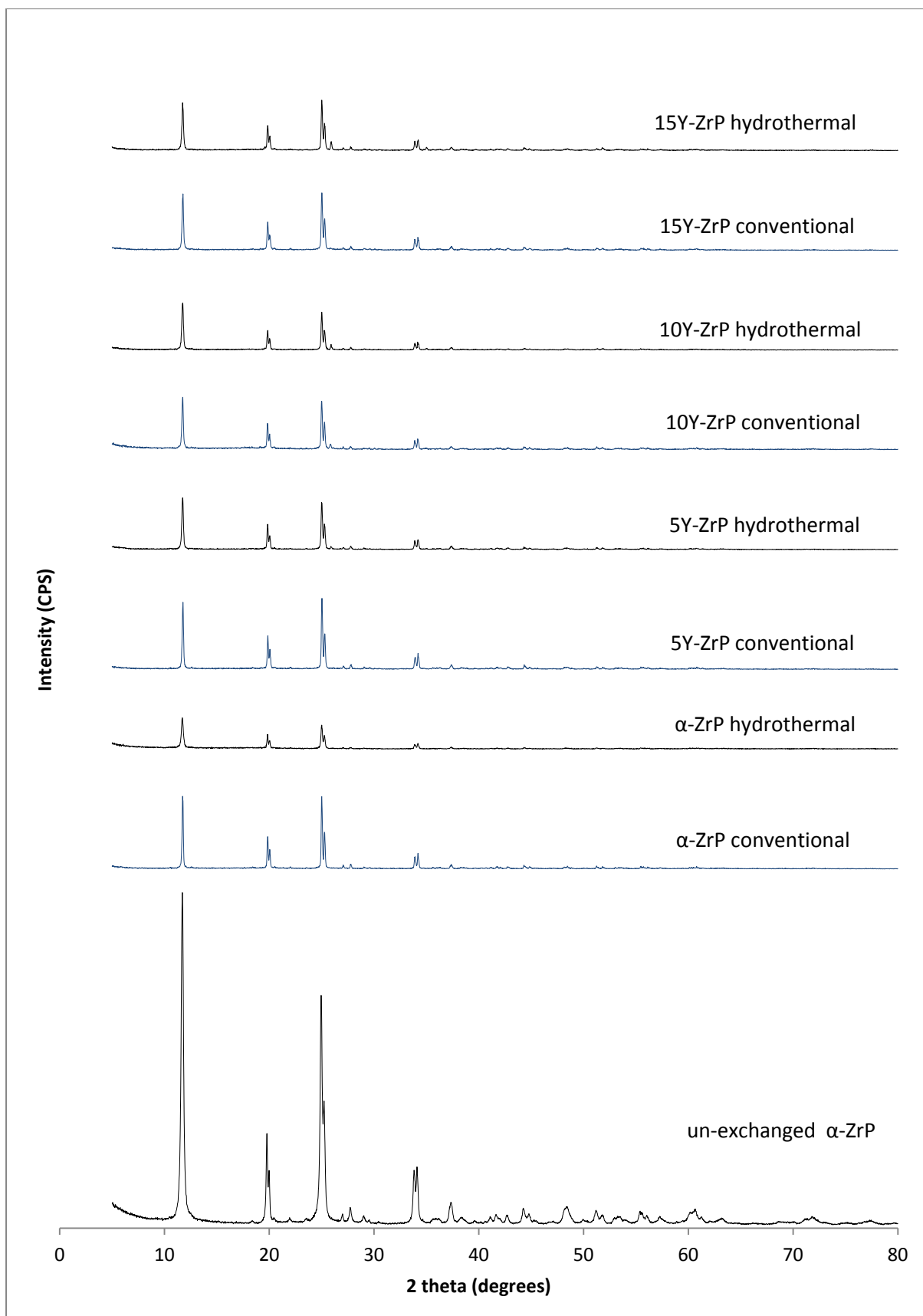


Figure 5. 6 XRD of caesium-calcium exchange

The XRD results shown in the figure 5.6 for caesium-calcium exchange indicates a high loss of crystallinity of the products that is evident from the low signal to noise ratio of the characteristics peaks. However, the presence of typical peaks of α -ZrP type structure in all the exchanged products clearly indicates that a successful exchange of cations had taken place and the basic layered structure of the materials is conserved. But the possibility of partial breakdown of the exchanged products is present due to the reduced crystallinity. Also the appearance of a low intensity peak at $2\theta = 26^\circ$ is observed in all Y-ZrP samples which remains un-identified in the literature as discussed previously and no online match was found with the PDF crystal database.

The XRD pattern of the cobalt-calcium exchanged products is shown in the Figure 5.7 below.

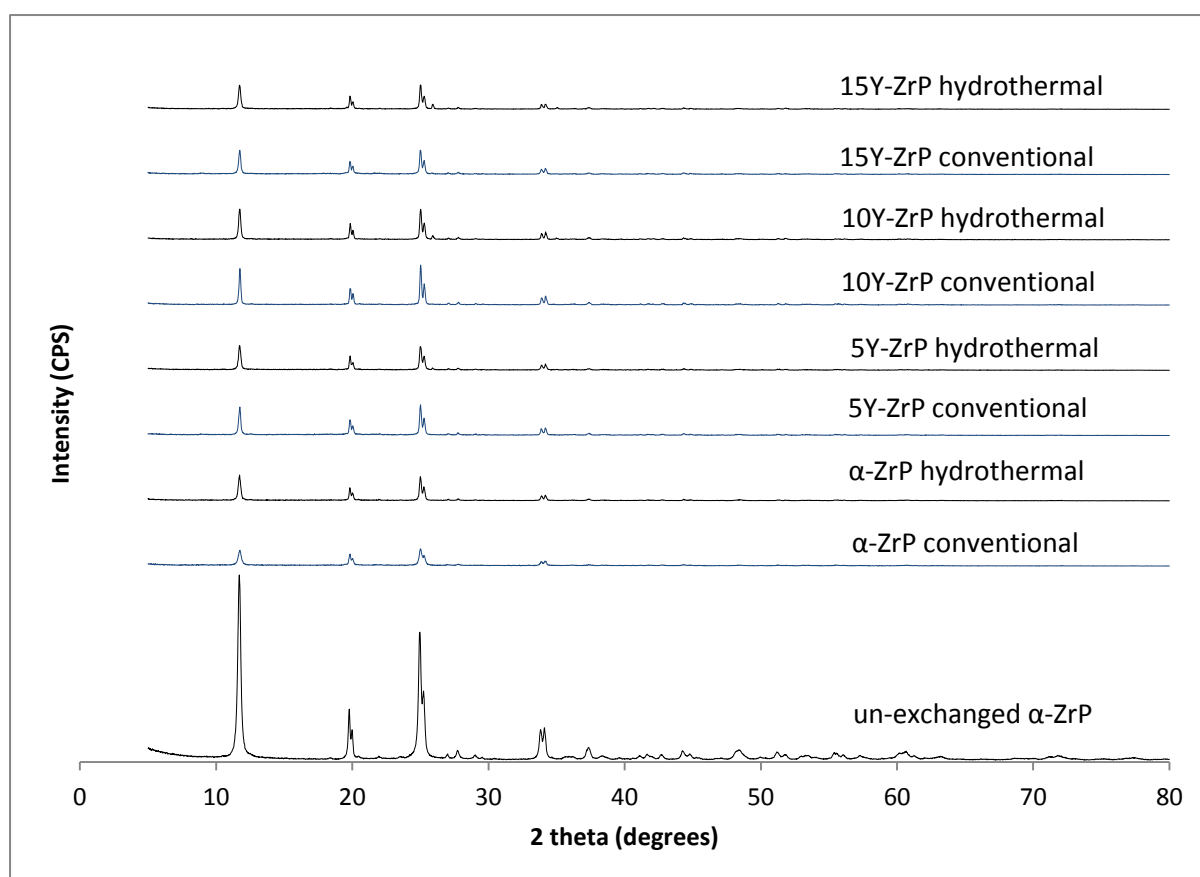


Figure 5. 7 XRD of cobalt-calcium exchange

The results shown in the figure 5.7 for cobalt-calcium exchange indicates a loss in crystallinity for the exchanged Y-ZrP and α -ZrP products. The presence of all the characteristic peaks of the parent α -ZrP type sample indicates that the layered

structure of the exchanged products is maintained however there is a loss of intensity of all the peaks. Few minor peaks were seen throughout the pattern but due to extremely small intensity no identification could be made with known crystal structures.

5.6.2 XRF analysis of competitive exchange with calcium

The result for the XRF analysis is shown in the Table 5.17 and it compares that the extent of exchange for Sr^{2+} , Co^{2+} and Cs^+ ions with Ca^{2+} ions.

Table 5. 17 XRF of competitive exchange with calcium

Sample	Extent of exchange					
	Sr-Ca exchange		Cs-Ca exchange		Co-Ca exchange	
	$\frac{Sr}{Y + Zr}$	$\frac{Ca}{Y + Zr}$	$\frac{Cs}{Y + Zr}$	$\frac{Ca}{Y + Zr}$	$\frac{Co}{Y + Zr}$	$\frac{Ca}{Y + Zr}$
α -ZrP conventional	0.1085(1)	0.0607(1)	0.0231(2)	0.0278(3)	0.0384(3)	0.0435(1)
α -ZrP hydrothermal	0.1105(2)	0.0647(3)	0.0313(2)	0.0337(4)	0.0368(1)	0.0407(3)
5Y-ZrP conventional	0.1131(1)	0.0702(1)	0.0300(1)	0.0304(2)	0.0413(3)	0.0485(2)
5Y-ZrP hydrothermal	0.1251(3)	0.0751(2)	0.0319(2)	0.0356(1)	0.0521(2)	0.0626(2)
10Y-ZrP conventional	0.1081(2)	0.0625(3)	0.0317(3)	0.0356(4)	0.0344(1)	0.0417(3)
10Y-ZrP hydrothermal	0.1122(3)	0.0656(2)	0.0273(2)	0.0252(2)	0.0399(2)	0.0426(1)
15Y-ZrP conventional	0.1193(1)	0.0654(1)	0.0414(2)	0.0457(2)	0.0387(3)	0.0472(1)
15Y-ZrP hydrothermal	0.1192(3)	0.0662(2)	0.0266(1)	0.0336(1)	0.0365(2)	0.0418(2)

It was observed that the strontium-calcium exchange showed a higher Sr^{2+} uptake and in particular for 5% Y-ZrP hydrothermally synthesised as compared to the α -ZrP. However the Ca^{2+} uptake was more or less uniform for both Y-ZrP and α -ZrP samples except for the 5% Y-ZrP samples of both routes of reflux which showed

slightly increased exchange capacity for both Sr^{2+} and Ca^{2+} ions from the solution. But overall, strontium uptake was lower than the single exchange experiments (Table 4.2) but followed a similar trend of exchange for both Y-ZrP and α -ZrP sample and the Ca^{2+} uptake was highest for strontium-calcium exchange as compared to the other two exchanges.

For the caesium-calcium exchange, it was seen that there is no distinct trend but there was a slightly increased uptake of Cs^+ ions by both Y-ZrP and α -ZrP samples. The trend of exchange of Cs^+ ions in Y-ZrP samples did not follow that of the single exchange experiment (Table 4.9). Also the exchange capacity of the Cs^+ ions in Y-ZrP samples was slightly higher in the presence of Ca^{2+} ions compared to the α -ZrP samples. This is explained by the fact that the incoming Ca^{2+} ions in the interlayer spacing can expand the layers to allow the larger Cs^+ ions exchange in the cavities by replacing lattice water. However, this exchange may lead to a partial breakdown of the structure as indicated by the XRD results. But overall, it was observed from caesium-calcium exchange that Y-ZrP samples showed a slight increase in Cs^+ ions uptake as compared to the α -ZrP samples in the presence of Ca^{2+} ions, but the uptake of Ca^{2+} ions was more or less uniform for all the samples except for 15% Y-ZrP refluxed conventionally, that showed a considerably high Cs^+ and Ca^{2+} ion uptake.

The cobalt-calcium exchange on the other hand showed a marked increase in Co^{2+} ion uptake for both Y-ZrP and α -ZrP samples as compared to the single ion exchange experiments (Table 4.15). Also, the synthesised Y-ZrP samples of both routes of reflux had a higher Co^{2+} ion uptake as compared to the α -ZrP samples but the Ca^{2+} ion uptake was more or less uniform for both Y-ZrP and α -ZrP samples. However the 5% Y-ZrP sample synthesised hydrothermally showed the highest Co^{2+} and Ca^{2+} ion uptake among all the products. But overall, cobalt-calcium exchange showed a higher degree of Co^{2+} ion uptake in the presence of Ca^{2+} ions that again may be caused due to an increase in the interlayer distance making subsequent change more facile.

5.6.3 pH analysis of competitive exchange with calcium

The result for the pH analysis of the filtrate from the three competitive exchanges with calcium is shown in the Table 5.18 below and it indicates the extent of pH drop of the Y-ZrP compared to the α -ZrP samples.

Table 5. 18 Summary of pH results for competitive exchange with calcium

Samples	Sr-Ca exchange Stock pH = 6.50	Cs-Ca exchange Stock pH = 6.40	Co-Ca exchange Stock pH = 4.10
α -ZrP conventional	2.42	3.70	1.80
α -ZrP hydrothermal	2.33	3.70	2.02
5Y-ZrP conventional	2.20	3.23	1.78
5Y-ZrP hydrothermal	2.30	2.35	1.30
10Y-ZrP conventional	2.38	3.10	2.40
10Y-ZrP hydrothermal	2.17	2.95	2.35
15Y-ZrP conventional	2.33	3.50	1.76
15Y-ZrP hydrothermal	2.40	2.95	1.25

The results shown above clearly indicate a decrease in pH of the filtrate solutions for all the three competitive exchanges with calcium. The decrease in the pH shows that H^+ ions has been lost from the materials and replaced by the cations from the exchange solution. Also it can be seen from the above results that the decrease in pH is the highest for strontium-calcium exchanged solutions followed by cobalt-calcium and caesium-calcium exchanges. This explains the fact that the extent of exchange is also highest for strontium-calcium exchanged products and follows the same trend. Moreover, it can be seen from all the three competitive exchange experiments that Y-ZrP products showed a higher decrease in pH for its filtrate solutions compared to α -ZrP samples, especially the 5%Y-ZrP and 15% Y-ZrP which showed the greatest decrease throughout. These results are consistent with the XRF findings.

The FT-IR analysis was done on Y-ZrP and α -ZrP products of competitive exchange experiments with calcium as interfering ion. These results provide an insight about the changing chemical environment of the exchanged products due to the incoming

cations. Also, any change in the framework of the Y-ZrP and α -ZrP samples can be observed from the FT-IR spectrums of the exchanged products and compared with the pristine α -ZrP type structure.

The FT-IR spectrums for strontium-calcium exchanged products are shown in the figure 5 of Appendix 5 along with a summary of the ideal FT-IR peaks from strontium-calcium exchanged α -ZrP type product shown in table 5. It was seen from the FT-IR spectra that the exchanged products showed a similar chemical environment as that of un-exchanged α -ZrP however, the peaks present in the region of 950-1050 cm^{-1} exhibit a noticeable change in the intensity suggesting that the P-O stretching vibrations are reduced (at ca. 1030 cm^{-1}) as compared to the bending vibrations (at ca. 965 cm^{-1}). This is explained by the fact that the incoming cations shows steric hindrance on the localised phosphate groups that somewhat counters the stretching force of the P-O bonds. Also, the O-H stretching and bending vibration peaks (at ca. 1620 cm^{-1} and 3000-3500 cm^{-1}) showed a slight variation in the intensities, which suggests a high loading of exchanged cations into the lattice structure that led to the displacement of few water molecules from the cavities along with the outgoing protons. This is supported by the diminishing O-H (out of plane) vibration peak at ca. 650 cm^{-1} in all the strontium-calcium exchanged products as opposed to a clear peak observed in the pristine α -ZrP.

The FT-IR spectrums of caesium-calcium exchanged Y-ZrP and α -ZrP products are shown in the figure 6 of Appendix 5 along with a summary of ideal FT-IR peaks from an ideal caesium-calcium exchanged α -ZrP type product shown in table 6. It was seen from the results that the Y-ZrP and α -ZrP products from caesium-calcium exchange solution yielded similar spectrums to that of pristine α -ZrP with all the characteristic bonding peaks at the same wavenumber. However few minor variations were observed in the regions of 1000-1200 cm^{-1} which indicates a change in the P-O stretching vibrations. Also there is a slight variation in the intensities of few peaks such as in the region 950-1050 cm^{-1} and 3000-3500 cm^{-1} , but these changes are not recognised in the literature and are believed to be contributed due to changing crystallinity and the presence of non-framework cations that induces steric hindrance on the framework phosphate units. Overall, the exchanged products showed similar FT-IR spectrums of exchange as compared to pristine α -ZrP type

structures with slight changes that are contributed to the changing P-O and O-H vibrations.

The FT-IR spectrums for cobalt-calcium exchanged Y-ZrP and α -ZrP products of both routes of reflux are shown in the figure 7 of Appendix 5 along with a summary of the FT-IR peaks from an ideal cobalt-calcium exchanged α -ZrP type product shown in table 7. It was seen from the results that subtle changes were observed in the peak shape and intensities at the regions of 950-1200 cm^{-1} that indicates a change in the P-O bending and stretching vibrations due to incoming cations that are exchanged for protons on the phosphate group. Two minor peaks were observed at ca. 1345 cm^{-1} and 1429 cm^{-1} but these peaks were not recognised in the literature. However these peaks were not observed in the single ion exchange experiment with cobalt and hence are believed to be associated with calcium ion. Overall, apart from these few subtle changes in the P-O vibrations, no visible change was observed for peaks at 3000-3500 cm^{-1} indicating that the O-H stretching vibrations remain unaffected and hence no exchange had taken place in the water filled cavities. This confirms the XRD and XRF results that indicate an interlayer accumulation of the cations on exchange with the protons within the planes.

5.6.4 ICP-MS analysis for competitive exchange with calcium

The filtrate solutions from the exchanged Y-ZrP and α -ZrP products of competitive exchanges with calcium ions were analysed by ICP-MS in order to determine the amount of cations exchanged into the samples. A summary of the ICP-MS results for all three competitive exchanges with calcium is shown in the tables below.

Table 5. 19 Summary of ICP-MS result for strontium-calcium exchange

Samples	X = Amount of ions remaining (ppm)		% of ions incorporation $\frac{M_{ppm} - X_{ppm}}{M_{ppm} \text{ of } 0.1M} \times 100$	
	$X_1 = Sr^{2+}$	$X_2 = Ca^{2+}$	$M_1 = Sr^{2+}$ (8800 ppm)	$M_2 = Ca^{2+}$ (4000 ppm)
α -ZrP conventional	6419(2)	2589(2)	27.056	35.275
α -ZrP hydrothermal	6766(3)	2859(1)	23.113	28.525
5Y-ZrP conventional	6544(2)	2252(1)	25.636	43.7
5Y-ZrP hydrothermal	6041(1)	2142(2)	31.352	46.45
10Y-ZrP conventional	6092(3)	2134(4)	30.772	46.65
10Y-ZrP hydrothermal	6085(1)	2436(2)	30.852	39.1
15Y-ZrP conventional	6640(3)	2659(1)	24.545	33.525
15Y-ZrP hydrothermal	6074(2)	2114(1)	30.977	47.15

It can be seen from the above results that the synthesised Y-ZrP samples showed higher percentages of cation exchange from the competitive solution as compared to the α -ZrP. Both Sr^{2+} and Ca^{2+} ions were exchanged in higher quantities into the Y-ZrP samples as compared to α -ZrP, especially the 5% Y-ZrP synthesised hydrothermally showing the highest uptake for both the cations. However, the extent of Ca^{2+} uptake from the ICP-MS results is higher as compared to the XRF measurements. This is because of the poly-atomic interferences that can affect the analysis of certain atoms in the ICP-MS and can be avoided using a different matrix or better sample preparation using alternative isotope and applying elemental correction equations.^[11] Unfortunately, these errors could not be overcome for the ion-exchanged samples, probably due to the presence of complex solution matrix. Nevertheless, these results are generally in agreement with the XRF and pH results discussed above concluding that the synthesised Y-ZrP were efficient exchangers of both strontium and calcium ions from competitive solution.

However, XRD results suggests a possible breakdown of structure for the exchanged products hence a further investigation was done to determine the leached framework ions (Y^{3+} and Zr^{4+}) from the filtrate solutions. A summary of the results is provided in the Table 5.20 below.

Table 5. 20 Summary of leached ions for strontium-calcium exchange

Samples	Concentration of ions	
	Y ³⁺ (ppm)	Zr ⁴⁺ (ppm)
α-ZrP conventional	-	1.169(3)
α-ZrP hydrothermal	-	1.064(1)
5Y-ZrP conventional	1.112(1)	2.614(4)
5Y-ZrP hydrothermal	0.243(1)	0.201(1)
10Y-ZrP conventional	1.795(3)	0.082(1)
10Y-ZrP hydrothermal	1.310(2)	0.338(2)
15Y-ZrP conventional	1.096(2)	0.046(1)
15Y-ZrP hydrothermal	2.598(3)	0.027(1)

It is seen from the above results that the α-ZrP samples showed a considerable amount of Zr⁴⁺ ions leaching, whereas the synthesised Y-ZrP products showed a comparatively higher amount of Y³⁺ ions leaching. These results support the XRD analysis to explain the fact that the possible breakdown of sample structures did occur partially and the leaching results of framework ions of Y-ZrP products indicate that the yttrium rich regions underwent the distortion as opposed to the α-ZrP samples that leached only the zirconium ions. Further investigations and repetitive experiments are required to establish these results confidently.

The ICP-MS analysis for the caesium-calcium exchanged Y-ZrP and α-ZrP products are shown in the Table 5.21 below.

Table 5. 21 Summary of ICP-MS result for caesium-calcium exchange

Samples	X = Amount of ions remaining (ppm)		% of ions incorporation $\frac{M_{ppm} - X_{ppm}}{M_{ppm} \text{ of } 0.1M} \times 100$	
	X ₁ = Cs ⁺	X ₂ = Ca ²⁺	M ₁ = Cs ⁺ (13290.55 ppm)	M ₂ = Ca ²⁺ (4000 ppm)
α-ZrP conventional	12750(4)	2916(2)	4.0671	27.1
α-ZrP hydrothermal	12836(3)	2923(1)	3.420	26.925
5Y-ZrP conventional	11780(1)	2856(2)	11.365	28.6
5Y-ZrP hydrothermal	12100(3)	2774(3)	8.957	30.65
10Y-ZrP conventional	12380(4)	2811(2)	6.851	29.725
10Y-ZrP hydrothermal	12790(2)	2927(4)	3.766	26.825
15Y-ZrP conventional	11270(2)	2677(6)	15.202	33.075
15Y-ZrP hydrothermal	12163(3)	2861(2)	8.483	28.475

It can be seen from the above analysis that extent of exchange for caesium ions was more or less similar for the Y-ZrP and α-ZrP samples of both routes of synthesis. However, an increased uptake of Cs⁺ ions was observed for the 5% Y-ZrP hydrothermally synthesised and 15% Y-ZrP conventionally refluxed samples. A similar trend was also observed for the calcium ions exchanged into both Y-ZrP and α-ZrP samples however the extent of Ca²⁺ ion uptake was less than that from the strontium-calcium exchange as shown above. These results are in agreement with both XRF and pH analysis as discussed previously and hence concludes that only a slight increase was observed in the Cs⁺ ion uptake in the presence of calcium ion as compared to the single exchange experiments and both Y-ZrP and α-ZrP samples showed a similar trend of exchange of both the cations from the competitive exchange solution. But the overall Ca²⁺ ion uptake was higher as compared to the Cs⁺ uptake on contrary to the XRF results that showed nearly similar uptake. This might be due to the poly-atomic interferences that can affect the analysis of certain atoms in the ICP-MS, as discussed previously.

However, the XRD results indicates a possible breakdown of structure, therefore a further analysis of the filtrate solution was done to determine the amount of leached

framework ions (Y^{3+} and Zr^{4+}) into the solution and the results are shown in the Table 5.22 below.

Table 5. 22 Summary of leached ions for caesium-calcium exchange

Samples	Concentration of ions	
	Y^{3+} (ppm)	Zr^{4+} (ppm)
α -ZrP conventional	-	4.795(3)
α -ZrP hydrothermal	-	5.767(4)
5Y-ZrP conventional	2.673(4)	0.292(1)
5Y-ZrP hydrothermal	1.542(1)	0.740(1)
10Y-ZrP conventional	1.152(3)	1.590(3)
10Y-ZrP hydrothermal	0.930(1)	2.512(4)
15Y-ZrP conventional	1.559(2)	1.014(2)
15Y-ZrP hydrothermal	2.397(1)	0.548(1)

It can be seen from the above results that both Y-ZrP and α -ZrP samples showed a considerable amount of leached ions (Y^{3+} and Zr^{4+}) present in the filtrate solution indicating a significant degree of structure breakdown. Also the leaching results from the Y-ZrP samples indicate the possibility of structure distortion at the yttrium rich regions within the crystal lattice that can have severe effect on the crystallinity as already demonstrated by the XRD analysis. However such results are expected in case of Cs^+ ions exchange into the lattice structure as discussed previously.

A summary of the results from the ICP-MS of the cobalt-calcium exchanged Y-ZrP and α -ZrP products is provided in the Table 5.23 below.

Table 5. 23 Summary of ICP-MS result for cobalt-calcium exchange

Samples	X = Amount of ions remaining (ppm)		% of ions incorporation $\frac{M_{ppm} - X_{ppm}}{M_{ppm} \text{ of } 0.1M} \times 100$	
	X ₁ = Co ²⁺	X ₂ = Ca ²⁺	M ₁ = Co ²⁺ (5893.32 ppm)	M ₂ = Ca ²⁺ (4000 ppm)
α-ZrP conventional	5260(4)	2650(1)	10.746	33.75
α-ZrP hydrothermal	5200(1)	2878(3)	11.764	28.05
5Y-ZrP conventional	5180(3)	2228(2)	12.103	44.3
5Y-ZrP hydrothermal	5040(2)	2148(4)	14.479	46.3
10Y-ZrP conventional	5270(5)	2455(2)	10.576	38.625
10Y-ZrP hydrothermal	5280(3)	2624(1)	10.407	34.4
15Y-ZrP conventional	5260(4)	2484(1)	10.746	37.9
15Y-ZrP hydrothermal	5130(6)	2165(3)	12.952	45.875

It is seen from the results presented above that the extent of Co²⁺ ions exchanged for Y-ZrP and α-ZrP samples showed a slight increase as compared to the single exchange experiments. Also the synthesised Y-ZrP samples showed a higher uptake of Co²⁺ ions in the presence of calcium ions, especially the 5% Y-ZrP sample synthesised hydrothermally that showed the highest cobalt uptake. Also a similar trend of Ca²⁺ ion exchange was observed for both Y-ZrP and α-ZrP samples and overall the extent of exchange was similar to that of strontium-calcium exchange. However, there appears to be more Ca²⁺ ion uptake as compared to the Co²⁺ uptake that is not matching the XRF results, but as discussed previously this might be due to poly-atomic interferences that can affect the analysis of certain atoms in the ICP-MS. Overall these results complement the XRF and pH analysis done previously and hence concludes that the synthesised Y-ZrP samples are efficient cobalt exchangers even in the presence of interfering calcium ions.

However the XRD results also indicates a possible breakdown of structure which affects the crystallinity of the exchanged products, hence a further analysis of the filtrate solutions were done to determine the amount of leached framework ions (Y³⁺ and Zr⁴⁺) present in the solution and a summary of the results is shown in the Table 5.24.

Table 5. 24 Summary of leached ions for cobalt-calcium exchange

Samples	Concentration of ions	
	Y ³⁺ (ppm)	Zr ⁴⁺ (ppm)
α-ZrP conventional	-	2.620(3)
α-ZrP hydrothermal	-	2.630(2)
5Y-ZrP conventional	1.978(2)	1.210(1)
5Y-ZrP hydrothermal	0.603(1)	0.292(4)
10Y-ZrP conventional	1.964(4)	0.886(1)
10Y-ZrP hydrothermal	1.148(2)	1.026(3)
15Y-ZrP conventional	1.920(1)	0.877(1)
15Y-ZrP hydrothermal	0.553(1)	1.140(2)

It is seen from the above results that α-ZrP samples showed a considerable amount of leached Zr⁴⁺ ions in the filtrate solution as compared to the Y-ZrP samples that showed mixed results for the amount of leached Y³⁺ and Zr⁴⁺ ions. However, the amount of framework ions leached into the solutions is significant enough to support that fact that a partial breakdown of the α-ZrP type structures did occur from the competitive solution. These results are in consistent with the XRD and pH results that indicate a higher exchange of cations which can lead to partial structural damage. However, further investigation of the exchanged products and repetitive experiments are required to establish these results.

5.7. Competitive exchange with magnesium

The synthesised Y-ZrP and α-ZrP samples were subjected to a competitive exchange solution with Sr²⁺, Cs⁺ and Co²⁺ ions in the presence of magnesium as an interfering ion. Three different competitive solutions with 0.1M each of nitrate salts were used for exchange experiments such as strontium-magnesium, caesium-magnesium and cobalt-magnesium. The resulting products and filtrate solutions were then characterised using the techniques described previously, except for XRF which was not suitable for analysing the magnesium content, instead EDX/SEM was used to obtain semi-quantitative results.

5.7.1 XRD analysis of competitive exchange with magnesium

The XRD results for the competitive exchange experiments using magnesium as the interfering ion is shown in the following figures. The XRD patterns for the strontium-magnesium exchanged Y-ZrP and α -ZrP products are shown in the Figure 5.8 below.

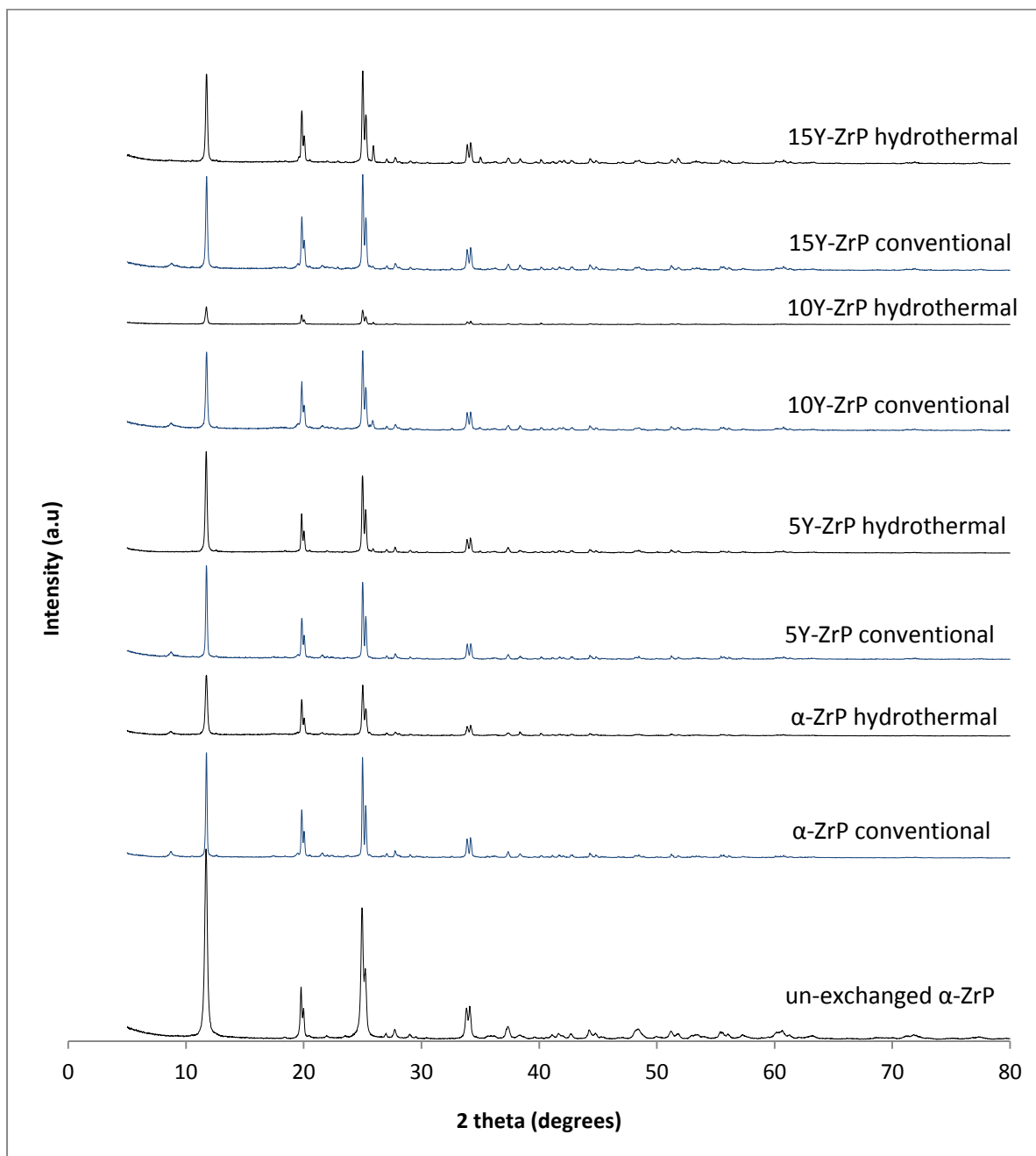


Figure 5. 8 XRD results for strontium-magnesium exchange

It is well evident from the above results that Y-ZrP and α -ZrP products from strontium-magnesium exchange showed only a partial loss in crystallinity as compared to the other strontium exchange experiments. The presence of relatively

high signal to noise ratio justifies the maintenance of crystallinity for both Y-ZrP and α -ZrP products in the presence of magnesium ions. However, such results might also indicate a limited or selective nature of exchange within the α -ZrP type products. But also, it was observed that there was a minor peak present at $2\theta = 8.83^\circ$ which might be due to the formation of $\text{ZrHSr}_{0.5}(\text{PO}_4)_2 \cdot 3.6\text{H}_2\text{O}$ as explained previously, in consistent with the literature ^[1, 2]. Also the presence of a strong distinct peak at $2\theta = 26^\circ$ is observed for some of the samples which is believed to be associated with most of the exchanges occurring in the α -ZrP type products. Therefore further investigation of the exchanged products is required along with repetitive experiments to establish these results.

The XRD patterns for the caesium-magnesium exchanged Y-ZrP and α -ZrP products are shown in the Figure 5.9 below.

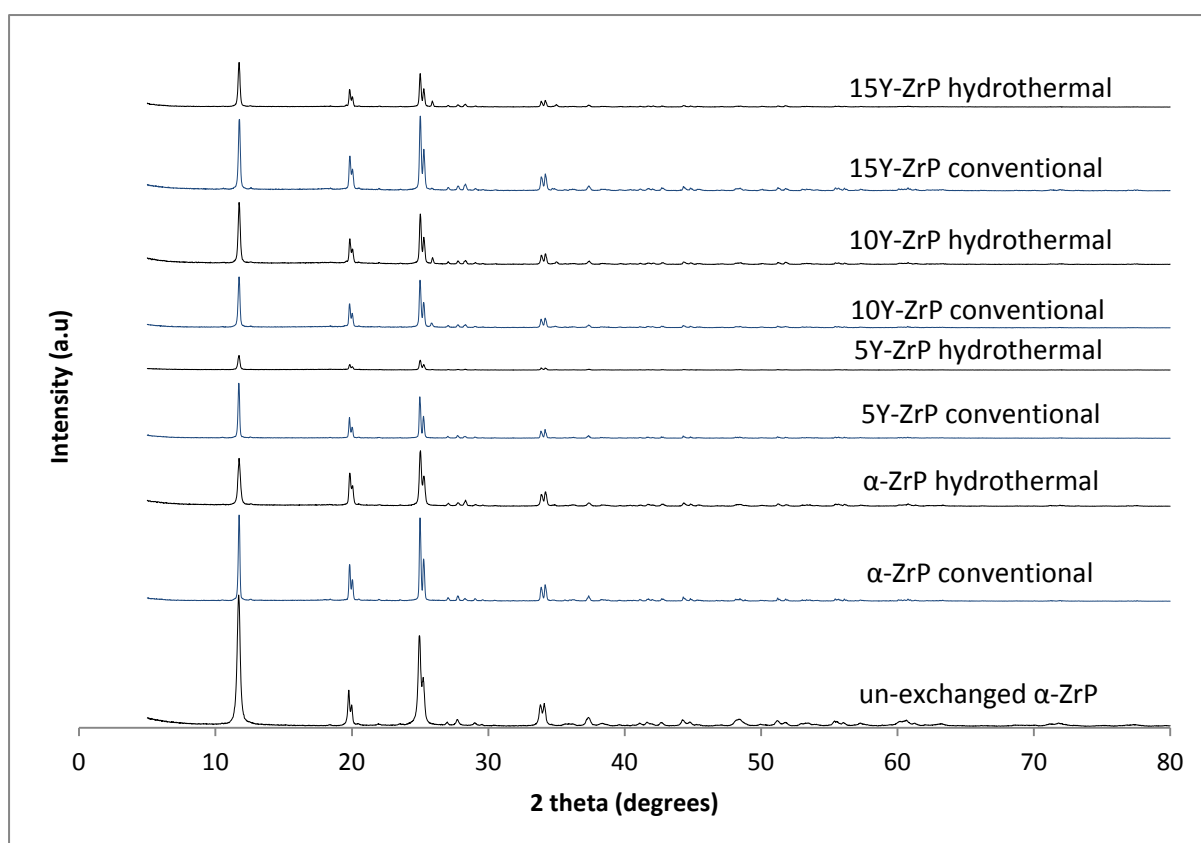


Figure 5. 9 XRD results for caesium-magnesium exchange

It can be seen from the above results for Y-ZrP and α -ZrP products from caesium-magnesium exchange that the degree of crystallinity is only partially reduced as compared to the pristine α -ZrP. This suggests that the structural breakdown was reduced in the presence of Mg^{2+} ions as compared to other single and competitive

exchanges that showed a high decline in the signal to noise ratio. Also, such a result can indicate a limited exchange of both Cs^+ and Mg^{2+} ions within the layers as compared to other exchange experiments. However two distinct low intensity peaks were observed at $2\theta = 26^\circ$ and 28.3° of which the former is not matched to any specific known crystal structure and is seen to be present in most exchanges occurring in the α -ZrP type structures. But the peak at $2\theta = 28.3^\circ$ is matched with the online PDF crystal database (as shown in figure 3 of appendix 4) to Cs_3PO_4 (caesium phosphate) therefore it suggests a possible exchange of Cs^+ ions for protons from interlayer phosphate units.

The XRD patterns for the Y-ZrP and α -ZrP samples for cobalt-magnesium exchange are shown in the Figure 5.10 below.

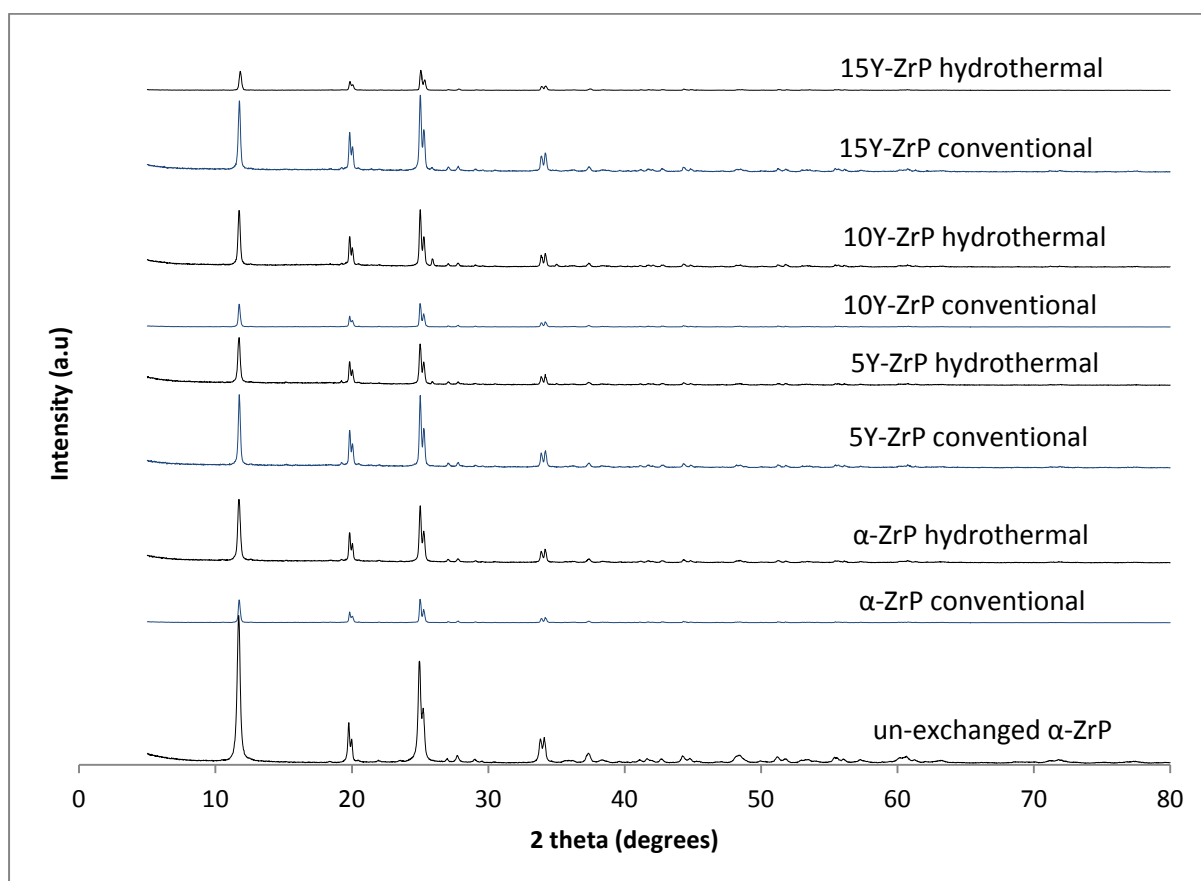


Figure 5. 10 XRD results for cobalt-magnesium exchange

The results shown above for cobalt-magnesium exchanged Y-ZrP and α -ZrP products indicate a crystalline structure of the products in regards to the un-exchanged α -ZrP. These products show a higher degree of crystallinity as compared to the single and competitive exchanges of cobalt. However such a result can

indicate either a limited or selective nature of exchange but can also be related to the stability of the products and minimum structural damage due to favourable pH of the exchange solution. The presence of relatively higher signal to noise ratio also distinctly resolved few minor peaks that were observed at $2\theta = 15^\circ, 19^\circ, 20.2^\circ, 23^\circ$ and 26° . These peaks were matched to either dicobalt magnesium bis-phosphate ($\text{MgCo}_2[\text{PO}_4]_2$) or magnesium phosphate (MgP_2O_6) using the online PDF crystal database as shown in the figure 4 of appendix 4. This indicates either the site selective exchange of Mg^{2+} and Co^{2+} ions or possible precipitation of cationic phosphates due to partial breakdown of the structure. Therefore, further investigation of these products and repetitive experiments are required to confirm these results and further characterise the exchanged products to study the site and mechanism of exchange from the competitive solution.

5.7.2 EDX/SEM results for competitive exchange with magnesium

The elemental analysis using the handheld XRF was not suitable to analyse magnesium exchanged products as the K lines for elements lighter than Al ($Z=13$) are too low to be detected. Therefore as an alternative EDX/SEM was used to provide a semi-quantitative result for the exchanged products in terms of composition and a further analysis of filtrate solution using ICP-MS was carried out later to support these results. A summary of the EDX/SEM results for the cobalt-magnesium exchanged products is provided in the Table 5.25.

Table 5. 25 EDX/SEM results for competitive exchange with magnesium

Sample	EDX/SEM elemental composition					
	Sr-Mg exchange		Cs-Mg exchange		Co-Mg exchange	
	Sr At%	Mg At%	Cs At%	Mg At%	Co At%	Mg At%
α -ZrP conventional	5.29(2)	0.60(2)	0.45(3)	0.71(3)	1.01(4)	0.93(2)
α -ZrP hydrothermal	4.96(1)	0.83(3)	0.59(2)	1.32(2)	1.07(3)	0.83(4)
5Y-ZrP conventional	6.66(3)	0.78(2)	0.77(4)	0.72(1)	1.43(2)	1.04(2)
5Y-ZrP hydrothermal	6.74(3)	0.95(1)	0.70(2)	0.57(3)	1.07(1)	1.01(2)
10Y-ZrP conventional	5.74(2)	0.92(4)	0.51(1)	1.04(2)	0.30(3)	0.66(1)
10Y-ZrP hydrothermal	5.88(2)	0.94(5)	0.33(1)	1.61(3)	0.91(2)	0.73(1)
15Y-ZrP conventional	5.82(4)	1.50(2)	0.46(2)	1.64(1)	1.64(1)	1.09(3)
15Y-ZrP hydrothermal	5.76(2)	1.23(1)	0.53(3)	0.43(1)	0.76(4)	0.80(2)

It can be seen from the above results for strontium-magnesium exchange that the extent of Sr^{2+} and Mg^{2+} ion exchange is slightly higher for Y-ZrP products as compared to that of α -ZrP. However no clear trend of exchange could be identified as compared to that yttrium concentration of the parent Y-ZrP samples but the 5% Y-ZrP samples showed the highest Sr^{2+} ion uptake among the other products.

Also, the EDX/SEM results for caesium-magnesium exchange showed that there is a non-uniform trend of exchange for both Cs^+ and Mg^{2+} ions in the Y-ZrP and α -ZrP samples, however 5% Y-ZrP samples showed the highest Cs^+ uptake and 10% and 15% Y-ZrP samples showed the highest Mg^{2+} uptake. Therefore, further characterisation using ICP-MS is needed to confidently determine the extent of exchange for both the cations since EDX/SEM is a semi-quantitative technique and no prior calibration was carried out for the ions of interest hence these results can be associated with significant errors such as matrix effects and spot size related errors.

In addition, the EDX/SEM results for cobalt-magnesium showed slightly mixed results for Co^{2+} and Mg^{2+} ion uptake for Y-ZrP and α -ZrP samples since some of the samples such as the 10% Y-ZrP hydrothermally synthesised sample showed almost similar or reduced extent of exchange for both the cations. However, 5% Y-ZrP and 15% Y-ZrP refluxed conventionally showed the highest amount of exchange for both the cations as compared to the rest of the samples although further investigation is needed in terms of ICP-MS analysis of the filtrate solution to confidently determine the extent of exchange for all the samples.

But overall, it was observed from EDX/SEM results that the highest amount of Mg^{2+} ion uptake was achieved for caesium-magnesium exchange followed by strontium-magnesium and cobalt-magnesium exchange. This indicates that the corresponding cations (Sr^{2+} , Cs^+ and Co^{2+}) from all the three exchanges followed a similar trend as that of Mg^{2+} ion uptake. The order of selectivity is $\text{Sr}^{2+} > \text{Co}^{2+} > \text{Mg}^{2+} > \text{Cs}^+$ but further characterisation of samples is needed to provide a firm conclusion about the nature and extent of exchanges occurring from such competitive solutions.

5.7.3 pH analysis of competitive exchange with magnesium

The pH results for the filtrate solutions separated from the Y-ZrP and α -ZrP products were obtained for all the three competitive exchanges and a summary is presented in the Table 5.26 below.

Table 5. 26 Summary of pH results for competitive exchange with magnesium

Samples	Sr-Mg exchange	Cs-Mg exchange	Co-Mg exchange
	Stock pH = 5.80	Stock pH = 6.45	Stock pH = 4.55
α -ZrP conventional	2.35	3.8	2.92
α -ZrP hydrothermal	2.72	3.5	3.15
5Y-ZrP conventional	2.50	3.45	3.45
5Y-ZrP hydrothermal	2.05	2.35	2.25
10Y-ZrP conventional	2.42	3.60	2.50
10Y-ZrP hydrothermal	2.65	2.95	2.75
15Y-ZrP conventional	2.65	3.45	4.10
15Y-ZrP hydrothermal	2.60	3.05	2.00

It can be seen from the above pH analysis that the decline in pH occurred for all the three competitive exchanges with magnesium, however the highest decrease in pH is observed for strontium-magnesium exchanged products that showed a nearly 50% decrease upon exchange. This suggests that both Y-ZrP and α -ZrP samples exchanged more protons for the cations from the strontium-magnesium competitive exchange solution indicating a higher capacity of exchange for both Sr^{2+} and Mg^{2+} ions. This is followed by caesium-magnesium and cobalt-magnesium exchange that showed a nearly similar extent of decline in the pH values after the exchange. These results are consistent with EDX/SEM results. However information regarding the selectivity and extent of exchange cannot be concluded from the pH measurements alone, therefore further analysis of the filtrate solution was carried out using the ICP-MS and the results are discussed in the following section.

The FT-IR spectra of the exchanged Y-ZrP and α -ZrP products for all the three competitive exchanges with magnesium were analysed in order to observe any

chemical changes that occur due to the exchange. The results can highlight the different chemical bonds that may be altered or formed due to the incoming cations.

The FT-IR spectra for strontium-magnesium exchange are shown in the figure 8 of Appendix 5 along with a summary of the peaks for an ideal strontium-magnesium exchanged product shown in the table 8. It can be seen from the results that FT-IR spectra for Y-ZrP and α -ZrP products resemble closely to that of pristine α -ZrP. However, subtle changes in peak intensities were observed in the range of 950-1050 cm^{-1} and 3000-3500 cm^{-1} that explains the variation in the P-O and O-H vibrations of the exchanged samples. Also, two extra minor peaks were observed at ca. 853 cm^{-1} and 1373 cm^{-1} which remains unidentified in the literature but is believed to be associated with Sr-O-P type bonding since it appears in all strontium exchange experiments. Therefore, it is concluded that a successful exchange of cations did occur from the competitive exchange solutions but further investigation of the products is required to understand the mechanism and extent of exchange.

The FT-IR spectrums for the caesium-magnesium exchanged Y-ZrP and α -ZrP products are shown in the figure 9 of Appendix 5 along with a summary of the peaks from an ideal caesium-magnesium exchanged product shown in table 9. It can be observed from the results that both Y-ZrP and α -ZrP exchanged products show a similar FT-IR spectrums to that of pristine α -ZrP. No distinctive changes were observed in terms of peak positions and types of peaks, however subtle changes can be seen in the peak intensities of the exchanged products especially for the P-O and O-H vibrational peaks observed in the range of 950-1050 cm^{-1} and 3000-3500 cm^{-1} .

The FT-IR spectrums for cobalt-magnesium exchanged Y-ZrP and α -ZrP products are shown in the figure 10 of Appendix 5 along with a summary of an ideal cobalt-magnesium exchanged product is provided in the table 10. It can be seen from the results for cobalt-magnesium exchange that both Y-ZrP and α -ZrP products had a similar FT-IR spectrum as that of pristine α -ZrP. However there are few subtle changes in the intensities of peaks at 950-1050 cm^{-1} and 3000-3500 cm^{-1} that explains the variations in the P-O and O-H vibrations due to incoming cations within the structure. Also, two minor peaks were distinctly seen at ca. 820 cm^{-1} and 1383 cm^{-1} similar to that of strontium-magnesium exchange as these were not identified in

literature but is believed to be associated with the successful exchanges occurring within the α -ZrP type structures.

5.7.4 ICP-MS analysis of the competitive exchange with magnesium

The filtrate solutions from all the three competitive exchanges after separating the Y-ZrP and α -ZrP samples were analysed using the ICP-MS for determining the extent and selectivity of the exchanged cations.

A summary of results from strontium-magnesium exchange is shown in the Table 5.27 below and it indicate that the Y-ZrP exchanged higher Sr^{2+} and Mg^{2+} as compared to the α -ZrP.

Table 5. 27 Summary of ICP-MS results for strontium-magnesium exchange

Samples	X = Amount of ions remaining (ppm)		% of ions incorporation $\frac{M_{ppm} - X_{ppm}}{M_{ppm} \text{ of } 0.1M} \times 100$	
	$X_1 = \text{Sr}^{2+}$	$X_2 = \text{Mg}^{2+}$	$M_1 = \text{Sr}^{2+}$ (8800 ppm)	$M_2 = \text{Mg}^{2+}$ (2430.5 ppm)
α -ZrP conventional	6762(3)	1904(2)	23.159	21.662
α -ZrP hydrothermal	6965(4)	2195(3)	20.852	9.689
5Y-ZrP conventional	6680(2)	1900(4)	24.090	21.826
5Y-ZrP hydrothermal	5674(3)	1757(2)	35.522	27.710
10Y-ZrP conventional	5914(3)	1860(3)	32.795	23.472
10Y-ZrP hydrothermal	7015(4)	2166(5)	20.284	10.882
15Y-ZrP conventional	6580(2)	2026(2)	25.227	16.642
15Y-ZrP hydrothermal	5837(4)	1803(3)	33.670	25.817

It is seen from the above ICP-MS results that both Y-ZrP and α -ZrP samples exchanged Sr^{2+} and Mg^{2+} ions from the competitive solution. The synthesised Y-ZrP showed an increased extent of exchange for both the cations as compared with the α -ZrP samples, especially the 5%Y-ZrP synthesised by both routes showing the highest amount of Sr^{2+} and Mg^{2+} ion exchange. Also, the uptake of Sr^{2+} is similar to that of the Sr-Ca exchange experiment shown in Table 5.19 above. However, significant deviation is observed as compared with the EDX/SEM results shown

above which is explained due to semi-quantitative nature of the technique and also the EDX/SEM was not calibrated specifically for the ions of interest. Therefore, the ICP-MS is deemed reliable in this case as it provides a higher degree of accuracy for quantification of exchanged ions.

Also, it is of interest to analyse the amount of framework ions that are leached into the solution due to structure breakdown. A summary of the results is provided in the table 5.28.

Table 5. 28 Summary of leached ions for strontium-magnesium exchange

Samples	Concentration of ions	
	Y ³⁺ (ppm)	Zr ⁴⁺ (ppm)
α-ZrP conventional	-	1.530(3)
α-ZrP hydrothermal	-	2.297(4)
5Y-ZrP conventional	0.542(3)	0.400(2)
5Y-ZrP hydrothermal	0.268(2)	0.470(1)
10Y-ZrP conventional	0.827(1)	0.650(2)
10Y-ZrP hydrothermal	1.313(2)	0.137(1)
15Y-ZrP conventional	0.333(4)	0.091(1)
15Y-ZrP hydrothermal	0.344(2)	0.292(3)

It is seen from the above results that both Y-ZrP and α-ZrP samples showed low amount of leached framework ions into the solution. This shows that the damage to the lattice structure due to extent of ion-exchange is less as compared to other competitive exchanges and therefore low degree of structure breakdown occurred. However, 10% Y-ZrP synthesised hydrothermally showed a slightly higher Y³⁺ ion leaching that indicates a higher degree of structural damage which in turn is observed from the XRD pattern shown that shows a decrease in crystallinity. These results are also consistent with the pH results as low amount of Y³⁺ and Zr⁴⁺ ions are leached that does not increase the acidity of the filtrate solutions. Hence it confirms that Y-ZrP samples showed a good exchange capacity for both strontium and magnesium ions with lower degree of structural damage.

A summary of the ICP-MS results for caesium-magnesium exchange is shown in the Table 5.29 below.

Table 5. 29 Summary of ICP-MS results for caesium-magnesium exchange

Samples	X = Amount of ions remaining (ppm)		% of ions incorporation $\frac{M_{ppm} - X_{ppm}}{M_{ppm} \text{ of } 0.1M} \times 100$	
	X ₁ = Cs ⁺	X ₂ = Mg ²⁺	M ₁ = Cs ⁺ (13290.55 ppm)	M ₂ = Mg ²⁺ (2430.5 ppm)
α-ZrP conventional	9460(5)	1775(3)	28.821	26.969
α-ZrP hydrothermal	10840(2)	2131(2)	18.438	12.322
5Y-ZrP conventional	11170(4)	2104(3)	15.955	13.433
5Y-ZrP hydrothermal	8215(3)	1564(2)	38.189	35.651
10Y-ZrP conventional	9735(2)	1971(4)	26.752	18.905
10Y-ZrP hydrothermal	9245(4)	1841(3)	30.439	24.254
15Y-ZrP conventional	8497(2)	1661(3)	36.067	31.660
15Y-ZrP hydrothermal	9148(3)	1739(4)	31.169	28.450

The results shown above for caesium-magnesium exchange indicates that both Y-ZrP and α-ZrP samples exchanged Cs⁺ and Mg²⁺ ions from the competitive solution. The extent of exchange for both the cations was slightly higher for Y-ZrP samples as compared to the α-ZrP samples, especially the 5% Y-ZrP sample synthesised hydrothermally that showed the highest exchange. However, no clear trend was observed for Cs⁺ and Mg²⁺ exchange with respect to the yttrium concentration of the Y-ZrP but overall it was seen that the magnesium ion uptake was increased in the presence of Cs⁺ ions as compared to that of Sr²⁺ ions. Also slight deviations were observed from EDX/SEM results presented above which is again attributed to semi-quantitative nature of the technique and lack of proper calibration for the ions of interest. Therefore, ICP-MS results are considered more accurate and reliable for quantifying the extent and nature of exchange occurring in the samples.

In addition, it is required to analyse the filtrate for the amount of leached framework ions into the solution, therefore a summary of the findings is provided in the table 5.30.

Table 5. 30 Summary of leached ions for caesium-magnesium exchange

Samples	Concentration of ions	
	Y ³⁺ (ppm)	Zr ⁴⁺ (ppm)
α-ZrP conventional	-	2.083(4)
α-ZrP hydrothermal	-	1.073(2)
5Y-ZrP conventional	0.358(2)	0.040(1)
5Y-ZrP hydrothermal	0.947(3)	0.822(2)
10Y-ZrP conventional	0.358(2)	0.594(3)
10Y-ZrP hydrothermal	0.249(3)	0.146(3)
15Y-ZrP conventional	0.380(4)	0.270(2)
15Y-ZrP hydrothermal	0.078(1)	0.261(1)

It is seen from the table above that both Y-ZrP and α-ZrP samples showed low amounts of leaching for the framework ions in the filtrate solutions, however 5% Y-ZrP sample synthesised hydrothermally showed a relatively higher amount of Y³⁺ and Zr⁴⁺ ions. This result complement the XRD analysis shown previously that clearly indicates a reduced crystallinity of the same sample as compared to the other Y-ZrP and α-ZrP samples which is evident from the lower intensity characteristic peak pattern. Therefore these results indicates that the caesium-magnesium exchanged products showed a lower degree of structural breakdown as compared with other caesium exchanges except for 5% Y-ZrP sample synthesised hydrothermally that showed a higher leaching of framework ions and hence suggested a higher degree of structural damage upon ion exchange.

A summary of the cobalt-magnesium exchange for Y-ZrP and α-ZrP samples is provided in the Table 5.31 below.

Table 5. 31 Summary of ICP-MS results for cobalt-magnesium exchange

Samples	X = Amount of ions remaining (ppm)		% of ions incorporation $\frac{M_{ppm} - X_{ppm}}{M_{ppm} \text{ of } 0.1M} \times 100$	
	X ₁ = Co ²⁺	X ₂ = Mg ²⁺	M ₁ = Co ²⁺ (5893.32 ppm)	M ₂ = Mg ²⁺ (2430.5 ppm)
α-ZrP conventional	5530(2)	2112(3)	6.164	13.104
α-ZrP hydrothermal	5490(1)	2144(2)	6.843	11.787
5Y-ZrP conventional	5230(3)	2093(4)	11.255	13.886
5Y-ZrP hydrothermal	5210(2)	2020(1)	11.594	16.889
10Y-ZrP conventional	5530(3)	2163(3)	6.164	11.005
10Y-ZrP hydrothermal	5500(4)	2104(2)	6.673	13.433
15Y-ZrP conventional	5540(2)	2194(1)	5.995	9.730
15Y-ZrP hydrothermal	5450(2)	2184(4)	7.522	10.141

It is observed from the above results for cobalt-magnesium exchange that extent of Co²⁺ exchange is reduced for both Y-ZrP and α-ZrP samples as compared to that of other cobalt exchange experiments. Also, the extent of Mg²⁺ ion was observed to be the lowest as compared to strontium-magnesium and caesium-magnesium exchange. The reason for this is attributed to the competitive inhibition of exchange due to the presence of similar ion exchange selectivity of both Co²⁺ and Mg²⁺ ions. However, since Mg²⁺ ions (ionic radius = 0.72 Å) are slightly smaller in size to Co²⁺ ions (ionic radius = 0.74 Å) therefore they might be preferred for exchange. Also, it was seen that the extent of Co²⁺ and Mg²⁺ ion exchange was more or less uniform for both Y-ZrP and α-ZrP samples for both routes of reflux, except for the 5% Y-ZrP samples that showed a slightly higher capacity of exchange, however a slight deviation of these results is noticed as compared to the EDX/SEM findings as seen in other competitive exchanges.

In addition, it is also required to analyse the filtrate solutions for the amount of leached framework ions as a consequence of structural damage, therefore a summary of leached amount of ions is provided in the table 5.32.

Table 5. 32 Summary of leached ions for cobalt-magnesium exchange

Samples	Concentration of ions	
	Y ³⁺ (ppm)	Zr ⁴⁺ (ppm)
α-ZrP conventional	-	6.020(3)
α-ZrP hydrothermal	-	2.133(2)
5Y-ZrP conventional	0.288(2)	0.190(1)
5Y-ZrP hydrothermal	0.475(1)	0.110(1)
10Y-ZrP conventional	1.011(3)	4.630(4)
10Y-ZrP hydrothermal	0.877(4)	0.859(2)
15Y-ZrP conventional	0.947(3)	0.803(1)
15Y-ZrP hydrothermal	0.698(2)	2.823(4)

It is observed from the above results that the α-ZrP sample synthesised conventionally showed a higher amount of Zr⁴⁺ ion leaching as compared to hydrothermally synthesised sample. Also, the 10% Y-ZrP samples refluxed conventionally and 15% Y-ZrP samples refluxed hydrothermally showed a higher amount of leached framework which indicates a higher degree of structural breakdown as compared to the other samples. These results are consistent with the XRD findings that clearly demonstrate a lower intensity XRD pattern for these samples indicating a reduced crystallinity and a higher degree of structural damage occurring due to competitive exchange.

5.8. Competitive exchange with sodium

The final experiments involve exchange of Sr²⁺, Cs⁺, Co²⁺ together with sodium as an interfering ion from 0.1M nitrate salt solutions of each. The resulting products were characterised XRD, FT-IR, ICP-MS and EDX/SEM.

5.8.1 XRD analysis of competitive exchange with sodium

The XRD analysis was carried out for all samples and the obtained XRD patterns of all the exchanged products were compared with that of un-exchanged α-ZrP in order to observe any qualitative changes occurring in the structure of the products.

The XRD pattern of strontium-sodium exchanged products is provided in the Figure 5.11 below and shows that the exchanged samples maintained crystalline structure along with presence of few extra peaks.

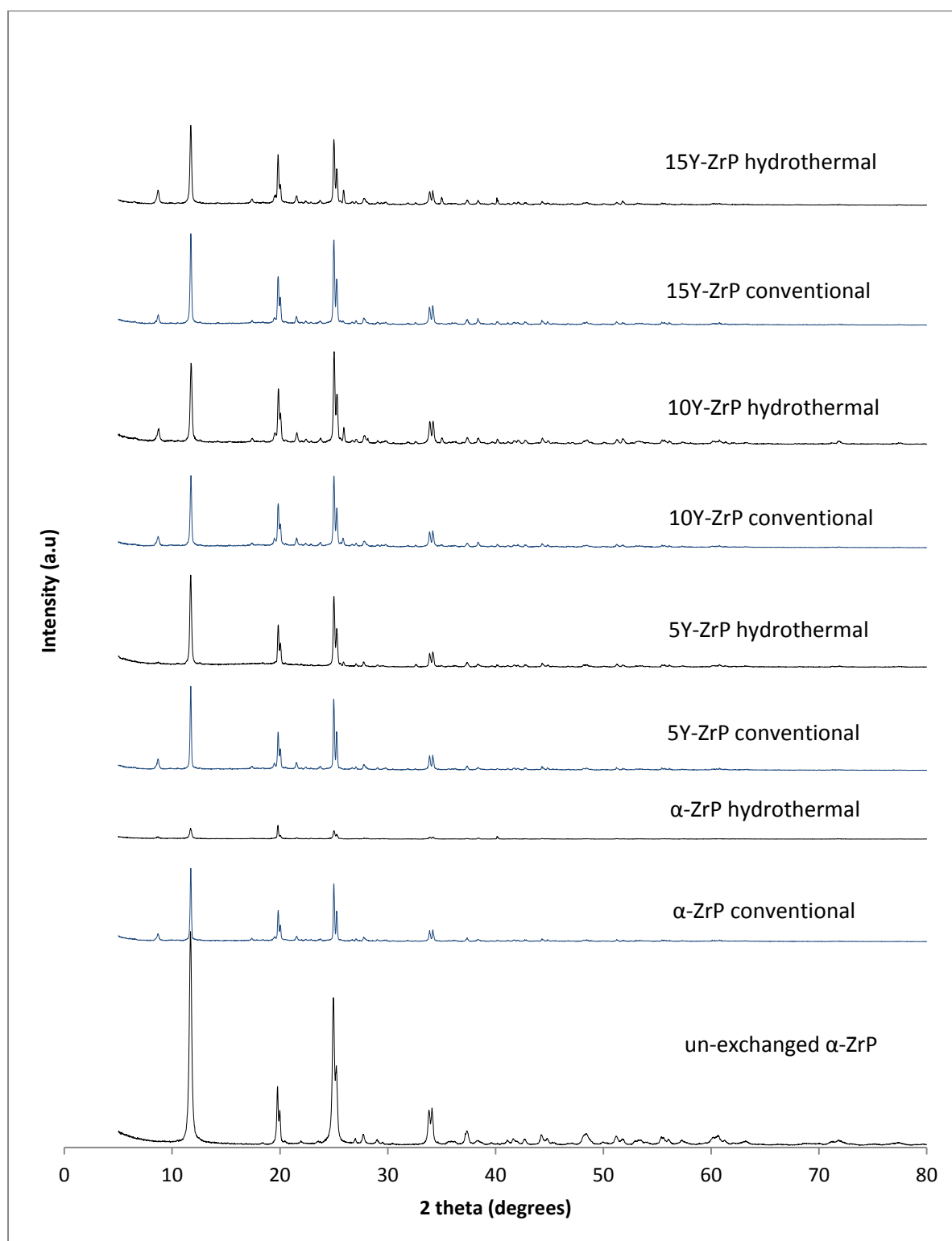


Figure 5. 11 XRD results for strontium-sodium exchange

It can be observed from the strontium-sodium exchanged results that both Y-ZrP and α -ZrP products showed a similar XRD pattern as compared to that of α -ZrP type structures. This indicates that a layered structure is maintained after the exchange but a decrease in peak intensities was observed that refers to slight decrease in crystallinity of all samples. However the α -ZrP samples of both routes of synthesis showed greater decrease in crystallinity as compared to the Y-ZrP products that showed a much higher degree of crystallinity for the exchanged products. These results are consistent with literature ^[9, 10] that indicates relatively amorphous products due to sodium exchange with α -ZrP. But the results for Y-ZrP indicates that Y-ZrP samples of both routes of synthesis were highly stable towards the strontium-sodium exchange as compared to that of α -ZrP samples that tend to undergo structural damage due to exchange. However, the extent of exchange might be considered as a factor for decreasing crystallinity of the products hence a further characterisation using EDX/SEM and ICP-MS was carried out to determine the exchange capacities of the products and the results are discussed in the following sections.

Also, it was seen from the above results that few extra peaks were observed at $2\theta = 8.75^\circ, 17.43^\circ, 21.55^\circ$ and 26° . These peaks were matched with sodium phosphate hydrate and strontium-zirconium phosphate using the online PDF crystal database, as shown in the figure 5 of appendix 4. The presence of sodium-zirconium phosphate indicates a successful exchange of both Sr^{2+} and Na^+ ions into the lattice structure for both Y-ZrP and α -ZrP products.

The XRD result for caesium-sodium exchanged products is shown in the Figure 5.12 below.

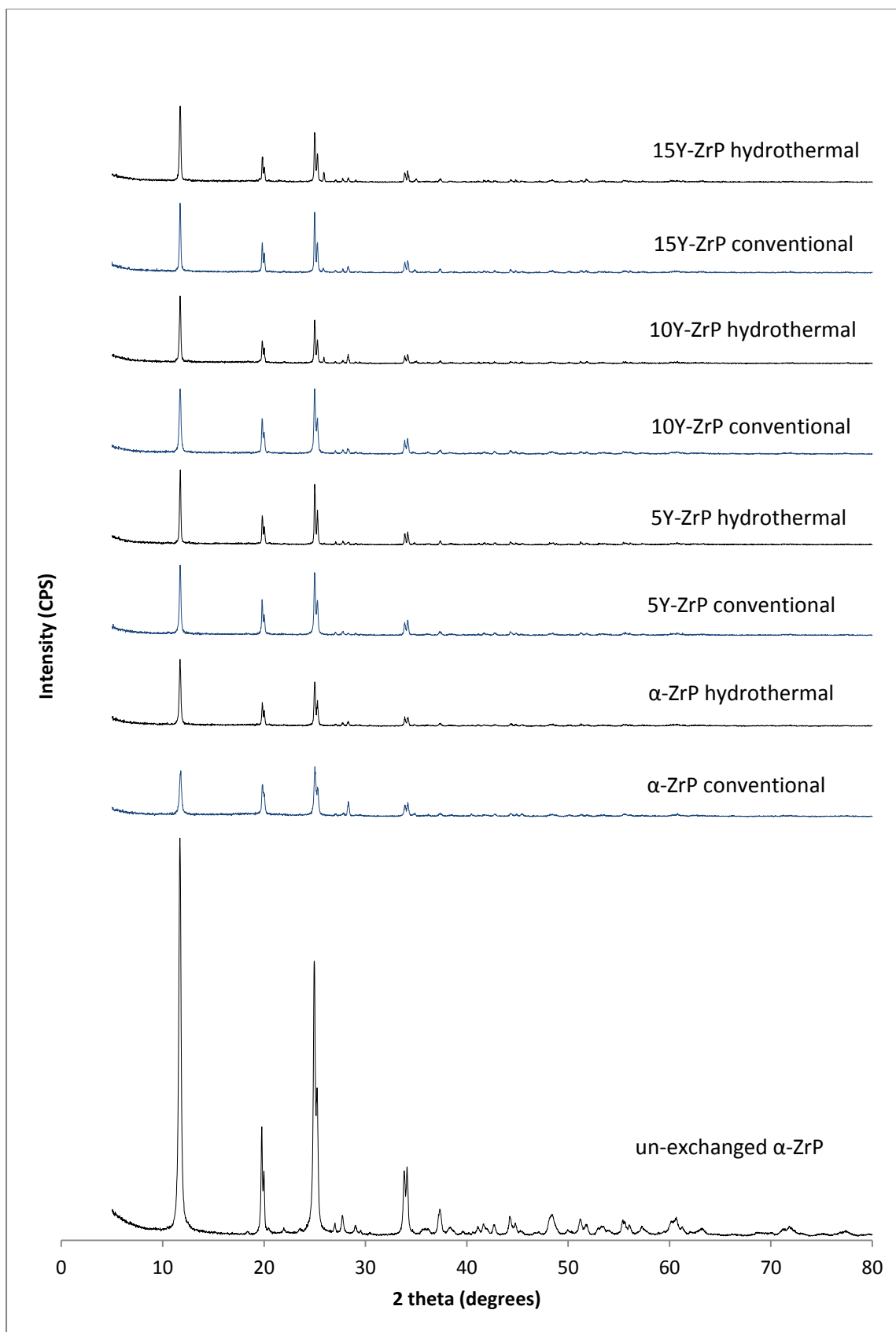


Figure 5. 12 XRD results of caesium-sodium exchange

It is seen from the above results that both Y-ZrP and α -ZrP exchanged products show a decrease in crystallinity which is evident from the decline in relative intensities of all the characteristic peaks as compared to that of pristine α -ZrP. However, there are no distinct extra peaks observed in the XRD patterns of both Y-ZrP and α -ZrP samples due to low peak to signal ratio of the peaks and also no potential match was found from the online PDF crystal database search. This indicates a very limited extent of exchange for cations (Cs^+ and Na^+) for both Y-ZrP and α -ZrP samples and also the reduced crystallinity is representative of a partial structural damage as seen previously for the Cs^+ ion exchange. Therefore further characterisation of the exchanged products was done to confirm these results as discussed in the following sections.

The XRD result for the cobalt-sodium exchanged products is shown in the Figure 5.13 below.

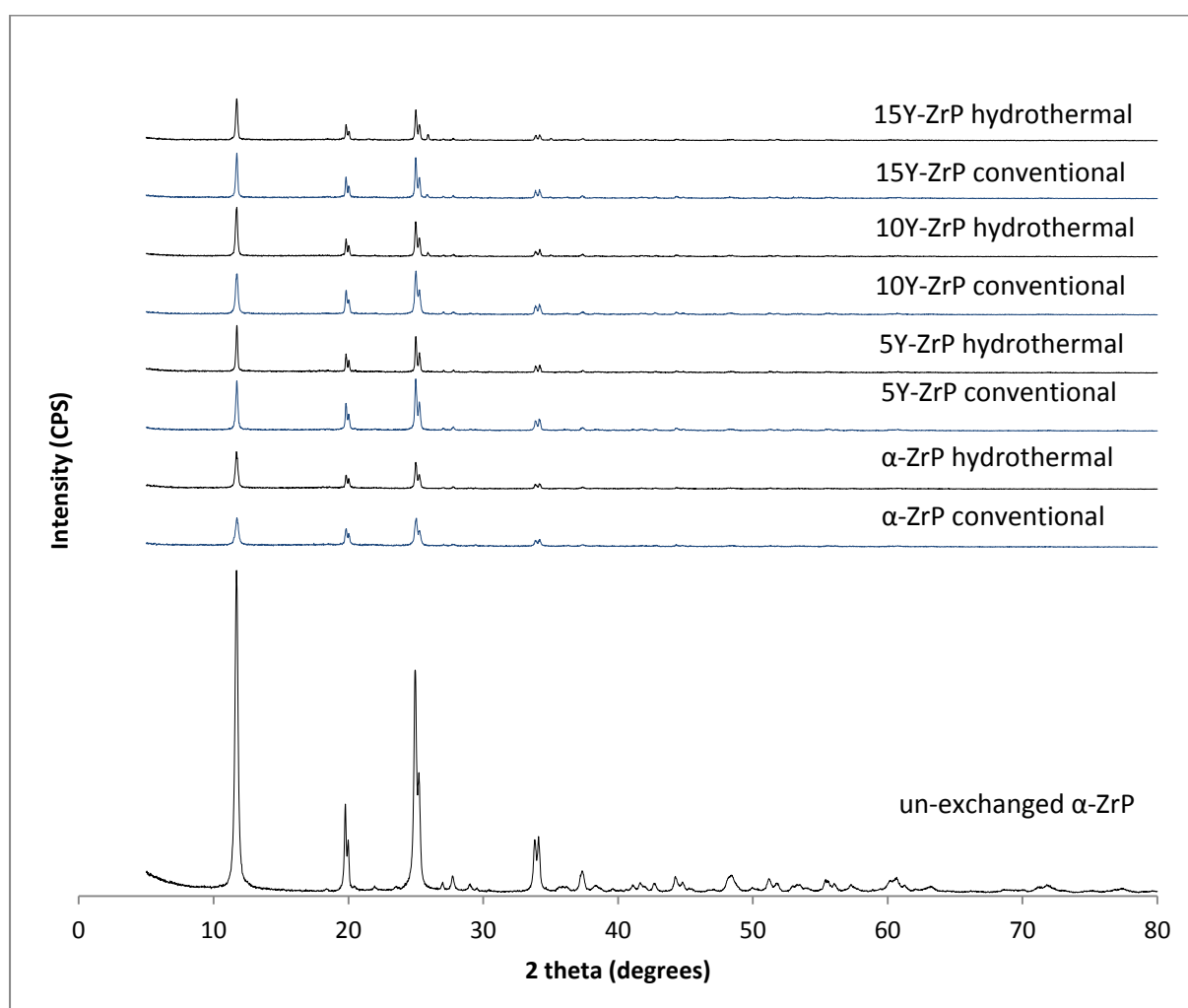


Figure 5. 13 XRD results for cobalt-sodium exchange

The results shown above for cobalt-sodium exchanged Y-ZrP and α -ZrP samples indicate a decrease in crystallinity of the products as evident from the reduced intensities of the characteristic peaks as compared to the pristine α -ZrP. However, no extra peaks were observed and the patterns did not lead to a confident match using the online PDF crystal database. Therefore, further investigation of the exchanged products was done in order to study the extent of exchange and the possibility of structure breakdown that resulted in the decline of crystallinity for the products.

5.8.2 EDX/SEM analysis of the competitive exchange with sodium

The competitive exchanged products of Y-ZrP and α -ZrP samples were analysed by EDX/SEM to provide information on the elemental composition of the products. A summary of the EDX/SEM results for strontium-sodium, caesium-sodium and cobalt-sodium exchanged products is shown in the Table 5.33 below.

Table 5. 33 EDX/SEM results for competitive exchange with sodium

Sample	EDX/SEM elemental composition					
	Sr-Na exchange		Cs-Na exchange		Co-Na exchange	
	Sr At%	Na At%	Cs At%	Na At%	Co At%	Na At%
α -ZrP conventional	2.91(3)	1.37(4)	0.96(1)	0.53(3)	1.47(4)	1.98(1)
α -ZrP hydrothermal	2.84(4)	2.51(3)	0.93(4)	0.58(2)	1.34(2)	1.87(2)
5Y-ZrP conventional	1.62(2)	1.79(2)	1.03(1)	0.65(4)	1.13(4)	1.97(3)
5Y-ZrP hydrothermal	1.23(4)	2.07(3)	0.87(3)	0.34(3)	1.85(3)	2.45(4)
10Y-ZrP conventional	2.62(2)	1.94(2)	0.90(1)	0.43(4)	1.54(3)	2.07(2)
10Y-ZrP hydrothermal	2.87(3)	2.63(1)	1.13(3)	0.66(3)	1.34(2)	1.87(4)
15Y-ZrP conventional	1.56(3)	1.42(4)	1.21(4)	0.65(2)	1.08(1)	1.98(2)
15Y-ZrP hydrothermal	1.63(2)	3.08(2)	0.95(2)	0.45(2)	1.48(1)	1.93(4)

It is seen from the above results that strontium-sodium exchange showed the highest amount of Na^+ ions exchanged followed by cobalt-sodium exchange and then caesium-sodium exchange that showed the least capacity among all the three competitive exchanges. This is explained by the fact that the hydrated ionic radii (4.12 Å) and the ionic radius of Sr^{2+} (1.18 Å) is more than the hydrated ionic radii

(3.58 Å) and the ionic radius (1.02 Å) of Na⁺ ion. Also, the cationic replacement ability of Sr²⁺ is also slightly lower than that of Na⁺ ions therefore the sodium exchange will be preferred compared to the strontium exchange. Similar result is expected for the cobalt-sodium exchange too since the hydrated ionic radius of Co²⁺ is 4.23 Å is higher compared to Na⁺ ion with hydrated ionic radius of 3.58 Å. However, Cs⁺ has higher cationic replacement ability compared to that of Na⁺ but since the ionic radius of Cs⁺ ions (1.67 Å) is greater than Na⁺ ions (1.02 Å), there appears to be a competitive inhibition occurring between the two ions that lead to an overall low extent of exchange for both the ions. But overall it was seen that the extent of Sr²⁺ ions exchange is higher as compared to the Co²⁺ and Cs⁺ ions that indicates that strontium ions are preferred for exchange in the presence of sodium ions. The reason for this is accounted to the higher cationic replacement capacity of strontium as compared to that of cobalt and that the large radii Cs⁺ ions cannot be easily exchange within the layers, so it can only occupy the larger cavities by displacing water molecules from it.

5.8.3 pH analysis of competitive exchange with sodium

The filtrate solutions from the exchanged Y-ZrP and α-ZrP samples were analysed for the change in the pH before and after the exchange. A summary of the results is provided in the Table 5.34 below.

Table 5. 34 Summary of pH results for competitive exchange with sodium

Samples	Sr-Na exchange Stock pH = 6.73	Cs-Na exchange Stock pH = 5.42	Co-Na exchange Stock pH = 7.63
α-ZrP conventional	2.30	3.15	2.66
α-ZrP hydrothermal	2.10	3.33	2.75
5Y-ZrP conventional	2.40	2.70	2.41
5Y-ZrP hydrothermal	2.30	2.13	2.30
10Y-ZrP conventional	2.65	2.46	2.26
10Y-ZrP hydrothermal	1.95	2.18	1.93
15Y-ZrP conventional	2.45	3.53	2.73
15Y-ZrP hydrothermal	1.87	2.21	1.99

It is seen from the above results that there is a decrease in pH for the filtrate solutions after the exchange, indicating a successful exchange of cations for the framework protons. The highest decline in pH is seen for cobalt-sodium exchange that shows a nearly 60% drop in pH followed by strontium-sodium exchange and then the caesium-sodium exchange that showed the lowest decrease in the pH among all the three exchanges. This indicates that the extent of exchange of cations is the highest for cobalt-sodium exchange followed by strontium-sodium and the least for caesium-sodium exchange. These results are similar to SEM/EDX results except that the strontium-sodium exchange was found to show the highest extent of exchange from the SEM/EDX results. Since no clear conclusion can be drawn about the selectivity and individual extents of exchange for the cations from the SEM/EDX and pH results, therefore further analysis of these filtrate solutions was carried out by using ICP-MS.

The Y-ZrP and α -ZrP products from strontium-sodium, caesium-sodium and cobalt-sodium exchange are analysed by FT-IR in order to understand any changes in the chemical environment due to the exchange.

The FT-IR spectrums for the exchanged products from strontium-sodium exchange are shown in the figure 11 of Appendix 5 along with a summary of the peaks representing the type of chemical bonds for an ideal strontium-sodium exchange shown in table 11. The results for Y-ZrP and α -ZrP products show similar FT-IR spectrums to that of pristine α -ZrP samples that indicates a similar chemical environment of all the products. However, slight differences were observed in the peak intensities and peak profiles showing a subtle shoulder to the peaks present in the range of 950-1050 cm^{-1} and 3000-3500 cm^{-1} . This indicates variations in the P-O and O-H vibrations due to incoming cations that replace the protons from the phosphate group. However, no distinct new peaks were observed for the strontium-sodium exchanged products except for a minor peak arising at ca. 1365 cm^{-1} which remains unidentified in literature but is observed to be associated with most of the strontium exchanges.

The FT-IR results for caesium-sodium exchanged Y-ZrP and α -ZrP products are shown in the figure 12 of Appendix 5 along with a summary of the characteristic peaks representing the type of bonding environment for an ideal caesium-sodium

exchanged product shown in table 12. The results for Y-ZrP and α -ZrP products show that the FT-IR spectrums of the exchanged products are similar to that of the pristine α -ZrP with slight changes to the peak intensities in the region of 950-1050 cm^{-1} and 3000-3500 cm^{-1} . This indicates a very limited exchange of cations into the parent samples that caused subtle variations in the P-O and O-H bonding vibrations, however no extra peaks or distinct changes in the spectrums were observed.

The FT-IR result for the Y-ZrP and α -ZrP samples from cobalt-sodium exchange is shown in the figure 13 of Appendix 5 along with a summary of the peaks corresponding to their chemical bonds for an ideal cobalt-sodium exchanged product shown in table 13. The results shown above for Y-ZrP and α -ZrP products from cobalt-sodium exchange exhibit similar FT-IR spectrums to that of pristine α -ZrP except for the emergence of two new minor peaks at 1978 cm^{-1} and 2029 cm^{-1} respectively. These peaks were not clearly identified in the literature but are believed to be associated with sodium exchange phases of α -ZrP. Therefore, further characterisation of these products is required to provide a clear insight about the changing chemical environment due to exchanged Co^{2+} and Na^+ ions in parent samples.

5.8.4 ICP-MS analysis of competitive exchange with sodium

The filtrate solutions from all the Y-ZrP and α -ZrP exchanged products from all three competitive exchanges were analysed to determine the extent of exchange of cations and their selectivity.

A summary of the results for strontium-sodium exchanged products is provided in the Table 5.35 below.

Table 5. 35 Summary of ICP-MS result for strontium-sodium exchange

Samples	X = Amount of ions remaining (ppm)		% of ions incorporation $\frac{M_{ppm} - X_{ppm}}{M_{ppm} \text{ of } 0.1M} \times 100$	
	X ₁ = Sr ²⁺	X ₂ = Na ⁺	M ₁ = Sr ²⁺ (8800 ppm)	M ₂ = Na ⁺ (2300 ppm)
α-ZrP conventional	5575(3)	1090(2)	36.647	52.608
α-ZrP hydrothermal	5237(5)	1034(4)	40.488	55.043
5Y-ZrP conventional	6863(3)	1477(5)	22.011	35.782
5Y-ZrP hydrothermal	6228(2)	1210(2)	29.227	47.391
10Y-ZrP conventional	5544(3)	1078(3)	37.000	53.130
10Y-ZrP hydrothermal	5332(2)	1073(2)	39.409	53.347
15Y-ZrP conventional	5806(2)	1379(3)	34.022	40.043
15Y-ZrP hydrothermal	6265(5)	1227(2)	28.806	46.652

It is seen from the above analysis that both Y-ZrP and α-ZrP samples exchanged high amounts of Sr²⁺ and Na⁺ ions from the competitive exchange solution. However, the extent of exchange is similar for α-ZrP samples of both routes of reflux as compared to Y-ZrP samples that showed relatively lower capacities for both the cations, especially the 5% Y-ZrP samples that showed the lowest exchange among all the samples. These ICP-MS results strongly support the XRD analysis that suggested a limited degree of exchange for Y-ZrP samples since they exhibited a higher degree of crystallinity as compared to the α-ZrP samples. However, it is interesting to note that Y-ZrP samples showed an approximately equal extent of exchange for both Sr²⁺ and Na⁺ ions but had a relatively higher crystallinity as compared to α-ZrP. Therefore it is of interest to analyse the degree of structural damage of both Y-ZrP and α-ZrP products by measuring the amount of leached framework ions to the solution.

A summary of the leached framework ions from filtrate solutions of all the products is provided in the Table 5.36.

Table 5. 36 Summary of leached ions for strontium-sodium exchange

Samples	Concentration of ions	
	Y ³⁺ (ppm)	Zr ⁴⁺ (ppm)
α-ZrP conventional reflux	-	57.880(3)
α-ZrP hydrothermal reflux	-	29.800(2)
5Y-ZrP conventional reflux	0.874(2)	2.585(2)
5Y-ZrP hydrothermal reflux	0.321(1)	0.192(1)
10Y-ZrP conventional reflux	1.202(3)	0.082(1)
10Y-ZrP hydrothermal reflux	1.254(2)	0.795(2)
15Y-ZrP conventional reflux	1.892(4)	1.389(2)
15Y-ZrP hydrothermal reflux	0.380(1)	1.434(4)

It is seen from the above results that α-ZrP samples showed a substantially high amount of Zr⁴⁺ ions in the filtrate solution for both synthesis methods. However, the amount of both Y³⁺ and Zr⁴⁺ ions from the filtrate solutions of Y-ZrP products were found to be much lower, indicating a very low amount of leaching of framework ions due to structural damage. Hence it can be concluded that these results complement the XRD analysis that suggested a lower degree of structural breakdown of Y-ZrP samples as compared to α-ZrP that are deemed to undergo heavy distortion in the presence of sodium exchange solutions^[9, 10]. Overall it was seen that Y-ZrP samples maintained a high extent of exchange for both Sr²⁺ and Na⁺ ions while still maintaining a high crystallinity of the products as opposed to the α-ZrP samples that exchange a similar amount of these ions while exhibiting a much lower structural stability.

A summary of the ICP-MS results for caesium-sodium exchange is provided in the Table 5.37 below.

Table 5. 37 Summary of ICP-MS result for caesium-sodium exchange

Samples	X = Amount of ions remaining (ppm)		% of ions incorporation $\frac{M_{ppm} - X_{ppm}}{M_{ppm} \text{ of } 0.1M} \times 100$	
	X ₁ = Cs ⁺	X ₂ = Na ⁺	M ₁ = Cs ⁺ (13290.55 ppm)	M ₂ = Na ⁺ (2300 ppm)
α-ZrP conventional	12100(3)	2070(2)	8.957	10.000
α-ZrP hydrothermal	12130(5)	1991(2)	8.732	13.434
5Y-ZrP conventional	12090(4)	1972(4)	9.033	14.260
5Y-ZrP hydrothermal	12000(3)	1999(3)	9.710	13.086
10Y-ZrP conventional	12200(4)	2104(2)	8.205	8.521
10Y-ZrP hydrothermal	11900(2)	2065(1)	10.462	10.217
15Y-ZrP conventional	12110(5)	1990(3)	8.882	13.478
15Y-ZrP hydrothermal	12010(2)	1983(2)	9.635	13.782

It is observed from the above analysis that both Y-ZrP and α-ZrP products show a very limited exchange for Cs⁺ ions in the presence of Na⁺ ions as compared to single exchange experiments. Also, the extent of exchange for Na⁺ ions is reduced as compared to the strontium-sodium exchange. These results suggest a competitive inhibition of exchange for both the monovalent cations consistent with the XRD results discussed before. This shows that the caesium-sodium exchange facilitate Na⁺ ions more than Cs⁺ ions due to a difference in the relative sizes that allows the Na⁺ ions to exchange within the interlayer spaces as opposed to the larger Cs⁺ ions that can only occupy the cavities. These results also compliment the EDX/SEM results. However it is of interest to analyse the possibility of structural damage for the exchange products as largely expected from ion exchanges involving caesium ions. Therefore a summary of the amount of leached framework ions for all the products is provided in the Table 5.38.

Table 5. 38 Summary of leached ions for caesium-sodium exchange

Samples	Concentration of ions	
	Y ³⁺ (ppm)	Zr ⁴⁺ (ppm)
α-ZrP conventional	-	5.987(4)
α-ZrP hydrothermal	-	4.876(3)
5Y-ZrP conventional	0.987(3)	1.876(3)
5Y-ZrP hydrothermal	1.345(2)	1.098(2)
10Y-ZrP conventional	1.324(5)	0.987(1)
10Y-ZrP hydrothermal	1.786(3)	1.955(4)
15Y-ZrP conventional	1.346(2)	1.098(2)
15Y-ZrP hydrothermal	0.655(1)	2.235(3)

The results shown above indicates a loss of significant amount of Zr⁴⁺ ions from the α-ZrP samples of both routes of synthesis, whereas the filtrate solutions from Y-ZrP products showed relatively higher amounts of Y³⁺ ions. These results indicate a significant amount of structural damage for both Y-ZrP and α-ZrP samples as observed from the XRD results discussed previously. Hence it can be concluded from all these results that caesium-sodium competitive exchange showed lower exchange capacities for both Y-ZrP and α-ZrP samples and the stability of the samples were severely affected under such condition.

A summary of the ICP-MS results for cobalt-sodium exchange is provided in the Table 5.39 below.

Table 5. 39 Summary of ICP-MS result for cobalt-sodium exchange

Samples	X = Amount of ions remaining (ppm)		% of ions incorporation $\frac{M_{ppm} - X_{ppm}}{M_{ppm} \text{ of } 0.1M} \times 100$	
	$X_1 = \text{Co}^{2+}$	$X_2 = \text{Na}^+$	$M_1 = \text{Co}^{2+}$ (5893.32 ppm)	$M_2 = \text{Na}^+$ (2300 ppm)
α -ZrP conventional	5134(3)	1393(4)	12.884	39.434
α -ZrP hydrothermal	5191(2)	1401(2)	11.917	39.086
5Y-ZrP conventional	5087(5)	1387(3)	13.682	39.695
5Y-ZrP hydrothermal	5065(2)	1376(2)	14.055	40.173
10Y-ZrP conventional	5199(3)	1399(1)	11.781	39.173
10Y-ZrP hydrothermal	5166(2)	1409(3)	12.341	38.739
15Y-ZrP conventional	5093(3)	1391(3)	13.580	39.521
15Y-ZrP hydrothermal	5072(4)	1363(2)	13.936	40.739

It is seen from the above results that both Y-ZrP and α -ZrP samples show good extent of exchange for both Co^{2+} and Na^+ ions. The synthesised samples followed a similar trend of exchange as that of single exchange experiment but the extent of exchange for Co^{2+} was increased slightly in the presence of Na^+ ions. Also, it was seen that the Na^+ exchange capacity was high similar to that of the strontium-sodium exchange that showed the highest capacity among all the three competitive exchanges. Also it was seen that the synthesised Y-ZrP samples showed a slightly higher extent of Co^{2+} ion exchange as compared to that of α -ZrP samples and similar results were found to be true for Na^+ ions as well. These results compliment the EDX/SEM results, suggesting that increased sodium and cobalt ion exchange was achieved from the competitive solution. However, it is of interest to analyse the possibility of structure breakdown for both Y-ZrP and α -ZrP samples, hence a further investigation for the amount of leached framework ions were done by ICP-MS and the results are summarised in the table 5.40.

Table 5. 40 Summary of leached ions for cobalt-sodium exchange

Samples	Concentration of ions	
	Y ³⁺ (ppm)	Zr ⁴⁺ (ppm)
α -ZrP conventional	-	6.097(4)
α -ZrP hydrothermal	-	5.987(2)
5Y-ZrP conventional	1.632(4)	1.098(2)
5Y-ZrP hydrothermal	1.646(3)	1.345(3)
10Y-ZrP conventional	0.875(2)	1.098(1)
10Y-ZrP hydrothermal	1.230(3)	2.098(3)
15Y-ZrP conventional	1.324(2)	0.987(1)
15Y-ZrP hydrothermal	0.908(1)	1.456(2)

The results shown in the above table indicates that α -ZrP samples had a significant amount of Zr⁴⁺ ion leaching, whereas the Y-ZrP samples showed a relatively higher Y³⁺ ion leaching for some of the samples. This explains the possibility of a partial structural damage as indicated by the XRD results discussed previously. Overall it can be concluded from all these results that both Y-ZrP and α -ZrP samples exchanged good amounts of cobalt and sodium ions from the competitive solution with a partial structural breakdown that is attributed to the reaction conditions such as pH and stirring effects.

5.9. Unit cell refinement of the ion-exchanged samples

It is of interest to analyse the various ion-exchanged samples to study the changes in the crystal system such as the unit cell dimensions by using a CELREF refinement software. However, due to time constraints only a pilot study is done for partial refinement of the lattice parameters for the 5% Y-ZrP synthesised hydrothermally since it showed the highest exchange capacity and affinity for ions of interest. The refinement was carried out using the refined lattice parameters of α -ZrP with $P2_1/c$ space group as provided by Burnell and Readman ^[12] and the results of the CELREF refinement is presented in the Table 5.41 below.

Table 5. 41 Refined lattice parameters of ion-exchanged 5% Y-ZrP hydrothermal

Ion exchange solution	a (Å)	b (Å)	c (Å)	α (°)	β (°)	γ (°)
α -ZrP ^[12]	9.0634(2)	5.2906(1)	16.24603(6)	90	111.40(2)	90
Sr(NO ₃) ₂	9.0558	5.293	16.2416	90	111.29	90
Sr(CH ₃ CO ₂) ₂	9.0249	5.2971	16.2681	90	111.39	90
Sr(OH) ₂	9.0641	5.2913	16.2757	90	111.46	90
CsNO ₃	9.0657	5.2872	16.2414	90	111.27	90
CsCH ₃ CO ₂	9.0478	5.2945	16.2347	90	111.36	90
CsOH	-	-	-	-	-	-
CoNO ₃	9.0564	5.2679	16.2437	90	111.35	90
Co(CH ₃ CO ₂) ₂	9.0447	5.2973	16.217	90	111.35	90
Co(OH) ₂	-	-	-	-	-	-
Sr-Cs	9.0595	5.2926	16.2366	90	111.48	90
Cs-Co	9.0441	5.2927	16.247	90	111.36	90
Sr-Co	9.0528	5.2942	16.2437	90	111.37	90
Sr-Cs-Co	9.0544	5.2879	16.2337	90	111.25	90
Sr-Ca	9.0581	5.293	16.2394	90	111.43	90
Sr-Mg	9.0619	5.2937	16.2395	90	111.39	90
Sr-Na	9.046	5.298	16.2422	90	111.47	90
Cs-Ca	9.0561	5.2924	16.2451	90	111.4	90
Cs-Mg	9.0525	5.2925	16.241	90	111.39	90

Cs-Na	9.0591	5.2897	16.2379	90	111.38	90
Co-Ca	9.0509	5.2954	16.2452	90	111.51	90
Co-Mg	9.0533	5.2911	16.2362	90	111.36	90
Co-Na	9.0554	5.2921	16.2338	90	111.39	90

These results highlight two important points with regards to the unit cell dimensions. Firstly, all of the ion-exchanged samples were indexed and refined according to monoclinic symmetry using refined lattice parameters of α -ZrP with $P2_1/c$ space group, therefore some of the peaks (especially those with $2\theta \leq 10^\circ$) were not included in the refinement by default, as shown in the refined peaks lists present in Table 1 to 20 of Appendix 6. Therefore, any changes in the crystal system or symmetry were not found and most of the ion-exchanged samples showed a satisfactory refined monoclinic unit cell, except for CsOH and $\text{Co}(\text{OH})_2$ since the powder x-ray diffraction pattern for CsOH was relatively amorphous and $\text{Co}(\text{OH})_2$ experiments were not performed as discussed previously. Secondly, some of the ion-exchanged samples showed a significant reduction in the *a*-axis dimension such as from $\text{Sr}(\text{CH}_3\text{CO}_2)_2$, $\text{Co}(\text{CH}_3\text{CO}_2)_2$ and Sr-Na exchanges. These results are consistent with XRD, XRF, pH measurements and ICP-MS results that indicated a high level of exchange from these exchange solutions that caused a reduction in crystallinity of the products and mixed phases were observed. However, the products did maintain a similar XRD pattern compared to un-exchanged α -ZrP in addition to few extra peaks, which strongly suggests that products did maintain the structure post ion-exchange.

5.10. Summary of the results

Competitive exchange experiments were carried out using 0.1 M individual nitrate solutions of strontium, caesium, cobalt, sodium, magnesium and calcium. The strontium-caesium exchange experiments indicate a higher loss of crystallinity for the hydrothermally synthesised samples compared to conventionally synthesised. However the compositional analysis indicate that overall strontium uptake was reduced by approximately 30% compared to single ion exchange, whereas the

caesium exchange was increased to almost double the single ion exchange capacity. The Y-ZrP samples showed slight increase (2 to 5%) in the exchange capacity compared to α -ZrP for both routes of synthesis, especially the 5% Y-ZrP synthesised hydrothermally that showed the highest extent of exchange for both Sr^{2+} and Cs^{2+} ions. However, significant leaching of framework ions were also observed from the ICP-MS results indicating that strontium-caesium exchange led to partial structural damage, degree of which was higher for hydrothermally synthesised samples.

Caesium-cobalt exchanges showed a similar trend of exchange but both caesium and cobalt exchange capacities were increased by approximately 50% compared to the single exchange experiments. The 5% Y-ZrP from both routes of synthesis showed the highest extent of exchange for both the ions. However, X-ray diffraction and ICP-MS results confirm lower crystallinity and partial structural damage that had occurred due to the leaching of the framework ions during the exchange. However, strontium-cobalt results indicate a decrease in strontium uptake by approximately 30% but the cobalt exchange had increased by 50% compared to the single exchange experiments. The highest extent of exchange was achieved by 5% Y-ZrP samples from both routes of synthesis. However, the crystallinity of the products were affected by the exchange as observed from the XRD analysis and only low amount of leaching of framework ions was observed from the ICP-MS results.

On the other hand, strontium-caesium-cobalt exchange showed that strontium exchange was reduced by almost 70%, but caesium and cobalt exchange capacities were increased by approximately 50% and 40% respectively. The highest exchange was observed for 5% Y-ZrP from both routes of synthesis that showed the highest extent of exchange. However, the XRD and ICP-MS studies indicate partial structural damage due to moderate release of framework ions during the exchange.

The results from competitive exchanges with calcium show that strontium exchange was reduced by approximately 20% but both caesium and cobalt extents were increased to 30% and 80% respectively, in the presence of calcium ion. Also, the calcium exchange capacity was the highest from strontium-calcium solution, followed by cobalt-calcium and caesium-calcium solution. Again, the highest extent of exchanges were observed for 5% Y-ZrP samples of both routes of synthesis

showing an almost 30% higher strontium and cobalt extent and 5% caesium extent compared to α -ZrP. However, low structural damage was observed for strontium-calcium and cobalt-calcium exchanges, whereas higher amount of framework ions were leached from caesium-calcium exchange leading to partial structural breakdown.

Competitive exchanges with magnesium showed similar results to that of calcium as the ICP-MS and SEM/EDX analysis indicate that strontium and cobalt uptakes were similar in presence of magnesium in regards to calcium, but the caesium uptake increased by almost 30%. Also, the XRD analyses show that the degree of crystallinity is better than other competitive exchanges, but was slightly reduced overall compared to un-exchanged α -ZrP. However, competitive exchange with sodium showed that strontium exchange was increased (20%) compared to calcium and magnesium exchange experiments, but caesium and cobalt uptake were similar to magnesium based experiments. However, degree of crystallinity was higher for strontium-sodium exchange as compared to caesium-sodium and cobalt-sodium exchanges that showed relatively higher leaching of framework ions.

Overall, Y-ZrP samples showed an increase in the exchange capacities compared to α -ZrP from both routes of reflux, especially the 5% Y-ZrP samples that showed the highest extent of exchange from all ion-exchange experiments indicating that it has highest exchange capacity. Also, all the Y-ZrP samples have high affinity towards strontium ions, followed by cobalt and caesium ions respectively.

5.11. References

1. Alberti, G., Bertrami, R., Casciola, M., Costantino, U., Gupta, J. P. J. Inorg. Nucl. Chem., 38, 843 (1976)
2. Clearfield, A., Hagiwara, H J. Inorg. Nucl. Chem., 40, 907 (1978)
3. Clearfield, A. Ann. Rev. Mater. Sci., 14, 205 (1984)
4. Alberti, G., Giammari, G., Grassini-Strazza, G. J. Chromatog., 28, 118 (1967)
5. Clearfield A (1998) Metal phosphonate chemistry. In: Karlin KD (ed.) Progress in Inorganic Chemistry, Vol. 47. New York: John Wiley.
6. Alberti, G., Costantino, U., Allulli, S., Massucci, M. A., Pelliccioni, M., J. Inorg. Nucl. Chem., 35, 1347 (1973)
7. Borovkov, S. I., Sharygin, L. M., Russ. J. Appl. Chem., 78, 2, 229 (2005)
8. Alberti, G., Bertrami, R., Casciola, M., Costantino, U., Gupta, J. P. J. Inorg. Nucl. Chem., 38, 843 (1976)
9. Clearfield, A., Frianeza, T. N. J. Inorg. Nucl. Chem., 40, 1925 (1978)
10. Clearfield, A., Medina, A. S. J. Inorg. Nucl. Chem., 32, 2775 (1970)
11. Kenneth R. Neubauer, Ruth E. Wolf, Interference Removal and Analysis of Environmental Waters Using the ELAN DRC-e ICP-MS, retrieved on 23/06/2015 from http://www.perkinelmer.co.uk/CMSResources/Images/44-74184APP_InterferenceRemovalandAnalysisofEnvironmentalWatersUingtheELANDRCeICPMS.pdf
12. Burnell, V.A., Readman, J.E. Tang, C.C. Parker, J.E. Thompson, S.P. Hriljac, J.A. J. Sol. Stat. Chem., 183, 2196, (2010)
13. Laugier, J. and Bochu, B. CELREF. 2003

CHAPTER 6: CONCLUSION AND FUTURE WORK

6.1. Mixed Metal Phosphates

The work presented in this thesis provides a deeper insight to the solid solution limits and structural chemistry of a particular class of inorganic ion-exchangers that have a potential for remediation of nuclear wastes. The principal aims of this thesis were to synthesise mixed metal phosphates using trivalent cations substituted for zirconium in alpha-zirconium phosphates (α -ZrP). The structural and ion-exchange properties of α -ZrP ^[1-17] are well known and documented, however this study was focussed on investigating whether mixed valence metal phosphates with the layered alpha structure could be synthesised and if so, what are the solid solution limits and the effect which the new cation has on ion-exchange the properties of the host material. It was hypothesised that the substitution of trivalent cation in place for Zr^{4+} would create a charge imbalance (net negative charge) that is balanced by extra protons and hence it will alter the ion-exchange properties of the new materials. For this purpose, 3 synthesis routes were initially planned, namely conventional, hydrothermal and microwave synthesis and parent α -ZrP were synthesised by all. The results indicate very similar products, however the degree of crystallinity and particle size distribution were slightly improved from conventional synthesis to hydrothermal, followed by microwave synthesis. Rietveld refinement also showed similar lattice parameters for all the three routes of synthesis in regards to the reported refinement parameters. ^[18] However, microwave synthesis yielded low amounts of product, in addition to other technical constraints and so this route of synthesis was not utilised for mixed metal phosphates.

Investigations were carried out in a number of mixed metal phosphate systems using yttrium (Y^{3+}), iron (Fe^{3+}) and cerium (Ce^{3+}) as a substitute for Zr^{4+} in an alpha zirconium framework. It was noted that a full solid solution series could not be synthesised for any of the studied systems as miscibility gaps were found in all. Several structural changes were determined by the X-ray diffraction data in the Fe-ZrP and Ce-ZrP structures which prevented formation of a full solid solution altogether, for all attempts at substitution. However, Y-ZrP samples showed a

solution limit of 0.2 molar substitutions and any further substitution gave to mixed phase products. It was found that there was a lack of flexibility for the Y-ZrP structures to accommodate a higher level of yttrium substitution due to differences in the crystal ionic radii ^[21] of the metal cations ($Y^{3+} = 1.04 \text{ \AA}$ and $Zr^{4+} = 0.86 \text{ \AA}$). This can in turn cause straining of the structures on metal substitution and will lead to formation of separate phases that are mixed together. Also, some solution chemistry aspects also effect the formation of full solid solutions by restricting the formation of the gel precursors.

There are no literature reports for the yttrium-zirconium phosphates or layered iron-zirconium phosphates to the best of our knowledge and only a single study has been done recently on the possibility of a cerium-zirconium phosphate, ^[19] however, the product obtained was amorphous in nature and no structural analysis was done on the material to conclude a single phase product. For the first time, in this thesis, yttrium-zirconium phosphates (Y-ZrP) were synthesised by using 2 synthesis routes and Rietveld analysis of the powder X-ray diffraction was carried out to characterise the structures from both the routes. A range of Y-ZrP solid solutions were formed which showed isostructural substitution of yttrium for zirconium in the α -ZrP lattice and the products behaved similarly to the host material. Solid state ³¹P NMR studies were also conducted to determine the phase purity and the results for conventional Y-ZrP samples are consistent with that reported ^[20] previously for α -ZrP, showing that yttrium substitution occurred at Zr sites close to HPO_4^{2-} as it gave a signal -27.1 ppm. However, for hydrothermally synthesised Y-ZrP samples, an addition peak was present at -8.14 ppm which suggests that yttrium substitution occurred at Zr sites close to phosphate groups ($H_2PO_4^-$) with Q^0 connectivity. The lattice parameters which are presented in Table 12 and 16 of Chapter 3 show that the Y-ZrP products are structurally similar to α -ZrP with slight changes in the average metal-oxygen distances that were not linearly varying according to the percentage substitution. This indicates that the unit cell could not withstand any major alternations to the cell dimensions to accommodate high levels of substitution of the second metal. Also, the BET surface area results shown in Figure 18 of Chapter 3 indicate a decrease in surface area of the Y-ZrP with increasing percentage of substitution, suggesting that the Y-ZrP samples have high crystallinity and crystallite sizes increased with yttrium doping, as shown by particle size measurements in Figure 17 of Chapter 3.

6.2. Ion Exchange Studies

The synthesised mixed Y/Zr metal phosphates were evaluated for their phase purity and success of synthesis in order to study the effect of substitution on the ion-exchange behaviour. Single phase products were obtained for 5%, 10% and 15% yttrium substitution from both synthesis routes and ion-exchange studies were carried out to investigate their potential as nuclear waste stores. Two types of ion-exchange experiments were carried out; the first study was with single metal ion solutions of strontium, caesium and cobalt from their nitrate, acetate and hydroxide salts and the second studied the competitive exchanges between strontium, caesium and cobalt along with the presence of sodium, magnesium and calcium as the interfering ions. All ion-exchange experiments were carried out at room temperatures for extended periods (72 hours) in order to study the highest exchange capacity and selectivity of these products.

The single ion exchange experiment results indicate that $\text{Sr}(\text{NO}_3)_2$ exchanged products showed higher degree of stability and crystallinity compared to $\text{Sr}(\text{CH}_3\text{CO}_2)_2$ that had lower crystallinity and presence of mixed phases, followed by $\text{Sr}(\text{OH})_2$ showing loss of crystal structure and presence of unidentified phases. This was indicative of extent of exchange as seen from the XRF and ICP-MS analysis that showed about 25% exchange from nitrate solution, followed by almost 50% from acetate and beyond theoretical capacity from the hydroxide solution. Caesium exchange results on the other hand, showed lower extent overall as compared to strontium exchange, with CsNO_3 and CsCH_3CO_2 solutions leading to very limited exchange (2%) and higher degree of crystallinity as compared to the CsOH exchange where the exchange was higher (25%) but the samples did not maintain the structure and there was a great loss of crystallinity of the products. Similar results were obtained from cobalt ion exchanges, where the $\text{Co}(\text{NO}_3)_2$ solutions led to lower extent of exchange (2.5%) and higher degree of crystallinity compared to $\text{Co}(\text{CH}_3\text{CO}_2)_2$ exchange that showed significantly higher extent of exchange (50%) and slightly lower crystallinity with presence of a mixed phase.

Overall it is concluded from single ion exchange experiments that some of the Y-ZrP samples, especially 5% Y-ZrP samples showed 8 to 10% higher strontium exchange capacity from nitrate, acetate and hydroxide solutions, but there were similar results

for the caesium exchanges with a slight increase for the hydrothermally synthesised Y-ZrP samples compared to α -ZrP for both routes of synthesis. However, the Y-ZrP showed a remarkable increase in the cobalt exchange capacity from both the nitrate solutions (12 to 75% increase) and acetate solutions (20 to 400% increase) compared to α -ZrP for both routes of synthesis.

The competitive exchange experiments demonstrated that among all the strontium and cobalt exchanges, strontium-cobalt solution led to the highest exchange capacity of both Sr^{2+} and Co^{2+} ions, whereas strontium-caesium and caesium-magnesium exchanges led to the highest caesium uptakes. In addition, the sodium exchange experiments showed an increase in strontium uptake with extent similar to that of strontium-cobalt uptakes, but the cobalt and caesium uptakes did not show any marked increase compared to calcium and magnesium based experiments. Also, in a competitive solution, both α -ZrP and Y-ZrP showed lower selectivity towards ions of interest (Sr, Cs, Co) since other alkali and alkaline earth metals were also exchanged in substantial amounts. However, the strontium-caesium-cobalt exchange showed that Y-ZrP products have higher affinity for strontium ions from a mixed solution compared to α -ZrP and the order of selectivity is $\text{Sr}^{2+} > \text{Co}^{2+} > \text{Cs}^+$. This behaviour is slightly different to α -ZrP since its order of selectivity is reported [7, 10] as $\text{Sr}^{2+} > \text{Cs}^+ > \text{Co}^{2+}$. Also, among the different composition and types of Y-ZrP samples synthesised, 5% Y-ZrP samples showed the highest extent of exchange from all experiments with at least 10% higher uptakes of strontium, caesium and cobalt compared to α -ZrP.

6.3. Summary of the work reported in this thesis

- Three synthesis routes were used for the formation of layered metal phosphates using modified methodology incorporating sonication to aid substitution reactions
- Structural analysis of α -ZrP from all the three routes of synthesis was carried out using Rietveld refinement of powder x-ray diffraction data.
- Attempts to synthesise mixed iron-zirconium phosphate and cerium-zirconium phosphates using conventional and hydrothermal methods of synthesis.

- Successful synthesis of yttrium-zirconium phosphate (Y-ZrP), their characterisation and structural studies using Rietveld refinement methods.
- Study of acid stability of the synthesised Y-ZrP samples.
- Comprehensive study on the ion-exchange behaviour of both α -ZrP and Y-ZrP samples synthesised from conventional and hydrothermal methods, for removal of Sr^{2+} , Cs^+ and Co^{2+} using single ion and competitive exchange solutions.
- Comprehensive study on the ion-exchange behaviour of both α -ZrP and Y-ZrP samples of both routes of synthesis for removal of Sr^{2+} , Cs^+ and Co^{2+} from a competitive solution containing Na^+ , Mg^{2+} and Ca^{2+} as an interfering ion.

6.4. Future Work

Several areas of potential future work result from this project including further structural characterisation of the synthesised yttrium-zirconium phosphates. The following recommendations may be useful to lead the future projects in the inorganic mixed metal phosphates:

- The use of Pair Distribution Studies (PDF) and Rietveld refinement using high resolution synchrotron powder X-ray diffraction data could yield more accurate information about the synthesised mixed metal crystal lattice and also study the sites of exchange within the structural framework.
- It might be of interest to study the crystal defects and tailor the physio-chemical properties of these newly synthesised inorganic exchangers by varying the molar ratios and metal salt compositions of the precursors.
- The study of these materials could be performed in mixed acid environment using a range of molar solutions and salt anions. Chloride ions can be used as additional counter ions to study the variations in extents and nature of ion exchanges.

In regards to application, detailed study of the mechanism of ion exchange can be studied in future in order to determine the nature of exchange of Y-ZrP with respect to oxidation states and ionic radii of the ions of interest. Also, stepwise ion exchanges can be studied with different ions to tailor the selectivity and extent of

exchange. A titration study of the ion exchange experiments could yield more accurate results in terms of the limits of exchange and structural damage. This could aid in refinement studies of the exchanged product structure which can be undertaken to fully understand the site occupancies and structural distortions that occur during the ion exchange experiments. Finally, other potential application of these new class of inorganic ion-exchangers can be explored in fields such as catalysis, fuel cells and sensors, etc.

6.5. References

1. G. Alberti. Atti. Accad. Nazl. Lincei, Rend., Classe Sci. Fis., Mat. Nat 1961; 31: 427.
2. M. J. N. Costa, M. A. S. Jeronimo. J. Chromatog 1961; 5:456.
A. Clearfield, G. D. Smith. J. Inorg. Nucl. Chem 1968; 30:327.
3. G. Alberti, U. Costantino, S. Alluli, M. A. Massucci. J. Inorg. Nucl. Chem 1975; 37:1779.
4. S. Allulli, A. La Ginestra, M. A. Massucci, M. Pelliccioni, M. Tomassini. Inorg. Nucl. Chem. Lett 1974; 10:337
5. B. R. Palmer, Fuerstenau M. C.. Proc. Int. Miner. Process. Congr., 10th 1974:1123.
6. R. Smits, D. L., et al. Massart. Anal. Chem 1976; 48:458.
7. A. Clearfield, R. A. Hunter. J. Inorg. Nucl. Chem 1976; 38:1085.
8. G. Alberti, R. Bertrami, U. Costantino, J. P. Gupta. J. Inorg. Nucl. Chem 1977; 39:1057
9. S. Allulli, C. Ferragina, A. La Ginestra, M. A. Massucci, N. Tomasinni. J. Chem. Soc., Dalton Trans 1977; 19:1879.
10. A. Clearfield, H. Hagiwara. J. Inorg. Nucl. Chem 1978; 40:907.
11. M. A. Massucci, A. La Ginestra, C. Ferragina. Gazz. Chim. Ital 1980; 110:73.
12. L. Kullberg, A. Clearfield. J. Phys. Chem 1981; 85:1578.
13. G. Alberti, U. Costantino, M. Pelliccioni. J. Inorg. Nucl. Chem 1973; 35:1327.
14. G. Alberti, U. Costantino, J. P. Gupta. J. Inorg. Nucl. Chem 1974; 36:2109.
15. L. Kullberg, A. Clearfield. J. Phys. Chem 1981; 85:1585.
16. T. Shaheen, M. Zamin, S. Khan. Main Group Metal Chemistry 2001; 24:351.
17. C. H. Kim, H. S. Kim. Synth. Met 1995; 71:2051.
18. V.A. Burnell, J.E. Readman, C.C. Tang, J.E. Parker, S.P. Thompson, J.A. Hriljac, J. Solid State. Chem, 183, 2196, 2010.
19. B. Preetha, C. Janardanan, J. Indian Chem. Soc., 8, 1377-1382 (2011)
20. N. J. Clayden, Journal of the Chemical Society, Dalton Transactions 1987, 1877.
21. R. D. Shannon, et al., Act. Crystal. A32. 751 (1976)

APPENDICES

Appendix 1

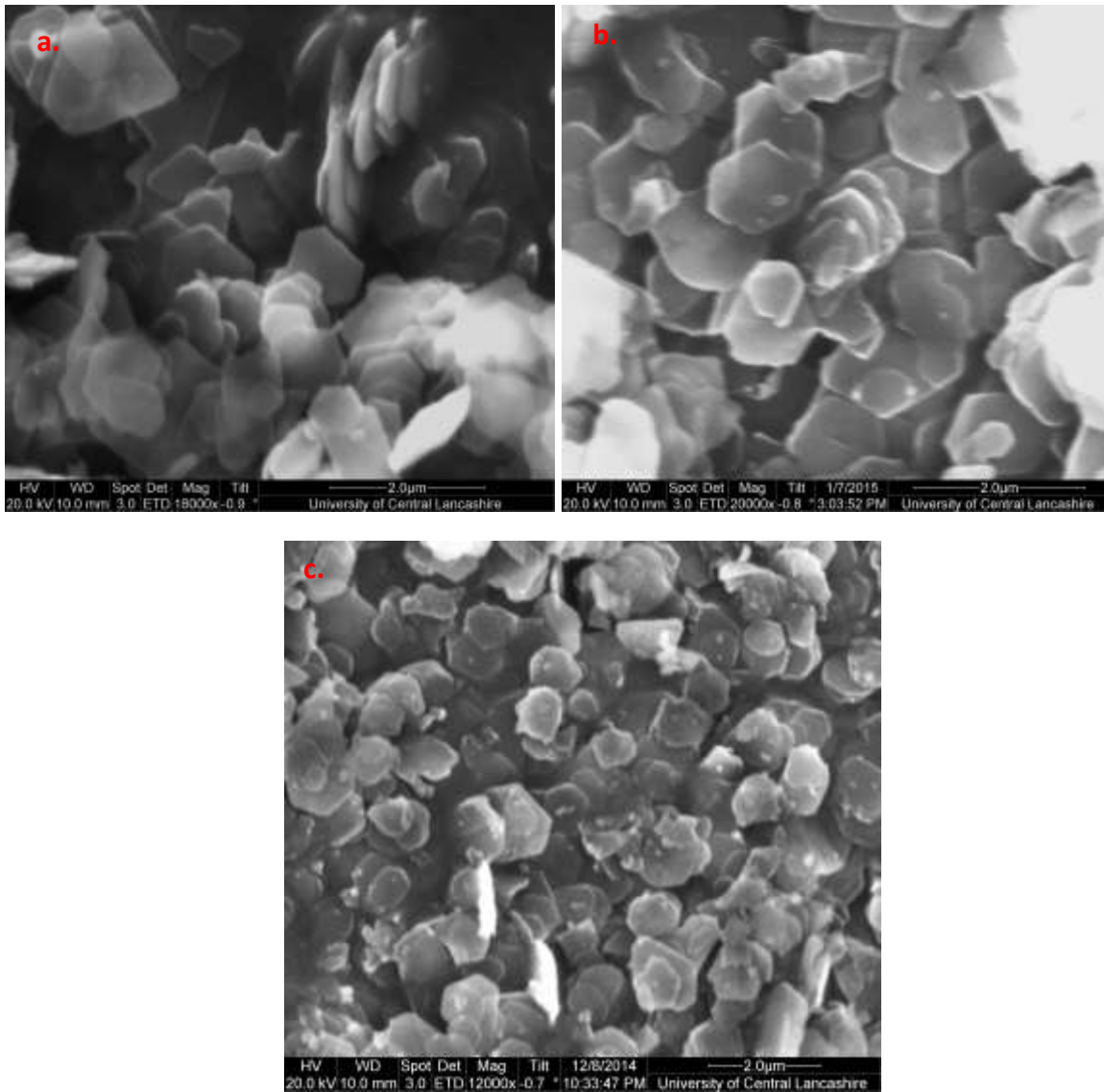


Figure1. SEM images showing morphology of α -ZrP (a. Conventional, b. Hydrothermal, c. Microwave)

Table 1. Calibration scheme for XRF measurements

Calibration of Yttrium w.r.t Zirconium						
Percentage Material	ZrO ₂	H ₂ NaO ₄ P	Y ₂ O ₃	Strontium oxide	Y/Zr% intensity ratio from calibration	Y/Zr% Peak area ratios
α- ZrP	1 g	2.2396 g	0	0	0	0
1 Y-ZrP	1 g	2.2396 g	0.00916 g	0	3.77	6.85
2 Y-ZrP	1 g	2.2396 g	0.01835 g	0	5.74	8.69
5 Y-ZrP	1 g	2.2396 g	0.0458 g	0	10.36	13.66
10 Y-ZrP	1 g	2.2396 g	0.0916 g	0	20.74	24.82
15 Y-ZrP	1 g	2.2396 g	0.1374 g	0	28.27	31.69
20 Y-ZrP	1 g	2.2396 g	0.1833 g	0	37.16	40.69
25 Y-ZrP	1 g	2.2396 g	0.2290 g	0	42.96	46.57
30 Y-ZrP	1 g	2.2396 g	0.2748 g	0	50.40	53.74
35 Y-ZrP	1 g	2.2396 g	0.3206 g	0	59.31	63.76
40 Y-ZrP	1 g	2.2396 g	0.3556 g	0	66.78	71.58
45 Y-ZrP	1 g	2.2396 g	0.4122 g	0	76.408	80.79
50 Y-ZrP	1 g	2.2396 g	0.4581 g	0	82.03	80.63
55 Y-ZrP	1 g	2.2396 g	0.5038 g	0	87.07	87.94
60 Y-ZrP	1g	2.2396 g	0.5497 g	0	89.09	89.83

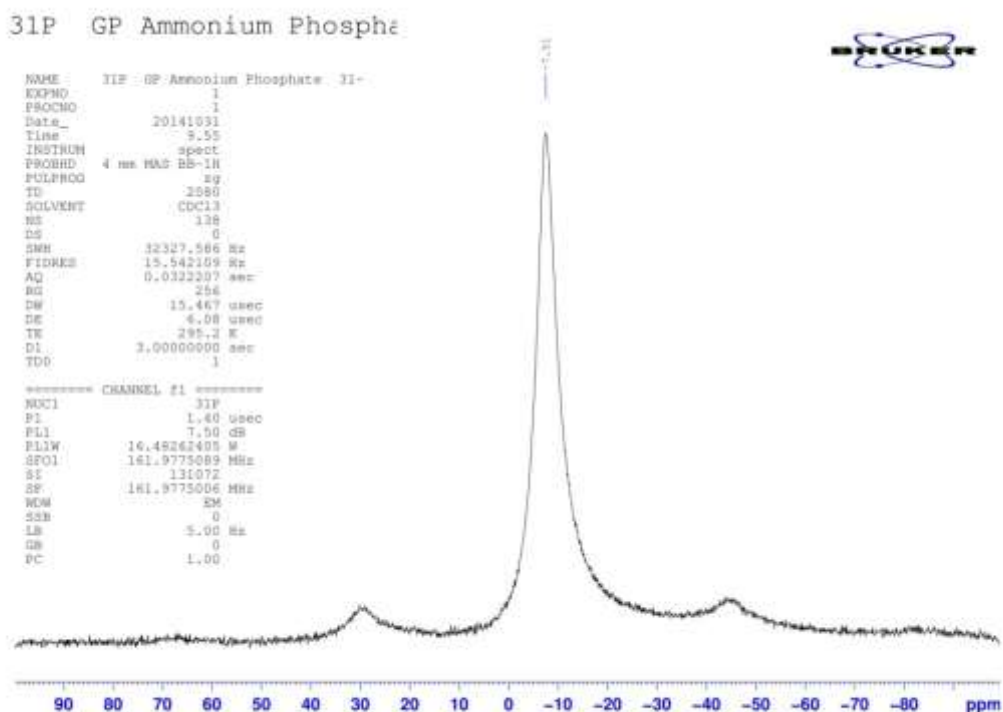


Figure 2. ³¹P MAS-NMR spectrum of ammonium phosphate as external standard

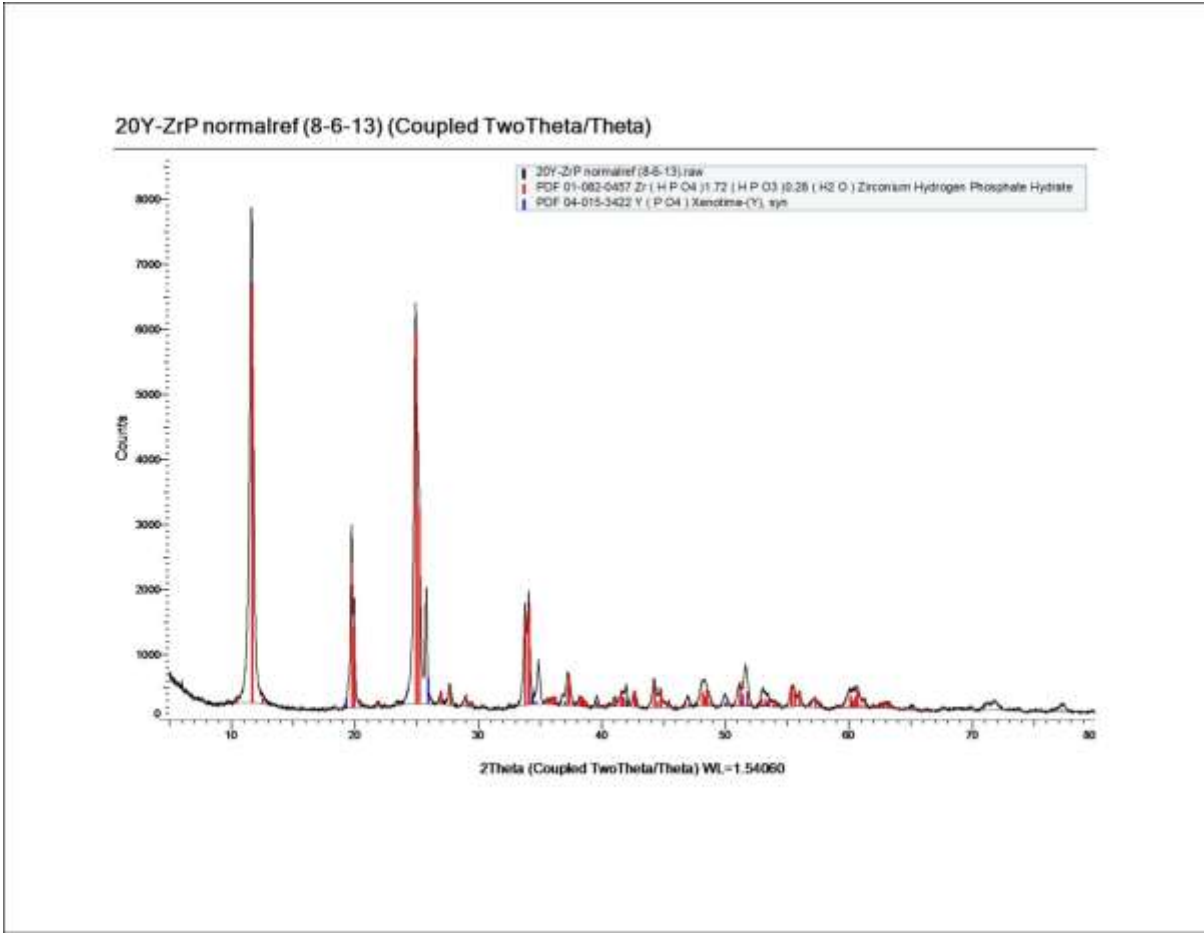


Figure 3.PDF match for 20% Y-ZrP using PDF 04-015-3422 for Xenotime

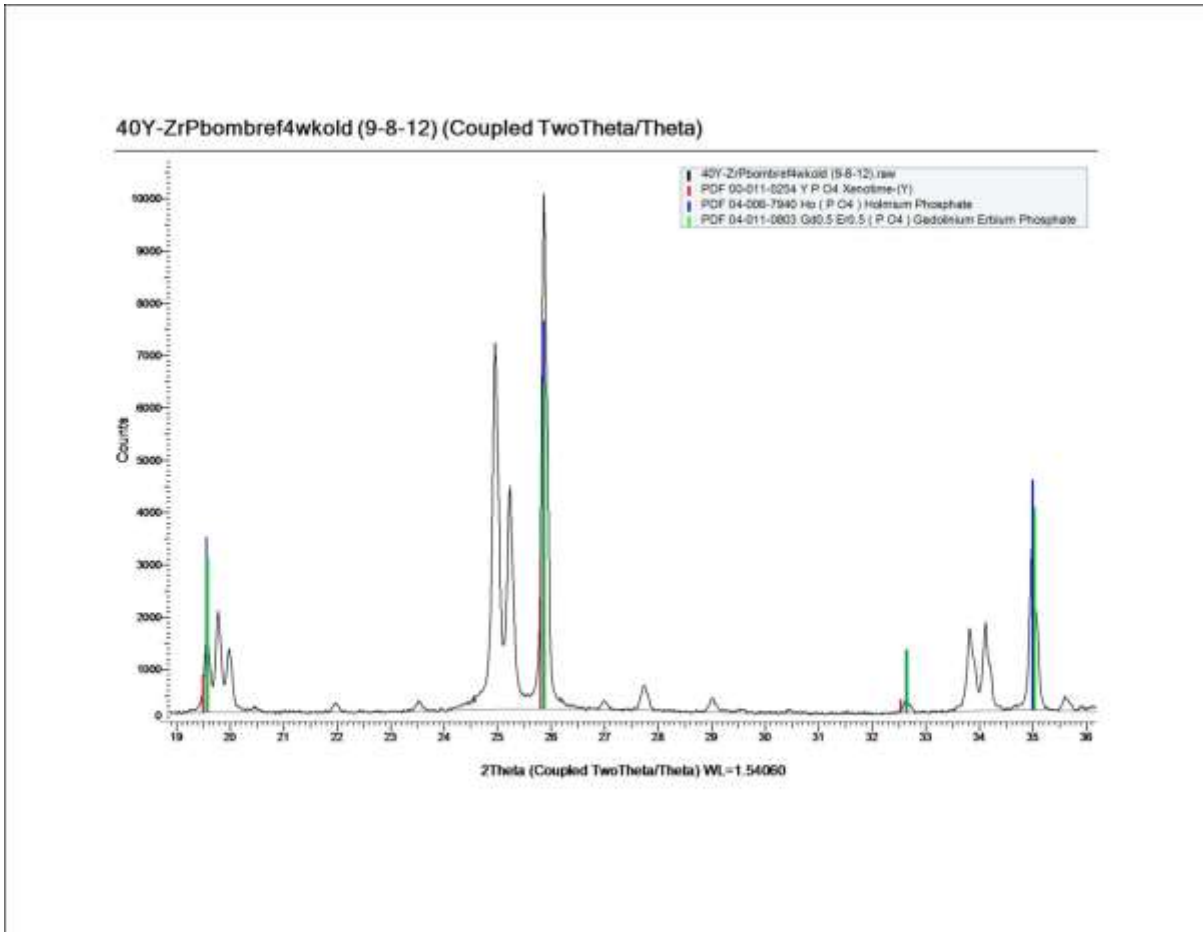


Figure 4.PDF matching for Xenotime (PDF 00-011-0254), Holmium phosphate (PDF 04-006-7940) and Gadolinium Erbium phosphate (PDF 04-011-0803)

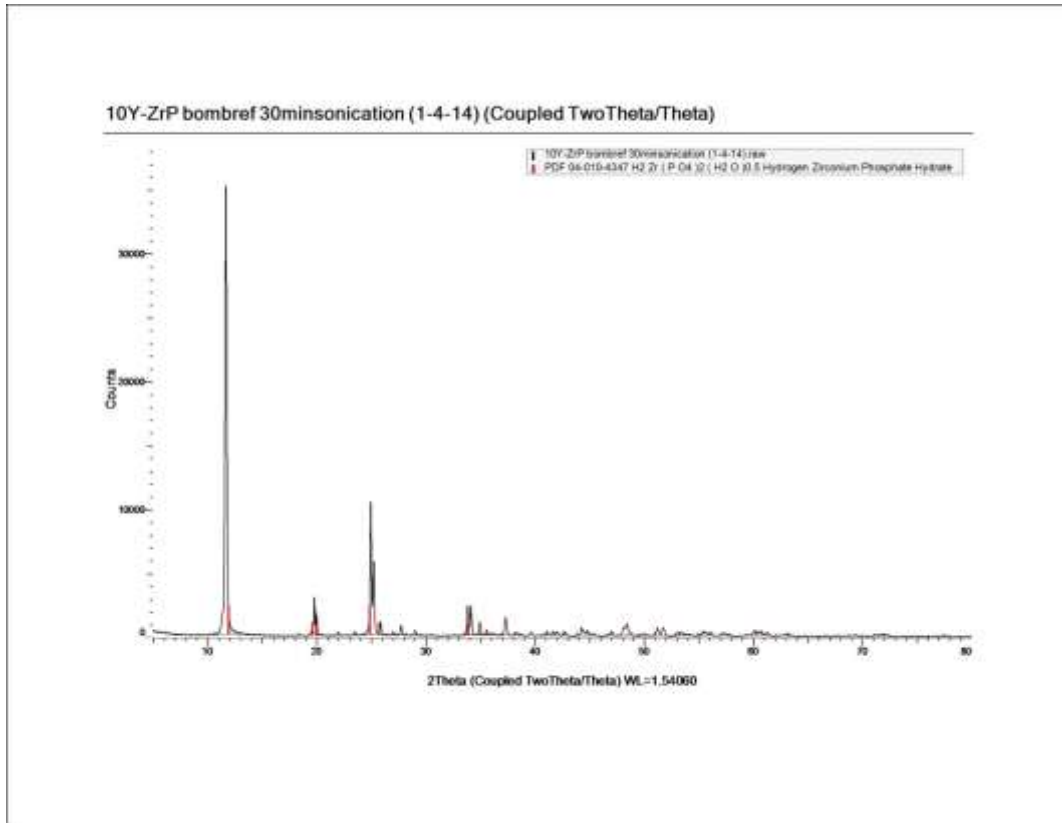


Figure 5.PDF match for 10% Y-ZrP with hydrogen zirconium phosphate hydrate (PDF 04-010-4347)

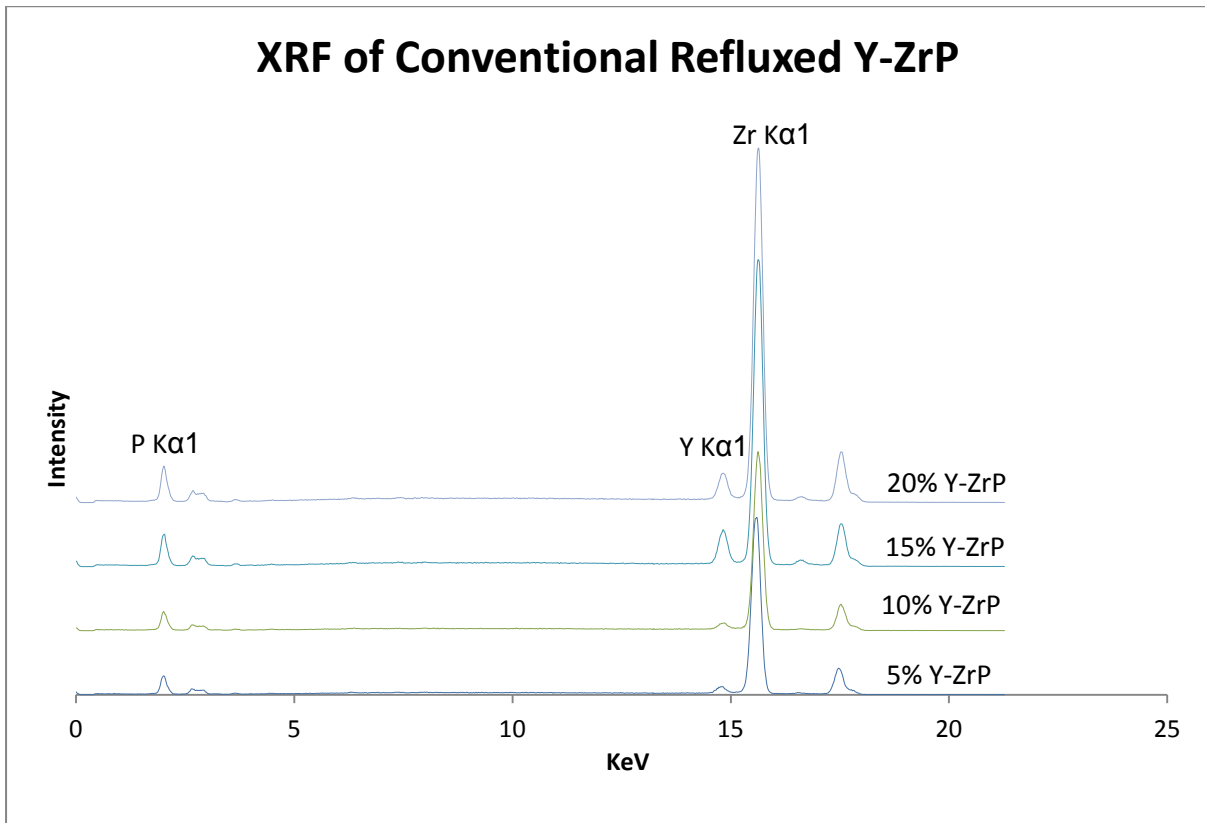


Figure 6.XRF for conventionally refluxed Y-ZrP products

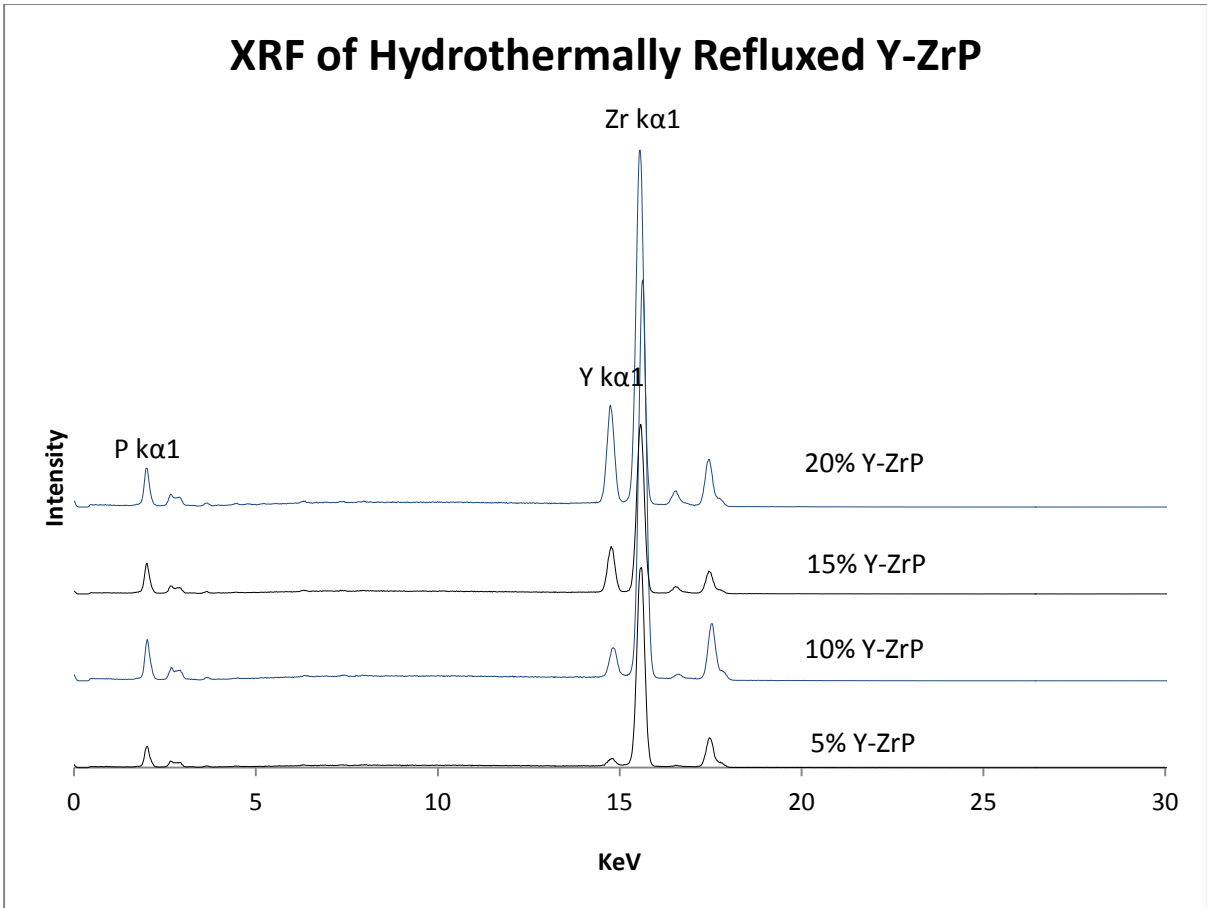


Figure 7. XRF for hydrothermally refluxed Y-ZrP products

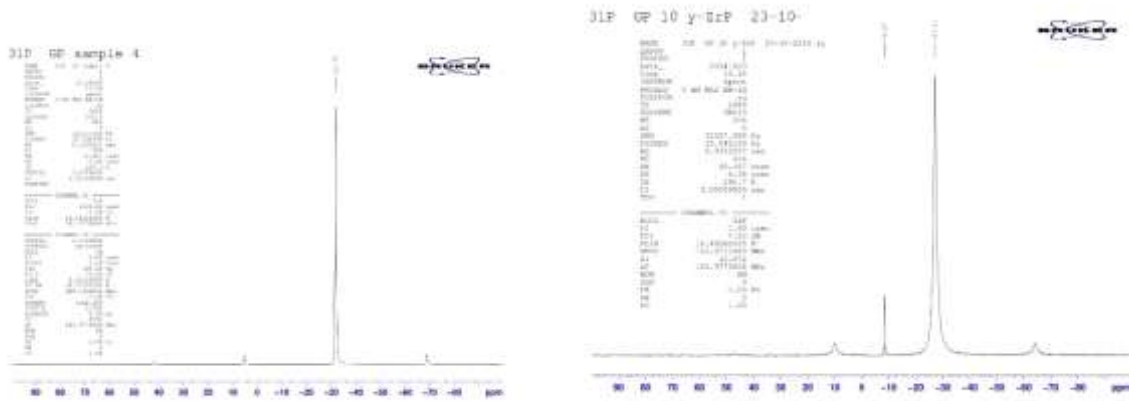


Figure 8. ^{31}P NMR for 10% Y-ZrP via conventional (left) & hydrothermal (right) route



Figure 9. ^{31}P NMR for 15% Y-ZrP via conventional (left) & hydrothermal (right) route



Figure 10. ^{31}P NMR for 20% Y-ZrP via conventional (left) & hydrothermal (right) route

31P GP YPO4 Bomb ref 2
 Bottle 15

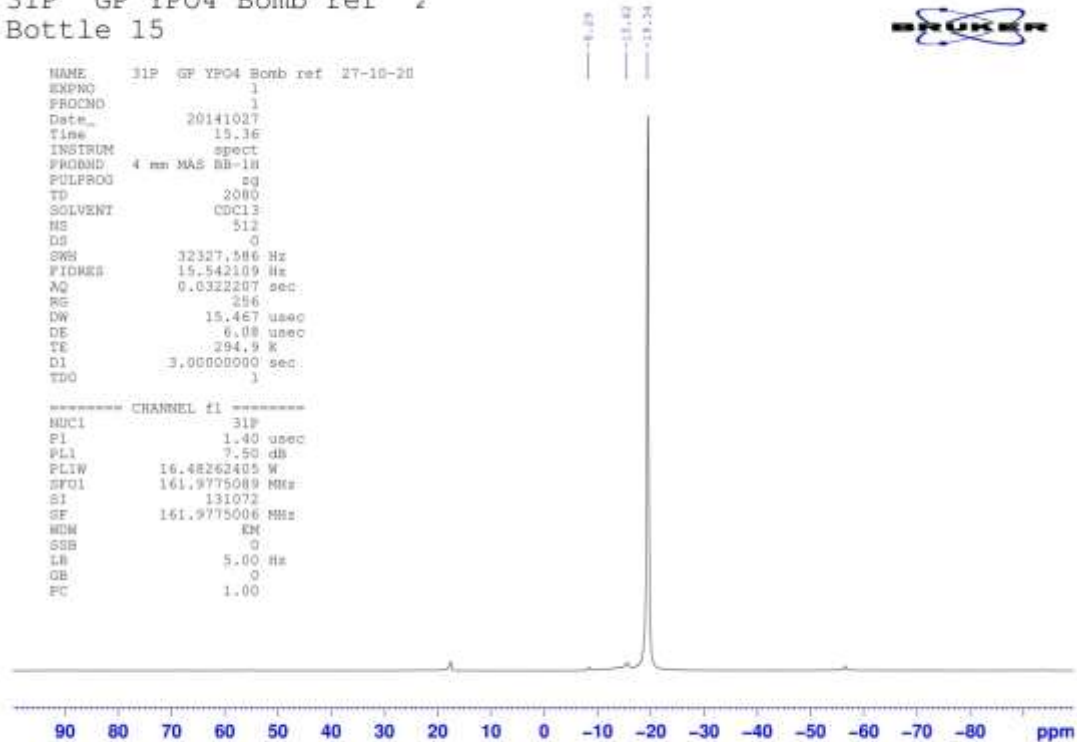


Figure 11. ³¹P NMR for hydrothermal refluxed YPO₄

Appendix 2

Table 1. Selected refined bond angles from Rietveld refinement for synthesised α -ZrP

Conventional Reflux		Hydrothermal Reflux		Microwave Reflux	
O1_Zr1_O2	93.18(21)	O2_Zr1_O3	108.234(6)	O1_Zr1_O2	56.86(11)
O1_Zr1_O3	72.01(23)	O2_Zr1_O4	69.378(6)	O1_Zr1_O3	90.41(20)
O1_Zr1_O5	84.90(29)	O2_Zr1_O5	45.27(13)	O1_Zr1_O5	82.67(17)
O1_Zr1_O7	98.11(24)	O2_Zr1_O6	66.00(7)	O1_Zr1_O6	91.50(20)
O1_Zr1_O8	171.65(27)	O2_Zr1_O7	65.42(11)	O1_Zr1_O8	167.49(31)
O2_Zr1_O3	160.171(1)	O2_Zr1_O8	29.60(4)	O2_Zr1_O3	78.20(16)
O2_Zr1_O5	74.52(12)	O3_Zr1_O4	91.159(7)	O2_Zr1_O5	76.16(18)
O2_Zr1_O7	102.28(8)	O3_Zr1_O5	147.84(15)	O2_Zr1_O6	147.53(25)
O2_Zr1_O8	80.36(10)	O3_Zr1_O6	62.68(14)	O2_Zr1_O8	114.31(21)
O3_Zr1_O5	115.87(12)	O3_Zr1_O7	171.11(12)	O3_Zr1_O5	152.99(26)
O3_Zr1_O7	93.02(8)	O3_Zr1_O8	88.58(10)	O3_Zr1_O6	96.66(26)
O3_Zr1_O8	112.93(8)	O5_Zr1_O6	107.38(22)	O3_Zr1_O8	96.43(15)
O5_Zr1_O7	31.58(5)	O5_Zr1_O7	30.65(6)	O5_Zr1_O6	109.55(21)
O5_Zr1_O8	98.33(13)	O5_Zr1_O8	72.26(13)	O5_Zr1_O8	86.53(19)
O7_Zr1_O8	88.49(16)	O6_Zr1_O7	108.47(24)	O6_Zr1_O8	98.07(18)
O1_P1_O2	112.767(2)	O6_Zr1_O8	36.47(9)	O1_P1_O2	75.758(3)
O1_P1_O4	112.631(5)	O7_Zr1_O8	83.11(16)	O1_P1_O3	93.852(2)
O2_P1_O4	84.096(3)	O4_Zr1_O5	64.44(17)	O1_P1_O4	92.831(6)
O3_P2_O5	58.51(10)	O4_Zr1_O7	92.17(12)	O2_P1_O3	151.367(2)
O3_P2_O6	64.75(13)	O4_Zr1_O8	91.17(15)	O2_P1_O4	130.192(2)
O3_P2_O7	92.92(10)	O5_P2_O6	105.22(18)	O3_P1_O4	76.067(2)
O3_P2_O8	153.6(4)	O5_P2_O7	43.073(3)	O5_P2_O6	74.019(5)
O5_P2_O6	105.233(4)	O5_P2_O8	94.67(26)	O5_P2_O7	80.651(4)
O5_P2_O7	34.506(0)	O6_P2_O7	141.77(20)	O5_P2_O8	114.496(4)
O5_P2_O8	129.5(4)	O6_P2_O8	37.52(15)	O6_P2_O7	45.629(4)
O6_P2_O7	128.503(4)	O7_P2_O8	112.05(32)	O6_P2_O8	145.253(3)
O6_P2_O8	89.43(35)	P2_O5_O2	129.23(23)	O7_P2_O8	161.930(1)
O7_P2_O8	99.8(4)	P2_O5_O7	36.827(3)	P1_O2_O2	100.927(5)

Table 2. Selected refined bond angles from Rietveld refinement for conventional reflux Y-ZrP

5% Y-ZrP		10% Y-ZrP		15% Y-ZrP	
O1_M1_O2	91.19(16)	O1_M1_O2	92.47(25)	O1_M1_O2	90.21(20)
O1_M1_O3	87.04(15)	O1_M1_O3	86.67(30)	O1_M1_O3	85.25(19)
O1_M1_O5	91.55(19)	O1_M1_O5	92.29(34)	O1_M1_O5	94.14(23)
O1_M1_O6	91.05(12)	O1_M1_O6	90.17(27)	O1_M1_O6	92.86(14)
O1_M1_O8	178.88(10)	O1_M1_O8	178.7(4)	O1_M1_O8	175.85(16)
O2_M1_O3	89.82(11)	O2_M1_O3	89.884(4)	O2_M1_O3	90.60(12)
O2_M1_O5	90.91(25)	O2_M1_O5	90.11(12)	O2_M1_O5	88.22(32)
O2_M1_O6	177.20(12)	O2_M1_O6	177.32(14)	O2_M1_O6	176.65(6)
O2_M1_O8	88.71(16)	O2_M1_O8	88.06(12)	O2_M1_O8	87.17(19)
O3_M1_O5	178.43(13)	O3_M1_O5	178.96(14)	O3_M1_O5	178.67(21)
O3_M1_O6	88.62(27)	O3_M1_O6	89.79(8)	O3_M1_O6	88.32(33)
O3_M1_O8	91.84(15)	O3_M1_O8	92.19(8)	O3_M1_O8	91.57(17)
O5_M1_O6	90.71(12)	O5_M1_O6	90.26(20)	O5_M1_O6	92.89(13)
O5_M1_O8	89.56(19)	O5_M1_O8	88.85(16)	O5_M1_O8	88.99(23)
O6_M1_O8	89.01(12)	O6_M1_O8	89.29(21)	O6_M1_O8	89.69(14)
O1_P1_O2	113.849(1)	O1_P1_O2	113.856(1)	O1_P1_O2	113.849(1)
O1_P1_O3	109.258(2)	O1_P1_O3	109.268(3)	O1_P1_O3	109.255(2)
O1_P1_O4	110.036(3)	O1_P1_O4	110.020(4)	O1_P1_O4	110.040(3)
O2_P1_O3	110.082(2)	O2_P1_O3	110.079(3)	O2_P1_O3	110.082(2)
O2_P1_O4	102.273(1)	O2_P1_O4	102.275(1)	O2_P1_O4	102.273(1)
O3_P1_O4	111.212(2)	O3_P1_O4	111.214(2)	O3_P1_O4	111.212(2)
O5_P2_O6	111.833(2)	O5_P2_O6	111.836(3)	O5_P2_O6	111.832(2)
O5_P2_O7	109.550(2)	O5_P2_O7	109.543(2)	O5_P2_O7	109.552(2)
O5_P2_O8	110.3(4)	O5_P2_O8	108.0(4)	O5_P2_O8	110.3(5)
O6_P2_O7	108.738(1)	O6_P2_O7	108.733(2)	O6_P2_O7	108.739(1)
O6_P2_O8	110.8(4)	O6_P2_O8	112.7(4)	O6_P2_O8	113.8(5)
O7_P2_O8	105.40(21)	O7_P2_O8	105.87(18)	O7_P2_O8	102.14(21)

Table 3. Selected refined bond angles from Rietveld refinement for hydrothermal reflux Y-ZrP

5% Y-ZrP		10% Y-ZrP		15% Y-ZrP	
O1_Zr1_O2	99.791(3)	O1_Zr1_O2	92.49(24)	O1_Zr1_O2	90.01(33)
O1_Zr1_O3	79.066(2)	O1_Zr1_O3	84.87(25)	O1_Zr1_O3	88.21(35)
O1_Zr1_O5	82.423(2)	O1_Zr1_O5	94.66(33)	O1_Zr1_O5	92.9(5)
O1_Zr1_O6	81.123(3)	O1_Zr1_O6	90.70(26)	O1_Zr1_O6	94.4(4)
O1_Zr1_O8	167.735(0)	O1_Zr1_O8	177.54(30)	O1_Zr1_O8	172.3(5)
O1_Zr1_Y13	114.651(3)	O2_Zr1_O3	89.648(4)	O2_Zr1_O3	89.629(7)
O2_Zr1_O3	94.590(3)	O2_Zr1_O5	89.67(14)	O2_Zr1_O5	92.96(25)
O2_Zr1_O5	88.750(3)	O2_Zr1_O6	176.80(17)	O2_Zr1_O6	170.06(22)
O2_Zr1_O6	166.000(0)	O2_Zr1_O8	88.53(14)	O2_Zr1_O8	85.76(24)
O2_Zr1_O8	92.392(3)	O3_Zr1_O5	179.15(17)	O3_Zr1_O5	177.18(30)
O3_Zr1_O5	161.487(1)	O3_Zr1_O6	90.34(10)	O3_Zr1_O6	81.61(18)
O3_Zr1_O6	99.282(3)	O3_Zr1_O8	92.90(10)	O3_Zr1_O8	85.35(15)
O3_Zr1_O8	98.674(2)	O5_Zr1_O6	90.37(24)	O5_Zr1_O6	95.7(4)
O5_Zr1_O6	77.487(3)	O5_Zr1_O8	87.58(19)	O5_Zr1_O8	93.7(4)
O5_Zr1_O8	99.374(2)	O6_Zr1_O8	88.27(24)	O6_Zr1_O8	88.8(4)
O6_Zr1_O8	87.402(3)	O1_P1_O2	113.861(1)	O1_P1_O2	106.108(3)
O1_P1_O2	134.071(1)	O1_P1_O3	109.275(3)	O1_P1_O3	123.936(5)
O1_P1_O3	87.544(2)	O1_P1_O4	110.006(5)	O1_P1_O4	120.026(7)
O1_P1_O4	142.843(2)	O2_P1_O3	110.084(4)	O2_P1_O3	95.916(6)
O2_P1_O3	112.050(3)	O2_P1_O4	102.274(1)	O2_P1_O4	88.557(3)
O2_P1_O4	66.503(2)	O3_P1_O4	111.209(2)	O3_P1_O4	111.234(5)
O3_P1_O4	115.066(1)	O5_P2_O6	111.849(4)	O5_P2_O6	106.275(7)
O5_P2_O6	116.049(3)	O5_P2_O7	109.533(2)	O5_P2_O7	93.436(5)
O5_P2_O8	139.632(1)	O5_P2_O8	106.3(4)	O5_P2_O8	107.7(5)
O6_P2_O8	91.514(2)	O6_P2_O7	108.724(2)	O6_P2_O7	114.037(3)

Appendix 3

Table 1.XRF calibration scheme for ions of interest

Total moles of metal (Zr+Y)	Moles % of ions of interest	Ratio of peak area Sr	Ratio of peak area Cs	Ratio of peak area Co	Ratio of peak area Ca
		$\frac{\text{Total metal}}$	$\frac{\text{Total metal}}$	$\frac{\text{Total metal}}$	$\frac{\text{Total metal}}$
0.00166	1%	0.03385	0.01551	0.1023	0.01136
	5%	0.15421	0.08817	0.6248	0.05147
	10%	0.42729	0.17825	1.1065	0.09205
	20%	0.60074	0.3569	1.795	0.1822
	30%	1.0497	0.5268	2.7239	0.27231
	40%	1.1430	0.66640	3.6758	0.40765
	50%	1.3742	0.85799	4.911	0.47528

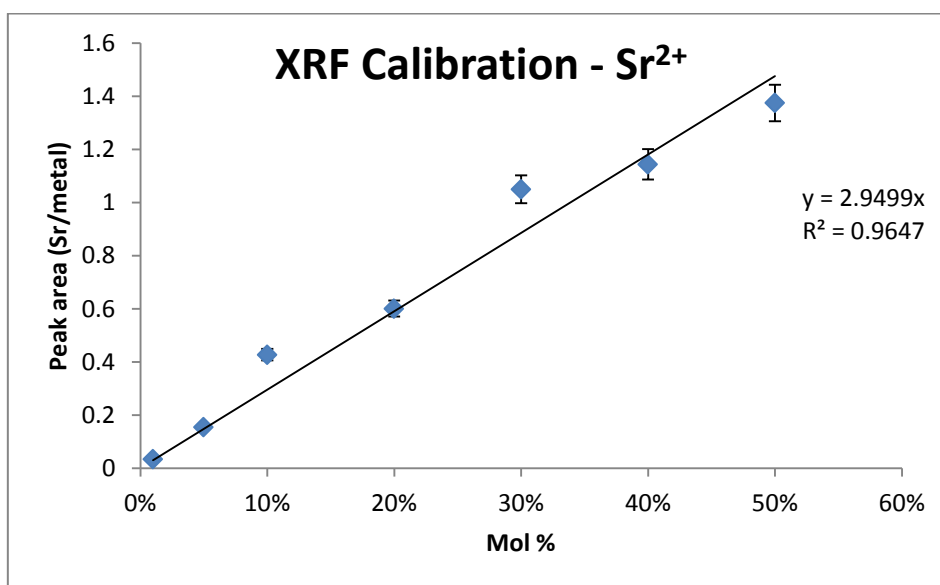


Figure 1.XRF calibration graph for strontium exchange

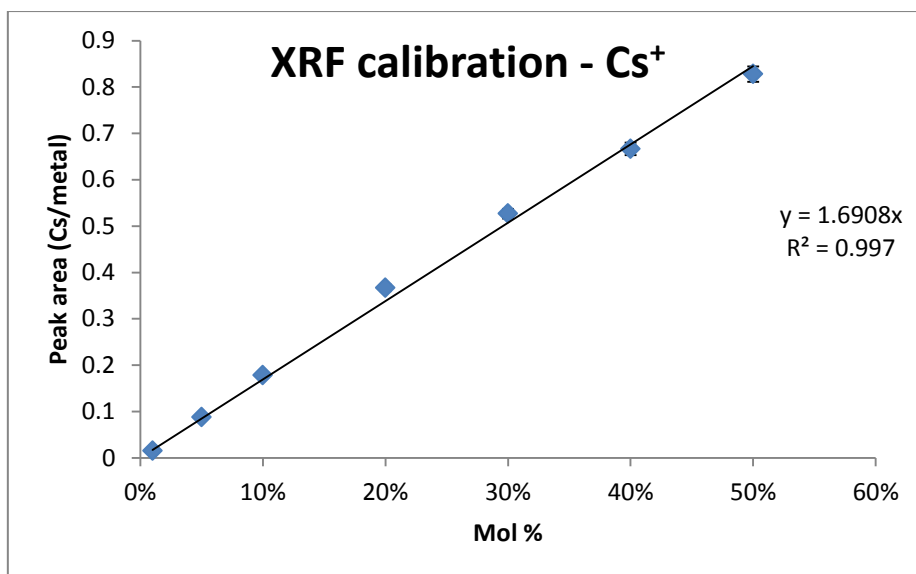


Figure 2.XRF calibration graph for caesium exchange

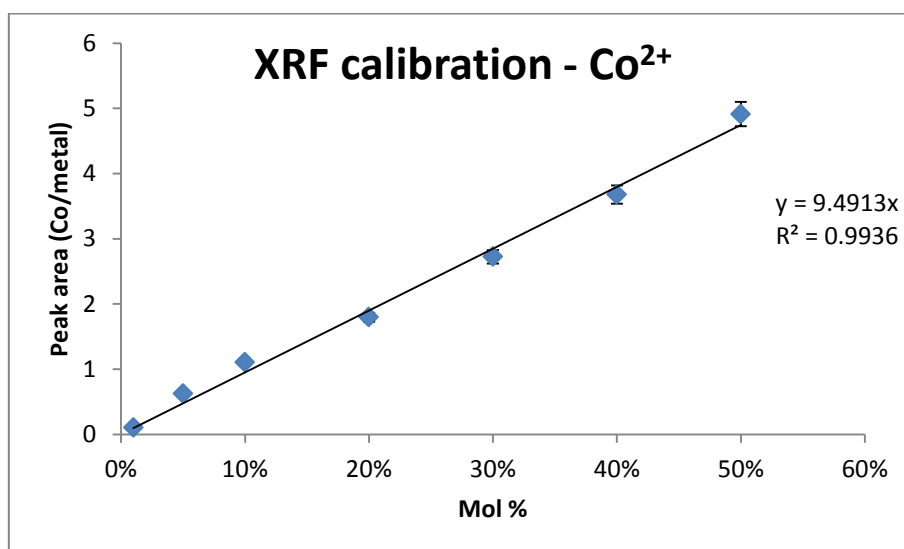


Figure 3.XRF calibration graph for cobalt exchange

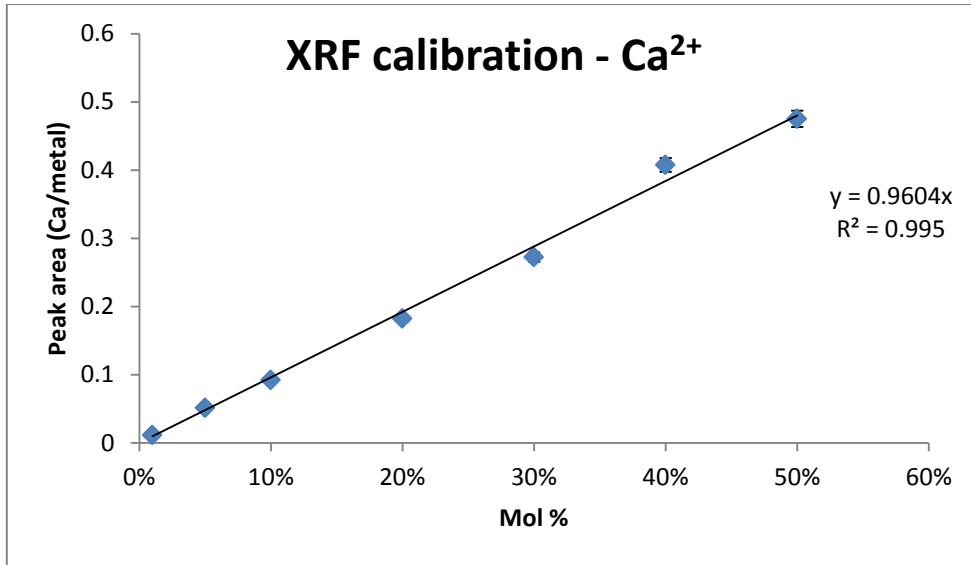


Figure 4.XRF calibration graph for calcium exchange

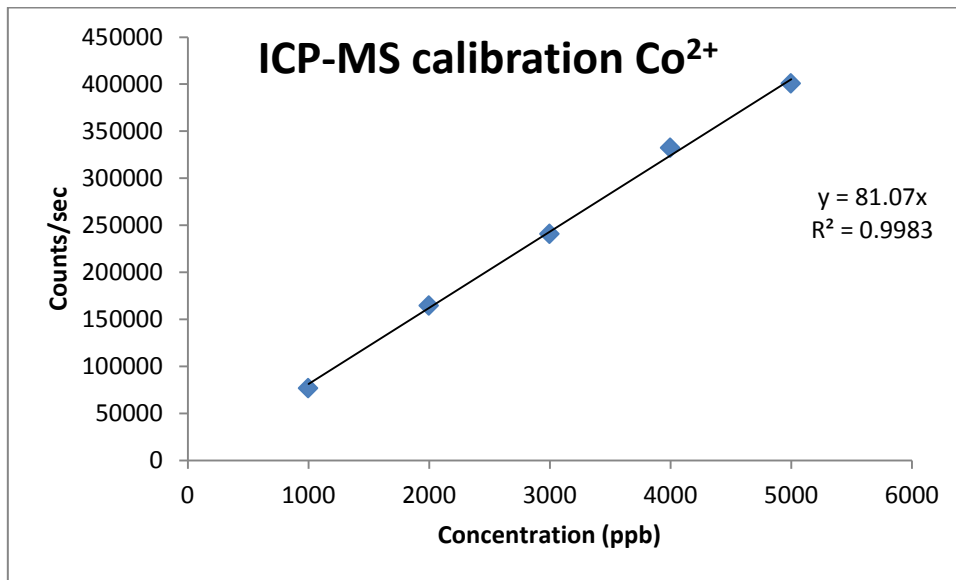


Figure 5.ICPMS calibration graph for cobalt exchange

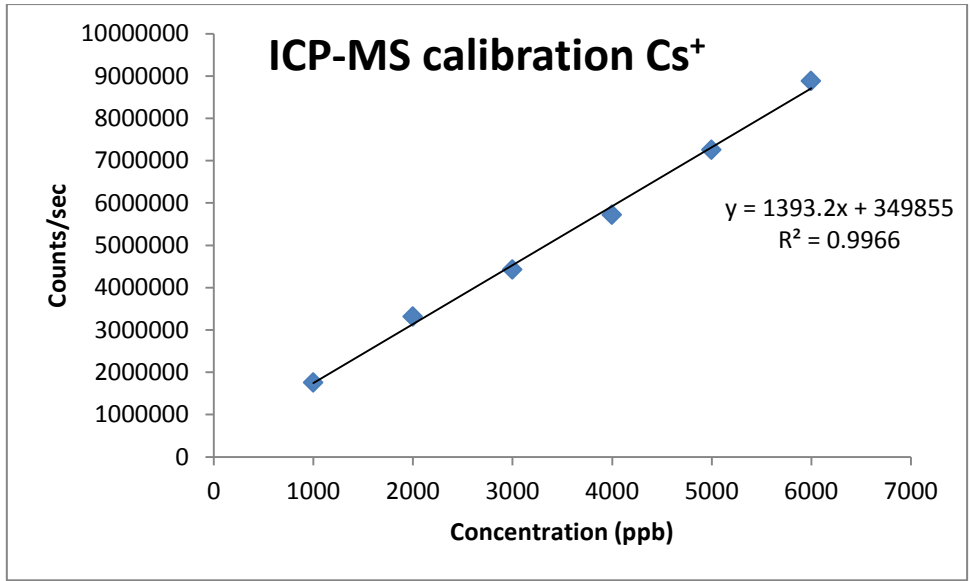


Figure 6. ICPMS calibration graph for caesium exchange

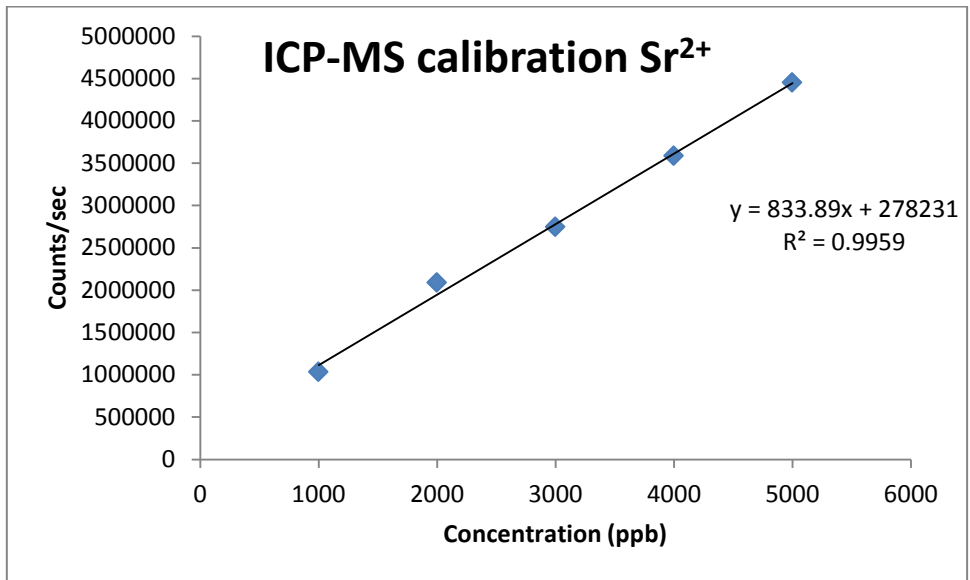


Figure 7. ICPMS calibration graph for strontium exchange

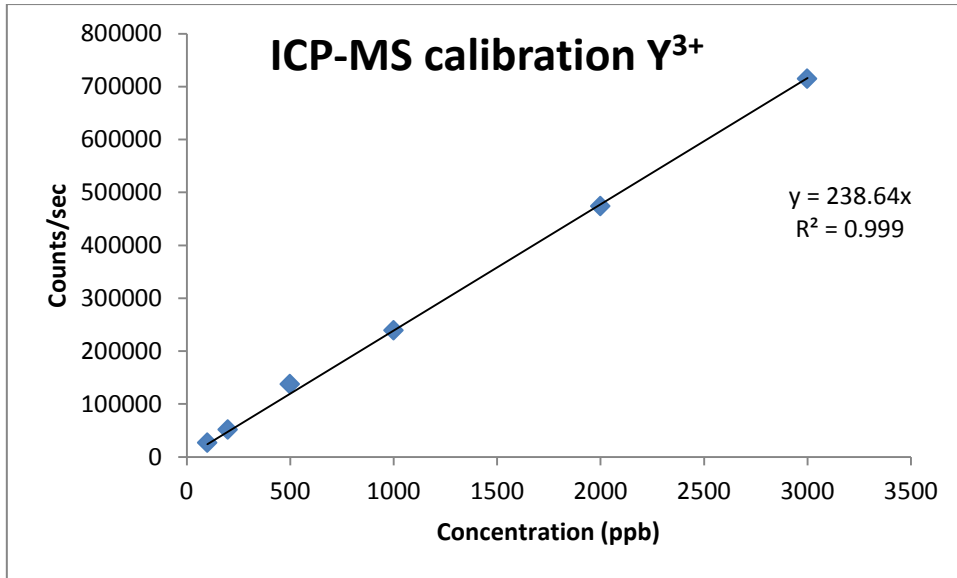


Figure 8. ICPMS calibration graph for yttrium exchange

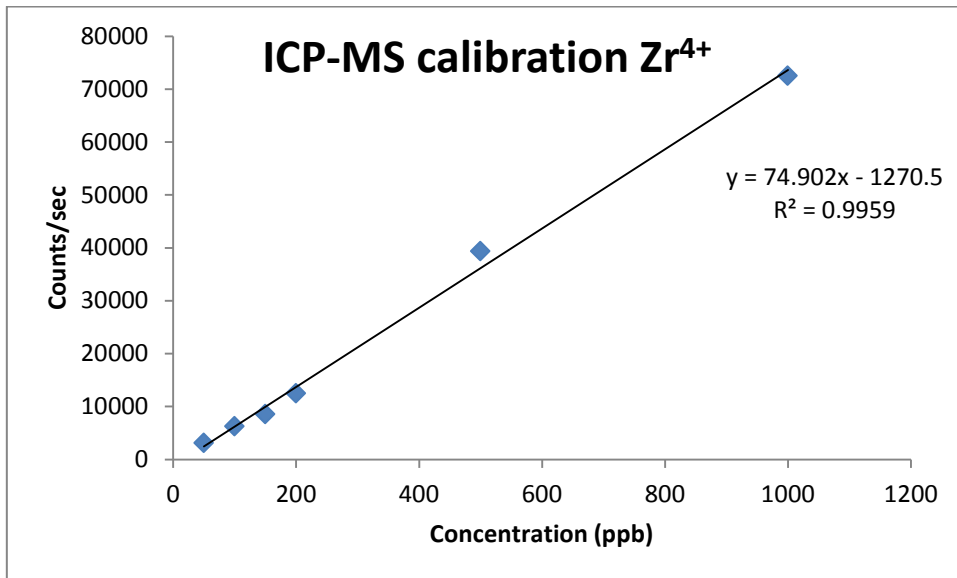


Figure 9. ICPMS calibration graph for zirconium exchange

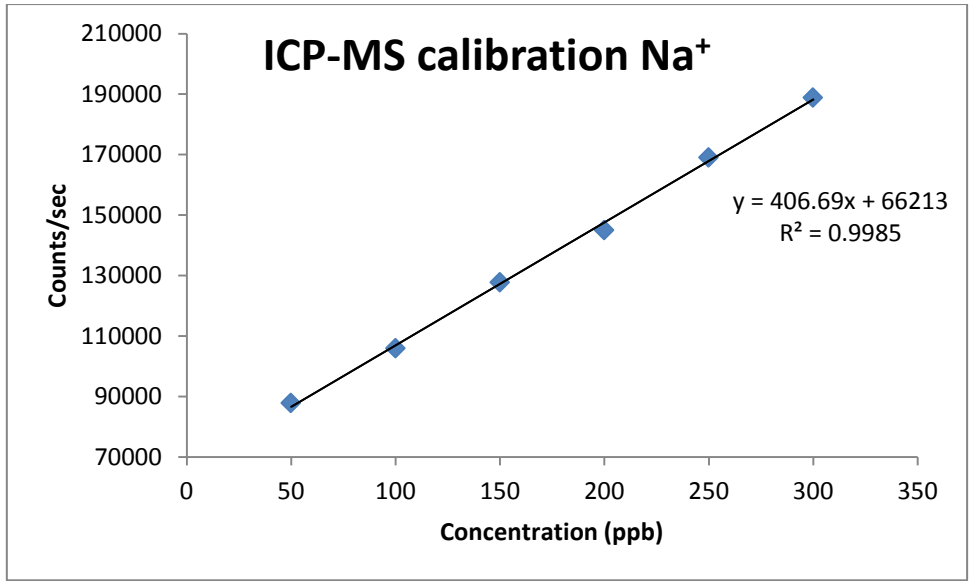


Figure 10. ICPMS calibration graph for sodium exchange

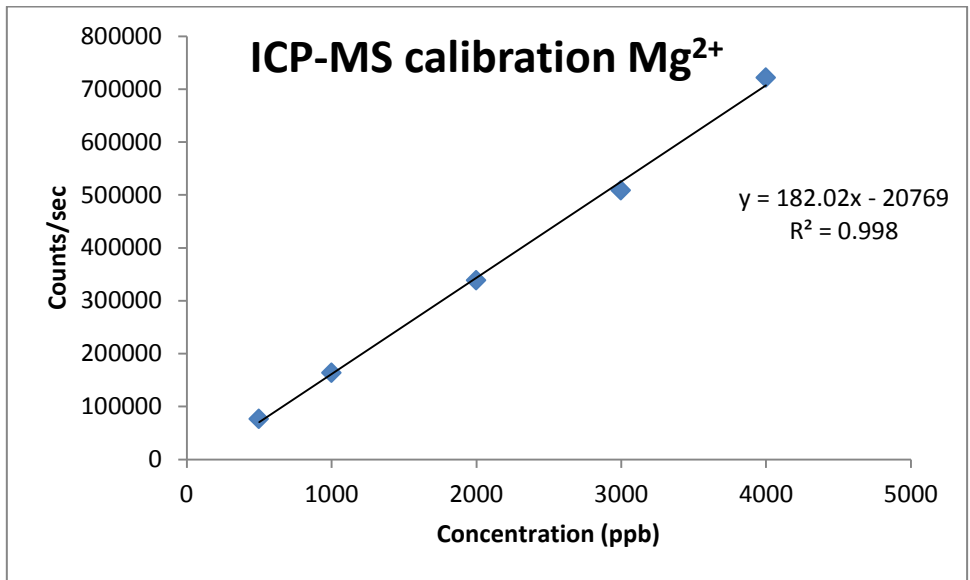


Figure 11. ICPMS calibration graph for magnesium exchange

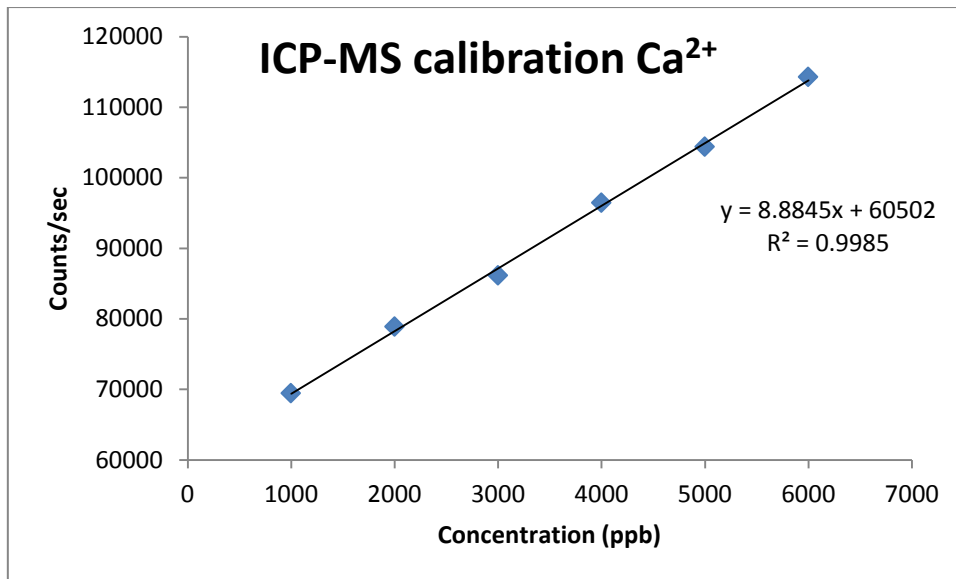


Figure 12. ICPMS calibration graph for calcium exchange

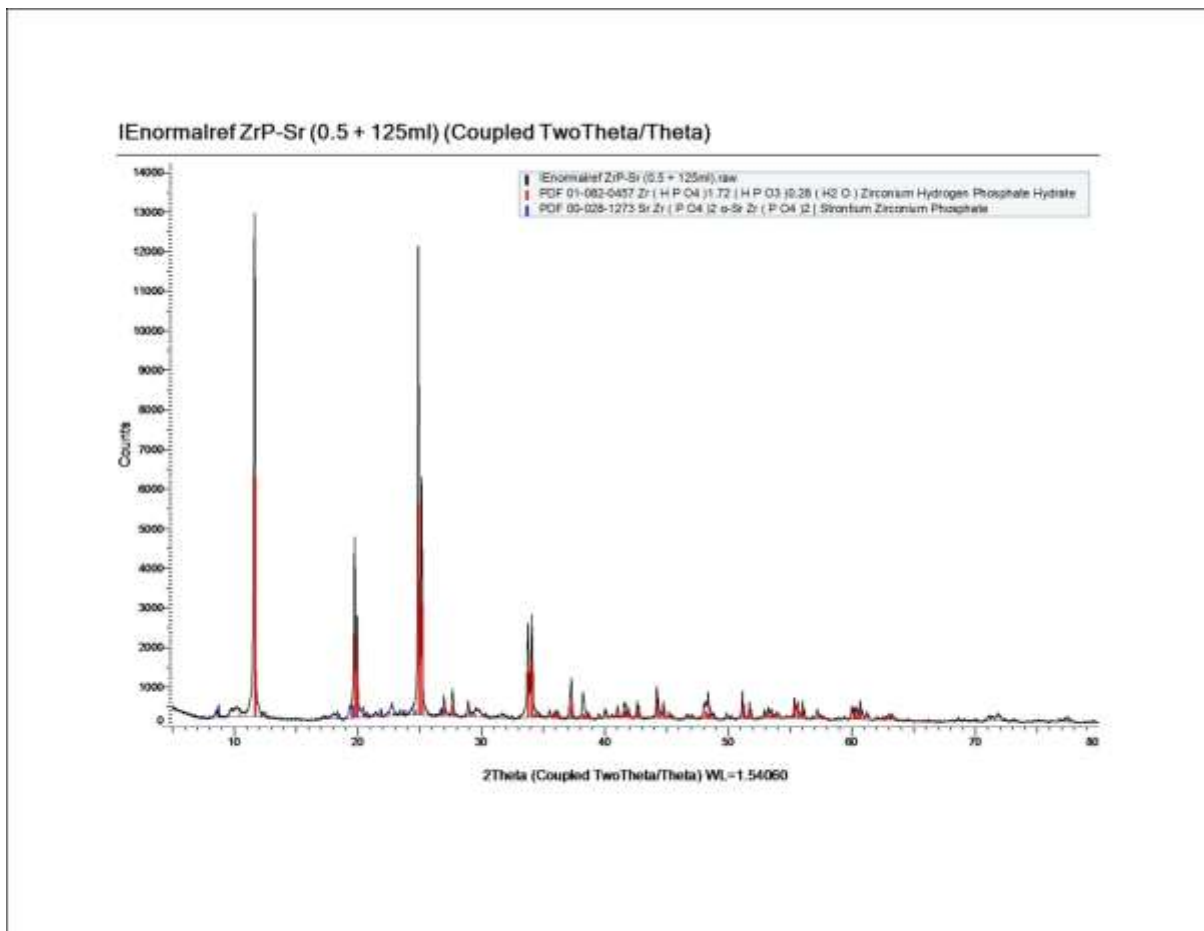


Figure 13. PDF database match for Sr(NO₃)₂ exchange (PDF 00-028-1273)

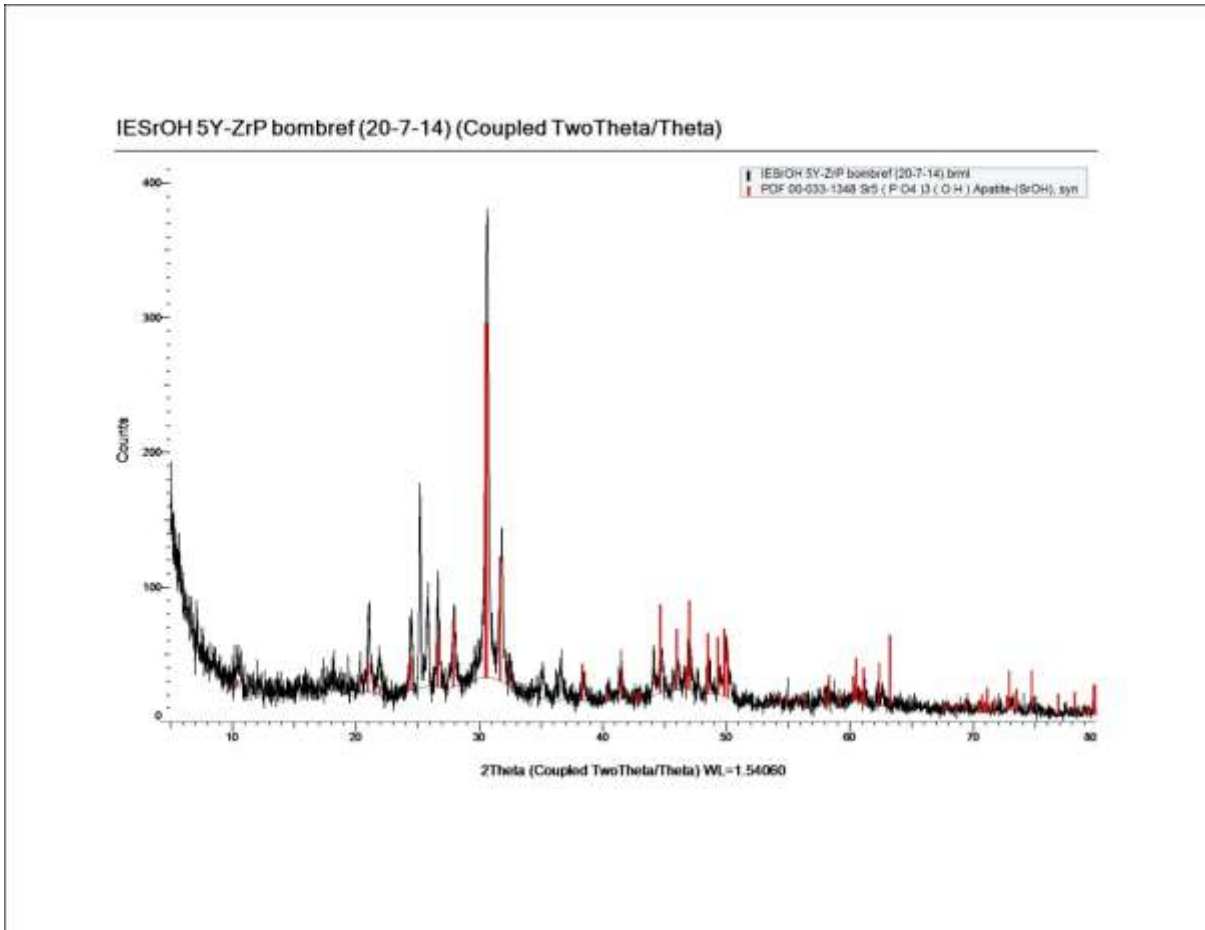


Figure 14. PDF database match for $\text{Sr}(\text{OH})_2$ exchange (PDF 00-033-1348)

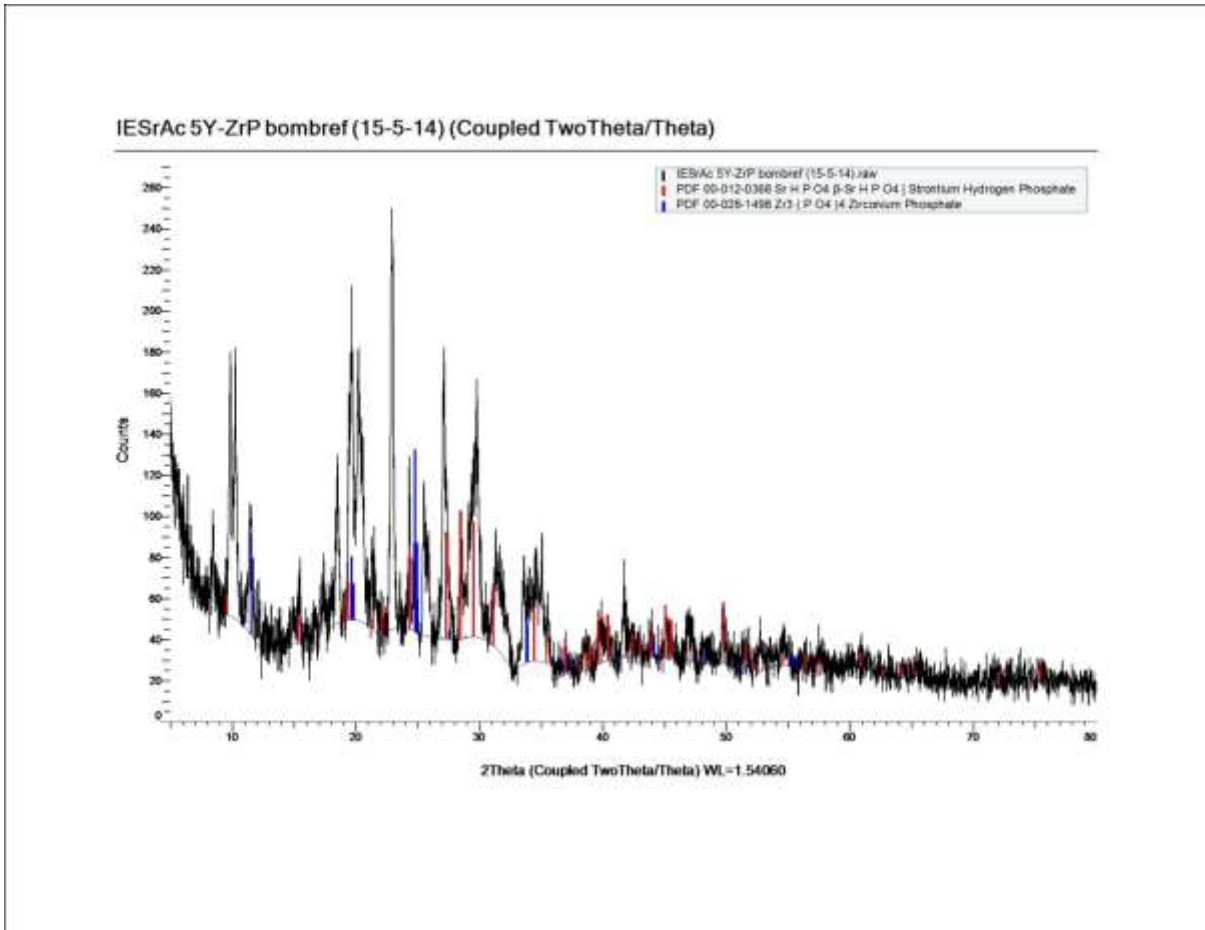


Figure 15. PDF database match for $\text{Sr}(\text{CH}_3\text{CO}_2)_2$ exchange (PDF 00-012-0368)

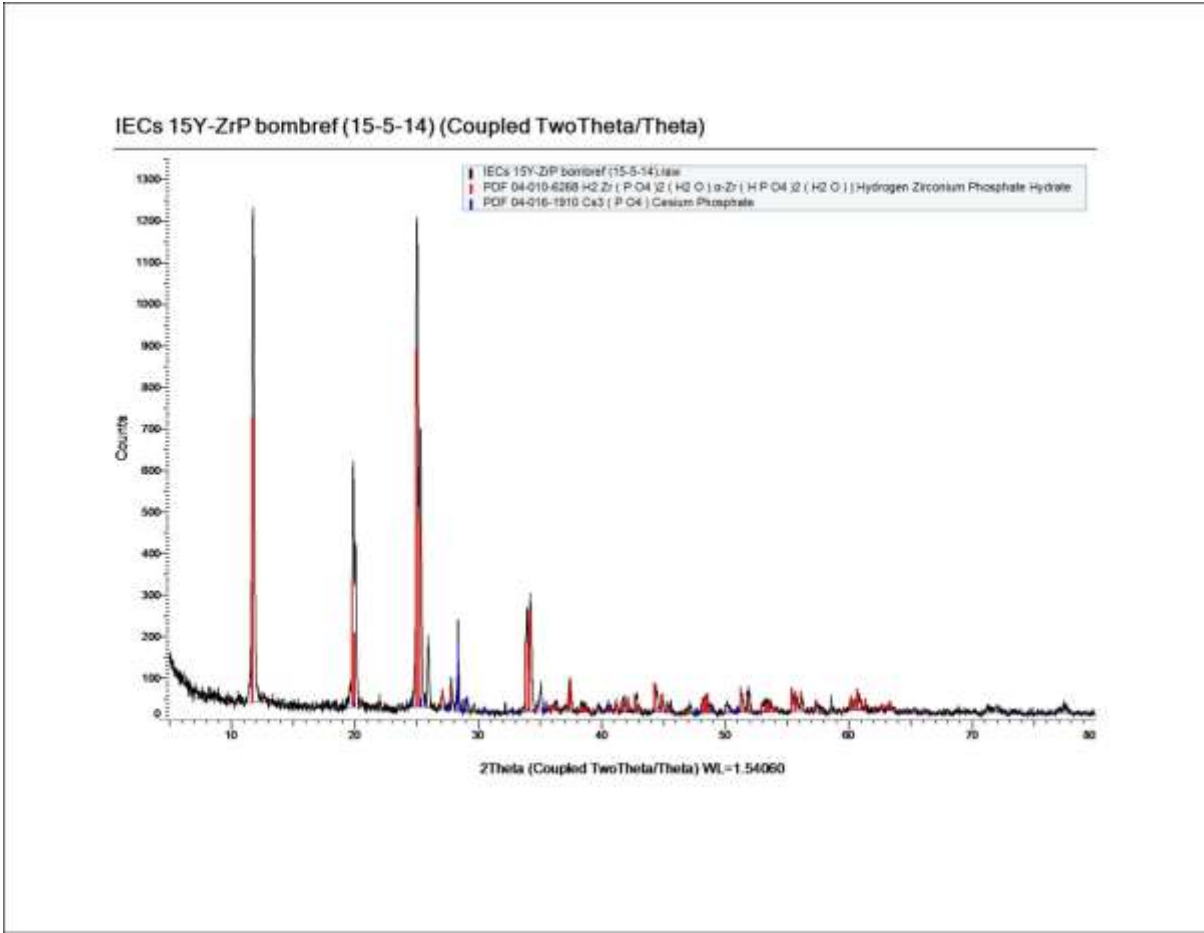


Figure 16.PDF database match for CsNO₃ exchange (PDF 04-016-1910)

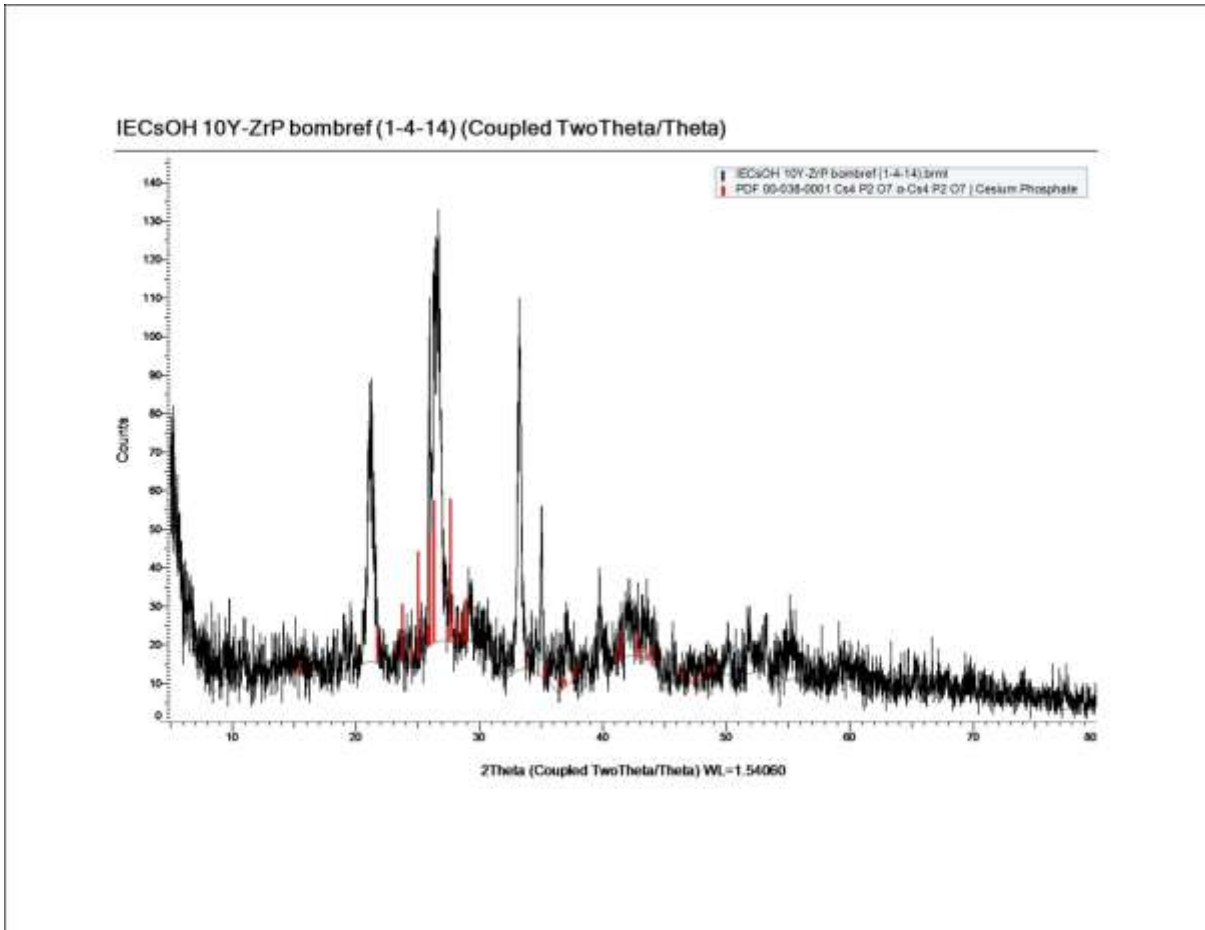


Figure 17.PDF database match for CsOH exchange (PDF 00-038-0001)

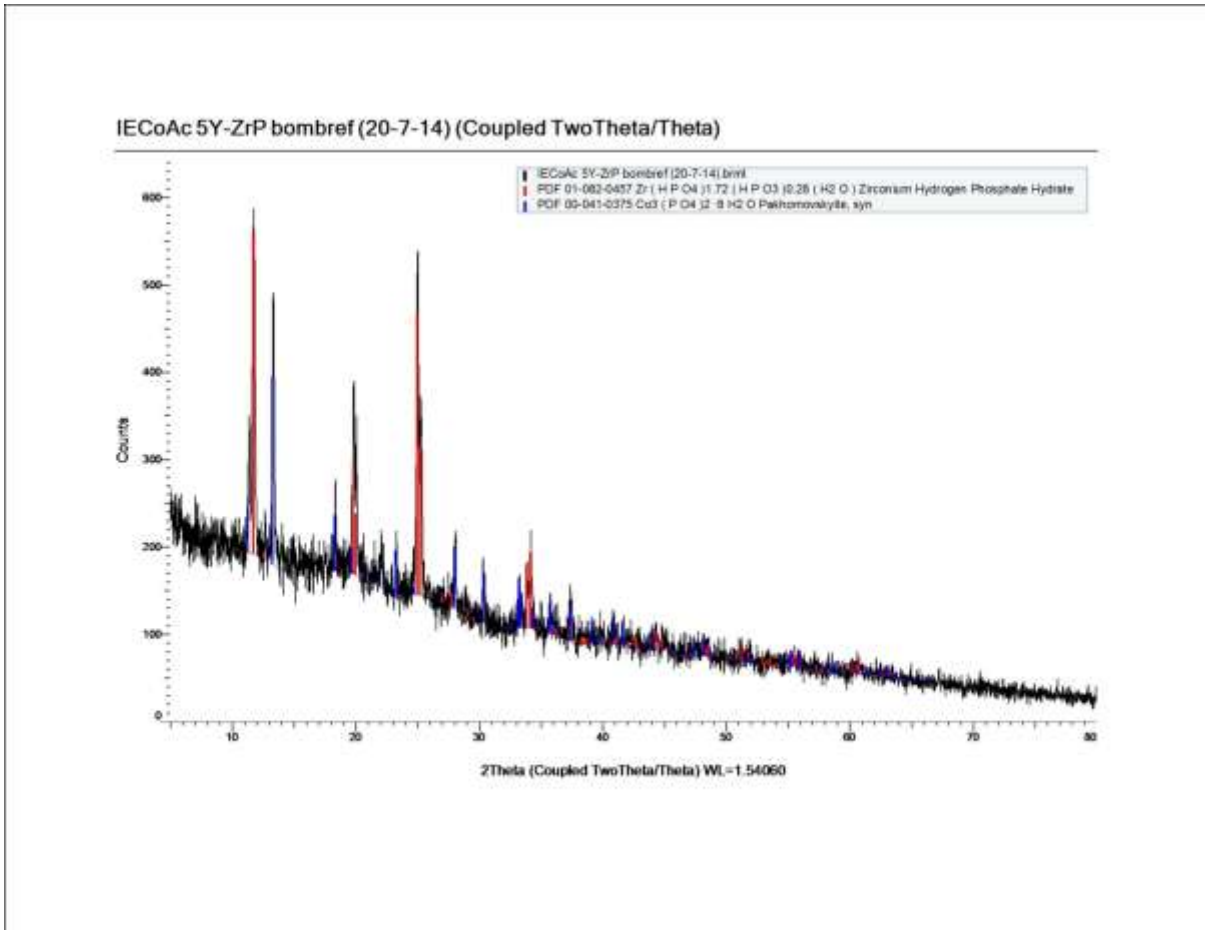


Figure 18. PDF database match for $\text{Co}(\text{CH}_3\text{CO}_2)_2$ exchange (PDF 00-041-0375)

Appendix 4

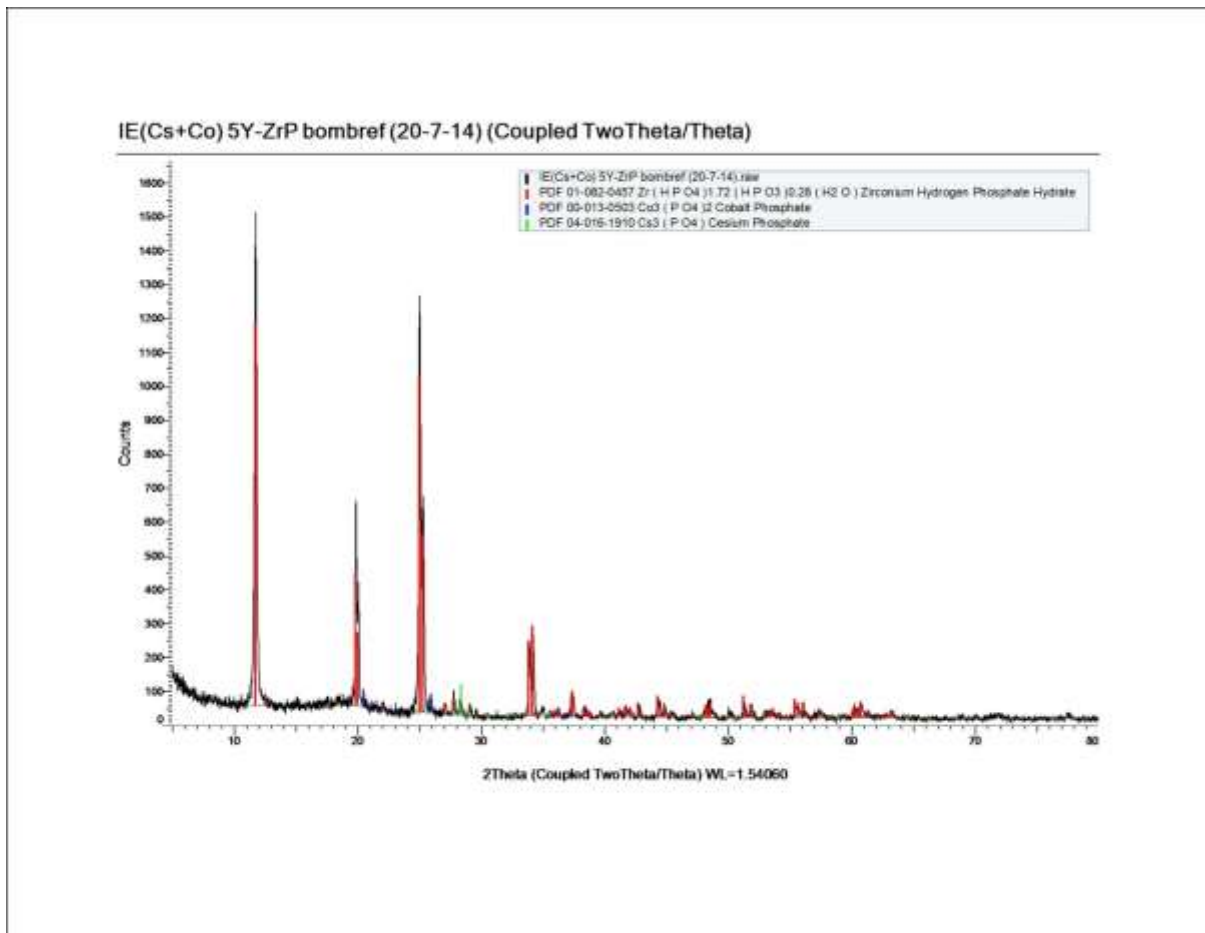


Figure 1. PDF database match for caesium-cobalt exchange (PDF 00-013-0503 and PDF 04-016-1910)

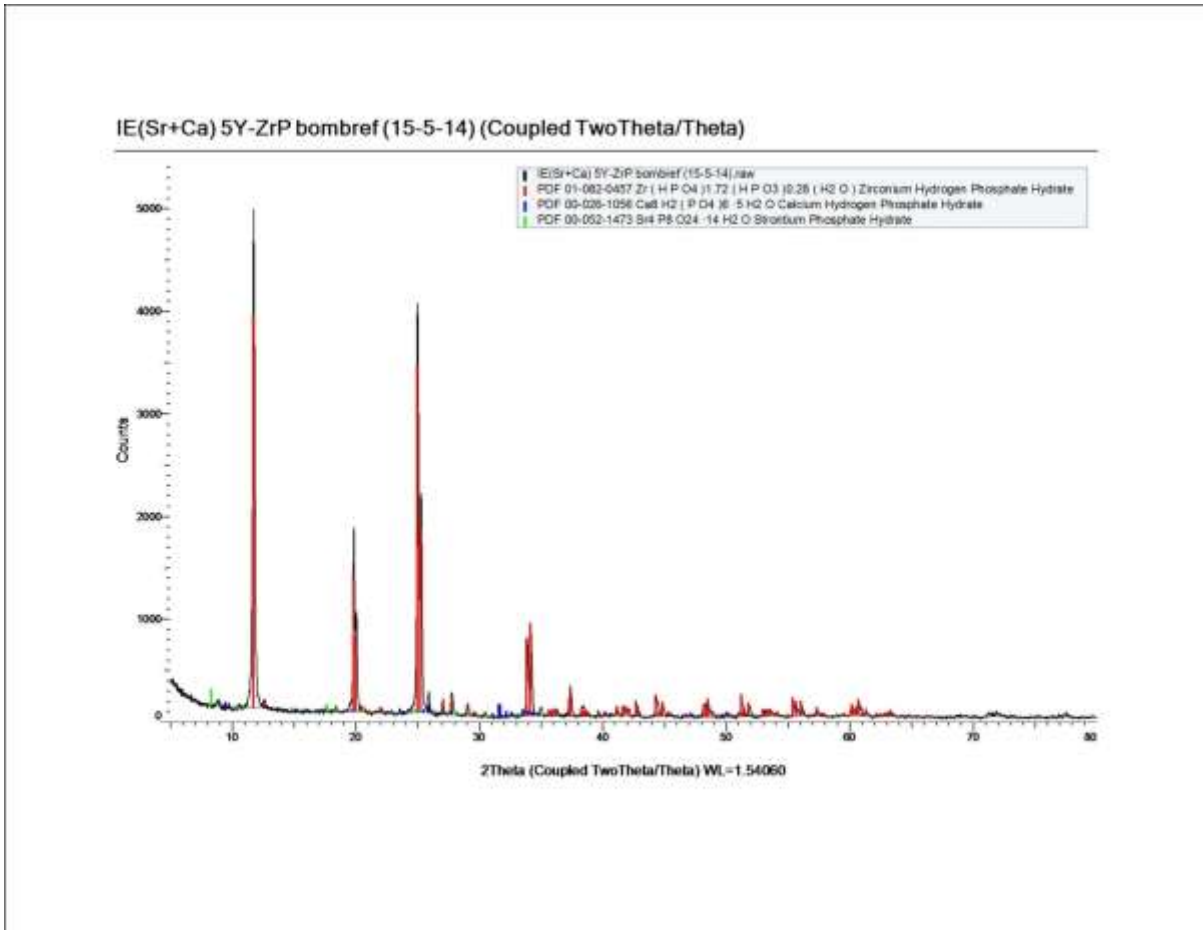


Figure 2. PDF database match for strontium-calcium exchange (PDF 00-026-1056 and PDF 00-052-1473)

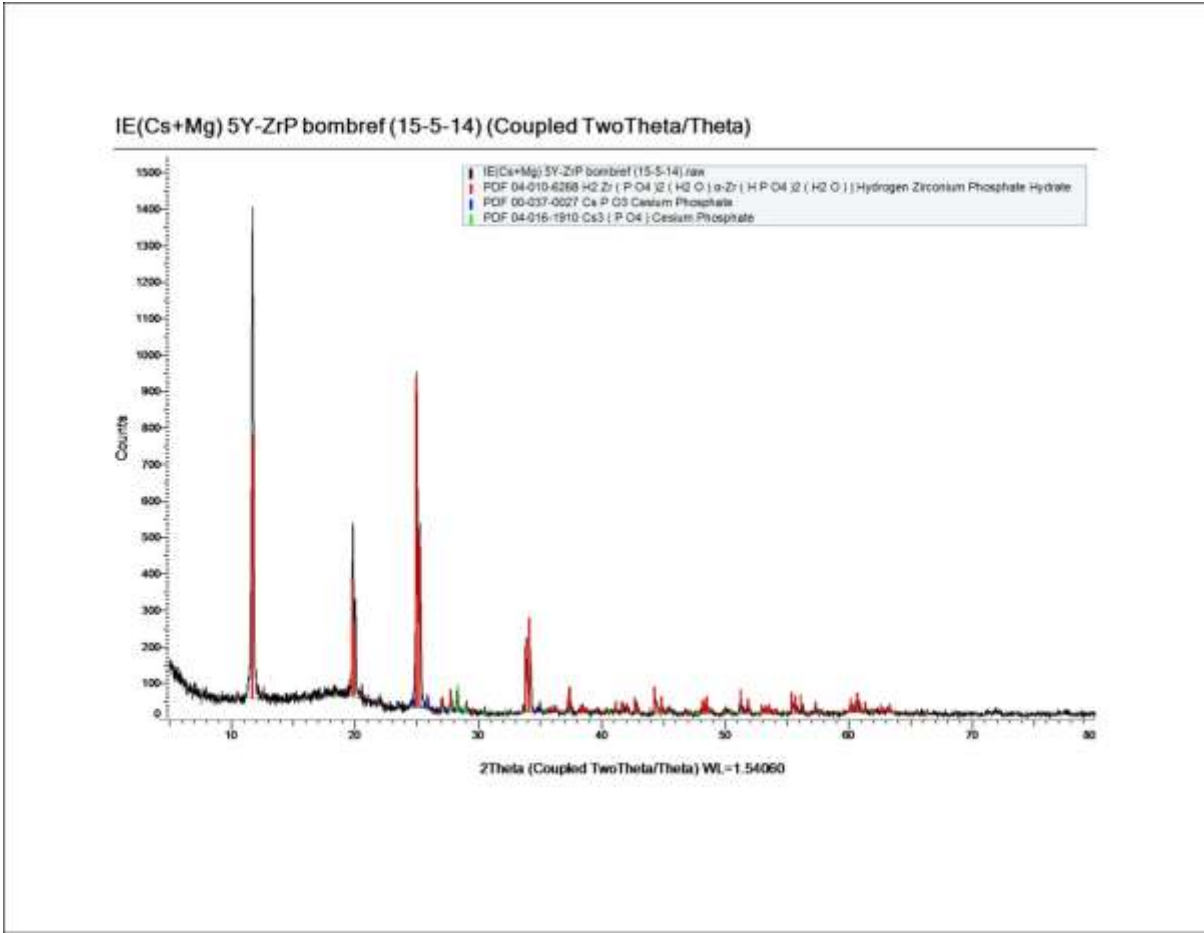


Figure 3. PDF database match for caesium-magnesium exchange (PDF 04-016-1910)

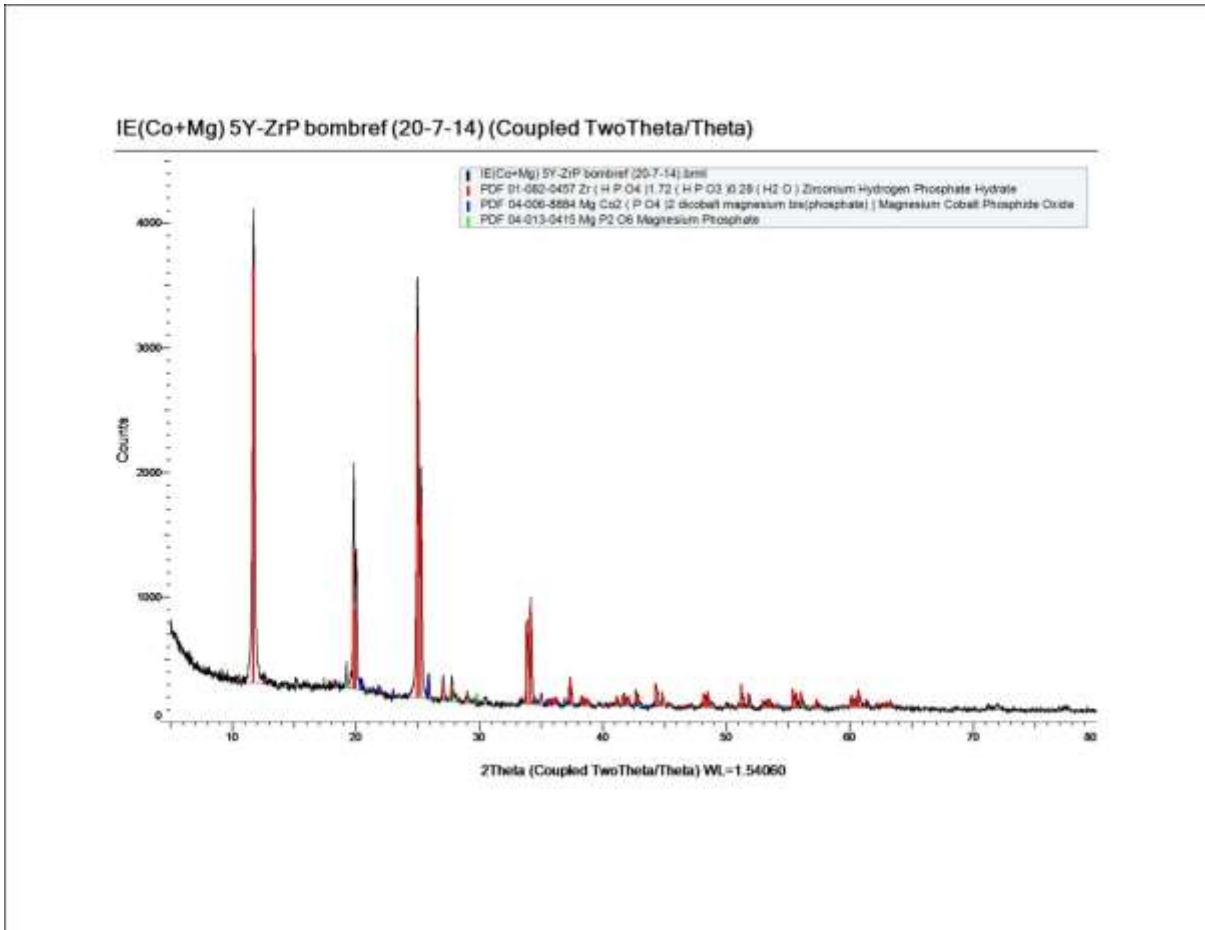


Figure 4. PDF database match for cobalt-magnesium exchange (PDF 04-006-8884 and PDF 04-013-0415)

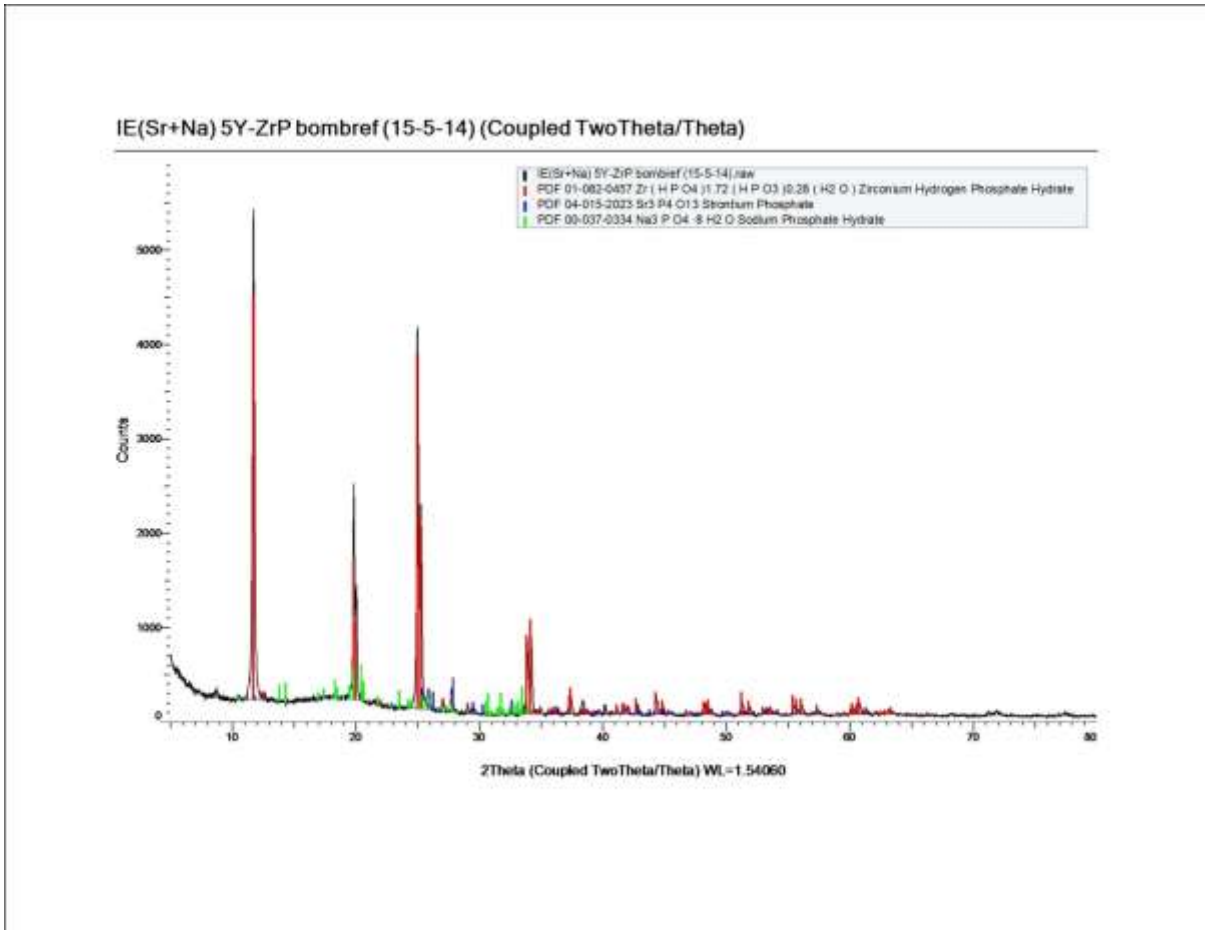


Figure 5. PDF database match for strontium-sodium exchange (PDF 04-015-2023 and PDF 00-037-0334)

Appendix 5

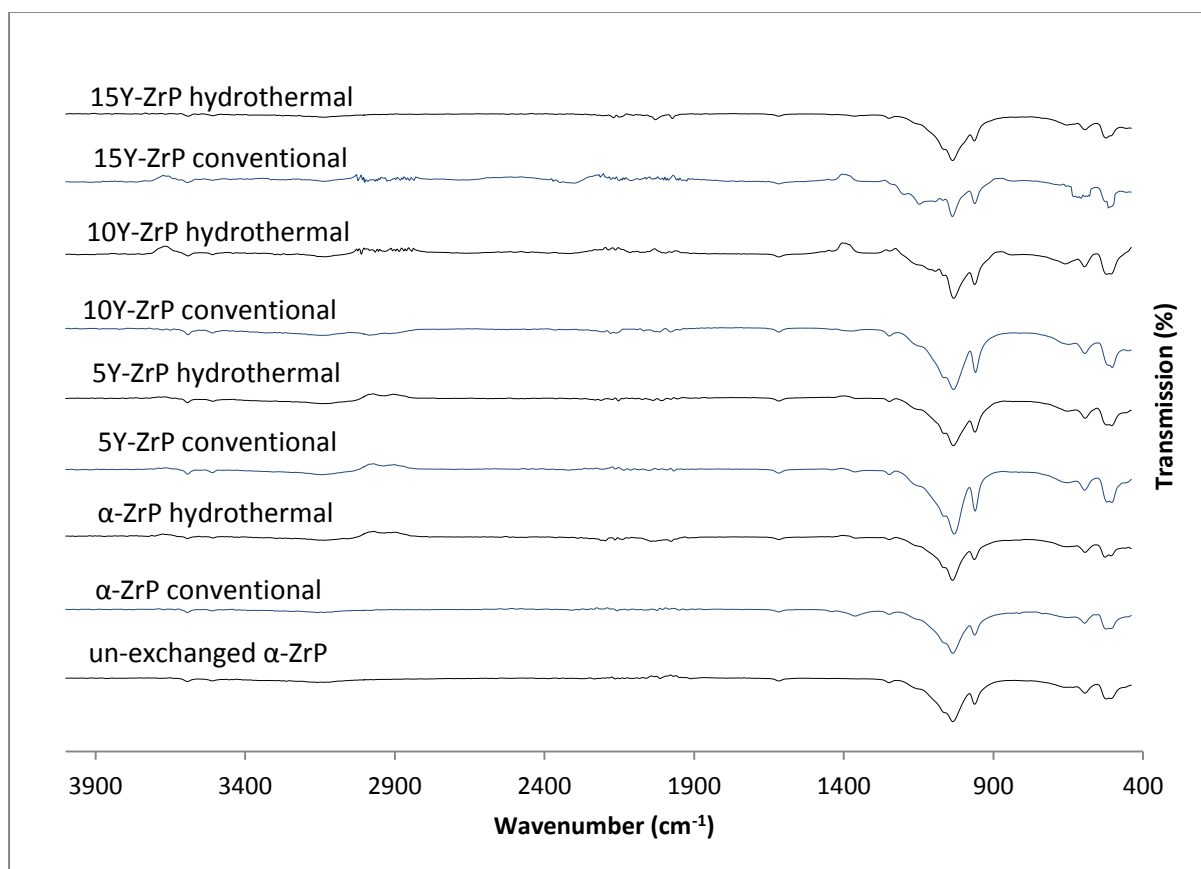


Figure 1. FT-IR analysis for strontium-caesium ion exchange

Table 1. Summary of FT-IR results for strontium-caesium exchange

Peak Wavenumber (cm ⁻¹)	Chemical bonds
505.24	P-O-P vibration
594.06	P-OH (out of plane)
652.93	O-H (out of plane)
962.07	P-O bending (in plane)
1033.99	P-O stretching (asym)
1247.78	P-O-H deformation
1617.04	O-H bending (asym)
2152.83	P-OH
3141.66	O-H stretching (sym)
3507.35	O-H stretching (asym)
3592.75	O-H stretching (asym)

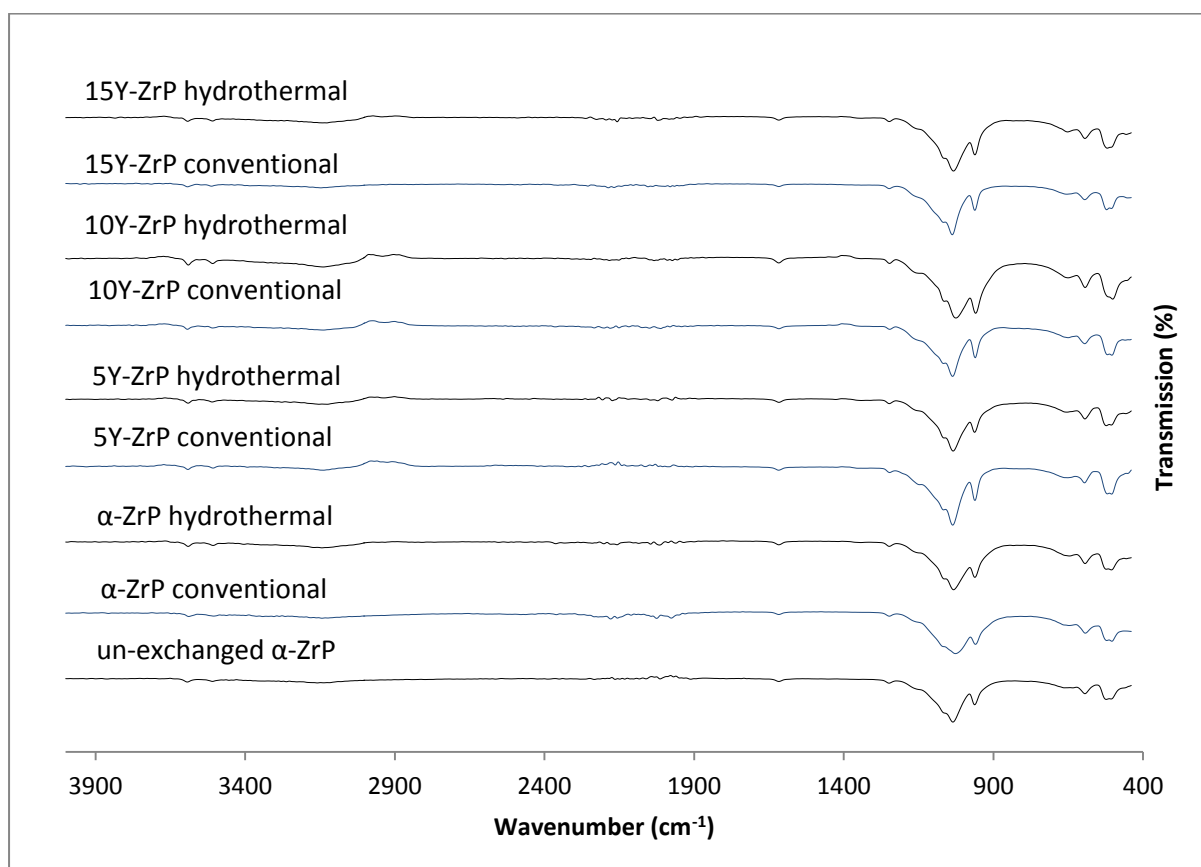


Figure 2. FT-IR analysis of the caesium-cobalt exchange

Table 2. Summary of FT-IR results for caesium-cobalt exchange

Peak Wavenumber (cm ⁻¹)	Chemical bonds
505.91	P-O-P vibration
595.92	P-OH (out of plane)
652.56	O-H (out of plane)
962.12	P-O bending (in plane)
1036.27	P-O stretching (asym)
1246.80	P-O-H deformation
1617.74	O-H bending (asym)
2163.85	P-OH
3138.51	O-H stretching (sym)
3507.33	O-H stretching (asym)
3591.37	O-H stretching (asym)

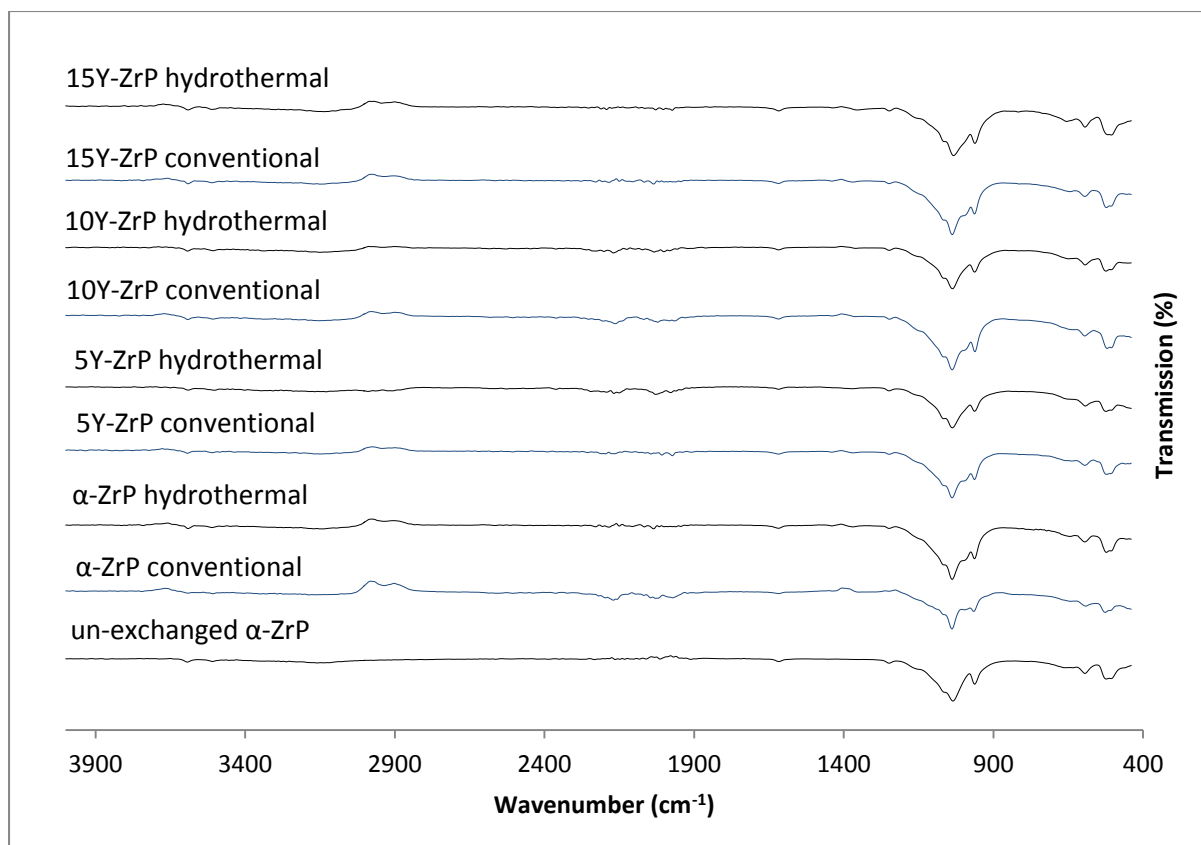


Figure 3. FT-IR of strontium-cobalt exchange

Table 3. Summary of FT-IR peaks for strontium-cobalt exchange

Peak Wavenumber (cm ⁻¹)	Chemical bonds
522.75	P-O-P vibration
594.93	P-OH (out of plane)
644.36	O-H (out of plane)
963.54	P-O bending (in plane)
1037.97	P-O stretching (asym)
1248.55	P-O-H deformation
1618.53	O-H bending (asym)
2184.94	P-OH
3149.55	O-H stretching (sym)
3510.76	O-H stretching (asym)
3590.72	O-H stretching (asym)

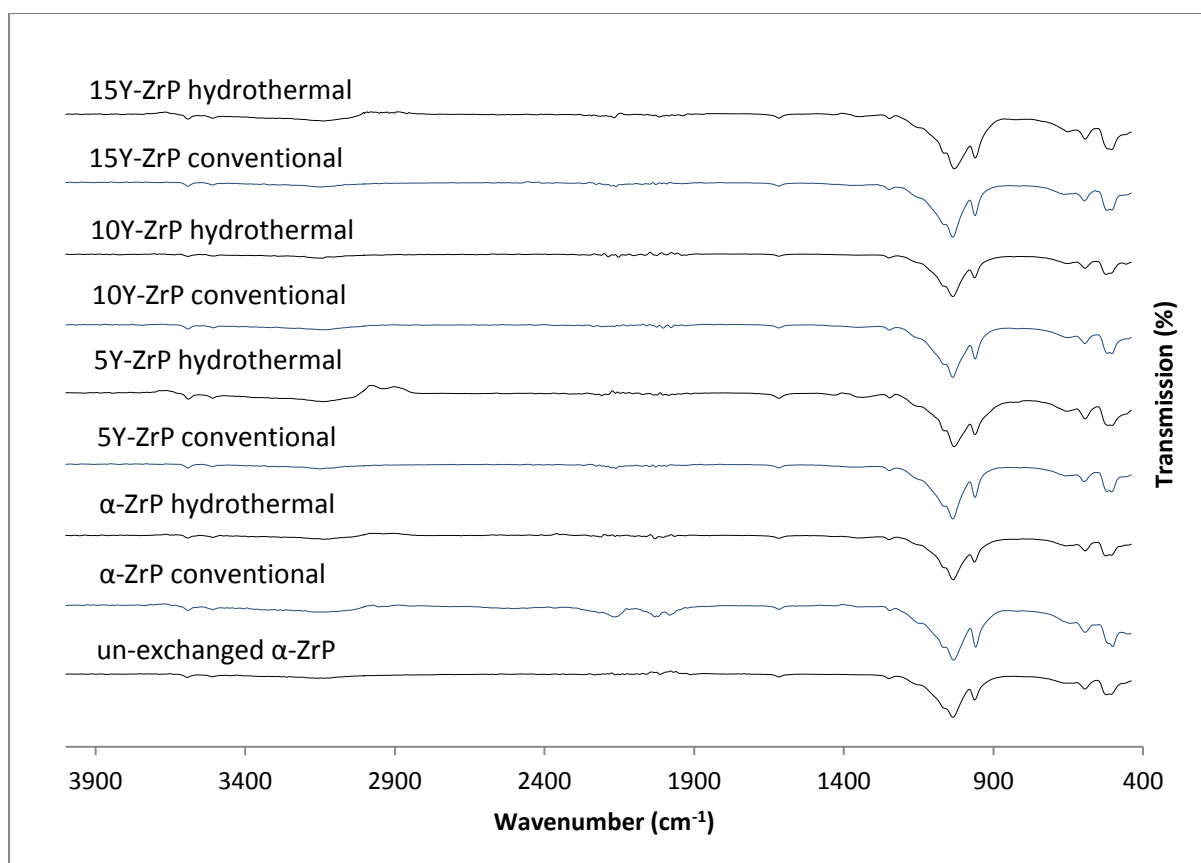


Figure 4. FT-IR of strontium-caesium-cobalt exchange

Table 4. Summary of FT-IR peaks for strontium-caesium-cobalt exchange

Peak Wavenumber (cm ⁻¹)	Chemical bonds
505.31	P-O-P vibration
593.74	P-OH (out of plane)
653.27	O-H (out of plane)
961.68	P-O bending (in plane)
1031.40	P-O stretching (asym)
1246.55	P-O-H deformation
1616.93	O-H bending (asym)
2163.36	P-OH
3139.58	O-H stretching (sym)
3508.62	O-H stretching (asym)
3589.68	O-H stretching (asym)

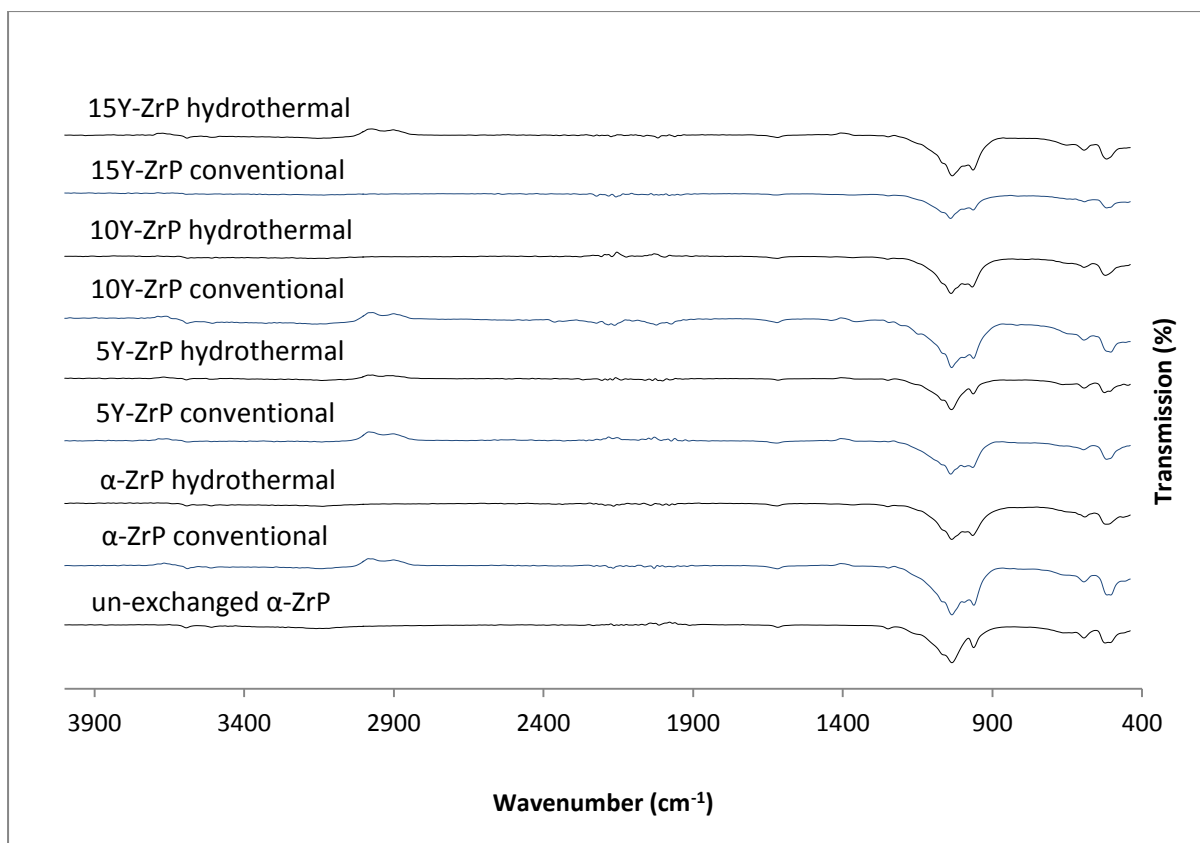


Figure 5. FT-IR results for strontium-calcium exchange

Table 5. Summary of FT-IR peaks for strontium-calcium exchange

Peak Wavenumber (cm ⁻¹)	Chemical bonds
519.55	P-O-P vibration
591.55	P-OH (out of plane)
966.09	P-O bending (in plane)
1036.06	P-O stretching (asym)
1249.62	P-O-H deformation
1619.91	O-H bending (asym)
2166.13	P-OH
3138.69	O-H stretching (sym)
3509.81	O-H stretching (asym)
3591.48	O-H stretching (asym)

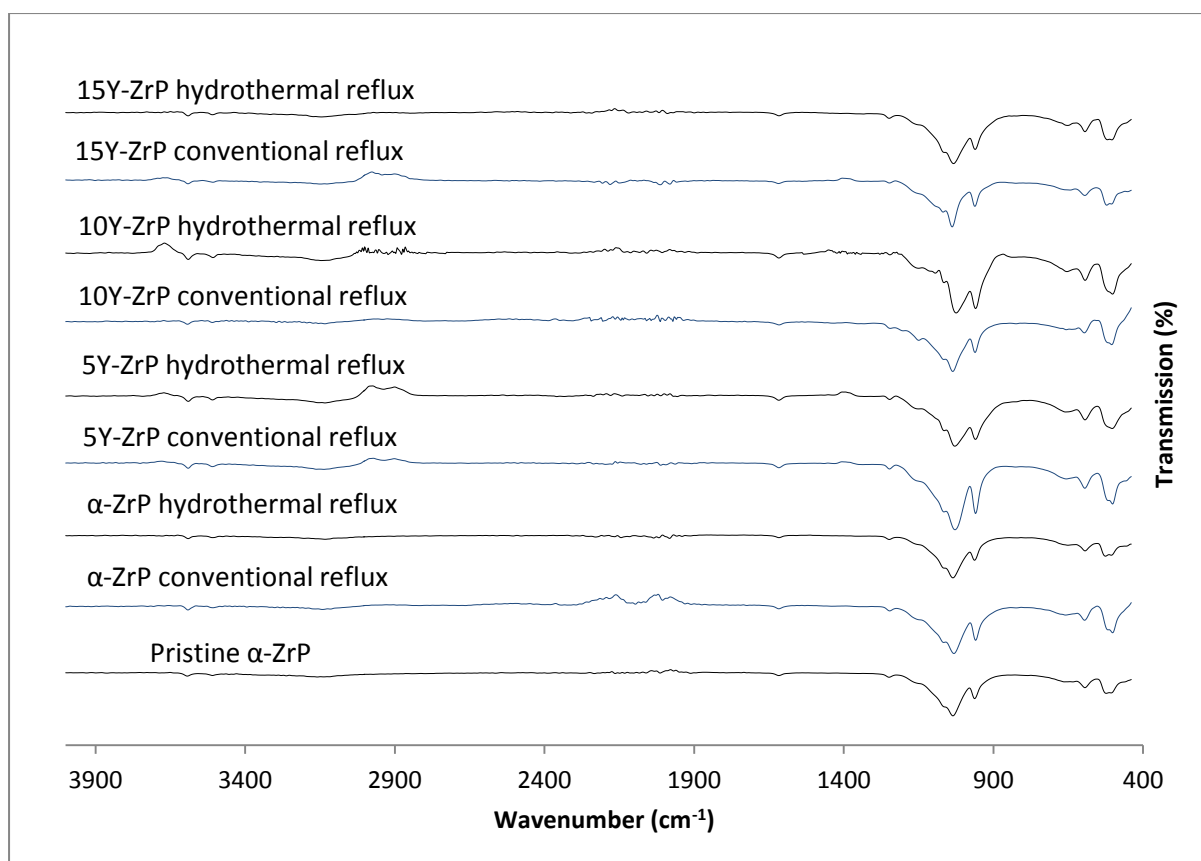


Figure 6. FT-IR results for caesium-calcium exchange

Table 6. Summary of FT-IR peaks for caesium-calcium exchange

Peak Wavenumber (cm ⁻¹)	Chemical bonds
503.69	P-O-P vibration
594.13	P-OH (out of plane)
658.55	O-H (out of plane)
960.21	P-O bending (in plane)
1029.01	P-O stretching (asym)
1246.90	P-O-H deformation
1617.20	O-H bending (asym)
2179.16	P-OH
3133.31	O-H stretching (sym)
3509.14	O-H stretching (asym)
3590.25	O-H stretching (asym)

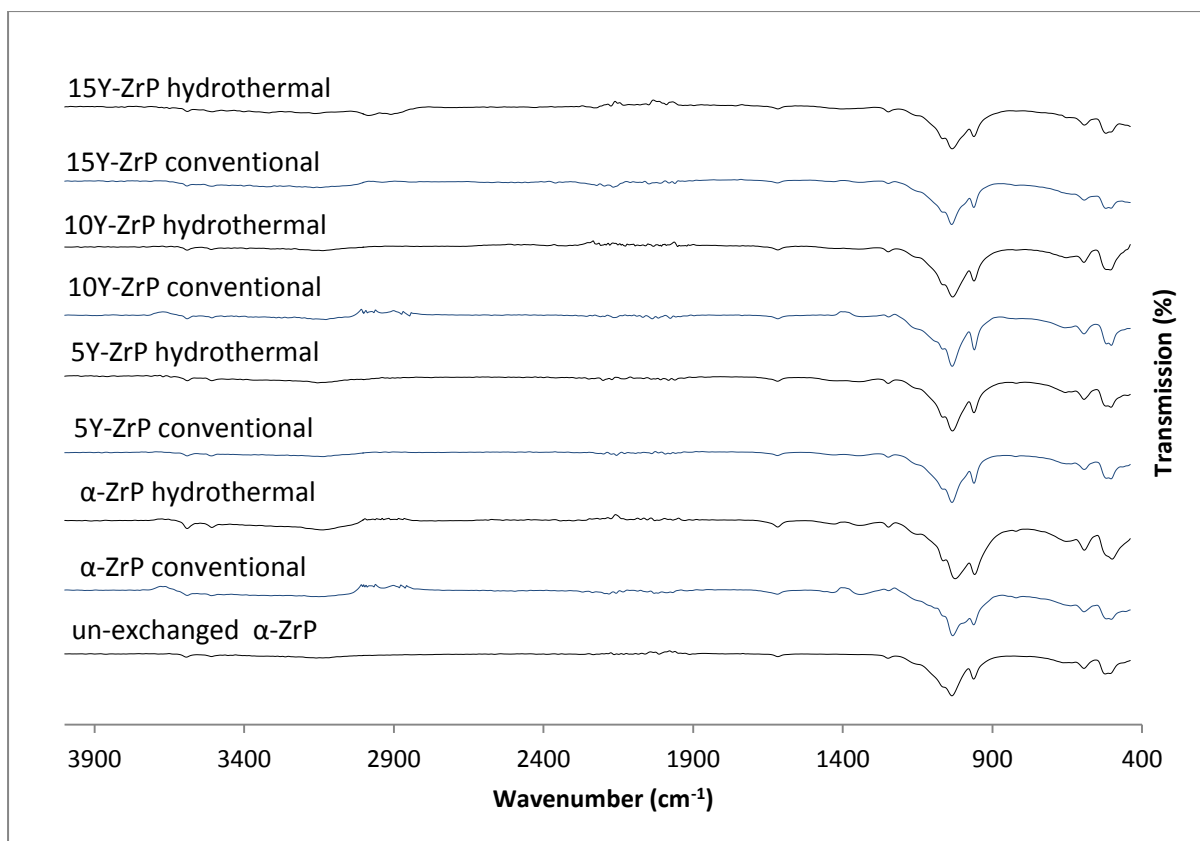


Figure 7. FT-IR results for cobalt-calcium exchange

Table 7. Summary of FT-IR peaks for cobalt-calcium exchange

Peak Wavenumber (cm ⁻¹)	Chemical bonds
500.42	P-O-P vibration
593.25	P-OH (out of plane)
652.80	O-H (out of plane)
959.57	P-O bending (in plane)
1024.53	P-O stretching (asym)
1247.38	P-O-H deformation
1617.65	O-H bending (asym)
2120.05	P-OH
3138.57	O-H stretching (sym)
3507.93	O-H stretching (asym)
3590.40	O-H stretching (asym)

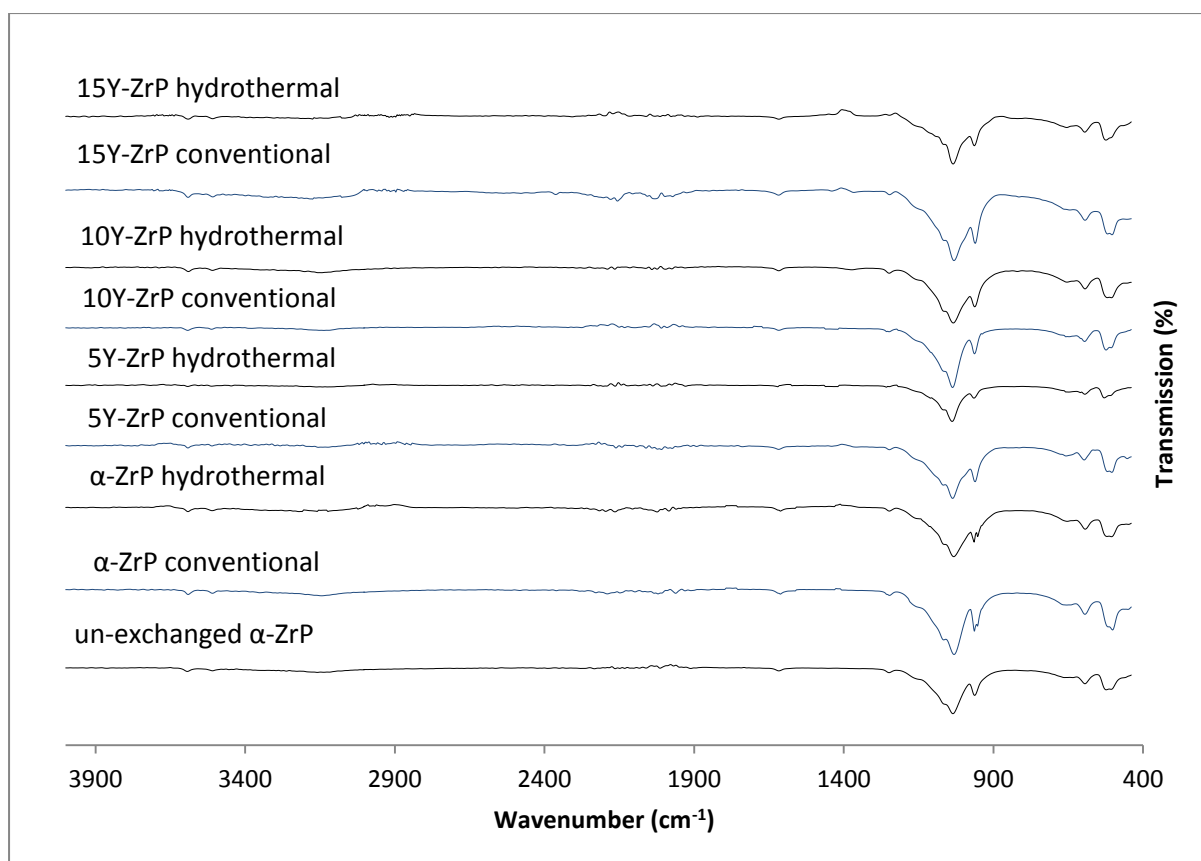


Figure 8. FT-IR spectra for strontium-magnesium exchange

Table 8. Summary of the FT-IR peaks of strontium-magnesium exchange

Peak Wavenumber (cm ⁻¹)	Chemical bonds
506.30	P-O-P vibration
594.15	P-OH (out of plane)
654.47	O-H (out of plane)
962.74	P-O bending (in plane)
1034.31	P-O stretching (asym)
1248.38	P-O-H deformation
1617.37	O-H bending (asym)
2140.97	P-OH
3144.72	O-H stretching (sym)
3509.18	O-H stretching (asym)
3589.81	O-H stretching (asym)

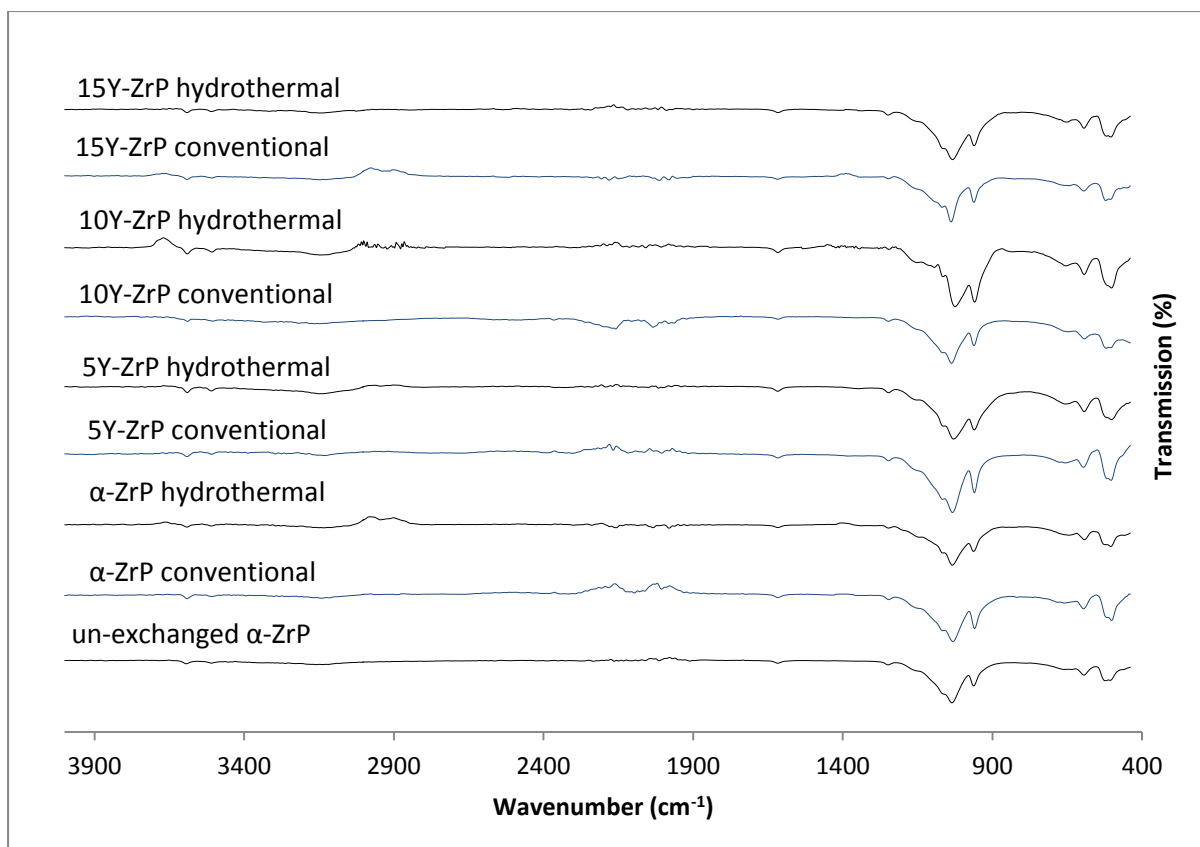


Figure 9. FT-IR spectrums for caesium-magnesium exchange

Table 9. Summary of FT-IR peaks for caesium-magnesium exchange

Peak Wavenumber cm^{-1})	Chemical bonds
502.47	P-O-P vibration
593.67	P-OH (out of plane)
656.29	O-H (out of plane)
960.86	P-O bending (in plane)
1029.72	P-O stretching (asym)
1247.37	P-O-H deformation
1617.66	O-H bending (asym)
2191.72	P-OH
3147.30	O-H stretching (sym)
3509.65	O-H stretching (asym)
3590.33	O-H stretching (asym)

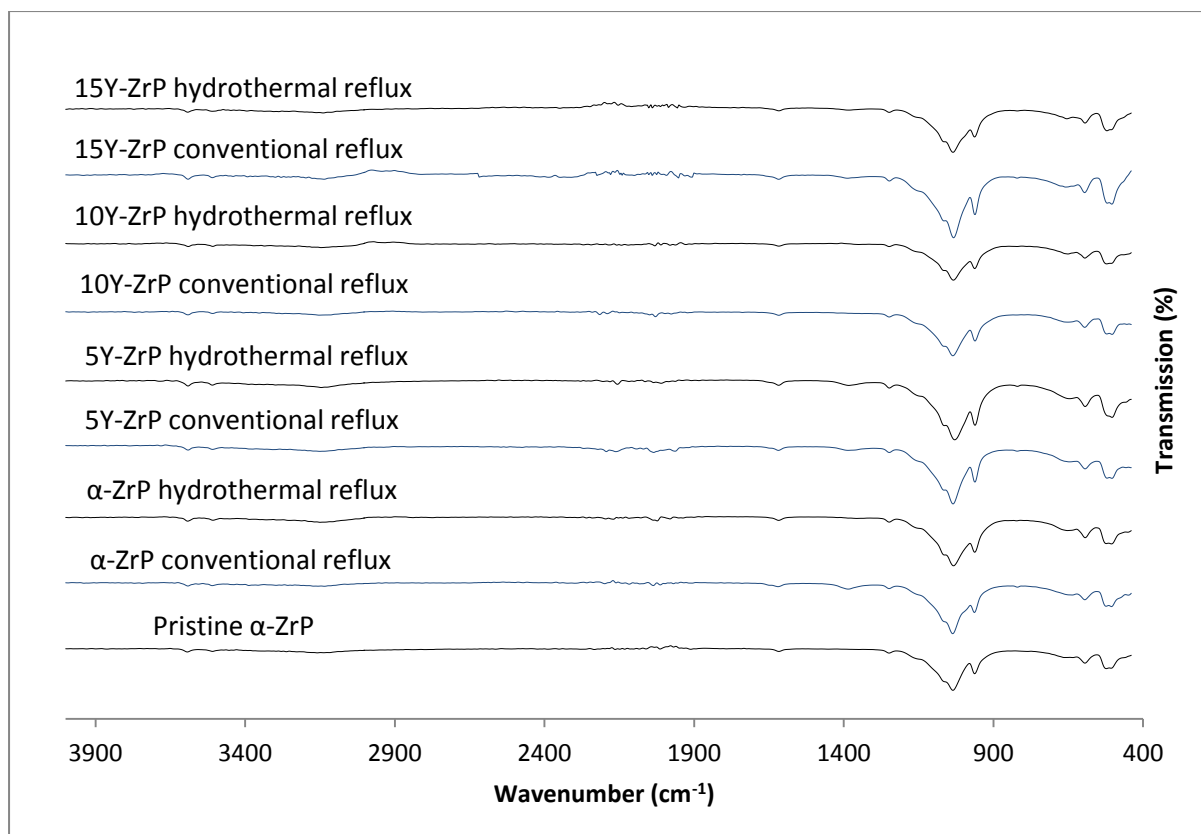


Figure 10. FT-IR spectrums for cobalt-magnesium exchange

Table 10. Summary of FT-IR peaks for cobalt-magnesium exchange

Peak Wavenumber (cm ⁻¹)	Chemical bonds
504.29	P-O-P vibration
593.73	P-OH (out of plane)
645.99	O-H (out of plane)
961.83	P-O bending (in plane)
1029.49	P-O stretching (asym)
1247.97	P-O-H deformation
1617.80	O-H bending (asym)
2156.34	P-OH
3146.15	O-H stretching (sym)
3509.60	O-H stretching (asym)
3591.06	O-H stretching (asym)

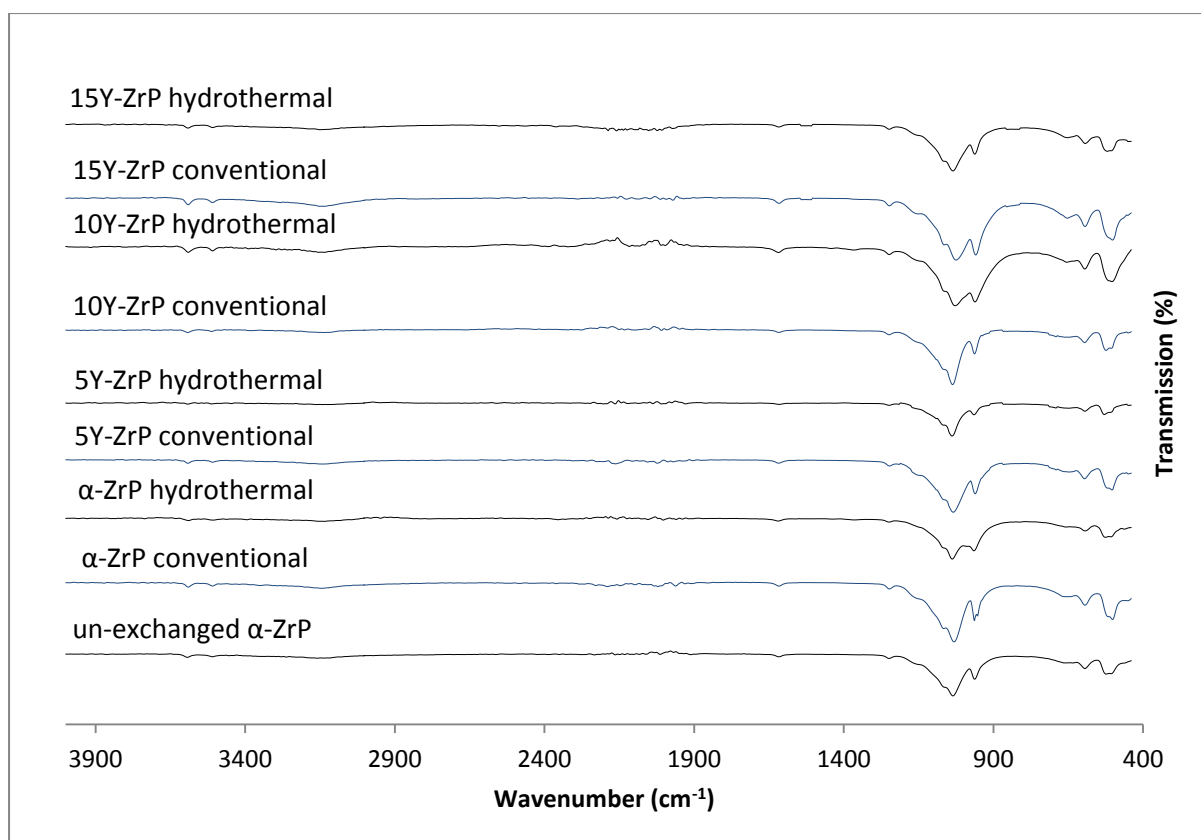


Figure 11. FT-IR results for strontium-sodium exchange

Table 11. Summary of FT-IR peaks for strontium-sodium exchange

Peak Wavenumber (cm ⁻¹)	Chemical bonds
504.52	P-O-P vibration
594.84	P-OH (out of plane)
654.67	O-H (out of plane)
961.82	P-O bending (in plane)
1028.30	P-O stretching (asym)
1248.31	P-O-H deformation
1618.58	O-H bending (asym)
2116.67	P-OH
3136.50	O-H stretching (sym)
3509.08	O-H stretching (asym)
3590.40	O-H stretching (asym)

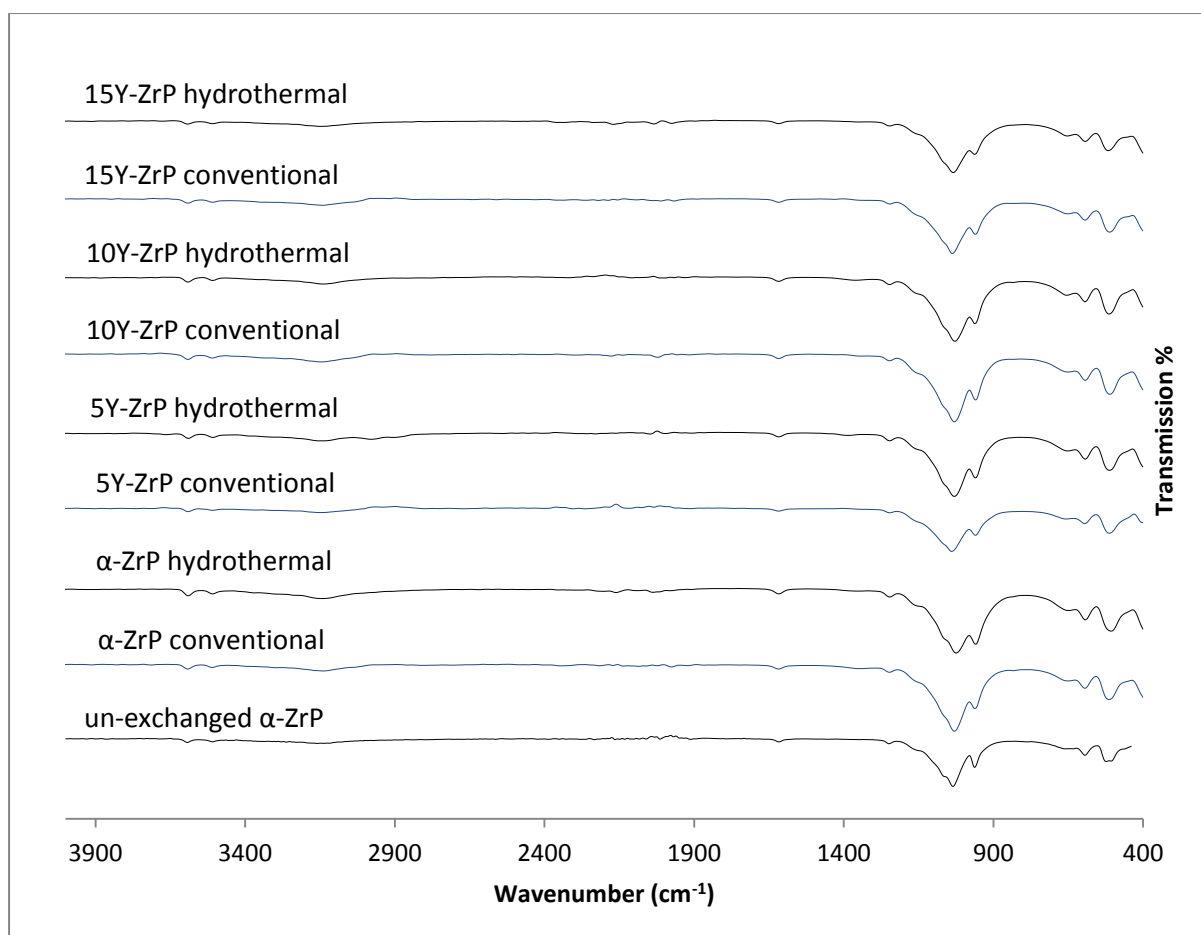


Figure 12. FT-IR results for caesium-sodium exchange

Table 12. Summary of FT-IR peaks for caesium-sodium exchange

Peak Wavenumber (cm ⁻¹)	Chemical bonds
513.60	P-O-P vibration
594.19	P-OH (out of plane)
654.74	O-H (out of plane)
962.31	P-O bending (in plane)
1029.07	P-O stretching (asym)
1247.22	P-O-H deformation
1617.80	O-H bending (asym)
2108.21	P-OH
3138.70	O-H stretching (sym)
3508.70	O-H stretching (asym)
3591.23	O-H stretching (asym)

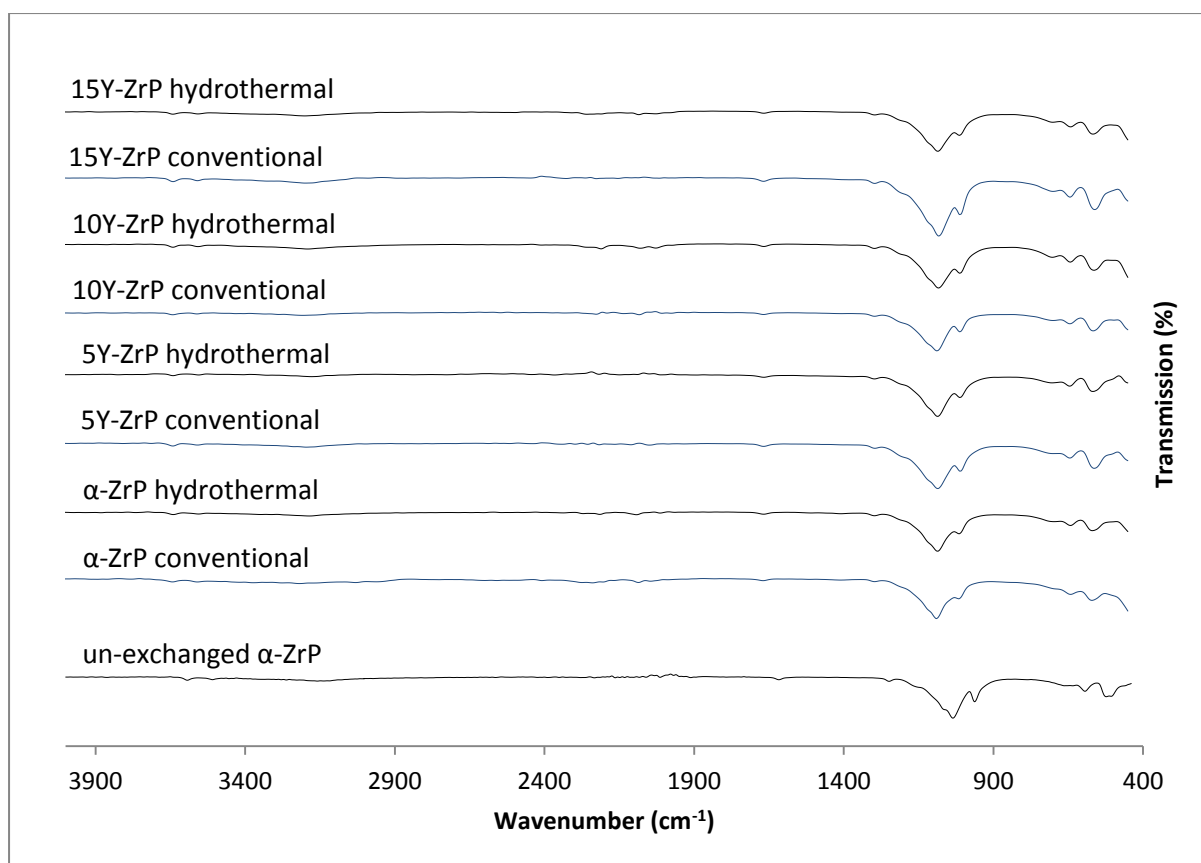


Figure 13. FT-IR results for cobalt-sodium exchange

Table 13. Summary of FT-IR peaks for cobalt-sodium exchange

Peak Wavenumber (cm ⁻¹)	Chemical bonds
514.17	P-O-P vibration
593.57	P-OH (out of plane)
653.29	O-H (out of plane)
962.86	P-O bending (in plane)
1033.87	P-O stretching (asym)
1247.61	P-O-H deformation
1617.60	O-H bending (asym)
1978.10	Na-O-P (unidentified)
2029.70	Na-O-P (unidentified)
2161.25	P-OH
3141.84	O-H stretching (sym)
3507.77	O-H stretching (asym)
3591.53	O-H stretching (asym)

Appendix 6

Table 1: Refined peaks for Sr(NO₃)₂ exchange of 5% Y-ZrP hydrothermal

2T(Obs) (°)	2Th(Cal) (°)	Difference (°)
11.7095	11.696	0.0135
19.827	19.8012	0.0258
20.05	20.0334	0.0166
24.9908	24.9618	0.029
25.2884	25.278	0.0104
25.89	25.9581	-0.0681
27.6873	27.6982	-0.0109
29.0262	29.012	0.0142
29.6213	29.5958	0.0255
33.8779	33.8725	0.0054
34.1889	34.1979	-0.009
37.3601	37.3852	-0.0251

Table 2: Refined peaks for Sr(OH)₂ exchange of 5% Y-ZrP hydrothermal

2T(Obs) (°)	2Th(Cal) (°)	Difference (°)
21.0448	21.0639	-0.0191
21.8853	21.9319	-0.0466
24.4753	24.368	0.1073
25.1946	25.2114	-0.0168
27.0922	27.0357	0.0565
31.8092	31.8257	-0.0165
36.2415	36.2585	-0.017

36.6879	36.7285	-0.0406
37.3573	37.329	0.0283
38.3987	38.4139	-0.0152
44.0877	44.1122	-0.0245
44.7214	44.7233	-0.0019
45.614	45.6286	-0.0146
46.0603	46.0156	0.0447
49.9283	49.9349	-0.0066

Table 3: Refined peaks for Sr(CH₃CO₂)₂ exchange of 5% Y-ZrP hydrothermal

2T(Obs) (°)	2Th(Cal) (°)	Difference (°)
20.3977	20.4608	-0.0631
24.3401	24.3551	-0.015
29.1007	29.1043	-0.0036
29.3983	29.3674	0.0309
30.514	30.469	0.045
33.787	33.8337	-0.0467
34.2333	34.2816	-0.0483
35.4978	35.5404	-0.0426
39.6634	39.6704	-0.007
40.3328	40.2526	0.0802
41.7462	41.6998	0.0464
43.0107	42.9618	0.0489
44.0521	44.0902	-0.0381
45.0935	45.0825	0.011
45.9117	45.9469	-0.0352

Table 4: Refined peaks for CsNO₃ exchange of 5% Y-ZrP hydrothermal

2T(Obs) (°)	2Th(Cal) (°)	Difference (°)
11.7311	11.6945	0.0366
18.3148	18.3599	-0.0451
19.8409	19.8102	0.0307
20.0625	20.0153	0.0472
23.5218	23.513	0.0088
25.0043	24.9641	0.0402
25.2972	25.2696	0.0276
25.8997	25.9528	-0.0531
27.0179	27.0192	-0.0013
27.7929	27.7952	-0.0023
33.8896	33.9112	-0.0216
34.2078	34.1786	0.0292
37.3659	37.3945	-0.0286
41.746	41.7285	0.0175
44.4239	44.477	-0.0531
44.8702	44.8807	-0.0105
51.3416	51.2918	0.0498
51.8623	51.8854	-0.0231

Table 5: Refined peaks for CsCH₃CO₂ exchange of 5% Y-ZrP hydrothermal

<i>2T(Obs) (°)</i>	<i>2Th(Cal) (°)</i>	<i>Difference (°)</i>
11.7128	11.7067	0.0061
12.5729	12.5643	0.0086
19.8208	19.8052	0.0156
20.0598	20.0455	0.0143
20.472	20.4804	-0.0084
24.9968	24.9803	0.0165
25.292	25.283	0.009
25.903	25.9707	-0.0677
27.059	27.0485	0.0105
27.7606	27.7684	-0.0078
29.0262	29.0273	-0.0011
33.8756	33.8631	0.0125
34.1957	34.2188	-0.0231
37.3738	37.3986	-0.0248
42.7233	42.7281	-0.0048
44.3344	44.3234	0.011
44.9445	44.9226	0.0219
51.2672	51.2582	0.009

Table 6: Refined peaks for $\text{Co}(\text{NO}_3)_2$ exchange of 5% Y-ZrP hydrothermal

<i>2T(Obs) (°)</i>	<i>2Th(Cal) (°)</i>	<i>Difference (°)</i>
11.7328	11.6895	0.0433
18.3148	18.371	-0.0562
19.834	19.8146	0.0194
20.0727	20.0398	0.0329
22.0341	21.9948	0.0393
23.5218	23.5213	0.0005
25.0009	24.9708	0.0301
25.296	25.2926	0.0034
25.9104	25.9702	-0.0598
26.274	26.241	0.033
27.059	27.0367	0.0223
27.7713	27.8128	-0.0415
29.1006	29.0957	0.0049
29.601	29.6007	0.0003
33.8858	33.9064	-0.0206
34.2075	34.2106	-0.0031
37.3645	37.4066	-0.0421
42.8618	42.8689	-0.0071

Table 7: Refined peaks for $\text{Co}(\text{CH}_3\text{CO}_2)_2$ exchange of 5% Y-ZrP hydrothermal

<i>2T(Obs) (°)</i>	<i>2Th(Cal) (°)</i>	<i>Difference (°)</i>
11.7345	11.7185	0.016
12.6464	12.5751	0.0713
18.3403	18.4137	-0.0734
19.8247	19.7988	0.0259
20.0652	20.0552	0.01
22.0562	22.0145	0.0417
24.9963	24.9821	0.0142
25.2933	25.3049	-0.0116
33.2326	33.2296	0.003
33.8664	33.8698	-0.0034
34.1863	34.2235	-0.0372
37.3814	37.4277	-0.0463
39.0886	39.049	0.0396
41.6014	41.6528	-0.0514
44.3659	44.3161	0.0498

Table 8: Refined peaks for Sr-Cs-Co ion-exchange of 5% Y-ZrP hydrothermal

<i>2T(Obs) (°)</i>	<i>2Th(Cal) (°)</i>	<i>Difference (°)</i>
11.7218	11.6985	0.0233
12.5872	12.5691	0.0181
18.3148	18.371	-0.0562
19.834	19.8146	0.0194
20.0727	20.0398	0.0329
22.0341	21.9948	0.0393
23.5218	23.5213	0.0005
25.0009	24.9708	0.0301
25.296	25.2926	0.0034
25.9104	25.9702	-0.0598
26.274	26.241	0.033
27.059	27.0367	0.0223
27.7713	27.8128	-0.0415
29.1006	29.0957	0.0049
29.601	29.6007	0.0003
33.8858	33.9064	-0.0206
34.2075	34.2106	-0.0031
37.3645	37.4066	-0.0421

Table 9: Refined peaks for Sr-Cs exchange of 5% Y-ZrP hydrothermal

<i>2T(Obs) (°)</i>	<i>2Th(Cal) (°)</i>	<i>Difference (°)</i>
11.7083	11.715	-0.0067
12.5128	12.5478	-0.035
19.821	19.8077	0.0133
20.0525	20.0145	0.038
20.5464	20.4902	0.0562
23.5962	23.5548	0.0414
24.9879	24.9967	-0.0088
25.2813	25.2493	0.032
25.9027	25.9575	-0.0548
27.0418	27.0445	-0.0027
27.7602	27.7658	-0.0056
30.4395	30.4555	-0.016
33.8798	33.8756	0.0042
34.195	34.1873	0.0077
35.6465	35.6565	-0.01
37.3749	37.4033	-0.0284
44.2751	44.2758	-0.0007

Table 10: Refined peaks for Cs-Co exchange of 5% Y-ZrP hydrothermal

<i>2T(Obs) (°)</i>	<i>2Th(Cal) (°)</i>	<i>Difference (°)</i>
10.5045	10.5031	0.0014
11.7245	11.6974	0.0271
19.8443	19.8121	0.0322
20.0737	20.0514	0.0223
20.491	20.4797	0.0113
25.0049	24.98	0.0249
25.2993	25.2769	0.0224
25.9091	25.9811	-0.072
27.0849	27.0583	0.0266
27.7672	27.7594	0.0078
28.9519	29.015	-0.0631
29.6213	29.6346	-0.0133
33.8871	33.8748	0.0123
34.2068	34.2326	-0.0258
34.8282	34.7968	0.0314
37.3776	37.377	0.0006
42.713	42.734	-0.021
51.269	51.2576	0.0114

Table 11: Refined peaks for Sr-Co exchange of 5% Y-ZrP hydrothermal

<i>2T(Obs) (°)</i>	<i>2Th(Cal) (°)</i>	<i>Difference (°)</i>
11.7193	11.7009	0.0184
19.8246	19.8032	0.0214
20.0692	20.0339	0.0353
25.005	24.9749	0.0301
25.2976	25.2674	0.0302
25.9145	25.9632	-0.0487
27.0707	27.0409	0.0298
27.7861	27.7865	-0.0004
29.1006	29.1057	-0.0051
33.897	33.865	0.032
34.2184	34.2047	0.0137
37.359	37.3822	-0.0232
38.39	38.4089	-0.0189
40.1788	40.231	-0.0522
41.1307	41.1309	-0.0002
41.7215	41.7129	0.0086
44.356	44.3166	0.0394
44.878	44.8941	-0.0161
51.7788	51.8101	-0.0313

Table 12: Refined peaks for Sr-Ca exchange of 5% Y-ZrP hydrothermal

<i>2T(Obs) (°)</i>	<i>2Th(Cal) (°)</i>	<i>Difference (°)</i>
11.7326	11.7326	11.7088
19.8349	19.8349	19.8053
20.0739	20.0739	20.0201
25.0036	25.0036	24.9862
25.2989	25.2989	25.2561
25.9102	25.9102	25.9577
27.0539	27.0539	27.0401
27.7808	27.7808	27.7776
29.0621	29.0621	29.0335
33.8844	33.8844	33.8724
34.206	34.206	34.1907
34.7539	34.7539	34.7539
37.3778	37.3778	37.395
38.3243	38.3243	38.2865
41.1509	41.1509	41.1553
41.746	41.746	41.7296
41.9692	41.9692	42.0558
42.713	42.713	42.7189
44.3471	44.3471	44.33

Table 13: Refined peaks for Sr-Mg exchange of 5% Y-ZrP hydrothermal

<i>2T(Obs) (°)</i>	<i>2Th(Cal) (°)</i>	<i>Difference (°)</i>
11.7121	11.7051	0.007
12.5872	12.5522	0.035
19.8107	19.7993	0.0114
20.0524	20.0155	0.0369
24.9865	24.9739	0.0126
25.2795	25.2583	0.0212
25.8924	25.9485	-0.0561
27.0464	27.0264	0.02
27.7633	27.7629	0.0004
29.0391	29.026	0.0131
29.5469	29.575	-0.0281
30.4395	30.461	-0.0215
32.5223	32.5606	-0.0383
33.867	33.8473	0.0197
34.1854	34.1786	0.0068
37.3556	37.3923	-0.0367
38.3987	38.4148	-0.0161
44.3495	44.3105	0.039
44.8702	44.864	0.0062

Table 14: Refined peaks for Sr-Na exchange of 5% Y-ZrP hydrothermal

<i>2T(Obs) (°)</i>	<i>2Th(Cal) (°)</i>	<i>Difference (°)</i>
11.7156	11.7101	0.0055
18.4636	18.426	0.0376
19.8273	19.8009	0.0264
20.0701	20.0409	0.0292
24.9969	24.9899	0.007
25.2924	25.2616	0.0308
25.9062	25.9694	-0.0632
27.0619	27.0573	0.0046
27.7729	27.7778	-0.0049
29.0262	29.0262	0
32.6174	32.6078	0.0096
33.8792	33.8396	0.0396
34.2017	34.2179	-0.0162
37.3628	37.3828	-0.02
38.3702	38.3929	-0.0227
44.3399	44.3299	0.01
51.2592	51.2789	-0.0197

Table 15: Refined peaks for Cs-Ca exchange of 5% Y-ZrP hydrothermal

<i>2T(Obs) (°)</i>	<i>2Th(Cal) (°)</i>	<i>Difference (°)</i>
10.5045	10.492	0.0125
11.7257	11.7019	0.0238
19.832	19.8068	0.0252
20.0689	20.0254	0.0435
20.472	20.483	-0.011
25.0023	24.9801	0.0222
25.2945	25.2585	0.036
25.9045	25.9616	-0.0571
27.0723	27.041	0.0313
27.7781	27.7826	-0.0045
29.0412	29.0231	0.0181
33.8883	33.8764	0.0119
34.209	34.1976	0.0114
37.373	37.3835	-0.0105
44.2751	44.2975	-0.0224
44.7958	44.8147	-0.0189
51.2635	51.2576	0.0059
51.7879	51.817	-0.0291

Table 16: Refined peaks for Cs-Mg exchange of 5% Y-ZrP hydrothermal

<i>2T(Obs) (°)</i>	<i>2Th(Cal) (°)</i>	<i>Difference (°)</i>
11.7152	11.7044	0.0108
19.8326	19.8087	0.0239
20.0623	20.0334	0.0289
24.9969	24.9833	0.0136
25.2885	25.2673	0.0212
25.8994	25.9675	-0.0681
27.0634	27.0469	0.0165
27.7767	27.7892	-0.0125
29.0262	29.0272	-0.001
30.5139	30.4708	0.0431
33.8855	33.8762	0.0093
34.2065	34.208	-0.0015
34.7539	34.7728	-0.0189
37.3606	37.3908	-0.0302
42.713	42.7291	-0.0161
44.3442	44.3312	0.013

Table 17: Refined peaks for Cs-Na exchange of 5% Y-ZrP hydrothermal

<i>2T(Obs) (°)</i>	<i>2Th(Cal) (°)</i>	<i>Difference (°)</i>
11.726	11.7055	0.0205
19.8222	19.8116	0.0106
20.0549	20.0219	0.033
24.9947	24.9837	0.011
25.2844	25.2646	0.0198
25.9765	25.9616	0.0149
27.0448	27.0387	0.0061
27.7794	27.7891	-0.0097
33.8827	33.8946	-0.0119
34.1903	34.1935	-0.0032
37.3743	37.4009	-0.0266
42.8618	42.8839	-0.0221
44.3182	44.3341	-0.0159
44.7958	44.8352	-0.0394
45.3909	45.3513	0.0396
55.4322	55.4144	0.0178

Table 18: Refined peaks for Co-Ca exchange of 5% Y-ZrP hydrothermal

<i>2T(Obs) (°)</i>	<i>2Th(Cal) (°)</i>	<i>Difference (°)</i>
11.7278	11.7107	0.0171
19.4961	19.5263	-0.0302
19.8256	19.8063	0.0193
20.0647	20.0287	0.036
24.9973	24.9967	0.0006
25.2895	25.2481	0.0414
25.9057	25.9674	-0.0617
27.0586	27.0575	0.0011
27.7713	27.7722	-0.0009
29.0334	29.0321	0.0013
29.6217	29.6115	0.0102
33.8848	33.8569	0.0279
34.1974	34.2078	-0.0104
34.742	34.7617	-0.0197
37.3543	37.3826	-0.0283
40.2189	40.2374	-0.0185
41.6997	41.7301	-0.0304
42.9362	42.9924	-0.0562
44.3395	44.3432	-0.0037

Table 19: Refined peaks for Co-Mg exchange of 5% Y-ZrP hydrothermal

<i>2T(Obs) (°)</i>	<i>2Th(Cal) (°)</i>	<i>Difference (°)</i>
11.721	11.7052	0.0158
19.8256	19.8107	0.0149
20.0661	20.0349	0.0312
24.9963	24.9821	0.0142
25.2906	25.2759	0.0147
25.9034	25.9682	-0.0648
27.071	27.0445	0.0265
27.7804	27.7963	-0.0159
29.0262	29.0311	-0.0049
33.8809	33.8853	-0.0044
34.1993	34.2083	-0.009
37.3743	37.4009	-0.0266
44.3396	44.3314	0.0082
51.8182	51.821	-0.0028
55.4258	55.4215	0.0043
56.1149	56.1284	-0.0135
60.7547	60.7314	0.0233

Table 20: Refined peaks for Co-Na exchange of 5% Y-ZrP hydrothermal

<i>2T(Obs) (°)</i>	<i>2Th(Cal) (°)</i>	<i>Difference (°)</i>
11.7227	11.7096	0.0131
19.8183	19.808	0.0103
20.0574	20.0289	0.0285
20.5106	20.4884	0.0222
24.9931	24.9854	0.0077
25.2852	25.2707	0.0145
25.9029	25.9632	-0.0603
27.058	27.0423	0.0157
27.7828	27.7893	-0.0065
33.8844	33.8789	0.0055
34.1993	34.2003	-0.001
37.3855	37.4056	-0.0201